DEVELOPMENT OF CELL-BASED BIOSENSORS FOR BIOCIDE DETECTION APPLICATIONS IN WASTEWATER

DEVELOPMENT OF CELL-BASED BIOSENSORS FOR BIOCIDE DETECTION APPLICATIONS IN WASTEWATER

By PATRICK MORKUS, B.ENG.BIOSCIENCES

A Thesis Submitted to the School of Graduate Studies in Partial Fulfillment of the Requirements for the Degree Doctor of Philosophy

McMaster University

McMaster University DOCTOR OF PHILOSOPHY (2022) Hamilton, Ontario (Chemical Engineering)

TITLE: Development of cell-based biosensors for biocide detection applications in wastewater

AUTHOR: Patrick Morkus, B.ENG.BIOSCIENCES

SUPERVISORS: Associate Professor Dr. David R. Latulippe, P.Eng.
Professor Dr. Carlos D.M. Filipe, P.Eng.

NUMBER OF PAGES: xxiv, 238

Lay Abstract

The use of toxic chemicals in industrial processes results in the production of chemical-contaminated waters. Testing is required to determine whether these chemical-contaminated waters will disrupt a crucial biologically mediated process in wastewater treatment plants. However, the gold-standard test requires a person to replicate this biological process which is complex and time consuming (4 hours). Thus, a rapid (10 min) test was developed that uses bacteria as sensors to detect toxic chemicals and predict the impact of these waters on this process. Also, different methods for preparing these bacteria used as sensors were investigated. Sugars were mixed with the bacteria using various processes in a solution and dry format to preserve the bacteria for improved shelf-life, and to create an easy-to-use platform for rapidly detecting toxic chemicals. This test will enable a reduction in cost, testing time, and enable 'on-the-fly' decisions regarding treatment of these waters.

Abstract

Biocides, commonly used in industrial processes, are responsible for inhibiting a biologically mediated process in municipal wastewater treatment plants (WWTPs) known as nitrification. Testing wastewaters (WW) that contain biocides prior to their treatment at municipal WWTPs is critical; inhibition of nitrification may cause ammonia levels to exceed effluent limits and lead to the discharge of biocides and other chemical compounds into receiving waterways. The specific nitrification rate (SNR) batch test/nitrification inhibition test is considered the gold-standard test for this evaluation; however, it is cumbersome and requires approximately 4 hours to conduct. The focus of this thesis aims to address the critical need for the development of a rapid nitrification inhibition test by using bacteria as cell-based biosensors (CBBs). First, non-pathogenic *E. coli* and an off-the-shelf nucleic acid stain were used to detect three common biocides. Expanding on this work, six additional bacterial strains (nitrifying, non-nitrifying) as CBBs were selected and the combined response – a set of fluorescence signals ("fingerprint") – were found to successfully predict the nitrification inhibition potential of real industrial wastewater samples. Furthermore, changes in bacteria concentration and salinity content were found useful in manipulating biocide detection sensitivity. Efforts were also focused on preserving *E. coli*: storage temperature, salinity content, and a sugar-based polymer, pullulan, were important to maintaining a high level of survival in solution format. The benefits of sugars (pullulan and trehalose) in a dry format were also investigated: a miniature (1 L) electrospinning system was used to create thin and instantly dissolvable *E. coli*-embedded films to detect biocides. Finally, a new technique of aerosolizing bacteria while electrospinning sugar fibers was found to be gentler at incorporating bacteria into electrospun films when compared to electrospinning alone. Thus, this new technique could serve as a promising method of preserving the bacterial strains used as CBBs to predict nitrification inhibition potential.

Acknowledgements

I am incredibly grateful to have had this opportunity to continue my life-long journey of continuous learning by pursing my PhD in Chemical Engineering here at McMaster University, a place that I've called home for the last 11 years. These past five and half years as a graduate student were made possible by supervisors Dr. David Latulippe and Dr. Carlos Filipe who encouraged and inspired me to continue my studies beyond undergrad. To you both, I am sincerely thankful for your friendship and mentorship; you have taught me to think holistically about challenging problems, encouraged me when experiments were unsuccessful, and inspired me to work hard and never give up. I will never forget our meetings, particularly those in-person, where we would begin with sharing cheerful moments of our lives inside and outside of academic work, and then transition to our scientific discussions which I always looked forward to; I can honestly say that I don't remember a time leaving a meeting where I felt less motivated; and so, for that I thank you for those experiences. To my committee member, Dr. Tohid Didar, I thank you for your optimistic outlook and invaluable inputs in our group meetings that helped me acquire new perspectives when working on my project.

Many individuals have had such a profound impact on my experiences as a graduate student that it is difficult to mention these individuals in any particular order; but unfortunately, I cannot name them all at once and so here it goes. To Ryan, Scott, Mehdi, Salman, Damien, I will miss our lab experiences, but I am hopeful that we will work in the lab together once again. To Shabnam, Amir, Kimia, Wael, I looked up to you as I started my adventure and I wish you all the best. To Karina, Kurt, Reza, Satyam, Indranil, Melissa and

Blake, Noelle, Nicole, I will miss seeing you in the labs and sparking up conversations. To my star-studded student helpers (Lauren, Stephanie, Sarah, Danika, Matthew, Mikayil, James), you made my job so unbelievably easy because of your intelligence and your hardworking and friendly nature; I wish you the best in your futures – make our group proud! I would also like to thank Dawn White and Omar Salem for the guidance they provided me with respect to my early experimental work. From the Mobix Lab at McMaster University, I thank Laura Rossi for her help with Sanger sequencing of the bacterial strains. From the McMaster Regional Centre for Mass Spectrometry, I thank Dr. Kirk Green and Dr. Fan Fei for their guidance on running the GC-MS system and analyzing the results; also, I thank Salman for providing these data. From the City of Hamilton, I thank the Rocco at the Dundas Wastewater Treatment Plant for his assistance in providing the samples of return activated sludge that were used for the SNR batch tests. From the Department of Chemical Engineering at McMaster University, I thank Kristina, Michelle, and Linda for all their incredible support, and Paul Gatt and Michael Clarke for their help in machining and assembling a variety of equipment used in experimental work, particularly the electrospinning system used in Chapter 5 and 6. I also thank Brady Semple of the McMaster Manufacturing Research Institute (MMRI) for the 3D printing work of the electrospinning box. From the Canadian Centre of Electron Microscopy at McMaster University, I thank Marcia Reid for her help and patience in acquiring SEM images. From the Department of Chemistry & Chemical Biology, I thank Jose M. Moran-Mirabal for lending us his high voltage supply to conduct our electrospinning work. From Aevitas Inc. (our industrial partner), I thank Tom, Milos, Jo-Ann, and Rich for their time in meetings, providing industrial WW samples, and for their funding of this work in partnership with Ontario Centres of Excellence. I would also like to thank

Natural Sciences and Engineering Research Council of Canada (NSERC), Dillon Consulting and Canadian Water Resources Association (CWRA) for your incredibly generous grants.

Finally, to my parents, Miluse and Vaclav, I cannot thank you enough for your overwhelming support, steadfast encouragement, and guidance throughout this truly fulfilling and joyous schooling experience. To my loving, beautiful wife, Hilary, who I met in first year of undergrad, I thank you for the best 11 years of my life; you have been nothing but supportive along this entire journey and your continued backing of my ideas and potential endeavors remind how lucky I am to have you by my side.

Table of Contents

List of Abbreviations

ABS	acrylonitrile Butadiene Styrene
AIES	Atomizer Integrated Electrospinning System
BFE	Bacterial Filtration Efficiency
BOD	biological oxygen demand
BSC	biological safety cabinet
CBB	cell-based biosensor
CFU	colony forming unit
CMIT	5-Chloro-2-methyl-4-isothiazolin-3-one
CNC	computerized numerical control
COD	chemical oxygen demand
CTAB	cetyltrimethylammonium bromide
DCM	dichloromethane
DNA	deoxyribonucleic acid
DOE	design of experiments
eDNA	extracellular deoxyribonucleic acid
EDTA	ethylenediaminetetraacetic acid
FGM	fluorescent green microsphere
GC-MS	gas chromatography-mass spectrometry
HEPA	high-efficiency particulate absorbing
LB	Luria-Bertani
LC50	lethal concentration 50
LC-MS	liquid chromatography-mass spectrometry
LOD	limit of detection
LPM	liter per minute
MIT	2-Methyl-4-isothiazolin-3-one
MLF	maximum live fluorescence
MMRI	McMaster Manufacturing Research Institute
MSTFA	N-methyl-N-trimethylsilyl-trifluoroacetamide
NCS	new cell solution
NIPALS	non-linear iterative partial least squares
NRRL	Northern Regional Research Laboratory
NSERC	Natural Sciences and Engineering Research Council of Canada
OCE	Ontario Centres of Excellence
OD_{600}	Optical density 600
PBS	phosphate buffered saline
PCP	personal-care products
PCR	polymerase chain reaction
PLE	pressurized liquid extraction
PLS	partial least squares
PSI	pound per square inch
RAS	return activated sludge
RFU	relative fluorescence unit
RH	relative humidity
RNA	ribonucleic acid
RPM	revolutions per minute
rRNA	ribosomal ribonucleic acid
SEM	scanning electron microscope
SNR	specific nitrification rate
TEM	transition electron microscope
TSS	total suspended solids
ULPA	ultra-low particulate air
VBNC	viable but non culturable
VSS	volatile suspended solids
WW	wastewater
WWTP	wastewater treatment plant

List of Figures

List of Tables

Declaration of Academic Achievement

My research contribution and those of colleagues and other contributors are prefaced in each chapter, 2 through 6, with other acknowledgements made in the acknowledgement section.

1 Chapter 1: Introduction, Objectives and Thesis Outline

1.1 Biocide use and production of industrial wastewater

Many industries that produce goods rely on processes that generate wet waste (i.e., industrial wastewater) that have varying characteristics. These industrial wastewaters may contain high concentrations of oils, suspended solids, heavy metals and toxic compounds such as biocides. Biocides are broadly defined, and their definitions are geographically dependent. US and EU environmental agencies' definitions are largely the same,[1] with biocides defined in the US as "a diverse group of poisonous substances including preservatives, insecticides, disinfectants, and pesticides used for the control of organisms that are harmful to human or animal health or that cause damage to natural or manufactured products".[2] In Canada, pesticides and biocides are often used interchangeably.[1]

Biocide products are used across a wide range of industries, and because of their diverse end-use applications, there are many different types. They exist as alcohols, peroxygen compounds such as hydrogen peroxide, peracetic acid, phenols and phenolic type compounds, mineral and organic acids, quaternary ammonium compounds such as benzalkonium chloride, and other chlorine-based compounds such as chlorhexidine to name a few.[3] Automotive, aerospace, mining, steel/iron production, oil and gas, food processing, and the textile industries are all examples of industries that produce biocide-containing wastewaters. In manufacturing processes, cutting oils – that facilitate cutting or shaping of metals by lubricating, reducing heat and wear at the workpiece-tooling interface[4] – are mixed with commercially available biocides (e.g., Grotan BK, Protectol® PE) to control

microbial deterioration and thus maintain the quality of the cutting oil over time. Its use in cutting oils ultimately leads to a better performance of the cutting tools. In cooling towers, which are commonly used to reject heat from residential buildings and large power stations, biocides (e.g., Isothiazolin, DBNPA) are used to control the proliferation of *Legionella* and other microbial populations that exist on the inside surface of the equipment, or in the bulk water. Controlling the microbial contamination reduces fouling and corrosion of the cooling system. These are only a few, but common examples of biocide use that are necessary in maintaining operational efficiencies. There is an obvious financial tradeoff to using biocides, not only due to their inherent cost, but also with their treatment/separation out of the industrial wastewater produced. Total industrial water use (mainly from manufacturing, mining, oil and gas, and power) in the US is estimated to account for approximately 151 billion gallons per day with US industries spending $10.2 billion on water management of which 24% of that money is used for discharge treatment.[5]

1.2 Impact of inadequately treated biocide-containing wastewaters on receiving waterways and municipal WWTPs

Improper treatment of industrial wastewaters containing biocides could both directly and indirectly negatively influence aquatic environments.[6, 7]

Direct: Industrial WWs are often pretreated using a variety of treatment processes (e.g., coagulation, flocculation, sedimentation, aeration, filtration, adsorption) either on-site where the biocides are used,[8] and/or can be shipped to specialized treatment facilities prior to being sewered and sent to a municipal wastewater treatment plant (WWTP).[9] Municipal WWTPs rely heavily on the pretreatment performance of industrial WWs because

conventional WWTPs have difficulties separating out the complex chemical compounds prior to being discharged into our environment.[6, 10] In fact, the effluent of municipal WWTPs is considered the main emission source for biocides (e.g., triclosan,[11] artizine[12]) according to a few studies.[11, 12] In a study conducted by the United States Environmental Protection Agency (EPA), the occurrences of biocides – derived from industrial processes – in nine different WWTPs with similar treatment methodologies were monitored.[6] Four of the nine WWTPs monitored were selected for analysis due to their high influent volumes (between 10-20% of flow) coming from industrial sources. Some of the industrial sources included pharmaceutical, plastic, meat, and dairy processing plants. **Table 1-1** shows that many of the compounds found in the influent stream were also found in the effluent stream; the compounds found in this study are not statistically representative of the compounds found in other WWTPs.[6] All of the WWTPs were conventional activated sludge facilities with some plants having additional treatment such as powdered activated carbon (PAC) addition and sand filtration.

Table 1-1. Removal percentages and number of pesticide/biocide compounds across four municipal WWTPs with high influent volumes (between 10-20% of flow) derived from industrial sources; table adapted. Removal percentages and number of pesticide/biocide compounds across four municipal WWTPs with high influent volumes (between 10-20% of flow) derived from industrial sources; table adapted.[6]

Pesticide/Biocide Compounds	WWTP Influent	WWTP Effluent	Percent of Biocides Removed
Organochlorine (e.g., Chlorothalonil, cis-Nonachlor, Deldrin)	21	7	67%
Organophosphorous (e.g., Chlorpyriphos, Malathion, methyl parathion)	8	4	50%
Pyrethroid (e.g., Cis-Permethrin, Cypermethrins)	4	1	75%
Triazine (e.g., Desethyl atrazine, Hexazinone, Simazine)	4	4	0%

It was found that the municipal WWTPs are not designed to specifically remove these compounds, many of which (e.g, pyrethroids,[13] organophosporous chlorpyriphos[14]) are known to be toxic to aquatic invertebrates and fish.

Indirect: Poorly pretreated industrial wastewaters discharged into municipal WWTPs can disrupt a highly important biologically mediated process known as nitrification. Nitrification requires autotrophic nitrifying bacteria (e.g., *Nitrosomonas europaea*, *Nitrobacter*, *Nitrospira*) to facilitate the oxidation of ammonia into nitrate in the aeration stage (secondary treatment) of a WWTP. Under phased implementation set out in 2012, the Canadian government enacted the Wastewater Systems Effluent Regulations (WSER), made under the authority of the Fisheries Act. Those subject to the Regulations, are required to meet specific ammonia effluent limits which are dependent on nitrification performance in a municipal WWTP. As per the Regulation, the maximum concentration of un-ionized ammonia in the effluent is less than 1.25 mg/L when expressed as nitrogen (N) at 15°C.[15]

Ammonia effluent limits are established to avoid negatively affecting the health of aquatic organisms. When ammonia concentrations are elevated, aquatic organisms have difficulty excreting ammonia and thus may lead to accumulation of the deleterious substance resulting in potential death.[16] For example, at 0.06 mg/L, 0.2 mg/L and 2.0 mg/L of ammonia, fish may suffer from gill damage, trout and salmon begin to die, and higher-toxicity-tolerant fish such as carp begin to die, respectively.[17] The danger of ammonia to fish is also dependent on the temperature and pH of water; the toxicity of ammonia increases with increasing pH and temperature.[18]

1.3 Biocide detection techniques for biocide-containing wastewaters

Detecting biocides and/or assessing toxicity of industrial wastewater prior to entering a municipal WWTP is critical in the prevention of biocides entering our waterways. A variety of techniques have been used to identify and quantify chemical compounds including capillary electrophoresis-based techniques such as micellar electrokinetic capillary chromatography,[19] gas/liquid-chromatography-mass spectrometry, microfluidic sensors, spectrophotometry, colorimetry, and biosensors.[20]

Today, industries and commercial facilities that produce wastewater may decide to purchase commercially available colorimetric testing technologies to detect specific biocides. For example, non-oxidizing biocide test kits (Accepta) are used for testing Isothiazolinones (used in cosmetics, chemical additives for industrial use[21]), Tetrakis Hydroxymethyl Phosphonium Sulfate (THPS; commonly used in oil field operations to control biocorrosion, biofouling and reservoir souring[22]), 2,2-dibromo-3-

nitrilopropionamide (DBNPA; used in industrial cooling systems[23]), quaternary ammonium compounds (QAC; used in personal hygiene products, dyes, softeners, cosmetics[24]). For wastewaters that contain many biocides, chromatography-based methods (e.g., GC-MS, LC-MS)[20] or cell-based biosensor (CBB) technologies (e.g., Microtox®, Biocide Rapide™) could be selected to detect a wide range of compounds; commercial bacterial-based CBB technologies are used to assess general toxicity, however, provide little information in terms of compound identification. Though, because the bacteria in CBB technologies can be produced in large quantities using basic culturing practices and inexpensive nutrient media, the cost of testing is known to be less than that of other techniques.[25]

CBBs are particularly advantageous when assessing biological effects of target compounds such as biocides.[26] This makes CBBs a convenient and suitable candidate in the context of wastewater because nitrification in WWTPs is also a bacteria-driven process that is heavily influenced by biocides. Although bacteria such as *Vibrio fischeri* have been used to assess general toxicity in aquatic systems,[27] currently there is no commercial CBB test that utilizes the bacteria that are responsible for nitrification. Also, there is no commercial CBB test that provides information concerning the identity of the toxic compounds present in a tested sample. Most importantly, because many of the wastewaters produced are sewered and treated at municipal WWTPs, none of the techniques mentioned evaluate the impact/potential disruption of these wastewaters on the nitrification process, which is critical to meeting ammonia discharge limits.

The Specific Nitrification Rate (SNR) batch test or the International Standard ISO 9509 nitrification inhibition test are “legacy” techniques that exist to solve this problem.[28, 29]

They are used to model the performance of the nitrification but the complexity and time-consuming nature of these similarly conducted tests[28, 29] limit their widespread use. Thus, municipal WWTPs are prone to identifying disruptions in their nitrification process after they have already occurred. Therefore, personnel at municipal WWTPs are obliged to determine the origins of the wastewater and reach out to the facility(s) that was/were responsible for the disruption. These tests require access to activated sludge that contains the bacteria (nitrifiers) responsible for performing nitrification, a variety of expensive reagents (nitrate, nitrite, ammonia test kits) and instruments (pH probe, thermocouple, dissolved oxygen meter), along with trained personnel to perform a tedious, time-consuming (approximately 4 hours; and up to 24 hours[29]) and multi-step batch process (see Chapter 3 for a detailed description of the SNR process).[28, 29] Therefore, there is a critical need to develop a new technique/biocide detection technology that can rapidly assess the impact of industrial wastewaters containing biocides on the nitrification process in municipal WWTPs. This new technique could be implemented across the entire "supply chain" beginning at the source where biocides are used, before being treated onsite and/or sent out to intermediary treatment facilities, or before sewering to municipal WWTPs.

1.4 Preservation techniques for cell-based biosensors used for detection of biocides in the context of wastewater

CBBs are a convenient and suitable detection platform for evaluating toxicity and detecting a variety of compounds (e.g., phenol, acephate, atriazine) in wastewater.[30] The simple and inexpensive culture process[25] along with the constant sensing of their environment[31] has already proven suitable for water toxicity detection of heavy metals,

biological oxygen demand, pharmaceuticals and others.[30] However, creating operationally stable CBBs – in other words keeping CBBs alive and active – over the long-term (months) is challenging.

Various techniques for preserving CBBs have been investigated including lyophilization, vacuum desiccation, air-drying, immobilization in biocompatible polymers to retain operational stability.[31] Lyophilization or freeze drying is by far the most ubiquitous technique that has a proven industrial performance record,[31] and is the process by which commercially available biocide-sensing CBB tests such as *Vibrio fischeri*-based Microtox (Modern Water) are made. Products made via lyophilization are easily rehydrated in water which makes for detecting compounds in water convenient. However, the technique can be harsh to freeze-sensitive microorganisms,[31] is complex, and requires access to a freeze drier which is costly. The storage conditions for lyophilized CBB products are also less than desirable: lyophilized CBBs such as bioluminescent *E. coli* used for toxicity monitoring requires storage at -20°C and is functional over a time range anywhere from 10 days to several months, and other CBBs such as *Vibrio fischeri*-based Microtox test also requires storage at -20°C but is functional up to one year.[32, 33] Other preservation techniques such as immobilization/entrapping of CBBs in organic (e.g., hydrogels such as agar[31]) or inorganic (e.g., sol-gel) polymer gels have also been investigated, however, solute transport kinetics through and signal (e.g., optical) disruptions from the gels can add to the detection complexity.

There is currently no preservation technique at freezer (-20 °C), fridge (4 °C) or room temperatures (20-25 °C) which guarantees the same level of activity of various CBBs over

the advertised shelf-life of the products. These CBB products are said to be capable of 'maintaining' their activity, though some or most of their activity is lost over time.[31] Preservation techniques that 'maintain' a certain level of activity are more suitable as colorimetric tests in which the response is not continuous, but discrete and often binary (e.g., partially or completely yellow corresponds to 'insufficient biocide' and purple corresponds to 'sufficient biocide' as per the Biocide Rapide™ test). Many applications, however, would benefit from a greater response resolution (i.e., continuous), and thus to increase the widespread use of CBBs for toxicity detection and other detection alike, advances in preservation performance through new or modified existing techniques of CBBs are needed. Furthermore, obviating the need for cold chain would be beneficial when seeking to develop a CBB that enables on-site/in-the-field testing. Thus, developing a CBB that is equipped to handle temperature fluctuations in the field – when the kits are not used or transported – so as to not affect the performance of the CBB is desirable. Works by Dr. Filipe and his group,[34, 35] along with other groups,[36] have shown that sugars such as pullulan and/or trehalose act as stabilizing agents to better preserve a variety of biological materials such as phage, enzymes, and other biomolecules at room temperature or greater.

1.5 Objective & Thesis Outline

The successful development of a rapid (~10 minute) CBB 'next-generation' nitrification inhibition test to replace the cumbersome, time-consuming (4-6 hour) specific nitrification rate (SNR) batch test will be transformational in many ways. The development of this new test will enable both a reduction in cost and testing time, as well as enable quicker

treatment-related decisions that will have a positive impact in the ability of these WWTPs to meet standards set out by the WSER. For example, industrial/commercial facilities that generate biocide-containing wastewaters will be able to rapidly assess the impact their industrial wastewaters will have on municipal WWTPs prior to sewering, thus leading to a reduction in their use of biocides.

The main objective of this thesis was to develop a simple and rapid (~10 minutes) CBB technology that can be used to assess the impact of industrial WWs (containing biocides) on the nitrification process in municipal WWTPs. The work presented in this thesis investigated both a solution-based and electrospinning-based approach for making CBBs.

Chapter 2 presents the development of a simple to use CBB test which utilizes a non-pathogenic *E. coli* strain (as a model) and an off-the-shelf nucleic acid stain that probes for cellular activity and membrane integrity. The results demonstrate that the CBB test can be stored in the fridge for at least three months under certain conditions and still maintain a similar fluorescence response to three different biocides (see Appendix F). The results also demonstrate that pullulan sugar improves culturability, however, a decreasing culturability over the approximate three-month storage time does not necessarily dictate whether the fluorescence response to biocides will be maintained.

Chapter 3 explores the use of a panel of seven pure bacterial strains, an off-the-shelf nucleic acid stain, and partial least squares (PLS) modeling to predict the nitrification inhibition potential of real industrial WW samples. Each bacterial strain produces a different fluorescence signal when exposed to the same WW sample, therefore forming a fingerprint

of the WW sample when the signals are combined. The unique fingerprint, which is acquired in less than 10 minutes using a microplate reader, is then be correlated to the response of the SNR batch test using partial least squares (PLS) modeling. The results demonstrate that this method can be used to predict nitrification inhibition potential of industrial wastewater samples, and that of the seven bacterial strains, only four (*Nitrospira*, *Escherichia coli*, *Bacillus subtilis*, *Bacillus cereus*) were identified to be significant contributors in the model's prediction.

Chapter 4 focusses on two improvements: (1) increasing the sensitivity of fluorescence signals on three (*E. coli*, *B. subtilis*, *B. cereus*) of the four bacterial strains identified in Chapter 3, and (2) translating the technology to a handheld fluorometer to enable point-of-use detection of biocides. *Nitrospira* was not studied in this chapter mainly due to its slow culturing time (weeks).

Chapter 5 describes the development of a customized electrospinning setup that is miniature in size (approximately 1 L) and fully enclosed to create rapidly dissolvable bacteria-embedded pullulan-trehalose pills. Miniaturization was the key feature for two reasons: (1) it easily fits into a common Class II, Type A2 Biological Safety Cabinet to allow for work with biosafety level restrictions, and (2) it enables rapid manipulation and control of the relative humidity which is known to affect electrospinning performance. The results demonstrate that there is an optimal set of conditions (e.g., humidity, spinneret configuration and design) for producing high quality and highly reproducible bacteria-embedded pullulan-trehalose

films. With these conditions we demonstrate the application of preparing *E. coli*-embedded pills (cut from the films) used to detect two model biocides.

Chapter 6 demonstrates the benefits of integrating bacteria into a pullulan-trehalose fibrous network by aerosolizing bacteria and electrospinning pullulan-trehalose fibers simultaneously. The method was found to significantly increase the percent culturability of bacteria (which could be used as CBBs) present in the fibrous network when compared to electrospinning bacteria alone as demonstrated in Chapter 5.

Chapter 7 examines the major outcomes from this thesis work and provides recommendations for the future of this work that will ultimately be required to bring this technology to market.

1.6 References

1. Miller, J., *A Comparative Review of Biocidal Legislation in the EU, US and Canada*, in *compliance & risks*. 2020.
2. Sandle, T., *Disinfectants and Biocides*, in *Disinfection and Decontamination*. 2018, CRC Press. p. 7-34.
3. Ruiz, L. and A. Alvarez-Ordóñez, *The role of the food chain in the spread of antimicrobial resistance (AMR)*, in *Functionalized Nanomaterials for the Management of Microbial Infection*. 2017, Elsevier. p. 23-47.
4. Inc, A.L.M.F. *How Do We Choose the Best Cutting Oil?* 2017 [cited 2021 December 30].
5. Research, B., *U.S. industry spent $10.2 billion on water management in 2017 according to new study*, in *smart water magazine*. 2018.
6. Agency, U.S.E.P., *Occurrence of Contaminants of Emerging Concern in Wastewater From Nine Publicly Owned Treatment Works* 2009: U.S. Environmental Protection Agency Office of Water (4303T) 1200 Pennsylvania Avenue, NW Washington, DC 20460
7. Cooper, C., *Biological effects of agriculturally derived surface water pollutants on aquatic systems—a review.* Journal of environmental quality, 1993. **22**(3): p. 402-408.

8. Carrera, J., T. Vicent, and J. Lafuente, *Effect of influent COD/N ratio on biological nitrogen removal (BNR) from high-strength ammonium industrial wastewater.* Process Biochemistry, 2004. **39**(12): p. 2035-2041.
9. Aevitas. *Industrial Wastewater Treatment*. 2017 [cited 2021 December 30]; Available from: https://www.aevitas.ca/industrial-wastewater-treatment.html.
10. Ontario, G.o., *Water reclamation and reuse*. 2019.
11. Chen, Z.-F., et al., *Triclosan as a surrogate for household biocides: an investigation into biocides in aquatic environments of a highly urbanized region.* water research, 2014. **58**: p. 269-279.
12. Heeb, F., et al., *Organic micropollutants in rivers downstream of the megacity Beijing: sources and mass fluxes in a large-scale wastewater irrigation system.* Environmental science & technology, 2012. **46**(16): p. 8680-8688.
13. Werner, I. and K. Moran, *Effects of pyrethroid insecticides on aquatic organisms.* Synthetic pyrethroids: Occurrence and behavior in aquatic environments, 2008. **991**: p. 310-335.
14. Giesy, J.P., et al., *Ecological risk assessment of the uses of the organophosphorus insecticide chlorpyrifos, in the United States.* Ecological risk assessment for chlorpyrifos in terrestrial and aquatic systems in the United States, 2014: p. 1-11.
15. Canada, G.o. *Wastewater Systems Effluent Regulations: frequently asked questions*. 2021 [cited 2021 December 30]; Available from: https://www.canada.ca/en/environment-climate-change/services/wastewater/system-effluent-regulations-reporting/wastewater-systems-effluent-frequently-asked-questions.html.
16. Agency, U.S.E.P. *Aquatic Life Criteria - Ammonia*. 2021 [cited 2021 December 30]; Available from: https://www.epa.gov/wqc/aquatic-life-criteria-ammonia.
17. Sedna. *Water Quality Traceability and Salmon Quality*. 2021 [cited 2021 December 30]; Available from: https://sednatech.io/water-quality-traceability-and-salmon-quality/#:~:text=When%20levels%20reach%200.06%20mg,L%20usually%20indicate%20polluted%20waters.
18. Agency, U.S.E.P. *Ammonia*. 2021 [cited 2021 December 30]; Available from: https://www.epa.gov/caddis-vol2/ammonia.
19. Fang, R., et al., *Determination of eight triazine herbicide residues in cereal and vegetable by micellar electrokinetic capillary chromatography with on-line sweeping.* Food chemistry, 2014. **145**: p. 41-48.
20. Zulkifli, S.N., H.A. Rahim, and W.-J. Lau, *Detection of contaminants in water supply: A review on state-of-the-art monitoring technologies and their applications.* Sensors and Actuators B: Chemical, 2018. **255**: p. 2657-2689.
21. Silva, V., et al., *Isothiazolinone biocides: chemistry, biological, and toxicity profiles.* Molecules, 2020. **25**(4): p. 991.
22. Conlette, O.C., *Impacts of Tetrakis-hydroxymethyl Phosphonium Sulfate (THPS) based biocides on the functional group activities of some oil field microorganisms associated with corrosion and souring.* Microbiology Research Journal International, 2014: p. 1463-1475.

23. Klaine, S.J., et al., *An ecological risk assessment for the use of the biocide, dibromonitrilopropionamide (DBNPA), in industrial cooling systems.* Environmental Toxicology and Chemistry: An International Journal, 1996. **15**(1): p. 21-30.
24. Vereshchagin, A.N., et al., *Quaternary ammonium compounds (QACs) and ionic liquids (ILs) as biocides: From simple antiseptics to tunable antimicrobials.* International journal of molecular sciences, 2021. **22**(13): p. 6793.
25. Lim, J.W., et al., *Review of micro/nanotechnologies for microbial biosensors.* Frontiers in bioengineering and biotechnology, 2015. **3**: p. 61.
26. Eltzov, E. and R.S. Marks, *Whole-cell aquatic biosensors.* Analytical and bioanalytical chemistry, 2011. **400**(4): p. 895-913.
27. Johnson, B.T., *Microtox® acute toxicity test*, in *Small-scale freshwater toxicity investigations*. 2005, Springer. p. 69-105.
28. Bye, C.M., R.M. Jones, and P.L. Dold, *Pragmatic Nitrification Inhibition Testing for Robust Plant Design.* Proceedings of the Water Environment Federation, 2012. **2012**(12): p. 4222-4238.
29. Standard, I., *Water quality — Toxicity test for assessing the inhibition of nitrification of activated sludge microorganisms*, in *ISO 9509*. 2006: Switzerland.
30. Gupta, N., et al., *Cell-based biosensors: Recent trends, challenges and future perspectives.* Biosensors and Bioelectronics, 2019. **141**: p. 111435.
31. Bjerketorp, J., et al., *Advances in preservation methods: keeping biosensor microorganisms alive and active.* Current opinion in biotechnology, 2006. **17**(1): p. 43-49.
32. Gu, M.B., S.H. Choi, and S.W. Kim, *Some observations in freeze-drying of recombinant bioluminescent Escherichia coli for toxicity monitoring.* Journal of biotechnology, 2001. **88**(2): p. 95-105.
33. Shin, H.J., H.H. Park, and W.K. Lim, *Freeze-dried recombinant bacteria for on-site detection of phenolic compounds by color change.* Journal of biotechnology, 2005. **119**(1): p. 36-43.
34. Leung, V., et al., *Long-term preservation of bacteriophage antimicrobials using sugar glasses.* ACS Biomaterials Science & Engineering, 2017. **4**(11): p. 3802-3808.
35. Jahanshahi-Anbuhi, S., et al., *Pullulan encapsulation of labile biomolecules to give stable bioassay tablets.* Angew Chem Int Ed Engl, 2014. **53**(24): p. 6155-8.
36. Krumnow, A.A., et al., *Preservation of bacteria in natural polymers.* J Microbiol Methods, 2009. **78**(2): p. 189-94.

2 Chapter 2: Optimization of microorganism preservation conditions for the development of an acute toxicity bioassay for biocides

In this chapter, experiments were performed by myself, post-doctoral fellows Mehdi Zolfaghari, and Damien Parrello, and undergraduate students Matthew Csordas, Mikayil Malikov, under my supervision. Undergraduate students James Rose and Kenneth Byungjun Choi led preliminary work. This chapter was drafted by myself and edited by my academic supervisors, Dr. David R. Latulippe and Dr. Carlos D.M Filipe. The chapter and its appendix are presented with permission from Elsevier © 2022.

Optimization of microorganism preservation conditions for the development of an acute toxicity bioassay for biocides
Patrick Morkus, Mehdi Zolfaghari, Damien Parrello, Matthew Csordas, Mikayil Malikov, James Rose, Kenneth Byungjun Choi, Carlos D.M. Filipe, David R. Latulippe
Chemosphere 221 (2019): 45-54
DOI: 10.1016/j.chemosphere.2018.12.182

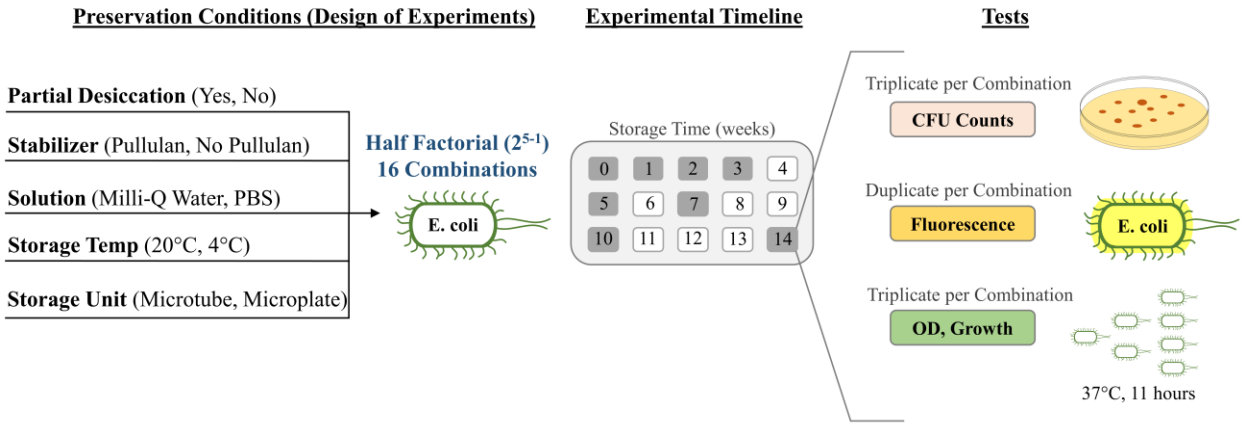

2.1 Abstract

Biocides, also referred to as 'microbicides' or 'inhibitors', are widely used in industrial processes (e.g. utility water in cooling towers) to control and/or eliminate the growth of microorganims. Because of their inherent toxicity, their presence in various sources (e.g., river sediments, potable water) can negatively affect ecosystems. Currently available biocide detection techniques are not suitable for 'point-of-use' applications since they are tedious, complicated, and often require experienced personnel to operate. To address this concern, we sought to develop a simple-to-use toxicity bioassay based on a model microorganism (*E. coli*) after short (< 30 min) exposure to known biocides that can be stored at room temperature (preferably) or the fridge. Based on recent work and our expertise in polymer-based preservation of biomolecules, we leveraged this knowledge to improve *E. coli* preservation for biocide detection purposes. A design-of-experiments strategy was used to evaluate 16 different preservation conditions from 5 process parameters (i.e. 2^{5-1} fractional factorial). It was found that pullulan, a sugar-based polymer, improved *E. coli* culturability by an order of magnitude after three months of storage. Also, it was found that storing *E. coli* in the fridge in Milli-Q water was favorable for maintaining a high level of culturability. Finally, the toxicity of three common biocides (Cetyltrimethylammonium bromide (CTAB), ProClin™ 300, and Grotan® BK) was evaluated using a fluorescence-based assay across all 16 preservation conditions. The response of the preserved *E. coli* was biocide specific but most importantly did not vary during the entire three-month storage period.

2.2 Introduction

There is great interest in the use of whole bacterial cells as biosensors for specific analytes due to their low cost, rapid-response, and capacity to be easily produced (Belkin, 2003). In general, these microbial-based sensors produce an optical or electrical signal that can be detected using either simple or specialized instruments. For example, an optical biosensor utilized a heavy metal responsive gene promoter zntA, lacZ reporter gene, and a cyan fluorescent protein carrying gene in *E. coli* to measure the concentration of mercury (Biran et al., 2003). Also, a genetically modified version of *Pseudomonas putida* (JS444) was used in an amperometric biosensor to measure the concentration of organophosphates such as fenitrothion (Lei et al., 2007). Researchers have also used non-genetically modified microbes as biosensors for the purposes of detecting a larger variety of analytes. For example, changes in the respiration rate of *Pseudomonas putida* (DSM 50026) were used to detect aromatic compounds (e.g., phenolic substrates) in a synthetic wastewater (WW) source (Timur et al., 2004). Also, naturally bioluminescent bacteria such as *P. fischeri* immobilized in thin films of poly(vinyl alcohol) cryogels have been used to evaluate the toxicity of phenolic materials in an industrial wastewater WW source (Philp et al., 2003). Researchers have also reported the use of a *Vibrio fischeri* bioluminescence assay to detect a wide range of chemicals (Girotti et al., 2008).

The strategy of using whole cell biosensors is particularly attractive in applications where a complex mix of potentially toxic compounds are present. One such application is the use of biocides in the production of commercial products and the operations of various industrial processes. For example, biocides are used to prolong the lifetime of recirculating

fluids and used to control the degree of bio-fouling on process surfaces (U.S. Army Corps of Engineers, 2012). There are over 75 different biocides approved by the U.S. Environmental Protection Agency to control microbial proliferation in metalworking fluids alone. Numerous types of biocides, from different 'families' such as isothiazolones, benzimidazoles, triazines, and nitromorpholines, are available as 'ready-to-use' formulations in liquid and powder form.

From an environmental perspective, there are multiple concerns about the widespread use of biocides. In a recent study, Malaj et al. (2014) reported that the biocide tributylin was one of the 'major contributors' to the acute and chronic effects on freshwater diversity that currently exists at a continent-wide scale. There is also the potential for biocides to indirectly affect water quality – because biocides are persistent and non-specific, they can inhibit the biological treatment processes that occur at most municipal wastewater treatment plants (e.g., nitrification). In such a situation, the decrease in effluent quality could negatively affect the ecosystems in the receiving water bodies of the plant effluent (Yan et al., 2017).

Depending on the scope of work and scale of study, a variety of techniques have been used to detect for biocides. For example, in their very large study of the toxicity data for hundreds of chemicals from thousands of sites, Malaj et al. (2014) used LC_{50} values for the three test species: *P. promelas* (fish), *D. magna* (planktonic crustacean), and *P. subcapitata* (algae). These sorts of tests are well accepted but they require between 48 and 96 hours to complete which is completely impractical for any 'point-of-use' applications. The specific nitrification rate (SNR) test is an alternative technique that can be used for biocide detection

(Bye et al, 2012); it still takes approximately 4-6 hours to compete and is rather tedious (requiring continuous monitoring, frequent sampling, and multiple analyses to be made on each sample) such that it requires the dedication of a full-time operator. It is challenging to run the SNR test on more than a few samples at once. Overall, the SNR test is also impractical to use in any 'point-of-use' applications. Many sophisticated techniques have been developed for identifying and/or detecting biocides in various environmental samples. For example, Massei et al. (2018) used pressurized liquid extraction (PLE) and a combination of liquid and gas chromatography techniques to detect for the presence of pesticides and biocides in river sediment samples. Helmi et al (2018) used a combination of flow cytometry and microbial strains from two different water sources (potable water sample, fresh river water sample) to detect for toxins in cooling tower water samples. The ability to integrate these sorts of detection techniques into a point-of-use application is greatly hindered by the need for sophisticated and expensive equipment.

Given the reasons listed above, it is believed that a detection technique based on the use of microbial biosensors would be ideal. However, a key challenge lies in the ability to maintain the stability and responsiveness of the microbial biosensors. It is known that the structure of the cellular membrane is an important factor in determining the best preservation conditions. For example, Gram-positive bacteria exhibited higher culturability in phosphate-buffered saline (PBS) while Gram-negative bacteria were better in pure water (Liao & Shollenberger, 2003). An early study showed that the soil-borne bacterium, *Ralstonia solancearum*, could be stored in tap water for many months (Kelman, 1956) and even multiply for several generations in pure water (Wakimoto et al., 2001). Another study

showed that phytopathogenic bacteria, *Agrobacterium tumefaciens,* along with *Pseudomonas syringae ssp. syringae*, could even survive in sterile water for at least 20 years (Iacobellis & DeVay, 1986). However, maintaining high culturability rates can be a problem. Therefore, there has been great interest in developing techniques to further improve preservation issues. Cryopreservation at very low temperatures (typically -80 °C) is a well-known technique that halts deleterious cellular instability and morphological changes (Kim and Kubica, 1972; Pegg, 1976). However, the requirement of having ultra-low temperature systems and possible limitations on the number of 'freeze-thaw cycles', makes that approach less favorable. Alternatively, lyophilization (also known as 'freeze drying' or 'spray drying') has been shown to effectively preserve many different bacterial strains (Joubert & Britz, 1987). However, osmotic stress and ice crystal formation due to lyophilization have been known to reduce cellular stability (Morgan et al., 2006) and this approach requires highly sophisticated and expensive equipment (Rojas-Tapias et al., 2013). An alternative preservation technique based on the use of biopolymers (e.g. pullulan, acacia gum, trehalose) has also been demonstrated to have relatively high survivability for approximately 80% of heterotrophic bacteria which can be stored in the fridge, or even at room temperature (Krumnow et al., 2009; Rojas-Tapias et al., 2013; Sorokulova et al. 2015). The principle advantage to this approach is its simplicity.

In previous studies led by one of us, it has been shown that pullulan is an effective preservation additive for biological molecules such as enzymes (Jahanshahi-Anbuhi et al., 2014) and bacteriophage antimicrobials (Leung et al., 2017). The motivation for our study was to leverage this expertise into developing an optimum preservation condition for storing

Escherichia coli (*E. coli*), as a model microorganism, so that it could be used as a microbial biosensor for the detection of biocides. In this study, we explored the effect of different preservation factors (storage temperature, solution conditions, biopolymer addition, preservation unit) on the survival of *DH5α E. coli* cells over a period of approximately three months. As a proof-of-principle, a 'live' fluorescence labelling fluorophore was used to evaluate the toxicity of three commonly used biocides.

2.3 Materials and methods

2.3.1 *DH5α E. coli* inoculation and preservation

DH5α E. coli was generously provided by the Biointerfaces Institute at McMaster University. The bacteria were grown in Lysogeny broth (LB) media (Sigma-Aldrich) in 14 mL polystyrene round-bottom Falcon tubes and placed into a Thermo MaxQ 8000 Shaker Incubator set to 37 °C at 225 rpm for 20 hours. After incubation, 10 tubes (5 mL solution each) were combined into a 50 mL polystyrene Falcon tube and centrifuged in a Thermo Scientific Sorvall ST 40R Centrifuge at 8 °C for 16 minutes. The supernatant was removed and replaced with an equal volume of phosphate buffered saline (PBS) solution (BioShop®). Then the maximum live fluorescence (MLF) signal was measured using a LIVE/DEAD™ *Bac*Light™ Bacterial Viability Kit (L7007 from Invitrogen™), 96-well Flat Bottom Black microplate (Eppendorf), and an Infinite M200 Pro plate reader (TECAN). If necessary, the solution was concentrated or diluted with PBS solution as required to obtain a MLF signal of approximately 20,000 arbitrary fluorescence units. In order to optimize the *E. coli* preservation conditions, a two-level, five-factor, fractional factorial (i.e. 2^{5-1} = 16 preservation conditions) design-of-experiment (DOE) study was established. To perform

triplicate analysis of the cell survivability (culturability) at eight different 'time points' (corresponding to weeks 0, 1, 2, 3, 5, 7, 10, and 14) for each preservation condition, a total of 384 'preservation' samples were required. The 'high' and 'low' conditions for each of the five factors in the DOE are shown in **Table 2-1**, with the exact details for each condition given below:

- One-half of the cell suspension in PBS solution was replaced with Milli-Q water and was concentrated five times to achieve a final cell concentration of approximately 3×10^9 CFU/mL (actual cell concentration was recorded to be between approximately 2.5×10^9 and 6.5×10^9 CFU/mL)
- 100 kDa desalinized pullulan (Polysciences, Inc.) was added to one-half of each cell solution (i.e., Milli-Q and PBS) to a final concentration of 10% w/w.
- One-half of each solution was aliquoted into 1.7 mL microcentrifuge tubes with each tube containing a final volume 150 µL (hereafter referred to as 'microtubes'); the other half of each solution was aliquoted into Falcon 96-well Flat Bottom with Low Evaporation Lid Tissue Culture Plates with each well containing a final volume 150 µL. As shown in **Figure A1** (in Appendix A), only the 60 'inside' wells of the microplate were used. For the one-half of the samples that did not require partial desiccation (see below for details), the microtubes were capped and Parafilm wrapped while the microplates were sealed tightly with a black AbsorbMax film (Sigma-Aldrich).
- For the other half of the samples that were subjected to partial desiccation, the samples were placed in a xL Bel-Art Vacuum Desiccator containing 100 g of Drierite

Desiccant (Calcium Sulphate Anhydrous) for 20 hours (see **Figure A2** in Appendix A). During the desiccation process, the relative humidity (RH) was measured via a USB-502 RH/Temperature Data Logger to be 25 ± 3% (see **Figure A3** in Appendix A). It is known that the RH is an important factor in the desiccation of bacterial cells (Ronan et al., 2013). After the desiccation process was complete, the microtubes were capped and Parafilm wrapped and the microplates were sealed tightly with the black AbsorbMax film.

- One half of the microtubes (192 in total) and one-half of the microplates (4 in total) were stored in the dark at room temperature (i.e. 20 ± 2 °C); the other 192 microtubes and 4 microplates were stored in the dark in a fridge (i.e. 4 ± 1 °C).

Table 2-1. Five factors used in the 2^{5-1} DOE study; 'high' conditions are denoted as Positive (+) and 'low' conditions are denoted as Negative (-).

Factor	Positive (+)	Negative (-)
x1	Partial Desiccation	No Desiccation
x2	Pullulan	No Pullulan
x3	Milli-Q Water	PBS
x4	Room Temperature (20 ± 2°C)	Fridge (4 ± 2°C)
x5	Microcentrifuge tube	96-well microplate

Note that for each of the 8 conditions that were stored in the 96-well microplates (i.e., 2 solutions × 2 pullulan conditions × 2 desiccation conditions × 2 temperatures), an extra number of samples were prepared in the microplate because we occasionally observed an inconsistent formation of the slight depressions in the AbsorbMax film after the first day in storage (see **Figure A4** in Appendix A). In our preliminary work, we discovered that they

were critically important to maintaining cell culturability. In order to better understand this phenomenon, we prepared a set of bacteria-free samples in the microplates at the exact same conditions and found that they never formed those slight depressions in the AbsorbMax film. Thus, the depressions are due to the presence of the bacteria; currently our hypothesis is that the depressions are formed by the slight vacuum that is created by the uptake of oxygen by *E. coli*. This topic will be studied further in depth and will be the subject of a forthcoming publication.

2.3.2 *E. coli* preservation analysis and response assays

At each 'time point' in the experiment, a total of 24 microtubes (triplicate samples for 8 different preservation conditions) and the microplates were removed from storage (24 wells used). In order to access the contents within each well of the microplate, a small sampling hole was created in the AbsorbMax film using a mechanical punch (pre-sterilized with 70% ethanol). For each sample (microplate well only), 150 μL of PBS solution was added and the contents pipetted 'up and down' to resuspend the preserved cells. Then, the entire cell solution was transferred to an empty sterile 1.7 mL microtube, centrifuged, and the supernatant was replaced with 1.5 mL of PBS; the resulting solution, hereafter referred to as the 'new cell solution' (NCS), was used for the various tests described below. For microtubes, the cell solution was centrifuged and the supernatant of the cell solution was simply replaced with 1.5 mL of PBS to generate the NCS.

2.3.2.1 Microbial CFU Enumeration

The enumeration of colony forming units (CFUs) was determined from a 10 × serial dilution (performed in triplicate) that was plated on LB-Agar culture plates, incubated upside down at 37 °C for 20 hours, and then counted visually.

2.3.2.2 Fluorescence assay

The MLF was determined by first adding 100 µL of NCS and 100 µL of dye solution (as per LIVE/DEAD™ *Bac*Light™ Bacterial Viability Kit L7007 from Invitrogen™ instructions) to a well of a 96-well Flat Bottom Black microplate (Eppendorf). Then, the plate was immediately placed inside an Infinite M200 Pro plate reader (TECAN) with a shaking frequency of 60 s, measurement frequency of 2 min, default gain of 60, and an excitation and emission wavelength of 485 nm and 530 nm, respectively. This test was performed in duplicates (two of three NCS solutions).

2.3.2.3 Growth Curve Evaluation

Triplicate 200 µL aliquots of the NCS were centrifuged in 1.7 mL microtubes and the supernatants were replaced with 200 µL of LB media. After resuspension, 150 µL from each triplicate was placed in a well of a Falcon Flat Bottom 96-well microplate with a Low Evaporation Lid Tissue Culture Plate and read by an Infinite M200 Pro plate reader (TECAN). The optical density value at 600 nm was measured at different intervals over the entire 11 h test with a microplate shaking interval of 60 s and a 1 mm linear setting.

2.3.2.4 Biocide Exposure Tests

The effect of three different biocides and control (Milli-Q water) on *E. coli* for all 16 preservation conditions was recorded at each of the eight timepoints over the 14-week test. A small volume (1.8 μL) of the stock biocide solution (see below for details) was added to a 150 μL aliquot of the NCS in a microtube and then the contents were rapidly mixed using a vortex mixer. After a one hour exposure time (however not necessary and could be done in less than 30 minutes), the MLF was measured. The technical details for the three biocides used in this study are given below:

- ProClin™ 300 (Sigma-Aldrich), a product that contains a mixture of 5-Chloro-2-methyl-4-isothiazolin-3-one (CMIT) and 2-Methyl-4-isothiazolin-3-one (MIT) is known to minimize microbial growth by inhibiting enzymatic activity and reducing the availability of ATP (Affatato et al., 2004). A stock solution was prepared by diluting the as-purchased liquid solution (containing 3% active ingredient) with Milli-Q water; the final concentration in the NCS was 300 ppm total or 9 ppm of active ingredient. According to the supplier, a 25 ppm active ingredient solution killed 10% of cells (but the exact cell type was not specified) within 15 min of exposure.
- Cetyltrimethylammonium bromide (CTAB) is a well-known corrosion inhibitor used in cooling water systems (Sherine, 2015). A stock solution was prepared by dissolving CTAB powder (Sigma) in Milli-Q water; the final CTAB concentration in the NCS was 20 ppm.

- Grotan® BK (Commercial Oil) contains 78.5% of Hexahydro-1,3,5,tris(2-hydroxyethyl)triazine and is commonly used to prevent demulsification of metalworking fluids (Urwin et al., 1976). A stock solution was prepared by diluting the as-received liquid solution with Milli-Q water; the final concentration in the NCS was 1,500 ppm which is within the concentration range as recommended by the manufacturer.

2.3.2.5 RNA concentration measurements

For a select number of preservation samples, an 800 µL aliquot of the NCS was processed as per the standard instructions for the PureLink® Quick Plasmid Miniprep Kits (Invitrogen). RNase-free buffers and RNase-free water were used to minimize the chance of RNA degradation; also DNase enzyme was not used in order to minimize the possibility of RNA degradation. The concentrations of RNA were determined using a Nanodrop™ One^{C} UV-Vis spectrophotometer (Thermo Scientific™).

2.4 Results and Discussion

2.4.1 *E. coli* cell storage evaluation: culturability and fluorescence assay

To enable a greater understanding of the effects of the DOE factors on microbial cell preservation, we organized all the experimental results into the format shown in **Figure 2-1**. Each panel corresponds to one specific preservation condition with CFU results (vertical bars) and MLF values (continuous line) displayed for the eight timepoints within the 14-week test period. The error bars for the CFU data series and MLF data series correspond to the standard deviation from the analysis of triplicate and duplicate samples, respectively.

The organization of the panels is displayed both on the periphery of **Figure 2-1** and in the accompanying caption. For clarity, some of the key details are outlined below:

- The top half of the figure (i.e., panels 1-4, 9-12) is for the samples prepared with PBS solution; the bottom half of the figure (i.e., panels 5-8, 13-16) is for the samples prepared with Milli-Q water.
- The second and fourth rows (i.e., panels 3, 4, 7, 8, 11, 12, 15, 16) are for the samples prepared with pullulan.
- The second and fourth columns (i.e., panels 2, 4, 6, 8, 10, 12, 14, 16) are for the samples where partial desiccation was done.
- The eight panels with the grey background shading (i.e., panels 1, 4, 6, 7, 10, 11, 13, 16) are for the samples that were prepared and kept in microtubes; the other eight panels are for the samples in the microplates.

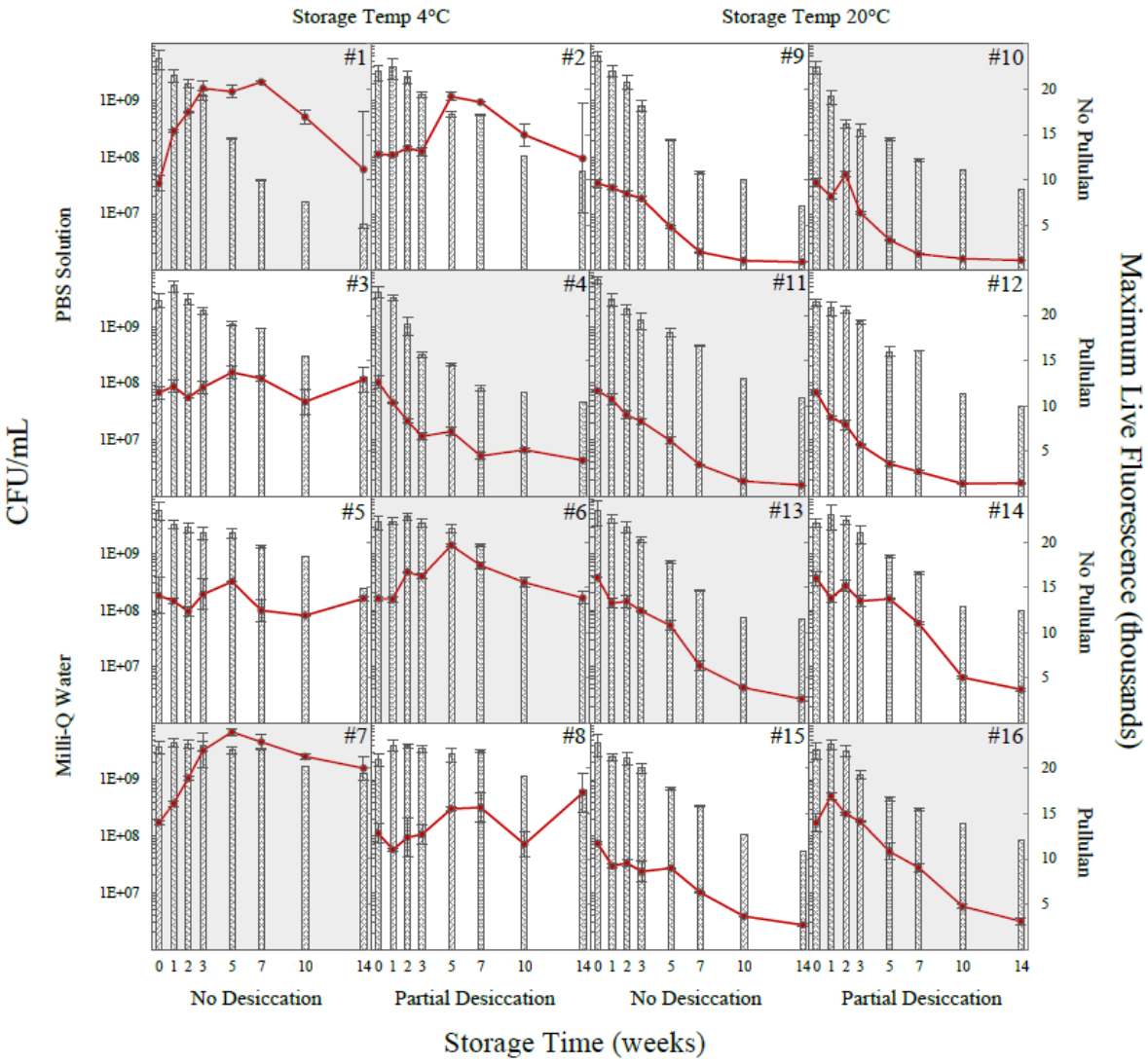

Figure 2-1. Comparison of all 16 preservation conditions from the 2^{5-1} DOE study in terms of the CFU/mL (primary axis with bar series plot) and Maximum Live Fluorescence (secondary axis with line series plot) across the eight timepoints of the 14-week storage period. The error bars for the CFU/mL data series and Maximum Live Fluorescence data series correspond to the standard deviation from the analysis of triplicate (three microtubes or microplate wells, each measured three times) and duplicate samples (two microtubes or microplate wells, each measured once) respectively. The exact condition for each panel is determined according to the following: the top and bottom halves are for samples prepared in PBS solution and Milli-Q water respectively; the left and right haves are for samples stored at 4 °C and 20 °C respectively; the second and fourth rows are for the samples prepared with pullulan; the second and fourth columns are for the samples where partial desiccation was done; the eight panels with the grey background shading are for the samples that were prepared in microtubes.

It is readily apparent that the preservation conditions had a significant effect on the CFU and MLF profiles. At the storage temperature of 20 °C (i.e., right half of the figure containing panels 9-16), both the CFU and MLF values continuously decreased with increasing storage time. **Figure A5** (Appendix A) shows that for all of these conditions, the CFU and MLF are positively correlated over a 14-week storage period. At the storage temperature of 4 °C (i.e., left half of the figure containing panels 1-8), it is hypothesized that the *E. coli* bacteria either remained intact, or entered 'viable-but-non-culturable' (VBNC) state in which cells are incapable of dividing, yet are still viable and responsive (Roszak and Colwell, 1987). This condition was of particular interest in our study where there were numerous instances where the MLF results remained constant or even increased over the 14-week test, but the CFU values declined; panel #1 is a good example of this observation. According to Oliver (2005), VBNC *E. coli* cells can be determined via acridine orange staining which probes cellular metabolic activity, or by *Bac*Light™ SYTO 9 and propidium iodide staining (which was used in our study) to probe for intact or disrupted cytoplasmic membranes. In **Figure 2-1**, for many of the conditions stored at 4 °C, the cytoplasmic membrane integrity of cells may have been preserved (evident in some cases by a horizontal MLF profile). Interestingly, in some cases, the MLF signal increased with increasing storage time (specifically panel 1, 7). It is our hypothesis that this phenomenon is due to a similar effect seen in eukaryotic microorganisms (e.g., yeast) where slower-growing cells subjected to external stresses (e.g., oxidative, temperature) lead to reduced fidelity of RNA polymerase (Van Dijk et al., 2015). This may be a reasonable comparison, since historically, *E. coli* have provided a model for transcription in eukaryotic organisms (Cooper, 2000). A reduced RNA polymerase fidelity

could result in more error prone RNA, which would potentially increase the quantity of non-coding RNA. This result could increase the binding capacity of nucleic acid bound SYTO 9 fluorophore, thereby increasing the overall live fluorescence signal. This phenomenon may also support the work done by Stevenson and Schmidt (1998) on *E. coli*, where slower-growing cells (controlled by changes in growth medium at 37 °C) contributed to an increase in RNA concentration by approximately 100%. In our study, for samples that were stored at 20 °C, it seemed that the cell's inability to maintain an intact cytoplasmic membrane structure, mitigated the effects of the slow-growing conditions necessary in increasing the overall RNA contents. Therefore, this result would allow propidium iodide to effectively displace the nucleic acid bound SYTO 9 fluorophore, resulting in a decreased MLF response.

Although this phenomenon offers an intriguing explanation, it may not explain the variation of MLF values between the different preservation conditions at the storage temperature of 4 °C. The MLF values for samples prepared in the microplate and stored at 4 °C (i.e., panels 2, 3, 5, 8) remained relatively constant over the entire 14-week test period and especially over the first three weeks. While for most of the conditions prepared in microtubes and stored at 4 °C (i.e., panels 1, 4, 6, 7), the MLF signals appeared to be amplified over the first three to five weeks in storage. This trend was not seen for preservation condition #4. A number of possible explanations exist. First, since the storage volume of the microtube (~1.7 mL) is over five-times larger than that of the microplate well (~300 mL), it is possible that the additional oxygen present in the microtube aided in higher cellular metabolic activity via aerobic respiration. Second, the presence of other compounds such as alcohols and organic acids could have been produced by *E. coli*, especially if the conditions

in the microtubes and/or microplate wells for anaerobic respiration were satisfied (Lacoursiere et al., 1986). Further studies are needed to precisely understand the effect of the storage vessel. It has been reported that the genes involved in respiration have a higher rate of expression in slower-growing isogenic cells (Van Dijk et al., 2015). Also, Riedel et al. (2013) showed that *E. coli* cells stored for 200 days at 24°C in a 5 × diluted LB solution experienced an increase in oxygen uptake rate in the post-death/long-term stationary phase (approximately 50 days after initial storage), where nutrients were considered limited. This potentially higher rate of oxygen uptake, and expression of genes involved in respiration, could promote an increase in RNA content and/or number of proteins, and therefore increase the MLF response. In order to test this hypothesis, we analyzed the intracellular RNA concentrations of extra samples from preservation conditions #1 and #10 after 28 weeks in storage at their respective conditions. As shown in **Table A1** in Appendix A, the MLF values were positively correlated with the measured concentration of intracellular RNA and the RNA/OD_{600} ratio.

The anomalies (dips and peaks) associated with the amplified signals occuring in the microplates could also be explained: in the cases where depressions did not form (poor film-to-plate seal), it was found that the culturability and MLF responses of the cells were significantly lower (results not shown). Therefore, since it was found that the depth of film depressions (thought to be caused by an uptake in oxygen by *E. coli*) appeared to have varied (see **Figure A4** in Appendix A), this could explain the variation in MLF responses from week to week.

2.4.2 Multiple linear regression model of cell preservation

In order to quantify the level of influence each factor and the interaction of factors had on MLF and culturability results, a multiple linear regression (MLR) analysis of the DOE results was conducted using R software (R Foundation for Statistical Computing). The quantitative measure was the ratio of CFU values from week 14 to week 0 (outputs of the DOE) – the results (MLR coefficient values) are shown as the Pareto plot in **Figure 2-2**. These values are calculated with the use of Yates' algorithm, and where the outputs of the DOE and the 'high' and 'low' values (+1 and -1, respectively) representing the factors are organized in matrix format (Spliid, 2002). The MLR factors on the x-axis act as variables in a multi-variable function and are added together. The y-axis depicts the MLR coefficient value (also the fraction of culturable cells remaining after 14 weeks) associated with each MLR factor with 'shading' of the bar (filled or empty) representing the sign of the coefficient value (positive (+) or negative (-), respectively). To determine the fraction of culturable cells for a particular condition, either a '+1' (denoted as high) or '-1' (denoted as low) will be substituted for each MLR factor. For example, if Milli-Q water was used, a '+1' will be substituted for x3, and if PBS was used, a '-1' will be substitued for x3. For multiple factor interactions (e.g., x1:x5), the individual factor values (+1 or -1) are multiplied together.

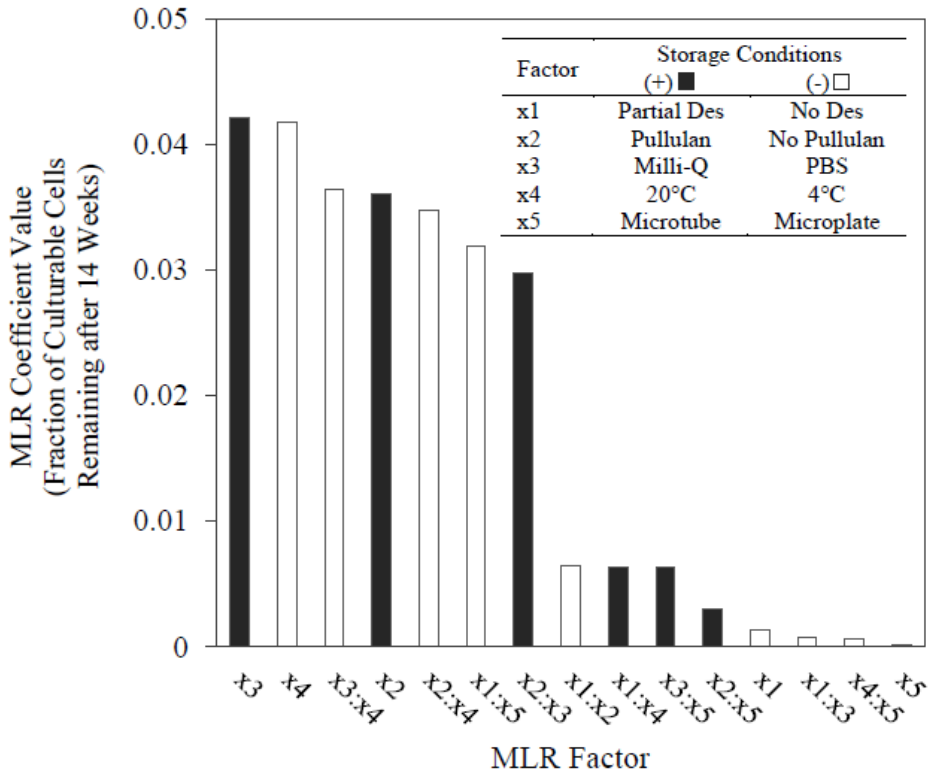

Figure 2-2. Pareto plot for the multiple linear regression (MLR) analysis of the CFU values from the DOE study in Figure 2-1. The fraction of culturable cells remaining after 14 weeks was determined from the ratio of CFU values at 14 weeks and 0 weeks. The y-axis values indicate the fractional increase or decrease in the fraction of culturable cells from the intercept value of 0.055 (average for all 16 conditions). The filled and empty bars represent positive (+) and negative (-) coefficients, respectively

The intercept value of 0.055 (not shown) corresponds to the average culturability as a fraction for all 16 preservation conditions. It was found that the solution condition (x3) and storage temperature (x4) had the highest impact of the five factors; the Milli-Q water and 4 ^{o}C storage temperature conditions were associated with a higher fraction of culturable cells. Thus, the MLR model predicts an increase in fraction of culturability by 0.042 (for both x3 and x4) after 14 weeks for *E. coli* cells that are either prepared in Milli-Q water solution or kept stored at 4 °C for 14 weeks. However, if both conditions are met (prepared in Milli-Q

water and stored at 4 °C), this does not simply equate to approximately 0.14 (0.055 + 0.042 + 0.042) since all coefficient factors must be accounted for in the calculation. These findings are in good agreement with those reported by Liao and Shollenberger where Milli-Q water and 4 °C improved culturability of a variety of Gram-negative bacterial cells (2003). Biopolymer (pullulan) addition (x2) also shows having a similar impact on culturability as solution condition (x3) and storage temperature (x4); the MLR model predicts an increase in fraction of culturability by 0.035 (the effect of pullulan is discussed in greater detail in the following section). On their own, the desiccation condition (x1) and storage unit (x5) were found to have no significant effect.

The impact of two-factor interactions on percent culturability was also investigated. In all cases, the most influential two-factor interactions were skewed heavily due to either the solution conditions (e.g. Milli-Q water) or storage temperature (e.g., 4 °C). Interestingly, the results in **Figure 2-2** show that the interaction factor between desiccation condition and storage unit (x1:x5) had a significant effect. However, the aliasing notations showed that this interaction was confounded with a three-factor interaction of biopolymer addition, solution conditions, and storage temperature (see the MLR Aliasing Notation section in Appendix A). These three conditions are associated with the two best performing preservation conditions after 14 weeks of storage in **Figure 2-1**: fraction of culturability of 0.333 (panel 7 in **Figure 2-1**) and 0.284 (panel 8 in **Figure 2-1**). Therefore, based on this finding, the interaction, x1:x5, was determined to be negligible. The next three best conditions, based on the highest fraction of culturability after 14 weeks, were 0.041 (panel 5 in **Figure 2-1**), 0.045 (panel 6 in **Figure 2-1**), and 0.044 (panel 3 in **Figure 2-1**). Compared to panels 7 and panel 8, these

values are approximately ten times lower and can be attributed to the absence of pullulan. This is a novel result, as many articles have been published which highlight the long term bacterial preservation efficacy of pullulan in a "fully" desiccated/dry state, however, to the best of our knowledge, improvements in preservation of bacteria in solution, rather than in dry form, have been under-reported.

A similar MLR analysis for the MLF results from **Figure 2-1** showed that storage temperature (x4) is the dominant factor in maintaining a high MLF level and therefore maintaining intact cytoplasmic membrane structure.

2.4.3 Additional culturability comparisons

A number of previous studies have demonstrated that the formation of fully dried pullulan tablets (sometimes referred to as pullulan pills) can be used to stabilize and preserve a wide range of enzymes (Jahanshahi-Anbuhi et al., 2014), phages (Leung et al., 2017), and bacteria (Sorokulova et al., 2015). The current working hypothesis is that the pullulan film hinders molecular motion and prevents the uptake of oxygen.[1] In some preliminary studies, we found that in the fully dried state there was a very low culturability of *E. coli* cells and also that it was quite difficult to redissolve the dried tablet. Given that the application of this work was to use a high number of cells for the detection of biocides in surrogate or actual wastewater samples, we concluded that a simpler approach would be to prepare a semi-homogeneous cell solution. But interestingly, as was previously discussed above, it was found that the addition of pullulan in solution had a positive effect on cell culturability.

In order to better highlight this effect, the CFU results for four preservation conditions (#5, #7, #10, and #12) are compared in **Figure 2-3**.

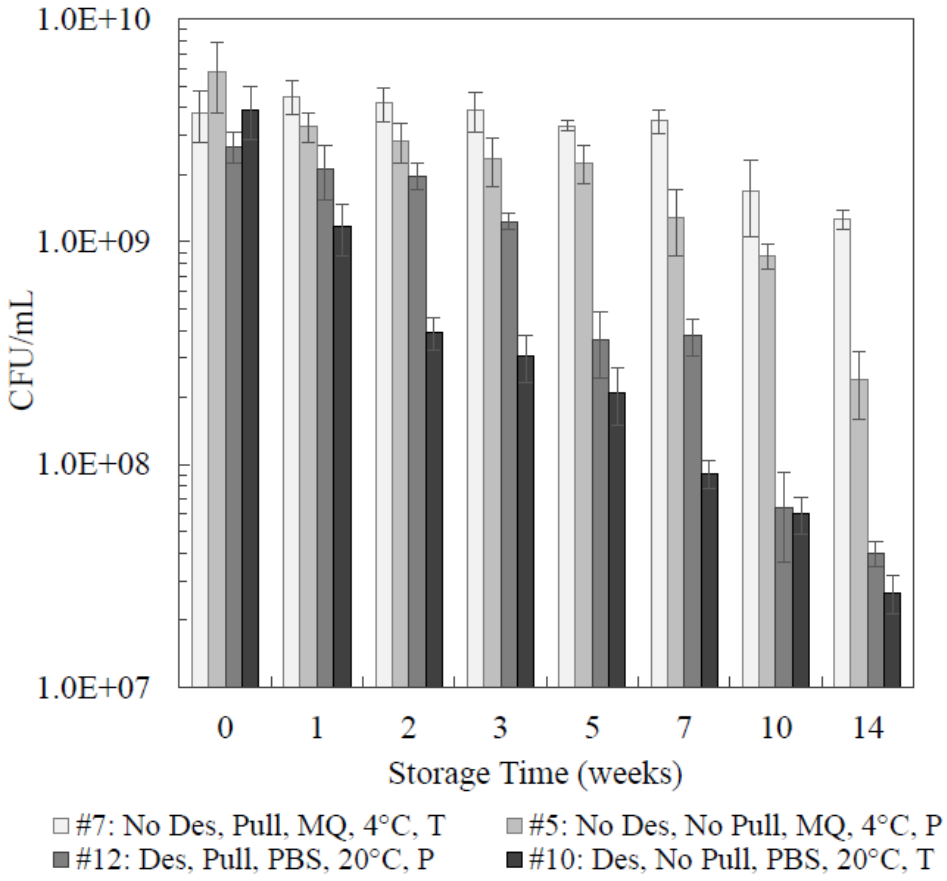

Figure 2-3. Comparison of a select number of preservation conditions from the 2^{5-1} DOE study in terms of the CFU/mL across the eight timepoints of the 14-week storage period – the same results were previously shown separately as panels 5, 7, 10, and 12 in Figure 2-1. Within the legend, 'Des' refers to partial desiccation, 'Pull' refers to pullulan, 'MQ' refers to Milli-Q water solution and 'T' and 'P' refer to microtube and microplate, respectively.

Note that these four conditions were chosen specifically as they contain two pairs for each factor in the DOE study. For example, the samples for conditions #5 and #7 were kept at the storage temperature of 4 °C while those for conditions #10 and #12 were kept at the storage temperature of 20 °C. Also, the samples for conditions #7 and #10 were prepared in microtubes (denoted as 'T') while those for conditions #5 and #12 were prepared in

microplates (denoted as 'P'). There was a slight variation in the CFU values for week 0 (between 2.5×10^9 and 6.5×10^9 CFU/mL) which is likely due to the inherent variation in the measurement technique. After one week in storage, there was already a noticeable decrease in the CFU values for the samples from condition #10 (partial desiccation, no pullulan, PBS solution, 20 ^oC storage temperature, microtube) and over the next 13 weeks the CFU values continued to decrease down to a final value of 2.7×10^7 CFU/mL or just 0.68% of the initial value for week 0. In comparison, for the samples from condition #7 (no desiccation, pullulan, Milli-Q water, 4 ^oC storage temperature, microtube) there was no significant change in CFU values over the first 7 weeks in storage; after 14 weeks, the CFU values decreased to approximately 33% of the initial value for week 0. We believe that there is a good opportunity to further optimize the preservation conditions and achieve an even higher culturability rate at these longer storage times by constructing another DOE focused around the conditions for those particular samples.

2.4.4 Optical density and growth curve analysis

The OD_{600} growth curves (at a temperature of 37 °C) over an 11 h incubation period at five different timepoints in the 14-week study (i.e., weeks 0, 2, 7, 10, and 14) are shown in **Figure 2-4** for the same four preservation conditions that were compared in **Figure 2-3**. **Figures A6, A7, A8**, and **A9** (in Appendix A) show growth curves for the other 12 preservation conditions.

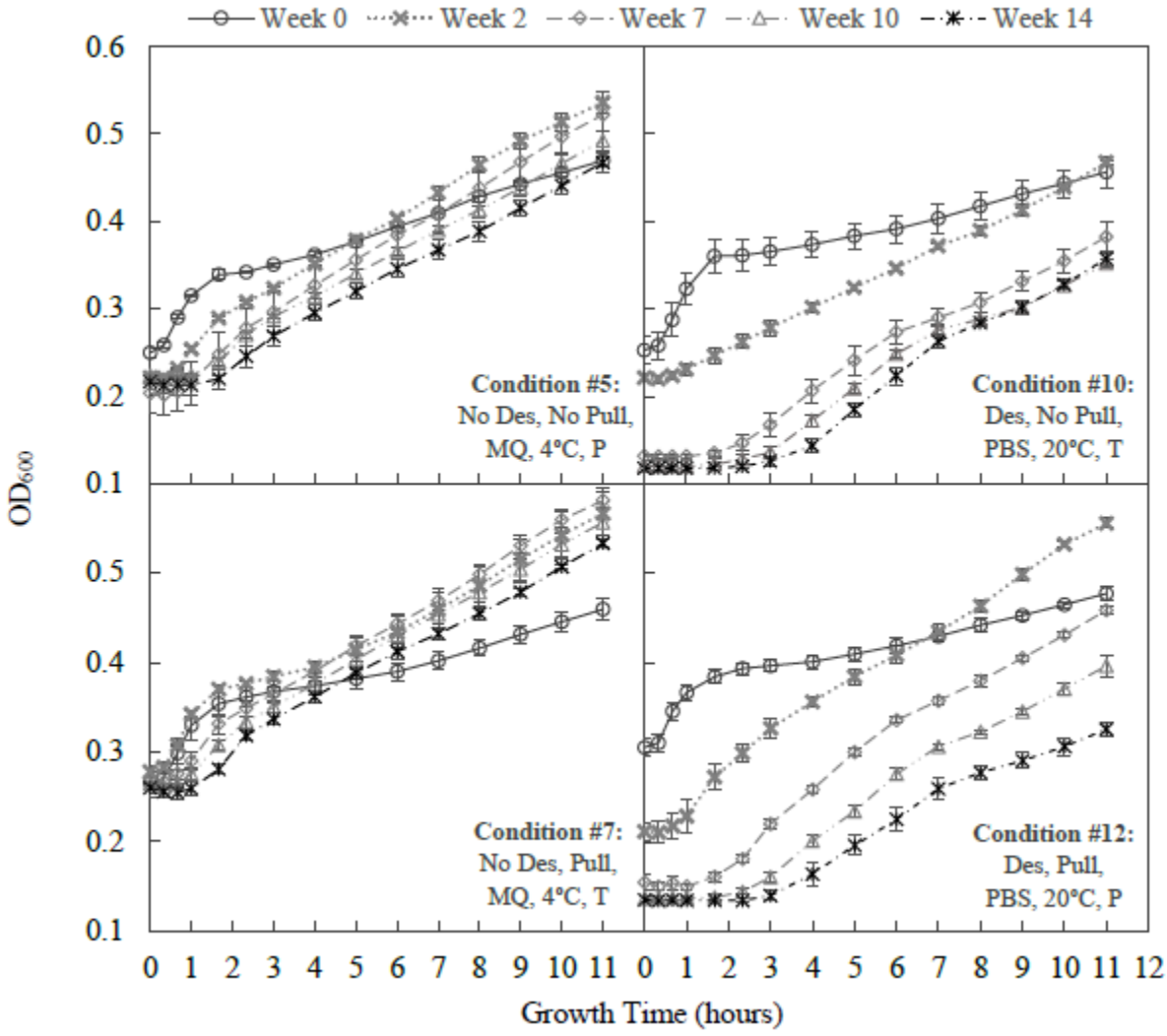

Figure 2-4. OD_{600} growth curves over an 11 h period at 37 °C for the four preservation conditions corresponding to panels 5, 7, 10, and 12 in Figure 2-1. The error bars correspond to the standard deviation from the analysis of triplicate samples (three microtubes or microplate wells, each measured one time). Refer to the caption in Figure 2-3 for a detailed explanation of the captions on each panel.

For the samples from conditions #10 and #12, in general there was good agreement between the initial OD_{600} values (i.e., $OD_{600,t=0}$) and the CFU results (analysis not shown) – both decreased with increasing storage time. There was also a noticeable increase in the lag phase

time of the OD_{600} growth curves. For example, for the samples from condition #12, the lag phase time increased from approximately 1 h in week 7 to approximately 2.5 h in week 14. For the samples from preservation conditions #5 and #7, there was no significant change in the $OD_{600,t=0}$ values with increasing storage time. This result supports the hypothesis that the cells that were stored at 4 °C remained intact throughout the 14-week storage period. For certain preservation conditions, it was interesting to find that there was no change in the $OD_{600,t=0}$ values at longer storage times but there was a noticeable increase in the lag phase time of the OD_{600} growth curves. A good example of this effect is shown in **Figure A6** (in Appendix A) for preservation condition #2. For those conditions in which the initial cell densities remained the same, the observed increase in the lag phase time is believed to be due to poor physiological adaptation of the cells to the new culture conditions (Maier and Pepper, 2015). This response could also be associated with the idea that some cells were considered VBNC. For conditions where initial cell densities decreased as a function of storage time, the increases in lag phase times could be a result of poor physiological adaptation, less VBNCs (instead the cells are lysed), as well as poor uptake and sharing of nutrients (Maier and Pepper, 2015).

2.4.5 Biocide exposure on preserved *E. coli* cells

As mentioned above, the effects of three different biocides (ProClin™ 300, CTAB, and Grotan® BK) on *E. coli* for all 16 preservation conditions were recorded at each of the eight timepoints over the 14-week test period. The MLF values are shown in **Figure 2-5** for the same four preservation conditions that were compared in **Figures 2-3** and **2-4**. **Figures A10, A11, A12,** and **A13** (in Appendix A) show the biocide exposure results for the other 12

preservation conditions. The results show that there was no significant difference between 300 ppm (9 ppm active ingredient) ProClin™ 300 and the Control (exposure to Milli-Q water) across all conditions; this result is in good agreement with the technical info provided by the supplier that active ingredient concentrations of 5 ppm and 25 ppm killed 0% and 10% of (unspecified) bacterial cells within 15 min, respectively.

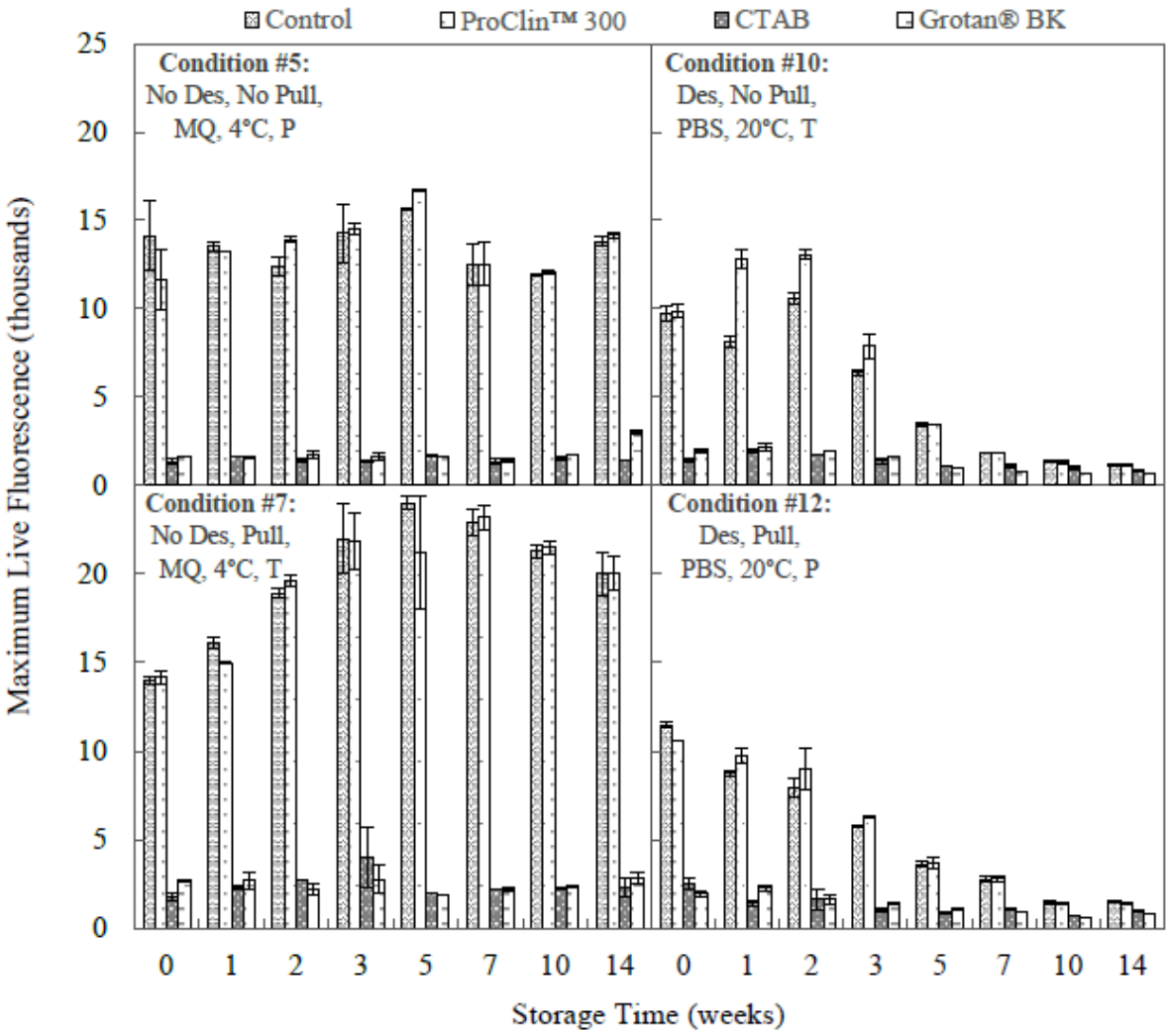

Figure 2-5. Comparison of the effect of biocide exposure on the Maximum Live Fluorescence values for the four preservation conditions corresponding to panels 5, 7, 10, and 12 in Figure 2-1. The different bars at each timepoint correspond to the samples that were exposed to the control (i.e., Milli-Q water) and ProClin™ 300, CTAB, and Grotan® BK samples with

concentrations of 300 ppm (9 ppm active ingredient), 20 ppm, and 1500 ppm, respectively. The error bars correspond to the standard deviation from the analysis of duplicate samples (two microtubes or microplate wells, each measured one time). Refer to the caption in Figure 2-3 for a detailed explanation of the captions on each panel.

For CTAB and Grotan® BK, both had a strong effect on *E. coli* and no significant difference was seen between them. Notably, the CTAB effect is also in good agreement with a previous study by Shanthy et al (2009), where 25 ppm was shown to be an optimum concentration for destroying *E. coli.* For conditions stored at 20 °C, the strong of effect of CTAB and Grotan® BK was mitigated by the poor cytoplasmic membrane integrity, compromised due to prolonged external stresses of long-term storage at this temperature. The results also show that conditions stored at 4 °C and in 96-well microplate wells, were capable of maintaining a relatively similar response to all three biocides over a 14-week storage period (e.g. condition #5 in **Figure 2-5**). Future work will include running additional biocide exposure tests to determine dose-response relationships for these three biocides and other commonly used biocides.

2.5 Conclusion

Based on our results, *DH5α E. coli* storage in microplates at 4 °C were capable of achieving relatively consistent maximum live fluorescence (MLF) responses for Control, CTAB, ProClin™ 300, and Grotan® BK biocides via *Bac*Light™ SYTO 9 and propidium iodide staining over a 14-week cell storage period. Maintaining intact cytoplasmic membrane integrity at 4 °C, and reducing oxygen availability by using lower volume microplate wells rather than higher volume microtube storage units may have played a crucial role in maintaining this consistency. This result was thought to be due to preserving intact cells or

possibly viable-but-non-culturable (VBNC) cells, and potentially due to an increase in intracellular RNA which lead to an increase in MLF response (increase uptake of fluorophore SYTO 9). This study also showed that pullulan played a valuable role in preserving long-term culturability. Although the temperature (4 °C) and storage solution (Milli-Q water) were the biggest contributors in maintaining high culturability over the first seven weeks of storage, pullulan was also shown to have a valuable impact after seven weeks, preventing almost a full order of magnitude drop in culturability after 14 weeks of storage. This study shows that there is a potential for developing a reliable biocide detection kit using *Bac*Light™ SYTO 9 and propidium iodide fluorophores, with a shelf-life of at least 14 weeks, and at a storage temperature of 4 °C using non-pathogenic *DH5α E. coli*.

2.6 References

Affatato, S., Bersaglia, G., Emiliani, D., Foltran, I., & Toni, A. (2004). Sodium-azide versus ProClin 300: influence on the morphology of UHMWPE particles generated in laboratory tests. *Biomaterials*, *25*(5), 835-842. doi.org/10.1016/S0142-9612(03)00603-3

Belkin, S. (2003). Microbial whole-cell sensing systems of environmental pollutants. *Current opinion in microbiology*, *6*(3), 206-212. doi.org/10.1016/S1369-5274(03)00059-6

Biran, I., Rissin, D. M., Ron, E. Z., & Walt, D. R. (2003). Optical imaging fiber-based live bacterial cell array biosensor. *Analytical biochemistry*, *315*(1), 106-113. doi.org/10.1016/S0003-2697(02)00700-5

Bye, C., Jones, R., & Dold, P. (2012). Pragmatic nitrification inhibition testing for robust plant design. *Proceedings of the Water Environment Federation,* 2012(12):4222-4238.

Cooper, G. M. (2000). Cell proliferation in development and differentiation. *The Cell: A Molecular Approach. 2nd edition. Sunderland (MA): Sinauer Associates*.

Girotti, S., Ferri, E. N., Fumo, M. G., & Maiolini, E. (2008). Monitoring of environmental pollutants by bioluminescent bacteria. *Analytica chimica acta*, *608*(1), 2-29. doi.org/10.1016/j.aca.2007.12.008

Helmi, K., David, F., Di Martino, P., Jaffrezic, M. P., & Ingrand, V. (2018). Assessment of flow cytometry for microbial water quality monitoring in cooling tower water and

oxidizing biocide treatment efficiency. *Journal of microbiological methods*. doi.org/10.1016/j.mimet.2018.06.009

Iacobellis, N. S., & DeVay, J. E. (1986). Long-term storage of plant-pathogenic bacteria in sterile distilled water. *Applied and environmental microbiology*, *52*(2), 388-389.

Jahanshahi-Anbuhi, S., Kannan, B., Leung, V., Pennings, K., Liu, M., Carrasquilla, C., ... & Filipe, C. D. (2016). Simple and ultrastable all-inclusive pullulan tablets for challenging bioassays. *Chemical Science*, *7*(3), 2342-2346. doi.org/10.1039/C5SC04184H

Jahanshahi-Anbuhi, S., Pennings, K., Leung, V., Liu, M., Carrasquilla, C., Kannan, B., ... & Filipe, C. D. (2014). Pullulan encapsulation of labile biomolecules to give stable bioassay tablets. *Angewandte Chemie International Edition*, *53*(24), 6155-6158. doi.org/10.1002/anie.201403222

Joubert, W. A., & Britz, T. J. (1987). A simple and inexpensive method for the long-term preservation of microbial cultures. *Journal of microbiological methods*, *7*(2-3), 73-76. doi.org/10.1016/0167-7012(87)90027-3

Kelman, A. (1956, January). Factors influencing viability and variation in cultures of *pseudomonas-solanacearum*. In *Phytopathology* (Vol. 46, No. 1, pp. 16-17). 3340 Pilot Knob Road, St Paul, MN 55121: Amer Phytopathological Soc.

Kim, T. H., & Kubica, G. P. (1972). Long-term preservation and storage of mycobacteria. *Applied microbiology*, *24*(3), 311-317.

Krumnow, A. A., Sorokulova, I. B., Olsen, E., Globa, L., Barbaree, J. M., & Vodyanoy, V. J. (2009). Preservation of bacteria in natural polymers. *Journal of microbiological methods*, *78*(2), 189-194. doi.org/10.1016/j.mimet.2009.05.017

Lacoursiere, A., Thompson, B. G., Kole, M. M., Ward, D., & Gerson, D. F. (1986). Effects of carbon dioxide concentration on anaerobic fermentations of Escherichia coli. *Applied microbiology and biotechnology*, *23*(5), 404-406.

Lei, Y., Mulchandani, P., Chen, W., & Mulchandani, A. (2007). Biosensor for direct determination of fenitrothion and EPN using recombinant Pseudomonas putida JS444 with surface-expressed organophosphorous hydrolase. 2. Modified carbon paste electrode. *Applied biochemistry and biotechnology*, *136*(3), 243-250. doi.org/10.1007/s12010-007-9023-9

Leung, V., Szewczyk, A., Chau, J., Hosseinidoust, Z., Groves, L., Hawsawi, H., ... & Filipe, C. D. (2017). Long-Term Preservation of Bacteriophage Antimicrobials Using Sugar Glasses. *ACS Biomaterials Science & Engineering*. doi.org/10.1021/acsbiomaterials.7b00468

Liao, C. H., & Shollenberger, L. M. (2003). Survivability and long-term preservation of bacteria in water and in phosphate-buffered saline. *Letters in applied microbiology*, *37*(1), 45-50. doi.org/10.1046/j.1472-765X.2003.01345.x

Maier, R. M., & Pepper, I. L. (2015). Bacterial growth. In *Environmental Microbiology (Third Edition)* (pp. 37-56). doi.org/10.1016/B978-0-12-394626-3.00003-X

Malaj, E., Peter, C., Grote, M., Kühne, R., Mondy, C. P., Usseglio-Polatera, P., ... & Schäfer, R. B. (2014). Organic chemicals jeopardize the health of freshwater ecosystems on the continental scale. *Proceedings of the National Academy of Sciences*, *111*(26), 9549-9554. doi.org/10.1073/pnas.1321082111

Massei, R., Busch, W., Wolschke, H., Schinkel, L., Bitsch, M., Schulze, T., ... & Brack, W. (2018). Screening of Pesticide and Biocide Patterns As Risk Drivers in Sediments of Major European River Mouths: Ubiquitous or River Basin-Specific Contamination? *Environmental science & technology*, *52*(4), 2251-2260. doi.org/10.1021/acs.est.7b04355

Morgan, C. A., Herman, N., White, P. A., & Vesey, G. (2006). Preservation of micro-organisms by drying; a review. *Journal of microbiological methods*, *66*(2), 183-193. doi.org/10.1016/j.mimet.2006.02.017

Oliver, J. D. (2005). The viable but nonculturable state in bacteria. *The Journal of Microbiology*, *43*(1), 93-100.

Pegg, D. E. (1976). Long-term preservation of cells and tissues: a review. *Journal of clinical pathology*, *29*(4), 271.

Philp, J. C., Balmand, S., Hajto, E., Bailey, M. J., Wiles, S., Whiteley, A. S., ... & Dunbar, S. A. (2003). Whole cell immobilised biosensors for toxicity assessment of a wastewater treatment plant treating phenolics-containing waste. *Analytica Chimica Acta*, *487*(1), 61-74. doi.org/10.1016/S0003-2670(03)00358-1

Riedel, T. E., Berelson, W. M., Nealson, K. H., & Finkel, S. E. (2013). Oxygen consumption rates of bacteria under nutrient-limited conditions. *Applied and environmental microbiology*, AEM-00756. doi.org/10.1128/AEM.00756-13

Rojas-Tapias, D., Ortiz-Vera, M., Rivera, D., Kloepper, J., & Bonilla, R. (2013). Evaluation of three methods for preservation of Azotobacter chroococcum and Azotobacter vinelandii. *Universitas Scientiarum*, *18*(2), 129-139. doi.org/10.11144/Javeriana.SC18-2.etmp

Ronan, E., Yeung, C. W., Hausner, M., & Wolfaardt, G. M. (2013). Interspecies interaction extends bacterial survival at solid–air interfaces. *Biofouling*, *29*(9), 1087-1096. doi.org/10.1080/08927014.2013.829820

Roszak, D. B., & Colwell, R. R. (1987). Survival strategies of bacteria in the natural environment. *Microbiological reviews*, *51*(3), 365.

Shanthy, P., Rengan, P., Chelvan, A. T., Rathika, K., & Rajendran, S. (2009). Corrosion inhibition and biocidal activity of a cationic surfactant.

Sherine, B. (2015). Biocidal Efficiency of Organic Inhibitor in Cooling Water Systems. *International Journal of Research and Development in Pharmacy and Life Sciences*, *4*(2), 1400-1406.

Sorokulova, I., Olsen, E., & Vodyanoy, V. (2015). Biopolymers for sample collection, protection, and preservation. *Applied microbiology and biotechnology*, *99*(13), 5397-5406. doi.org/10.1007/s00253-015-6681-3

Spliid, H. (2002). *Design and Analysis of Experiments with k Factors having p Levels*. Lyngby.

Stevenson, B. S., & Schmidt, T. M. (1998). Growth rate-dependent accumulation of RNA from plasmid-borne rRNA operons in Escherichia coli. *Journal of bacteriology*, *180*(7), 1970-1972.

Timur, S., Della Seta, L., Pazarlioğlu, N., Pilloton, R., & Telefoncu, A. (2004). Screen printed graphite biosensors based on bacterial cells. *Process Biochemistry*, *39*(11), 1325-1329. doi.org/10.1016/S0032-9592(03)00265-6

U.S. Army Corps of Engineers. (2012). Biocides for Industrial Use. glmris.anl.gov.

Urwin, C., Richardson, J. C., & Palmer, A. K. (1976). An evaluation of the mutagenicity of the cutting oil preservative Grotan BK. *Mutation Research/Genetic Toxicology*, *40*(1), 43-46. doi.org/10.1016/0165-1218(76)90021-5

Van Dijk, D., Dhar, R., Missarova, A. M., Espinar, L., Blevins, W. R., Lehner, B., & Carey, L. B. (2015). Slow-growing cells within isogenic populations have increased RNA polymerase error rates and DNA damage. *Nature communications*, *6*, 7972. doi.org/10.1038/ncomms8972

Wakimoto, S., Utatsu, I., Matsup, N., & Hayashi, N. (1982). Multiplication of Pseudomonas solanacearum in pure water. *Japanese Journal of Phytopathology*, *48*(5), 620-627. doi.org/10.3186/jjphytopath.48.620

Yan, D., Wang, Q., Li, Y., Ouyang, C., Guo, M., & Cao, A. (2017). Analysis of the inhibitory effects of chloropicrin fumigation on nitrification in various soil types. *Chemosphere*, *175*, 459-464. doi.org/10.1016/j.chemosphere.2017.02.075

3 Chapter 3: A Rapid Assay to Assess Nitrification Inhibition Using a Panel of Bacterial Strains and Partial Least Squares Modeling

In this chapter, experiments were performed by myself, post-doctoral fellow Mehdi Zolfaghari, and graduate student Salman Alizadeh Kordkandi. This chapter was drafted by myself and edited by Dr. Jake Nease who is knowledgeable in partial least squares modeling, and by my academic supervisors, Dr. David R. Latulippe and Dr. Carlos D.M Filipe. The chapter and its appendix are presented with permission from American Chemical Society © 2022.

A Rapid Assay to Assess Nitrification Inhibition Using a Panel of Bacterial Strains and Partial Least Squares Modeling

Patrick Morkus, Mehdi Zolfaghari, Salman Alizadeh Kordkandi, Jake Nease, Carlos D.M. Filipe, David R. Latulippe

Environmental science & technology 54, no. 1 (2019): 184-194
DOI: 10.1021/acs.est.9b04453

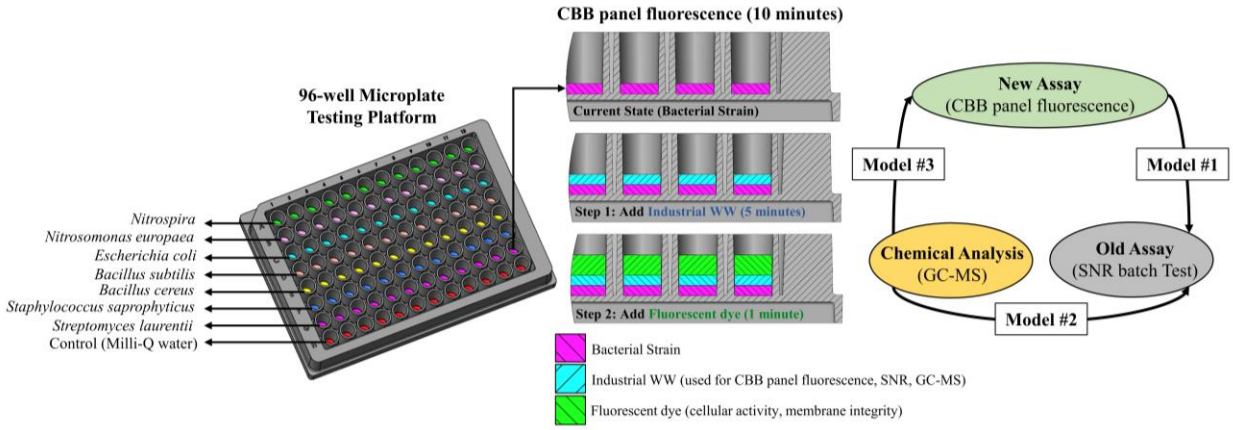

3.1 Abstract

As a proof of concept, a rapid assay consisting of a cell-based biosensor (CBB) panel of seven pure bacterial strains, a fluorescent dye, and partial least squares (PLS) modeling was developed to assess the nitrification inhibition potential of industrial wastewater (WW) samples. The current standard method used to assess the nitrification inhibition potential is the specific nitrification rate (SNR) batch test, which requires approximately 4 h to complete under the watch of an experienced operator. In this study, we exposed the CBB panel of seven bacterial strains (nitrifying and non-nitrifying) to 28 different industrial WW samples and then probed both the membrane integrity and cellular activity using a commercially available "live/dead" fluorescent dye. The CBB panel response ("fingerprint") acts as a surrogate measurement for the performance of nitrification. Of the seven strains, four (*Nitrospira*, *Escherichia coli*, *Bacillus subtilis*, *Bacillus cereus*) were identified via the modeling technique to be the most significant contributors for predicting the nitrification inhibition potential. The key outcome from this work is that the CBB panel fluorescence data (collected in approximately 10 min) can accurately predict the outcome of an SNR batch test (that takes 4 h) when performed with the same WW samples and has a strong potential to approximate the chemical composition of these WW samples using PLS modeling. Overall, this is a powerful technique that can be used for point-of-use detection of nitrification inhibition.

3.2 Introduction

Nitrification, the biologically mediated process of converting ammonia to nitrate, is widely used in municipal wastewater treatment plants (WWTPs) to meet strict ammonia effluent limits. Nitrifying microorganisms (i.e., nitrifiers), including *Nitrosomonas europaea* and *Nitrospira*, have been found in the activated sludge of WWTPs.[1-3] The rate of nitrification can be negatively affected by the presence of various chemical compounds in the influent to the municipal WWTP.[4] A variety of manufacturing plants from the food, automotive, pharmaceutical, metal working, and other industries use biocides (which include insecticides, fungicides, herbicides, acaricides) to enhance process performance by inhibiting microbial growth, inhibiting equipment corrosion, and other associated effects.[5-8] The wastewaters (WWs) generated by these industries are usually pretreated in industrial WWTPs prior to being directed to municipal WWTPs.[9] It is critical that an assessment of the potential effect of those incoming sources on the performance of the municipal WWTP is made; ideally this assessment should be (1) fairly simple to conduct, (2) fairly rapid in response, and (3) able to identify the source of the inhibitory chemical compounds. The current "gold-standard" method to assess nitrification inhibition is the specific nitrification rate (SNR) batch test.[10] This is a laborious method requiring frequent measurements of nitrate and nitrite concentrations, with and without the presence of potential nitrification inhibitors, over a few hours of operation. A rapid test to assess the toxicity of such WW sources would be beneficial to the operation of municipal WWTPs and could also be used for monitoring "point-of-use" of biocides at industrial/commercial facilities. Also, the SNR batch test gives no information about the source of the nitrification inhibition. Thus, additional

testing using sophisticated equipment, such as liquid chromatography-mass spectrometry (LC-MS) and/or gas chromatography-mass spectrometry (GC-MS), is used.[11] The complexity, time requirement, and large cost associated with this additional testing have created a space for innovating simpler methods/assays capable of assessing toxicity specifically with respect to nitrification inhibition.

Due to their relatively low-cost and rapid response kinetics, cell-based biosensors (CBBs) have gained significant attention for various applications in food, medical, environmental, and other industries.[12,13] In the environmental field specifically, the potential toxicity of various chemical compounds in water and soil samples has been determined using CBBs based on different microorganisms. For example, multi-bacterial toxicity assays such as MARA,[14] and LumiMARA,[15] which use absorbance and bioluminescence, respectively, have been used to assess the toxicity of environmental samples. However, these assays have not been used to assess nitrification. As another example, commercially available tests using bioluminescent *Vibrio fischeri* have been used to measure the toxicity of metals in environmental samples[16] and the concentration of biocides in paper mill process waters.[17] *Vibrio fischeri* has also been tested for its ability to predict the kinetics of nitrification with some success;[18] however, the long test time (approximately 1.5 h) and the inability to assess the source of inhibition are the major the limitations of this technique. This technique also does not consider the response of the nitrifying organisms which are responsible for nitrification. Nitrification inhibition assays based on pure cultures of *Nitrosomonas* and *Nitrobacter* were developed and tested on influent samples to municipal WWTPs[19] and

industrial WW samples.[20,21] However, these pure culture assays still required the same amount of incubation time (4 h) as a conventional activated sludge assay.

In order to solve the problem of developing a rapid assay of nitrification inhibition, we were inspired by the development of "soft sensor" technologies that have been used in various manufacturing industries to predict difficult-to-measure response variables using easy-to-measure process parameters.[22,23] For example, in the biotechnology industry, multiwavelength fluorescence spectra trajectories have been used to monitor cell densities, recombinant protein concentrations, and other time-consuming and/or difficult-to-measure components in mammalian cell cultures.[24] In another case, oxidation reduction potential and pH measurements were used to monitor for nitrogen and phosphorous removal in the biological treatment of municipal WW.[25]

In this study, we selected a diverse panel of seven bacterial strains (e.g., Gram-negative/Gram-positive, oval-shaped/rod-shaped, nitrifying): *Nitrospira*, *Nitrosomonas europaea*, *Escherichia coli*, *Bacillus subtilis*, *Bacillus cereus*, *Staphylococcus saprophyticus*, and *Streptomyces laurentii*. We used a fluorescent cell dye (SYTO 9, propidium iodide) to monitor for changes in membrane integrity and cellular activity upon exposure to a 'library' of industrial WW samples. This fluorescence cell dye is known for its ability to probe for intact and disrupted cytoplasmic membranes.[26-28] Also, because the dye binds to DNA and RNA,[29] it is hypothesized that this method would also probe for cellular activity (e.g., expression of genes upon exposure to stress).[30,31] Therefore, the combination of these two effects is anticipated to provide information about the interaction between each strain and the

chemical compounds present in a WW sample. Furthermore, because each strain (both nitrifying and non-nitrifying) behaves differently, combining the information from each strain allows for a greater understanding of the repercussions of the WW sample on bacteria that can be used as a surrogate measurement – in combination with a model – for the performance of various cellular functions (e.g., nitrification). The key advantage to this approach is that the CBB panel fluorescence data for all of the strains can be collected in approximately 10 min. In parallel to this work, we obtained SNR batch test and GC-MS data for the same "library" of WW samples. By combining these data/results (CBB panel fluorescence, SNR batch test, GC-MS) and partial least squares (PLS) modeling, we are able to predict the SNR outcome with a strong potential to approximate the chemical composition of the WW samples.

3.3 Materials and Methods

3.3.1 Preparation of Bacterial Strains

Seven bacterial strains were used in this study:

- *Nitrospira*, a Gram-negative and common aerobic chemolithoautotroph bacterium, was purchased from DSMZ (Braunschweig, Germany). *Nitrospira* has been commonly found in activated sludge (approximately 9% of total bacterial count) of WWTPs and is responsible for oxidizing nitrite to nitrate.[32] *Nitrospira* were grown at 28 °C over four weeks; it should be noted that the culturing conditions could be optimized to reduce the amount of time needed.[33] For the first two days, a Thermo MaxQ 8000 Shaker Incubator was used to shake the bacteria-media solution (see below) in a 100

mL Erlenmeyer flask set at 225 rpm to improve oxygen uptake; no shaking was done for the remainder of the four weeks. The media solution was made (as per DSMZ recommendations) by dissolving EDTA (1.4 mg/L), KH_2PO_4 (1.4 mg/L), $MgSO_4 \cdot 7H_2O$ (100 mg/L), $CaCl_2 \cdot 2H_2O$ (10 mg/L), $FeSO_4$ (5 mg/L), $NaNO_2$ (212 mg/L), K_2CO_3 (258 mg/L), $CuSO_4 \cdot 5H_2O$ (0.1 mg/L), $MnCl_2$ (1 mg/L), $ZnSO_4 \cdot 7H_2O$ (0.5 mg/L), and $Na_2MoO_4 \cdot H_2O$ (0.5 mg/L) in Milli-Q water. All the chemicals used were of analytical grade.

- *Nitrosomonas europaea*, a Gram-negative obligate chemolithoautotroph bacterium, was also purchased from DSMZ (Braunschweig, Germany). It has been found in activated sludge of WWTPs and operates under aerobic conditions oxidizing ammonia to nitrite.[3] *N. europaea* uses only ammonia as energy and only carbon dioxide as cellular carbon to function.[34] *N. europaea* were grown at 28 °C over four weeks (no shaking) in a 100 mL Erlenmeyer flask containing a media solution that was made (as per DSMZ recommendations) by dissolving Cresol red (1000 mg/L), KH_2PO_4 (54 mg/L), $MgSO_4 \cdot 7H_2O$ (49 mg/L), $CaCl_2 \cdot 2H_2O$ (147 mg/L), $FeSO_4$ (1 mg/L), NH_4Cl (535 mg/L), $NaHCO_3$ (1306.9 mg/L), NaCl (584 mg/L), and KCl (74 mg/L) in Milli-Q water. This solution was replenished once per week. All the chemicals used were of analytical grade.

- *Escherichia coli DH5α*, an abundant Gram-negative facultative anaerobic bacterium, was provided by the Biointerfaces Institute at McMaster University. It has been shown that the amount of *E. coli* can reach levels of approximately 10^3 to 10^5 cells per

gram of activated sludge.[35] *E. coli* were grown for 20 h in Lysogeny broth (LB) media (Sigma-Aldrich) in 14 mL polystyrene round-bottom Falcon tubes at 37 °C in a Thermo MaxQ 8000 Shaker Incubator set at 225 rpm.

- *Bacillus subtilis*, a Gram-positive aerobic bacterium that can grow in diverse environments, was provided by the Biointerfaces Institute at McMaster University. *B. subtilis* was included due to its role in bioflocculant production which is known to occur in activated sludge during the aeration process.[36] *B. subtilis* were grown for 20 h in LB media in 14 mL polystyrene round-bottom Falcon tubes at 26 °C in a Thermo MaxQ 8000 Shaker Incubator set at 225 rpm.

- *Bacillus cereus*, a Gram-positive aerobic and facultative anaerobic bacterium, was provided by the Agricultural Research Service Culture Collection (Peoria, IL). *B. cereus* is commonly found in a variety of environments and has been confirmed to exist in soils, water, food and activated sludge of WWTPs.[37] *B. cereus* were grown at the same conditions given for *B. subtilis*.

- *Staphylococcus saprophyticus,* a Gram-positive bacterium, was provided by the Biointerfaces Institute at McMaster University. *S. saprophyticus* belongs to the class *Staphylococci* which are commonly found in activated sludge of WWTPs.[38,39] In cases where biological aerobic treatment of saline wastewater is required, *Staphylococci* can act as a supplement in activated sludge to improve chemical oxygen demand (COD) removal rates.[40] *S. saprophyticus* were grown for 20 hours in Tryptic Soy Broth

media (Sigma Aldrich) in 14 mL polystyrene round-bottom Falcon tubes at 37 °C in a Thermo MaxQ 8000 Shaker Incubator set at 225 rpm.

- *Streptomyces laurentii*, a Gram-positive bacterium, was provided by the NRRL. *S. laurentii* can be typically found in soil and belongs to the class *Streptomyces* which are Gram-positive aerobic mycelial bacteria.[41] *Streptomyces* are also known to contribute to the removal of heavy metals, biological oxygen demand (BOD) and total suspended solids (TSS) from WW.[42] *S. laurentii* were grown for 20 h in Tryptic Soy Broth media (Sigma-Aldrich) in 14 mL polystyrene round-bottom Falcon tubes at 26 °C in a Thermo MaxQ 8000 Shaker Incubator set at 225 rpm.

The resulting bacteria-media solutions were transferred into 50 mL polystyrene Falcon tubes and then centrifuged at 8 °C and 4000 rpm for 16 min. The supernatant was replaced with an equal volume of phosphate buffered saline (PBS) solution (BioShop®) to make bacterial cell stocks**.** In order to confirm that the correct bacteria were received and successfully grown at the reported conditions, 10 µL aliquots of each cell stock was sent to the Mobix Lab at McMaster University for Sanger sequencing of the 16S rRNA gene. Each aliquot was prepared for sequencing according to the following three step sequence: boiling at 95 °C for 15 minutes; PCR amplification using 8f (5'-AGAGTTTGATCCTGGCTCAG-3') and 926r (5'-CCGTCAATTCCTTTRAGTTT-3') primers; column purification using the PureLink™ PCR Purification kit (Invitrogen). The strains were identified using BLAST search software, and all achieved a 99% identity to that which was expected.

3.3.2 Fluorescence Assay: CBB Panel Exposure to Wastewater

Twenty-eight WW samples were obtained from an industrial WWTP that receives WW derived from over 100 different clients from a variety of chemical, food, automotive, and other industries and discharges the treated WW at varying volumes (approximately 200000−500000 L per day) to a local municipal WWTP. The samples used in this study were treated physicochemically (e.g., flocculation-coagulation, hydrogen peroxide with aeration, sand filtration, adsorption via clay or activated carbon) at the industrial WWTP. The samples were collected over a period of approximately two months to help ensure diversity in the samples. Before testing, each WW sample was first centrifuged at 4000 rpm for 16 min to remove any suspended solid material.

Duplicate 50 µL aliquots of the supernatant from each WW sample were transferred into individual wells of a 96-well flat bottom black microplate (Eppendorf); duplicate 50 µL aliquots of Milli-Q water were also added to separate wells of the microplate as negative controls. An 8-channel pipet was used to add 50 µL of each bacterial cell stock into each well being tested. After 5 min, 100 µL of the LIVE/DEAD BacLight dye solution (prepared according to the manufacturer's instructions for the L7007 Bacterial Viability Kit) was added to each well using an 8- channel pipet; this step was completed in less than 1 min. The fluorescence signals of the contents within the 96-well microplate were determined using an Infinite M200 Pro multimode microplate reader (Tecan) at the following settings: shaking frequency of 2 min, shaking time of 30 s, default gain of 60, excitation wavelength of 485 nm, emission wavelength of 530 nm. The reported fluorescence signals for a given combination

of bacteria and WW were obtained by subtracting the "background" corresponding to the fluorescence signal from those wells containing only the WW and dye solution (i.e., no bacteria).

The fluorescence signals for each bacterial strain exposed to Milli-Q water (control) were 2900 ± 50, 2300 ± 25, 6100 ± 50, 19000 ± 500, 8800 ± 400, 4700 ± 50, and 24000 ± 100 relative fluorescence units (RFU) for *Nitrospira*, *Nitrosomonas europaea*, *Escherichia coli*, *Bacillus subtilis*, *Bacillus cereus*, *Staphylococcus saprophyticus*, and *Streptomyces laurentii*, respectively (**Figure B1** Appendix B). The differences in fluorescence readings were due to the differences in bacterial concentrations from strain to strain which was a result of implementing a convenient 20-h growth period for all strains (except for Nitrospira and N. europaea which was 4 weeks) regardless of their varying growth mediums and growth temperatures.43 In our preliminary testing (results not shown), we found that it was difficult to differentiate fluorescence signals of the same bacterial strain when exposed to different WW samples if a low control fluorescence signal (<1000) was used.

3.3.3 SNR Batch Test Assay

The SNR batch test assay used in this study was adapted from Bye et al.[10] As shown in **Figure B2** (Appendix B), eight 100 mL Erlenmeyer flasks were used to simultaneously test eight samples (typically seven WW samples and one Milli-Q water control). The following components were added to each flask:

- An 85 mL aliquot of return activated sludge (RAS) from the Dundas Valley WWTP in Dundas, Ontario. The as-received RAS was concentrated via a simple batch

centrifugation process to achieve a volatile suspended solids (VSS) value, as per the standard Method 1684,[44] in the range of 4400-5400 mg/L, which is typical in WWTPs.[45,46]

- A 10 mL aliquot of a synthetic mineral medium solution made in Milli-Q water (as per Seyhi et al.[47]) with the following chemicals (all of analytical grade) at the given concentrations: KH_2PO_4 (355 mg/L), $MgSO_4 \cdot 7H_2O$ (203 mg/L), $CaCl_2 \cdot 2H_2O$ (366 mg/L), $FeCl_3$ (15 mg/L), NH_4Cl (1920 mg/L), $NaHCO_3$ (421 mg/L), $CuSO_4 \cdot 5H_2O$ (0.4 mg/L), $MnSO_4 \cdot 4H_2O$ (0.4 mg/L), $ZnSO_4 \cdot 7H_2O$ (0.4 mg/L) and $Na_2MoO_4 \cdot H_2O$ (0.25 mg/L).
- A 5 mL aliquot of CH_3COONa solution (2970 mg/L in Milli-Q water) was used as a source of COD.

To start the SNR batch test, a 0.6 mL aliquot of the WW sample (or Milli-Q water for the control) was added to the mixture of components in each flask and then the air supply was immediately turned on; as shown in **Figure B2** (Appendix B), a custom-made manifold was used to deliver the air from a single supply to all eight flasks. The amount of dissolved oxygen within each flask was continuously monitored using a YSI 5000 dissolved oxygen meter to be in the range of 8 to 9 mg/L. The solution pH was continuously monitored via a VWR Benchtop pH meter and adjusted via the addition of 0.1 N H2SO4 solution (Sigma-Aldrich) to be in the pH range of 7 to 8; the maximum amount of acid added to any flask was 4 mL. A 1 mL sample was taken from each flask at three different time points (20, 45, and 75 min) after the air supply was turned on. Each sample was first centrifuged at 2000 rpm for

5 min, and then the nitrite-N and nitrate-N concentrations of the resulting supernatant were determined using a Nitrite TNTplus Vial Test HR kit (HACH), a NitraVer X Nitrogen-Nitrate Reagent Set HR kit (HACH), and a DR- 2800 spectrophotometer (HACH).

The SNR for each sample was determined from the slope of NO_x-N (total concentration (in mg/L) of nitrite-N and nitrate-N) versus time divided by the initial concentration (g/L) of VSS. According to Raboni et al.[48], the measured SNR values were normalized to 20 °C using:

$$\mathrm{SNR}_{20\,^{\circ}\mathrm{C}} = \frac{\mathrm{SNR}_{\mathrm{T}}}{1.07^{\mathrm{T}-20}} \qquad (1)$$

where T is the average temperature (in °C) that was measured using a standard glass thermometer throughout the 75 min test. The % SNR Difference was then calculated using:

$$\%\ \mathrm{SNR\ difference} = \frac{\mathrm{SNR}_{20\,^{\circ}\mathrm{C}}(\mathrm{sample}) - \mathrm{SNR}_{20\,^{\circ}\mathrm{C}}(\mathrm{control})}{\mathrm{Average}\ (\mathrm{SNR}_{20\,^{\circ}\mathrm{C}}(\mathrm{sample}), \mathrm{SNR}_{20\,^{\circ}\mathrm{C}}(\mathrm{control}))} \qquad (2)$$

From this, a % SNR difference of less than zero implies nitrification was not inhibited while a % SNR difference of greater than zero implies nitrification was inhibited. The acceptable level of nitrification inhibition will vary depending on the discharge limits of different jurisdictions.[49]

3.3.4 Gas Chromatography Mass Spectrometry (GC-MS) Analysis

A 100 mL aliquot of each industrial WW sample was pH-adjusted to 2.0 ± 0.2 via the addition of 1 N HCl solution (LabChem); this mixture was then combined with 100 mL of dichloromethane (DCM) (Caledon) in a separatory funnel, manually shaken for 1 min, then

allowed to rest for 5 min in order to partition into two separate phases. Approximately 100 mL of the bottom DCM rich phase was extracted from the separatory funnel and then dehydrated by pouring it through approximately 5 g of anhydrous sodium sulfate (Anachemia) on top of a 30 μm Whatman filter paper in a glass funnel. The dehydrated and filtered sample was then concentrated to 2 mL using a rotary vacuum evaporator operated at 37 °C. A 25 μL aliquot from the concentrated 2 mL sample was combined with 25 μL of N-methyl-N-trimethylsilyl-trifluoroacetamide (MSTFA) (Sigma-Aldrich) containing 1% trimethylchlorosilane (Fluka) and 5 μL of 9-anthracenemethanol (Sigma- Aldrich) in a 2 mL Clear Robo vial; 9-anthracenemethanol was included as an "internal standard" for the GC-MS analysis. This mixture was then placed in a 60 °C oven for 1 h.

The GC- MS analysis was performed using a 6890N gas chromatograph (Agilent) equipped with a DB-17ht column (30 m × 0.25 mm ID × 0.15 μm film, J & W Scientific) with a retention gap (deactivated fused silica, 5 m × 0.53 mm ID) and a 5973 MSD single quadruple mass spectrometer (Agilent). A 1 μL aliquot of the sample was injected into the chromatograph using a 7683 autosampler (Agilent) in splitless mode. The injector temperature was 250 °C, and the carrier gas (helium) flow rate was 1.1 mL/min. The transfer line temperature was 280 °C, and the MS source temperature was 230 °C. The column temperature was initially set at 50 °C which was then increased to 300 °C via an 8 °C/min ramp and held at 300 °C for 15 min for a total run time of 46.25 min. A full scan mass spectra between a mass-to-charge ratio of 50 and 800 was acquired; the multichannel ion detector

was turned off during the 0−2.5 and 2.8−3.9 min marks for toluene (solvent used as the stationary phase when the injection mode is splitless) and MSTFA, respectively

3.3.5 Partial Least Squares (PLS) Modeling

The PLS modeling was conducted using Aspen ProMV software (AspenTech) which uses the nonlinear iterative partial least- squares (NIPALS) algorithm.[50] For a detailed review of the mathematics and standard notation of PLS modeling, the reader is referred to the earlier work by Hö̈skuldsson.[51] Three separate PLS models were developed in this study:

1. CBB to SNR: this is the main model (i.e., "soft sensor") that was used to predict the % SNR difference based on the fluorescence signal of the CBB panel. The model input (X-space) contains the bacterial strains as variables (columns) and WW samples as observations (rows). The fluorescence signal for each bacterial strain and for each WW sample fills the X-space. The model output (Y- space) contains the % SNR difference as the only variable (column) and the same WW samples as observations (rows). Weight matrices, which define the orientation of the principal components, were labeled as 'W' for the CBB X-space and 'c' for the SNR Y-space; see **Figure B3** (Appendix B) for a schematic representation.
2. GC-MS to SNR: this model was used to determine which of the chemical compounds in the WW samples (**Table B2** Appendix B) contributed to nitrification inhibition. The model input (X-space) contains the chemical compounds as variables (columns) and WW samples as observations (rows). Standardized GC-MS peak area values fill the X-space; the integral area for each peak (i.e., chemical compound) was divided by the

integral area of the internal standard (see **Table B2**). The model output (Y- space) contains the % SNR difference as the only variable (column) and the same WW samples as observations (rows). Weight matrices which define the orientation of the principal components were labeled as 'W' for the GC- MS X-space and 'c' for the SNR Y-space; see **Figure B4** (Appendix B) for a schematic representation.

3. GC-MS to CBB: this model was used to determine which of the chemical compounds in the WW samples (**Table B2** Appendix B) contributed to a change in the fluorescence signals for two (*Nitrospira*, *Escherichia coli*) of the seven bacterial strains. The model input (X-space) contains the chemical compounds as variables (columns) and WW samples as observations (rows). Standardized GC-MS peak area values fill the X-space; the integral area for each peak (i.e., chemical compound) was divided by the integral area of the internal standard. The model output (Y-space) contains the two bacterial strains mentioned above as the variables (columns) and the same WW samples as observations (rows). Weight matrices which define the orientation of the principal components were labeled as 'W' for the GC-MS X-space and 'c' for the CBB subset Y- space; see **Figure B5** in Appendix B for a schematic representation

3.4 Results and Discussion

3.4.1 CBB Panel Fluorescence and SNR Batch Tests

The results collected from the CBB panel and SNR batch test for one of the industrial WW samples (WW #4) are shown in **Figure 3-1**. The fluorescence signals from the CBB panel corresponding to a unique "fingerprint" of the tested industrial WW are shown in the panel

on the left. A microplate reader was used to record the fluorescence signals over a 15 min reading period (as per the instructions provided by the manufacturer of the dye); however, it was found that only the initial fluorescence signal, which was retrieved 1 min after the addition of dye, was necessary to achieve a strong correlation to the SNR batch test (see section 3.4.2 for modeling result). Only the initial fluorescence signal was needed since the fluorescence signal was stable over the 15 min reading period (**Figure B6** in Appendix B); bacteria can adapt to stressful environment within minutes.[52] On the basis of modeling performance, it was found that there was no advantage to using the fluorescence signals over a 15 min period (results not shown). This outcome was convenient, as it reduced the complexity and the amount of time needed to test a WW sample. The results in the panel on the left in **Figure 3-1** show that after only 5 min of exposure to the WW sample and 1 min after the addition of the fluorescent dye, the change in fluorescence signal for the bacterial strains are markedly different after exposure to the same WW sample. For example, the fluorescence signal of *Nitrosomonas europaea* and *Escherichia coli* increased by 86% and 27%, respectively, while the fluoresence signal of *Bacillus subtilis* and *Streptomyces laurentii* decreased by 14% and 19%, respectively, relative to the control sample. It is assumed that the observed differences in the fluorescence signals are due to many factors including the bacterial strain type, structure (Gram-negative vs Gram-positive), and the chemical composition of the WW sample (see section 3.4.2 for a more detailed discussion).

The change in concentration of NO_x-N (nitrate-N and nitrite- N) during the SNR batch test is shown in the panel on the right. The % SNR difference was calculated from the NO_x-N production rate (slope), VSS measurement (4370 mg/L), and average temperature via

Equations 1 and 2. A linear regression analysis was used to capture the NO_x-N production rate since the expected change in the autotrophic bacterial population is negligible over the amount of time (75 min) required to run the test.[10] The % SNR difference for this WW sample was calculated to be +6.35, relative to the control, and thus is designated as a "fail" sample. The same sequence of testing was done for all of the other 27 industrial WW samples; those results are shown in **Table B1** (Appendix B). Of the 28 WW samples collected, 11 were designated as "pass" samples and 17 were designated as "fail" samples. Note that due to the high cost of reagents, only one SNR batch test was made for the majority of the WW samples. We are quite confident in the test reliability as a duplicate analysis of WW sample #2 gave values of +2.66 and +5.20 and a duplicate analysis of WW sample #18 gave values of +22.30 and +29.71.

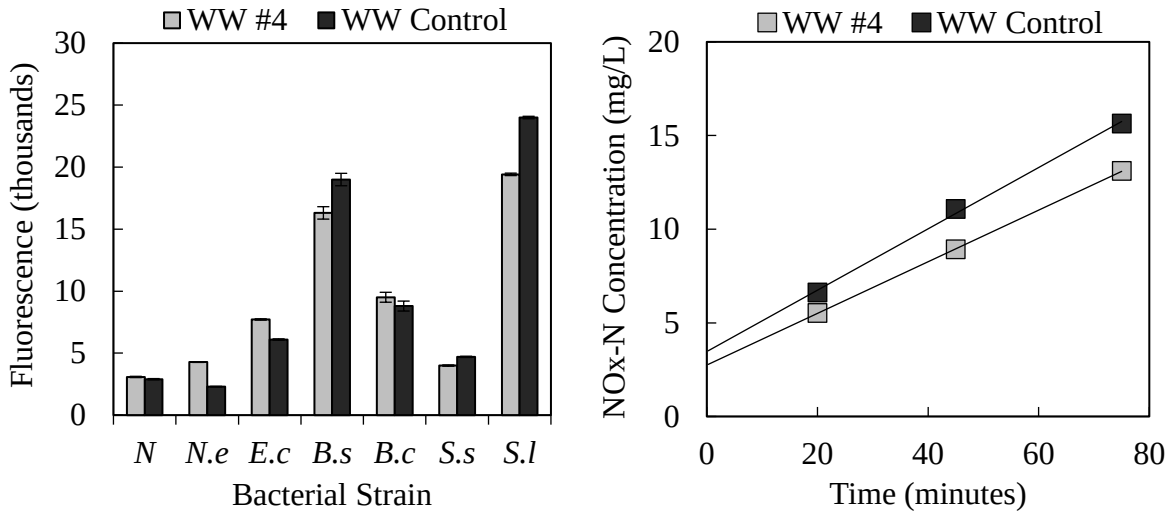

Figure 3-1. Left panel: Fluorescence data from CBB panel for industrial WW sample #4 (gray bars) and Milli-Q water control (black bars). The fluorescence signals show the initial fluorescence (1 min after dye addition) for each of the seven bacterial strains: *Nitrospira* (*N*), *Nitrosomonas europaea* (*N.e*), *Escherchia coli* (*E.c*), *Bacillus subtilis* (*B.s*), *Bacillus cereus* (*B.c*), *Staphylococcus saprophyticus* (*S.s*) and *Streptomyces laurentii* (*S.l*). Right panel: SNR batch test results for industrial WW sample #4 (gray square symbols) and Milli-Q water control

(black square symbols). The best-fit value of the slope corresponding to the NO_x-N (nitrate-N and nitrite-N) production rate was 0.1379 for WW sample #4 and 0.1638 for the control. The % SNR difference calculated for WW #4 was +6.35 and thus for this study is considered a 'fail' sample.

3.4.2 Prediction of the SNR outcome using the CBB panel fluorescence data and PLS modeling

In order to develop an appropriate model that can use the CBB panel fluorescence data to predict the % SNR difference of an industrial WW sample, all of the results shown in **Table B1** (Appendix B) were modeled using PLS. After modeling (setup shown in **Figure B3** of Appendix B), it was determined that WW samples #3 and #17 had relatively large squared residuals (165 and 554, respectively) compared to the average (21 ± 26) and therefore were excluded. The effect of using between one and five principal components in the PLS model is shown in **Table 3-1**. When three principal components were used, which means the first three principal components (1, 2, and 3) are used in the model, the R^2 value was 0.84.

Table 3-1. R^2 and Q^2 values for different numbers of principal components (1 to 5) in the CBB to SNR PLS Model for 26 industrial WW samples. Note that WW samples #3 and #17 were excluded from the model due to the large squared residuals (outliers).

Number of principal components used	R^2	Q^2
1	0.69	0.12
2	0.80	0.65
3	0.84	0.75
4	0.86	0.78
5	0.86	0.79

According to Chin,[53] an R^2 value of 0.67 or greater substantially explains model variance. In order to capture the predictive ability of the model, Q^2 is reported.[54] When three principal

components were used, the Q^2 was 0.75. This value is different than the R^2 value because the model uses a subset of the data (6/7ths) as the training set to predict the remaining subset (1/7th) of the data; Q^2 is calculated the same way as R^2 but with both subsets combined.[53] In this way, Q^2 is an indicator of how well the model can predict the % SNR difference of new WW samples from just the CBB panel fluorescence data. To prevent overfitting, three principal components were used in this model as there was only a small increase in both the R^2 (+0.02) and the Q^2 (+0.03) when the fourth principal component was used. In the context of our application, achieving a Q^2 of 0.75 is acceptable as there is significant value in determining whether or not nitrification inhibition is occurring; simply, a "pass" or "fail" determination is the most important. According to the literature, a Q^2 greater than zero indicates that a model has "predictive relevance".[55] However, the degree of predictive relevance seems to be subjective and application dependent. For example, according to the User Guide to SIMCA[56] and Heneseler et al.,[57] a "large" degree of predictive relevance is characterized by a Q^2 greater than 0.5 and 0.35, respectively. In biological applications of PLS modeling involving metabolite analyses for diagnostic applications, Q^2 values of 0.48 and 0.22 are deemed acceptable.[58,59] Those studies are relevant to this work since we are also investigating the impacts of metabolites/analytes (chemical compounds in WW samples) on bacteria that can be measured using fluorescence.

The effectiveness of using the CBB panel fluorescence data and PLS modeling to predict the % SNR difference is shown in **Figure 3-2**.

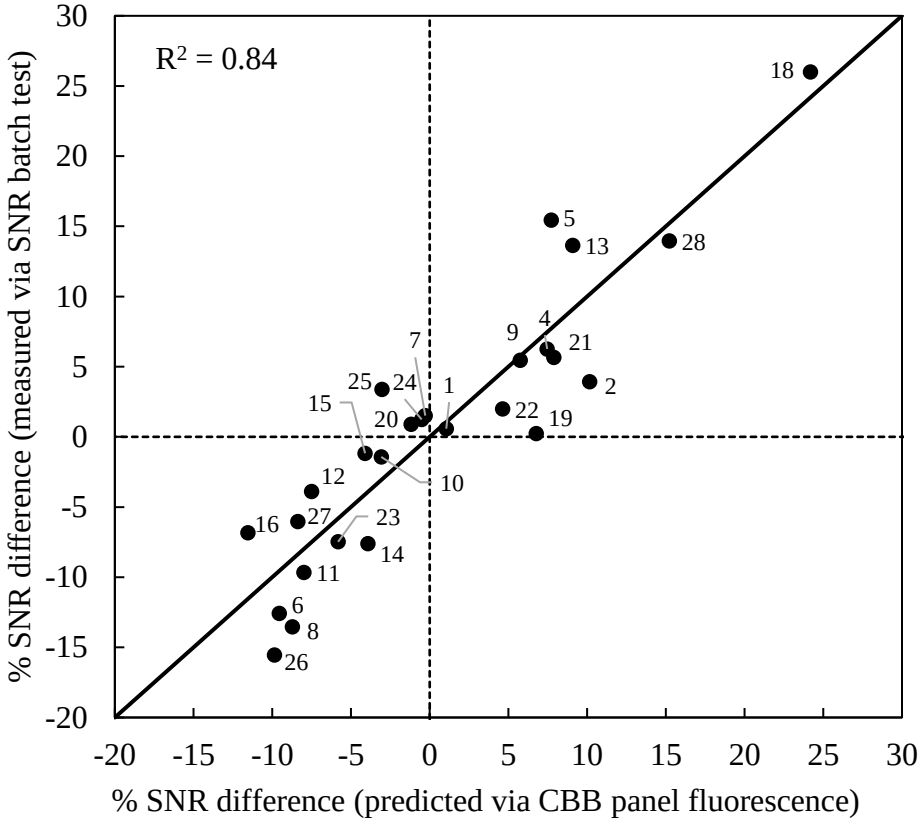

Figure 3-2. Comparison of the predicted % SNR difference values (from CBB panel fluorescence values) and the measured % SNR difference values (from SNR batch test) using PLS modeling and three principal components for 26 industrial WW samples. The solid diagonal line is included to indicate the perfect agreement between the two values. The Q^2 value (0.75) is close to the R^2 value (0.84) and therefore a testing set is not depicted (i.e., the testing data would look similar to the training data).

The WW samples are closely aligned to the solid diagonal line (i.e., perfect agreement between the measured and predicted values). This means that the fluorescence signals from the CBB panel that were obtained in approximately 10 min can be used to predict the outcome of the SNR batch test, which takes approximately 4 h to complete. So as to pragmatically and easily allow for a 10 min test time of the CBB panel without the need for constantly culturing the strains, it is anticipated that future developments of this technology

will involve preservation (e.g., using sugar films) of the strains which has been well documented in the literature.[60,61] As previously mentioned, it is of utmost importance to determine whether a sample is a "pass" or "fail", and therefore, the precise prediction of the % SNR difference may not be necessary. However, as the measured % SNR difference approaches the "pass-fail" criteria (which for this study was chosen to be zero), it becomes increasingly more difficult to predict. For example, WW samples #7, #20, #24, #25 are the only WW samples (of 26 samples) that were incorrectly predicted as "pass" samples; the measured % SNR difference values for these samples are +1.51, + 1.24, + 0.90, and +3.38, respectively, and the predicted % SNR difference values for these samples are −0.28, −0.51, −1.18, and −3.02, respectively. To better predict the values, specifically those that are close to the "pass-fail" criteria, more WW samples (preferably of varying compositions) should be collected and the results added to the model to further improve its predictive ability.

To gain insight into how the CBB panel fluorescence data predicts the % SNR difference, a T-score plot was generated and analyzed. The scores of the first and second principal component (the principal components which best explain variance in the training data) for each WW sample are displayed in **Figure 3-3**.

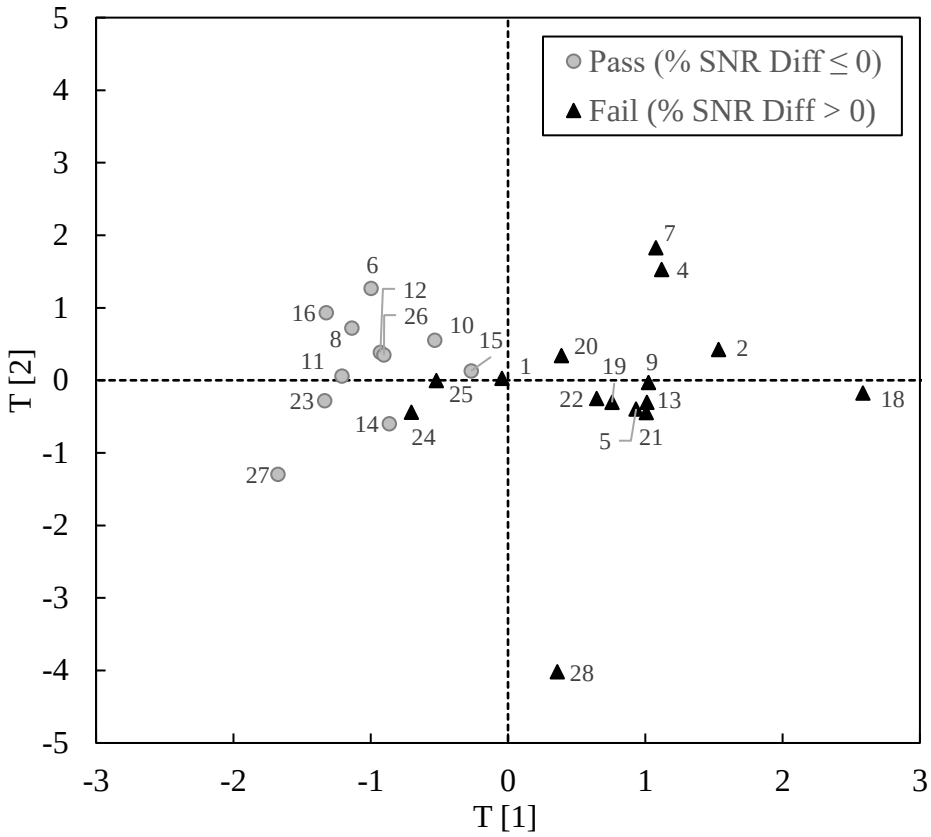

Figure 3-3. First and second principal component T-score plot for the X space of the CBB to SNR PLS model for 26 industrial WW samples. The grayed circle symbols represent the 11 WW samples with a "pass" rating (#6, #8, #10, #11, #12, #14, #15, #16, #23, #26, #27). The filled triangle symbols represent the 15 WW samples with a "fail" rating (#1, #2, #4, #5, #7, #9, #13, #18, #19, #20, #21, #22, #24, #25, #28).

By reducing the dimensionality to two (first and second score) using PLS modeling, the difference between "pass" and "fail" WW samples is evident. **Figure 3-3** shows that the "pass" WW samples tend to cluster together on the left side of the plot, while the "fail" WW samples tend to be distributed in various mid-to-right and lower-right regions of plot. This distribution can be attributed to the broad differences in effects of varying chemical compounds on each bacterial strain. By analyzing each cluster ("pass", "fail") with a

contribution plot, we can understand the behavior based on the fluorescence signal of each bacterial strain when exposed to a "pass" or "fail" WW sample.

The contribution plot for the PLS model is shown in **Figure 3-4**.

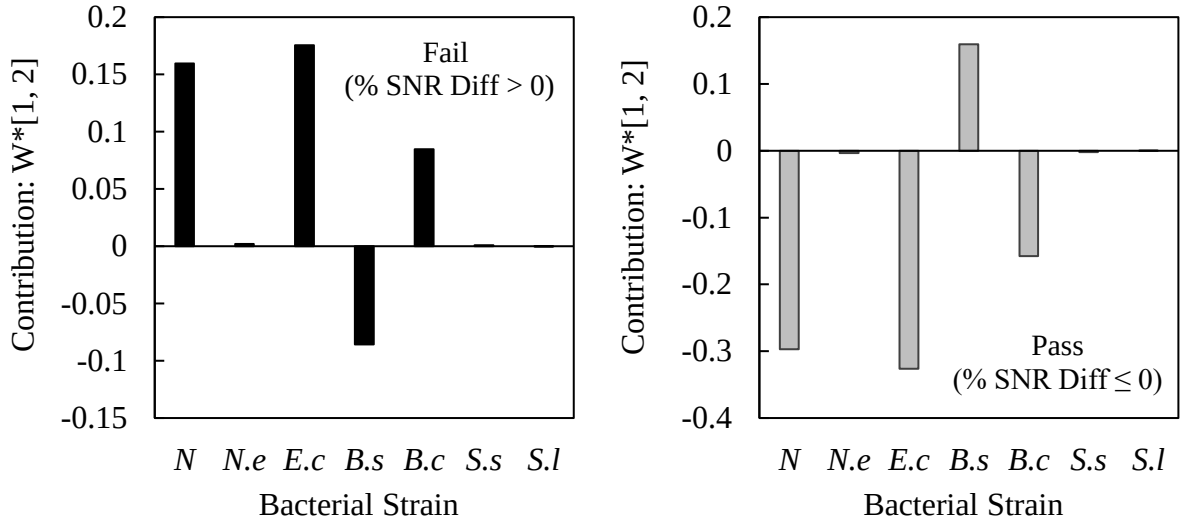

Figure 3-4. Contribution plot for the CBB to SNR PLS model. Average "fail" result (left) and "pass" result (right) of the seven bacterial strains (*Nitrospira* (*N*), *Nitrosomonas europaea* (*N.e*), *Escherchia coli* (*E.c*), *Bacillus subtilis* (*B.s*), *Bacillus cereus* (*B.c*), *Staphylococcus saprophyticus* (*S.s*) and *Streptomyces laurentii* (*S.l*)) measured as contributions for the first and second component. The weights without residuals (W*) are used. Contribution values greater than zero indicate a fluorescence signal that is greater than the average fluorescence signal for all WW samples, for that particular bacterial strain. Contribution values less than zero indicate the opposite (less than the average).

The reader is referred to the User Guide to SIMCA[56] to understand how the contribution values are calculated. Generally, for WW samples with a "fail" rating, *Nitrospira*, *Escherichia coli*, and *Bacillus cereus* have fluorescence signals higher than the average (for each strain), while *Bacillus subtilis* has fluorescence signals lower than the average. Interestingly, there was no significant effect found for *Nitrosomonas europaea*, *Staphylococcus saprophyticus* and *Streptomyces laurentii*; the contribution values for these three strains were -3.58×10^{-3},

-1.77×10^{-3}, and $+0.12 \times 10^{-3}$ for "pass" and $+1.92 \times 10^{-3}$,+ 0.95×10^{-3}, and -0.06×10^{-3} for "fail" samples, respectively. This is a surpising result, particularly for *Nitrosomonas europaea*, since it is a prominent nitrifying bacterium; we hypothesize that due to its high settleability rate (these bacteria form strong bacterial clumps or large flocs), the fluorescence signals are not as reliable as the other strains. The results in **Figure B1** (Appendix B) confirm this hypothesis since the fluorescence signals for *Nitrosomonas europaea* display a downward trend as the WW sample number increases from left to right. We believe that this trend represents the settling of the bacteria as the microplate was analyzed (from WW sample #1 to #28). For WW samples with a "pass" rating, *Nitrospira*, *Escherichia coli*, and *Bacillus cereus* have fluorescence signals lower than the average (for each strain), while *Bacillus subtilis* has fluorescence signals higher than the average (the opposite of the "fail" rating). Again, no effect is seen with *Nitrosomonas europaea*, *Staphylococcus saprophyticus* and *Streptomyces laurentii*. Although we do not fully understand the reason as to why certain strains behave the way they do, previous research indicates that an increase in the fluorescence signal for *E. coli* is correlated with an increase in the amount of intracellular RNA.[62] It is our hypothesis that an increase in the intracellular RNA, and hence an increase in the fluorescence signal, is due to an increase in cellular activity which is triggered by specific chemical compounds in the WW samples. A decrease in the fluorescence signal is likely due to an increase in cellular membrane porosity.[26,29] Since the "live" fluorescent dye (SYTO 9) used in this commerically provided kit works by primarily binding to nucleic acids such as DNA and RNA (as previously mentioned),[29] when the cellular membrane porosity increases, the SYTO 9 dye is replaced with propidium iodide (present in the dye), effectively decreasing the fluorescence signal.

However, we believe that these outcomes (increase in intracellular RNA, increase in membrane porosity) can occur simultaneously due to the many differences in the bacteria strains and their complex interactions with the wide range of chemical compounds present in each WW sample.

On the basis of the contribution results in **Figure 3-4**, it is interesting to note that of the four bacterial strains that contribute heavily to predicting the nitrification inhibition potential, two are Gram-negative (*Nitrospira*, *E. coli*) and two are Gram-positive (*Bacillus subtilis*, *Bacillus cereus*). Since both Gram-negative strains respond similarly with respect to each other when exposed to "pass" and "fail" samples, this may be one of many factors that can explain the differences in the fluorescence signals between strains. *Bacillus cereus* does not display the same effect as its Gram-positive counterpart, *Bacillus subtilis*, and therefore, the fluorescence signals are likely influenced by other factors (e.g., metabolism of specific chemical compounds) that may be bacterial strain specific. For example, it has been shown that approximately 30 genes for *Bacillus cereus* and 100 genes for *Bacillus subtilis* are transcribed upon exposure to environmental stress (e.g., acid stress) and therefore would react differently.[31] Gram-negative bacteria have a cell wall made of a thin peptidoglycan layer in comparison to Gram-positive bacteria,[63] and it has been reported that peptidoglycan may play a role in the permeability of the cell wall in bacteria that would affect which chemical compounds could enter the cell.[64] In some cases, certain chemical compounds such as surfactants (e.g., cetyltrimethylammonium bromide; CTAB) have been shown to increase the permeability of bacterial cells.[12] Once permeabilized, intracellular enzymes can perform their functions more quickly by allowing free diffusion of small molecules through the

membrane.[12] Another reason for the differences in the fluorescence signals between the strains could be due to the selective passage of chemical compounds through the hydrophilic Porins (channels) on the outer envelope of Gram-negative bacteria.[63] Gram-negative and Gram-positive bacteria are also known for their differences in regulating transcription and translation in response to the binding of riboswitches, which are stimulated in response to the binding of specific molecules.[65] Riboswitches generally attenuate transcription in Gram-positive bacteria and attenutate translation in Gram-negative bacteria.[66] Finally, researchers have shown that when bacterial cells are exposed to stressful environments that contain various metabolic toxins, the genes of the stress proteins are generally mutated which affects DNA and RNA synthesis.[30] Due to the many possible explanations for the differences in the fluorescence signals from strain to strain, future work will be done to better help understand the observed outcomes in this part of our study.

3.4.3 The Effect of Chemical Compounds on Nitrification Inhibition

The GC-MS to SNR PLS model was used to predict which chemical compounds are positively and negatively correlated to nitrification inhibition. This was made possible using the setup shown in **Figure B4** (Appendix B) and analyzing the contribution plot. Nineteen WW samples were used in the model. Five of the WW samples (#17, #18, #21, #25, and #26) were not used because they had GC-MS peak areas that were approximately 3 orders of magnitude lower than the average peak areas of all of the other WW samples (results not shown) and thus we were concerned that the results were unreliable. An additional four WW samples (#5, #15, #19, and #23) were not included (see **Table B2** in Appendix B) in the

model as they fell outside of the 95% confidence interval for the squared prediction error and Hotelling's T^2 values. Two principal components were used in this PLS model with large cumulative R^2 and Q^2 values (0.83 and 0.41, respectively) indicating the possibility of using GC-MS to predict the nitrification inhibition potential of a WW sample.

The impact of each chemical compound on the nitrification inhibition potential is shown as a contribution plot in **Figure 3-5**. The chemical compounds with positive x-axis values (e.g., benzyl alcohol, benzoic acid) are positively correlated with nitrification inhibition, and the chemical compounds with negative x-axis values (e.g., 2,3-butanediol, linalool) are negatively correlated with nitrification inhibition. The numerical value beside each bar is the number of times that particular compound was detected by GC-MS. It is interesting to note that diethylene glycol butyl ether appears in every one of the 19 WW samples and benzyl alcohol and 2-butoxyethanol each appear in 15 of the samples. Also, of the 51 chemical compounds present in these 19 WW samples, eight chemical compounds appear in at least half (i.e., 10 out of 19) of the samples. Seventeen of the 33 chemical compounds that are positively correlated with nitrification inhibition are carboxylic acids (black filled bars). We hypothesize that this result is likely due to the high electronegativity and therefore polarity of carboxylic acids[67] and since WW bacteria tend to be more hydrophilic than hydrophobic.[68] For example, it is shown that octanoic acid and 1-octanol are positively and negatively correlated with nitrification inhibiton, respectively. Also, the observed effects of aromatic chemical compounds (benzoic acid, phenol, and p-chlorocresol) on nitrification inhibition are consistent with previous studies.[69–71] However, it is also shown that some aromatic chemical compounds such as cyclohexanol and cresol are negatively

correlated with nitrification inhibition; we suspect that the competition between the chemical compounds plays a large role in the selective uptake in bacterial cells.

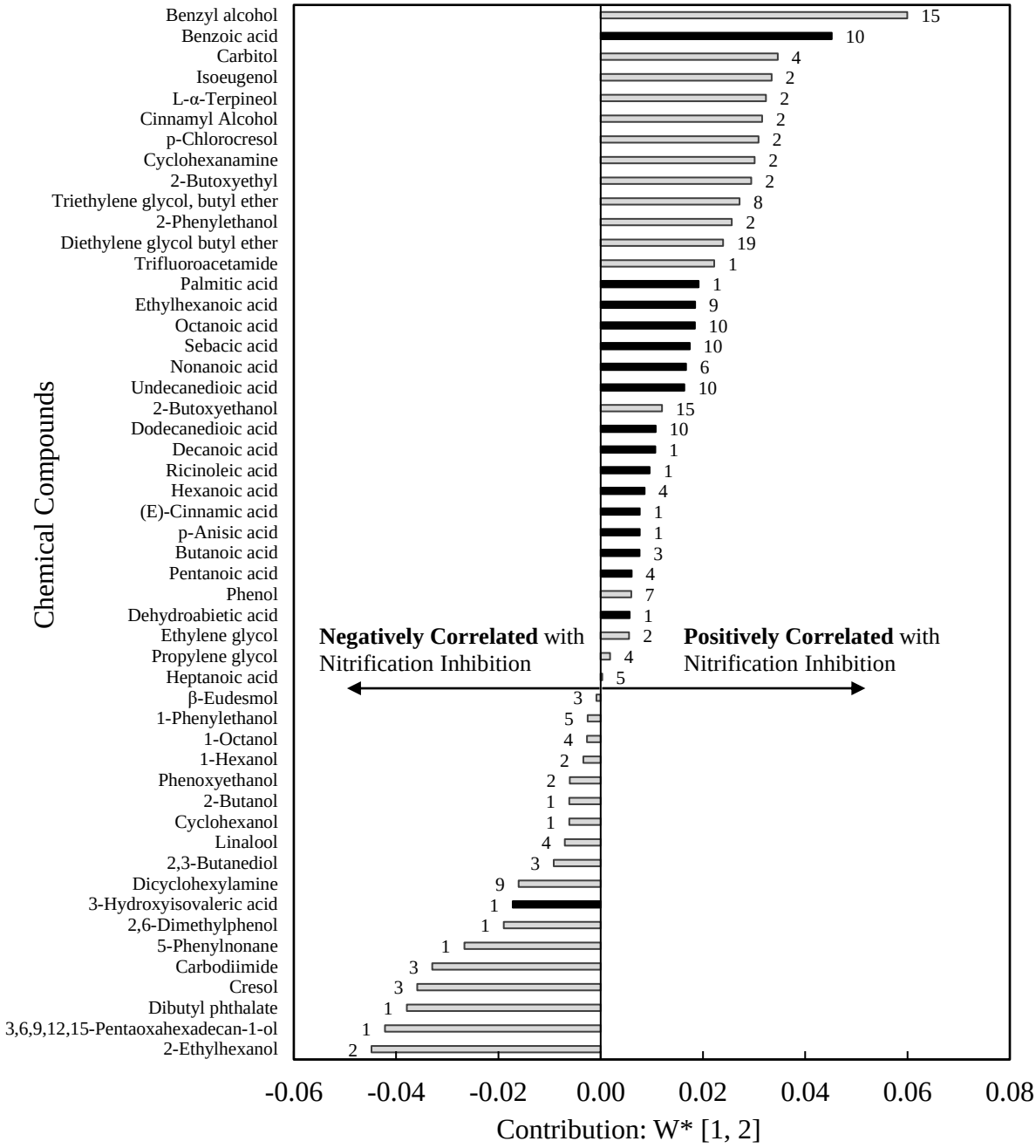

Figure 3-5. Contribution plot for the GC-MS to SNR PLS Model. The effect of 51 different chemical compounds from 19 WW samples on the % SNR difference is shown. The contributions of these 51 chemical compounds are shown for the first and second principal component; the weights without residuals (W*) are used. Dark bars (filled) are carboxylic acids, while light bars (grayed) are all other chemical compounds. The number beside each bar is the number of times that compound was detected in the 19 WW samples.

3.4.4 The Effect of Chemical Compounds on Bacteria Fluorescence Signal

The same 19 WW samples were used in a GC-MS to CBB PLS model (setup shown in **Figure B5** of Appendix B). In this model, we found that *Nitrospira* and *E. coli* were the only strains to have predictive relevance (Q2 > 0) for all of the principal components analyzed (**Table B3** in Appendix B) and therefore, only the fluorescence signals from *Nitrospira* and *E. coli* were included. This result may be due to their Gram-negative membrane structure; it is hypothesized that these strains can better discriminate between the compounds present in a WW sample due to the selective passage of hydrophilic compounds through Porins into the cell.[63] Two principal components were used in this PLS model; the cumulative R^2 and Q^2 values were 0.73 and 0.14, respectively (see **Table B4** in Appendix B for details on the other principal components). The large R^2 value with only two principal components indicates that this model can potentially be used to predict which chemical compounds are present in a WW sample based on the fluorescence signal of the two strains using a weight biplot (**Figure 5-6**). The low Q^2 value indicates that more WW samples need to be tested due to the large number of chemical compounds.

By analyzing the locations of the weights (left or right, top or bottom, diagonal) shown as empty circles for the chemical compounds and black squares for the strains, predictions can be made. For example, benzyl alcohol and pentanoic acid are present on the same side (right) of the weight biplot as *Nitrospira* and thus are positively correlated in the first principal component. However, benzyl alcohol is also present on the opposite side (bottom) of *Nitrospira* in the second principal component. This means that the presence of pentanoic acid is more likely to have a larger effect than benzyl alcohol on increasing the

fluorescence signal of *Nitrospira*. In another example, p-anisic acid and 2-ethylhexanol are present on the opposite side (left) of the weight biplot as *E. coli* and thus are negatively correlated in the first principal component. In addition, 2-ethylhexanol is also present diagonally of *E. coli* indicating they are also negatively correlated in the second principal component. This means that 2-ethylhexanol is more likely to have a larger effect than p-anisic acid on decreasing the fluorescence signal of *E. coli*. Therefore, by measuring the fluorescence signals of *Nitrospira* and *E. coli* and after consulting the weight biplot, there is a strong potential to estimate which chemical compounds are present in a WW sample.

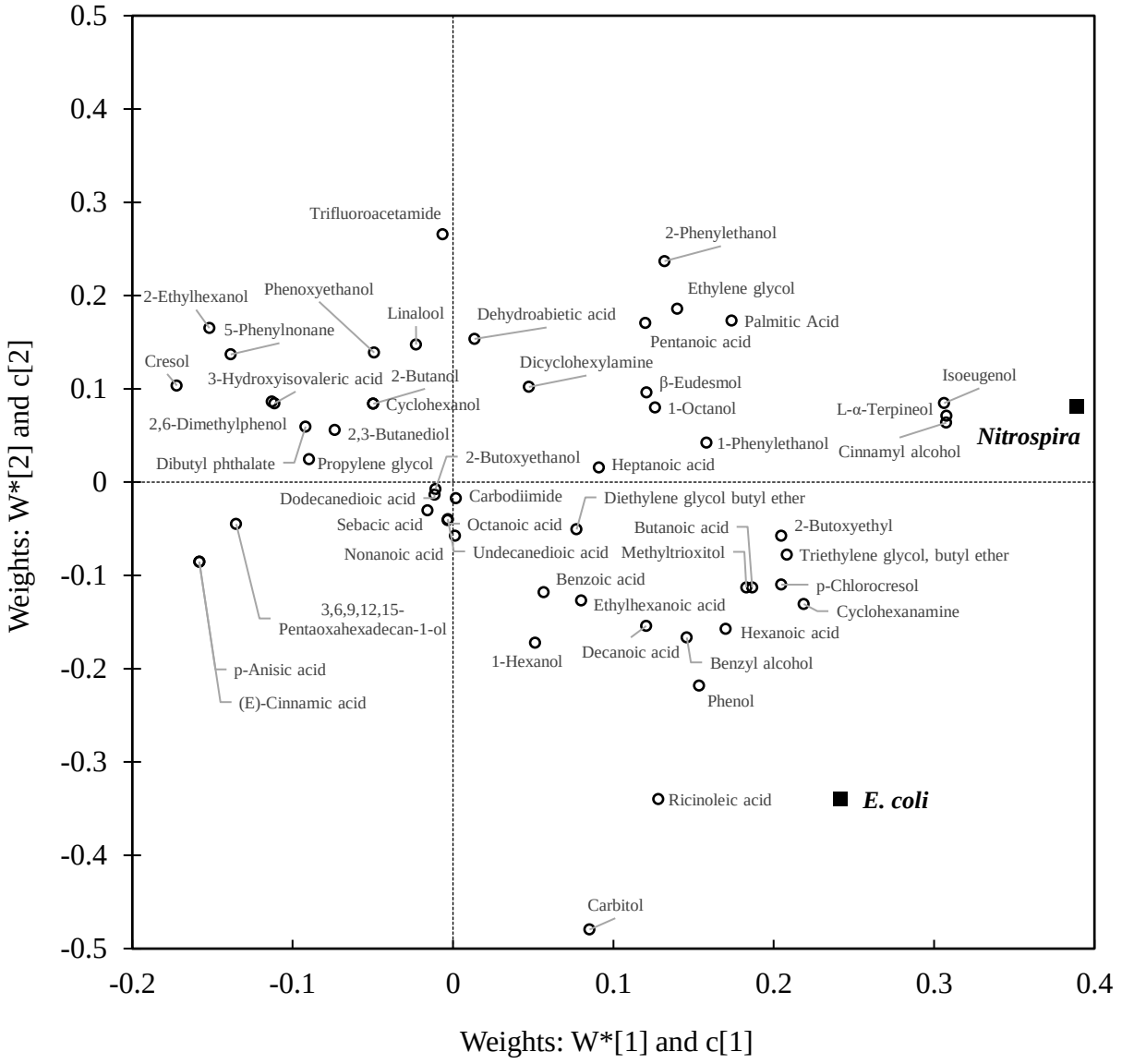

Figure 3-6. A weight bi-plot for the GC-MS to CBB PLS Model. Positively correlated weights for the X space (GC-MS) and Y space (CBB) appear on the same side (left or right, top or bottom) of the plot. Negatively correlated weights appear on opposite sides. Weights that appear in the same quadrant are more strongly correlated. Similar to **Figure 3-4** and **Figure 3-5,** the weights without residuals (W*) are used.

3.5 References

1. Comeau, Y. (2008). Microbial metabolism. Biological wastewater treatment: principles, modeling and design. London: IWA/Cambridge University Press, cap, 2, 9-32.
2. Juretschko, S., Timmermann, G., Schmid, M., Schleifer, K. H., Pommerening-Röser, A., Koops, H. P., & Wagner, M. (1998). Combined molecular and conventional analyses of nitrifying bacterium diversity in activated sludge: Nitrosococcus mobilis and Nitrospira-like bacteria as dominant populations. *Applied and environmental microbiology*, *64*(8), 3042-3051.
3. Chain, P., Lamerdin, J., Larimer, F., Regala, W., Lao, V., Land, M., ... & Sayavedra-Soto, L. (2003). Complete genome sequence of the ammonia-oxidizing bacterium and obligate chemolithoautotroph Nitrosomonas europaea. *Journal of bacteriology*, *185*(9), 2759-2773.
4. Henriques, I. D., & Love, N. G. (2004). Chemical inhibition of nitrification in activated sludge. *Biotechnology and bioengineering*, *85*(6), 683-694.
5. Iwasaki, T., Takeno, T., & Yamamoto, Y. (1988). *U.S. Patent No. 4,770,694*. Washington, DC: U.S. Patent and Trademark Office.
6. Affatato, S., Bersaglia, G., Emiliani, D., Foltran, I., & Toni, A. (2004). Sodium-azide versus ProClin 300: influence on the morphology of UHMWPE particles generated in laboratory tests. *Biomaterials*, *25*(5), 835-842. doi.org/10.1016/S0142-9612(03)00603-3
7. Sherine, B. (2015). Biocidal Efficiency of Organic Inhibitor in Cooling Water Systems. *International Journal of Research and Development in Pharmacy and Life Sciences*, *4*(2), 1400-1406.
8. Urwin, C., Richardson, J. C., & Palmer, A. K. (1976). An evaluation of the mutagenicity of the cutting oil preservative Grotan BK. *Mutation Research/Genetic Toxicology*, *40*(1), 43-46. doi.org/10.1016/0165-1218(76)90021-5
9. Ranade, V. V., & Bhandari, V. M. (2014). *Industrial wastewater treatment, recycling and reuse*. Butterworth-Heinemann.
10. Bye, C. M., Jones, R. M., & Dold, P. L. (2012). Pragmatic nitrification inhibition testing for robust plant design. *Proceedings of the Water Environment Federation*, *2012*(12), 4222-4238.
11. Farré, M., & Barceló, D. (2003). Toxicity testing of wastewater and sewage sludge by biosensors, bioassays and chemical analysis. *TrAC Trends in Analytical Chemistry*, *22*(5), 299-310.
12. D'Souza, S. F. (2001). Microbial biosensors. *Biosensors and Bioelectronics*, *16*(6), 337-353.

13. Pancrazio, J. J., Whelan, J. P., Borkholder, D. A., Ma, W., & Stenger, D. A. (1999). Development and application of cell-based biosensors. *Annals of biomedical engineering*, *27*(6), 697-711.
14. Kuhn, I., Colque-Navarro, P., Gabrielson, J., Iversen, A., McKenzie, J. D., & Hart, M. C. (2013). *U.S. Patent No. 8,551,921*. Washington, DC: U.S. Patent and Trademark Office.
15. Jung, Y., Park, C. B., Kim, Y., Kim, S., Pflugmacher, S., & Baik, S. (2015). Application of multi-species microbial bioassay to assess the effects of engineered nanoparticles in the aquatic environment: potential of a luminous microbial array for toxicity risk assessment (LumiMARA) on testing for surface-coated silver nanoparticles. *International journal of environmental research and public health*, *12*(7), 8172-8186.
16. Hsieh, C. Y., Tsai, M. H., Ryan, D. K., & Pancorbo, O. C. (2004). Toxicity of the 13 priority pollutant metals to Vibrio fisheri in the Microtox® chronic toxicity test. *Science of the total environment*, *320*(1), 37-50.
17. Rigol, A., Latorre, A., Lacorte, S., & Barceló, D. (2004). Bioluminescence inhibition assays for toxicity screening of wood extractives and biocides in paper mill process waters. *Environmental Toxicology and Chemistry: An International Journal*, *23*(2), 339-347.
18. Mamais, D., Noutsopoulos, C., Stasinakis, A. S., Kouris, N., & Andreadakis, A. D. (2008). Comparison of bioluminescence and nitrification inhibition methods for assessing toxicity to municipal activated sludge. *Water Environment Research*, *80*(6), 484-489.
19. Jönsson, K., Grunditz, C., Dalhammar, G., & Jansen, J. L. C. (2000). Occurrence of nitrification inhibition in Swedish municipal wastewaters. *Water Research*, *34*(9), 2455-2462.
20. Grunditz, C., Gumaelius, L., & Dalhammar, G. (1998). Comparison of inhibition assays using nitrogen removing bacteria: application to industrial wastewater. *Water Research*, *32*(10), 2995-3000.
21. Grunditz, C., & Dalhammar, G. (2001). Development of nitrification inhibition assays using pure cultures of Nitrosomonas and Nitrobacter. *Water research*, *35*(2), 433-440.
22. Kadlec, P., Grbić, R., & Gabrys, B. (2011). Review of adaptation mechanisms for data-driven soft sensors. *Computers & chemical engineering*, *35*(1), 1-24.
23. Kadlec, P., Gabrys, B., & Strandt, S. (2009). Data-driven soft sensors in the process industry. *Computers & chemical engineering*, *33*(4), 795-814.
24. Ohadi, S. K. (2014). Development of Soft Sensors for Monitoring of Chinese Hamster Ovary Cell Processes.
25. Luccarini, L., Porra, E., Spagni, A., Ratini, P., Grilli, S., Longhi, S., & Bortone, G. (2002). Soft sensors for control of nitrogen and phosphorus removal from wastewaters by neural networks. *Water science and technology*, *45*(4-5), 101-107.

26. Oliver, J. D. (2005). The viable but nonculturable state in bacteria. *The Journal of Microbiology*, *43*(1), 93-100.
27. Kim, H. J., Tango, C. N., Chelliah, R., & Oh, D. H. (2019). Sanitization Efficacy of Slightly Acidic Electrolyzed Water against pure cultures of Escherichia coli, Salmonella enterica, Typhimurium, Staphylococcus aureus and Bacillus cereus spores, in Comparison with Different Water Hardness. *Scientific reports*, *9*(1), 4348.
28. Díaz-Pascual, F., Hartmann, R., Lempp, M., Vidakovic, L., Song, B., Jeckel, H., ... & Nadell, C. D. (2019). Breakdown of Vibrio cholerae biofilm architecture induced by antibiotics disrupts community barrier function. *Nature microbiology*, 1-10.
29. Molecular Probes. (2003). *SYTO ® Green-Fluorescent Nucleic Acid Stains.*
30. Welch, W. J. (1993). How cells respond to stress. *Scientific American*, *268*(5), 56-64.
31. Desriac, N., Broussolle, V., Postollec, F., Mathot, A. G., Sohier, D., Coroller, L., & Leguerinel, I. (2013). Bacillus cereus cell response upon exposure to acid environment: toward the identification of potential biomarkers. *Frontiers in microbiology*, *4*, 284.
32. Juretschko, S., Timmermann, G., Schmid, M., Schleifer, K. H., Pommerening-Röser, A., Koops, H. P., & Wagner, M. (1998). Combined molecular and conventional analyses of nitrifying bacterium diversity in activated sludge: Nitrosococcus mobilis and Nitrospira-like bacteria as dominant populations. *Appl. Environ. Microbiol.*, *64*(8), 3042-3051.
33. Antoniou, P., Hamilton, J., Koopman, B., Jain, R., Holloway, B., Lyberatos, G., & Svoronos, S. A. (1990). Effect of temperature and pH on the effective maximum specific growth rate of nitrifying bacteria. *Water research*, *24*(1), 97-101.
34. Arp, D. J., Sayavedra-Soto, L. A., & Hommes, N. G. (2002). Molecular biology and biochemistry of ammonia oxidation by Nitrosomonas europaea. *Archives of microbiology*, *178*(4), 250-255.
35. Reinthaler, F. F., Posch, J., Feierl, G., Wüst, G., Haas, D., Ruckenbauer, G., ... & Marth, E. (2003). Antibiotic resistance of E. coli in sewage and sludge. *Water research*, *37*(8), 1685-1690.
36. Salehizadeh, H., & Yan, N. (2014). Recent advances in extracellular biopolymer flocculants. *Biotechnology advances*, *32*(8), 1506-1522.
37. Bartoszewicz, M., & Czyżewska, U. (2017). Spores and vegetative cells of phenotypically and genetically diverse Bacillus cereus sensu lato are common bacteria in fresh water of northeastern Poland. *Canadian journal of microbiology*, *63*(12), 939-950.
38. Börjesson, S., Matussek, A., Melin, S., Löfgren, S., & Lindgren, P. E. (2010). Methicillin-resistant Staphylococcus aureus (MRSA) in municipal wastewater: an uncharted threat?. *Journal of applied microbiology*, *108*(4), 1244-1251.
39. Ferreira, A. M., Bonesso, M. F., Mondelli, A. L., & de Souza, M. D. L. R. (2012). Identification of Staphylococcus saprophyticus isolated from patients with urinary

tract infection using a simple set of biochemical tests correlating with 16S–23S interspace region molecular weight patterns. *Journal of microbiological methods*, *91*(3), 406-411.
40. Abou-Elela, S. I., Kamel, M. M., & Fawzy, M. E. (2010). Biological treatment of saline wastewater using a salt-tolerant microorganism. *Desalination*, *250*(1), 1-5.
41. Doi, K., Fujino, Y., Nagayoshi, Y., Ohshima, T., & Ogata, S. (2016). Complete genome sequence of thiostrepton-producing *Streptomyces laurentii* ATCC 31255. *Genome announcements*, *4*(3), e00360-16.
42. Hozzein, W. N., Ahmed, M. B., & Tawab, M. S. A. (2012). Efficiency of some actinomycete isolates in biological treatment and removal of heavy metals from wastewater. *African Journal of Biotechnology*, *11*(5), 1163-1168.
43. Smejkalova, M., Mikanova, O., & Boruvka, L. (2003). Effects of heavy metal concentrations on biological activity of soil micro-organisms. *Plant Soil and Environment*, *49*(7), 321-326.
44. U.S Environmental Protection Agency Office of Water. (2001). *Total, Fixed, and Volatile Solids in Water, Solids, and Biosolids.* Washington, DC.
45. Hoilijoki, T. H., Kettunen, R. H., & Rintala, J. A. (2000). Nitrification of anaerobically pretreated municipal landfill leachate at low temperature. *Water Research*, *34*(5), 1435-1446.
46. Bourrain, M., Achouak, W., Urbain, V., & Heulin, T. (1999). DNA extraction from activated sludges. *Current microbiology*, *38*(6), 315-319.
47. Seyhi, B., Drogui, P., Buelna, G., & Blais, J. F. (2012). Removal of bisphenol-A from spiked synthetic effluents using an immersed membrane activated sludge process. *Separation and purification technology*, *87*, 101-109.
48. Raboni, M., Torretta, V., Viotti, P., & Urbini, G. (2014). Calculating specific denitrification rates in pre-denitrification by assessing the influence of dissolved oxygen, sludge loading and mixed-liquor recycle. *Environmental technology*, *35*(20), 2582-2588.
49. Government of Canada. (2012, June 29). *Wastewater Systems Effluent Regulations*. Retrieved from Justice Laws: https://laws-lois.justice.gc.ca/eng/regulations/sor-2012-139/fulltext.html
50. Holly, D. (2010). Online Process Monitoring of Part Manufacturing Using MVA. *McMaster University library, Hamilton*.
51. Höskuldsson, A. (1995). A combined theory for PCA and PLS. *Journal of Chemometrics*, *9*(2), 91-123.
52. Heipieper, H. J., Fischer, J., & Meinhardt, F. (2018). Cis–trans isomerase of unsaturated fatty acids: an immediate bacterial adaptive mechanism to cope with emerging membrane perturbation caused by toxic hydrocarbons. *Cellular Ecophysiology of Microbe: Hydrocarbon and Lipid Interactions*, 385-395.

53. Chin, W. W. (1998). The partial least squares approach to structural equation modeling. *Modern methods for business research*, *295*(2), 295-336.
54. Umetrics. (n.d.). *F.A.Q SIMCA-P and Multivariate Frequently Asked Questions, version 1.01.*
55. Hair Jr, J. F., Hult, G. T. M., Ringle, C., & Sarstedt, M. (2016). *A primer on partial least squares structural equation modeling (PLS-SEM)*. Sage Publications.
56. MKS Umetrics. (2012). *User Guide to SIMCA, Version 13.*
57. Henseler, J., Ringle, C. M., & Sinkovics, R. R. (2009). The use of partial least squares path modeling in international marketing. In *New challenges to international marketing* (pp. 277-319). Emerald Group Publishing Limited.
58. Slupsky, C. M., Steed, H., Wells, T. H., Dabbs, K., Schepansky, A., Capstick, V., ... & Sawyer, M. B. (2010). Urine metabolite analysis offers potential early diagnosis of ovarian and breast cancers. *Clinical cancer research*, *16*(23), 5835-5841.
59. Ubhi, B. K., Riley, J. H., Shaw, P. A., Lomas, D. A., Tal-Singer, R., MacNee, W., ... & Connor, S. C. (2012). Metabolic profiling detects biomarkers of protein degradation in COPD patients. *European Respiratory Journal*, *40*(2), 345-355.
60. Krumnow, A. A., Sorokulova, I. B., Olsen, E., Globa, L., Barbaree, J. M., & Vodyanoy, V. J. (2009). Preservation of bacteria in natural polymers. *Journal of Microbiological Methods*, *78*(2), 189-194.
61. Jahanshahi-Anbuhi, S., Pennings, K., Leung, V., Liu, M., Carrasquilla, C., Kannan, B., ... & Filipe, C. D. (2014). Pullulan encapsulation of labile biomolecules to give stable bioassay tablets. *Angewandte Chemie International Edition*, *53*(24), 6155-6158.
62. Morkus, P., Zolfaghari, M., Parrello, D., Csordas, M., Malikov, M., Rose, J., ... & Latulippe, D. R. (2019). Optimization of microorganism preservation conditions for the development of an acute toxicity bioassay for biocides. *Chemosphere*, *221*, 45-54.
63. Denyer, S. P., & Maillard, J. Y. (2002). Cellular impermeability and uptake of biocides and antibiotics in Gram-negative bacteria. *Journal of applied microbiology*, *92*, 35S-45S.
64. Burman, L. G., Nordström, K., & Bloom, G. D. (1972). Murein and the outer penetration barrier of Escherichia coli K-12, Proteus mirabilis, and Pseudomonas aeruginosa. *Journal of bacteriology*, *112*(3), 1364-1374.
65. Waters, L. S., & Storz, G. (2009). Regulatory RNAs in bacteria. *Cell*, *136*(4), 615-628.
66. Fernandez, J., Yaman, I., Huang, C., Liu, H., Lopez, A. B., Komar, A. A., ... & Lamers, W. H. (2005). Ribosome stalling regulates IRES-mediated translation in eukaryotes, a parallel to prokaryotic attenuation. *Molecular cell*, *17*(3), 405-416.
67. Siggel, M. R., Streitwieser, A., & Thomas, T. D. (1988). The role of resonance and inductive effects in the acidity of carboxylic acids. *Journal of the American Chemical Society*, *110*(24), 8022-8028.

68. Zita, A., & Hermansson, M. (1997). Determination of bacterial cell surface hydrophobicity of single cells in cultures and in wastewater in situ. *FEMS Microbiology Letters*, *152*(2), 299-306.
69. Kim, Y. M., Park, D., Lee, D. S., & Park, J. M. (2008). Inhibitory effects of toxic compounds on nitrification process for cokes wastewater treatment. *Journal of Hazardous Materials*, *152*(3), 915-921.
70. McCarty, G. W., & Bremner, J. M. (1986). Effects of Phenolic Compounds on Nitrification in Soil 1. *Soil Science Society of America Journal*, *50*(4), 920-923.
71. Gutierrez, M., Etxebarria, J., & De Las Fuentes, L. (2002). Evaluation of wastewater toxicity: comparative study between Microtox® and activated sludge oxygen uptake inhibition. *Water Research*, *36*(4), 919-924.

4 Chapter 4: Tuning the sensitivity of bacteria as point-of-use cell-based biosensors for the improved detection of biocides

In this chapter, experiments were performed by myself, and undergraduate students Sarah Rassenberg and Danika Montpetit, under my supervision. This chapter was drafted by myself and edited by my academic supervisors, Dr. David R. Latulippe and Dr. Carlos D.M Filipe.

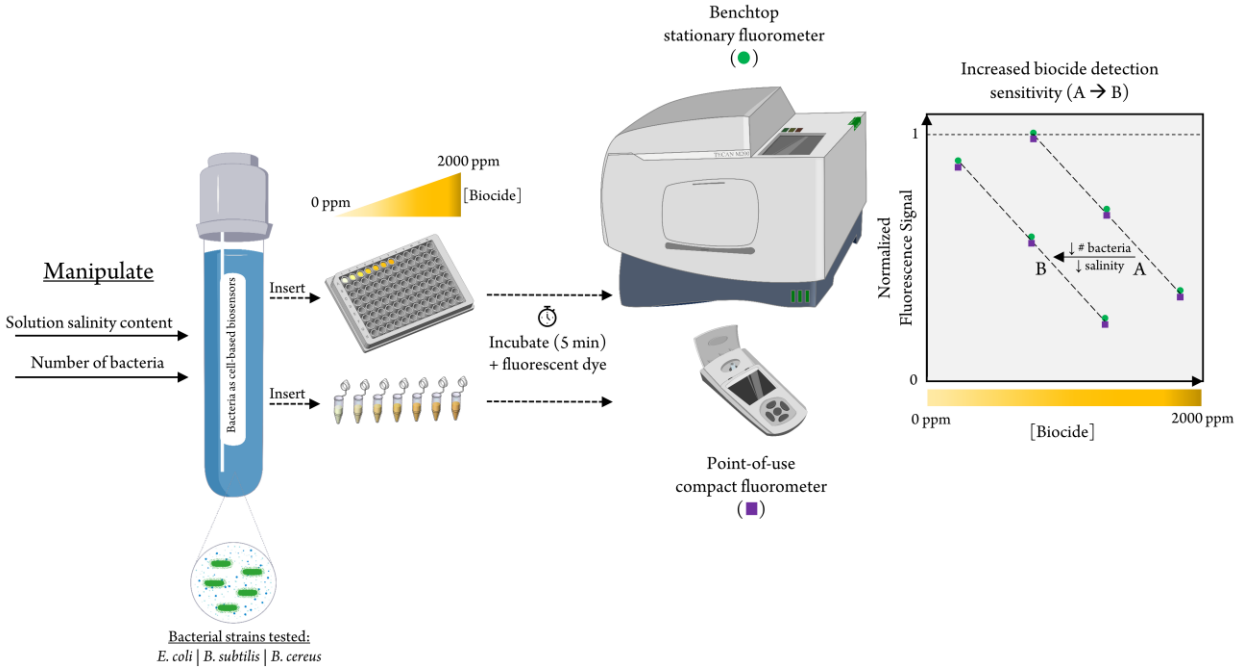

4.1 Abstract

The ability of many wastewater treatment plants (WWTPs) to reliably produce effluents with levels of ammonia below discharge limits depends on protecting the biological process of nitrification from being negatively affected. The bacteria responsible for this process are susceptible to inhibition due to the presence of toxic compounds, such as biocides, in the influent to these plants. In this paper, we describe an approach for creating cell-based biosensors (CBBs) with tunable levels of sensitivity, to detect the presence of these inhibitors when present at various concentrations. The CBB consists of a panel of bacterial strains (*E. coli*, *B. subtilis*, *B. cereus*) and the monitoring of fluorescence signal generation after exposure to biocides, as previously reported in the literature. We show that the sensitivity of these bacterial strains can be tuned by modulating the susceptibility of the cells to the biocides, which was found to be affected by the type/salinity of the buffer used to suspend the cells, and by changing the number of cells used in the assay. These changes enabled the detection of Cetyltrimethylammonium bromide (CTAB) at a concentration of 0.625 ppm and Grotan® BK at a concentration of 7.8 ppm. Finally, as a proof-of-concept, we demonstrate that the response of the bacterial strains and quantitative determination of the levels of toxicity of the specific agent can be determined with a low-cost (<$2000 CAD), compact commercially available fluorometer. Overall, the significance of this work will allow for greater accessibility via point-of-use testing and allow for better discrimination between biocide-containing samples of similar toxicity and detection of lower toxicity samples thereby improving the resolution of the CBB.

4.2 Introduction

Biosensors are widely used to detect a variety of analytes across a wide range of applications in the water/environmental, food, biomedical, and chemical industries. In general, a biosensor is a diagnostic device that transduces a biological signal generated by a biorecognition element into an electrochemical, optical/visual, piezoelectric, or thermal signal that can be interpreted using a simple or sophisticated instrument.[1, 2] Some common examples of biorecognition elements include enzymatic, DNA, and whole cell biosensors/cell-based biosensors (CBBs).[3, 4] CBBs are particularly suitable in situations where the goal is to assess the performance of the whole cells/living cells in a given application,[4] such as in wastewater treatment plants (WWTPs) that rely on the ability of nitrifying bacteria to oxidize ammonia into nitrate (i.e. nitrification) prior to discharging the water into various public waterways (e.g. lakes, rivers, oceans).[5] In this case, CBBs would be useful since they can provide direct functional information about the cell (i.e. the behavior)[4] when exposed to influent WW containing various analytes/chemical compounds. In addition, CBBs are easy to produce, at a low cost, and have rapid-response capabilities which make them strong candidates as sensors in the WW field.[6] One example of a commercially available CBB system used in the WW field is the *Aliivibrio fischeri* bioluminescence-based assay known as Microtox, which can take only minutes to use.[7] In one study,[8] Microtox was used to assess the toxicity of soil samples contaminated with biocides and biocide-degradation products as a result of them leaching from building materials (e.g. film preservatives in polymer resin-render and paint) due to rainfall. In other studies, Microtox was used to detect personal-care products (PCPs) including Triclosan,[9] ibuprofen,[10, 11] and

many others.[10] Other CBBs[9] have been developed using crustaceans (e.g. *Daphnia magna*) and algae to evaluate the toxicity of PCPs[9] and biocides,[12] however their long detection times (24 – 96 h) do not allow for rapid point-of-use testing. Respirometry[9] and Specific Nitrification Rate (SNR) batch tests[13] are other commonly used detection methods that use activated sludge (contains nitrifying bacteria and other bacteria) to assess the toxicity of WW. The SNR batch test is of particular interest to WWTPs because it is directly indicative of how influent WW will impact nitrification. However, these methods are complex and time-consuming, which limits the extent of adoption, and thus CBB assays provide a potential solution to these problems. CBB assays have been developed for easy and rapid monitoring of nitrification. The *Aliivibrio fischeri* toxicity test could predict the nitrification inhibition of a variety of WW samples (industrial, primary, secondary) from different WWTPs in approximately 1.5 h.[14] However, the results show that it is difficult to detect nitrification inhibition values of less than 20%.[14] In another example, pure cultures of *Nitrosomonas* and *Nitrobacter* (nitrifying bacteria) were used to detect the nitrification inhibition potential of industrial WW samples in approximately 4 h.[15] The limits of detection (LOD) for *Nitrosomonas* and *Nitrobacter* were reported as resulting in 11 and 13% inhibition, respectively. The drawbacks for both assays (*Aliivibrio fischeri*, *Nitrosomonas* and *Nitrobacter*) are that they are not faster than the SNR batch test and they are unable to measure/predict nitrification inhibition values across a wide range of values (including values closer to 0%). To solve for this, we recently developed a CBB technology utilizing a diverse panel of bacterial strains in combination with a commercially available fluorescent dye and partial least squares (PLS) modeling. This CBB technology can predict the

nitrification inhibition potential of a variety of industrial WWs ranging from -20% (nitrification stimulating) to +30% (nitrification inhibiting) in just 10 minutes.[16] Although we demonstrated success in detecting a wide range of nitrification stimulating and inhibiting WW samples, we determined that improvements in the resolution of this fluorescence-based technology were necessary in order to improve the precision of the nitrification inhibition prediction. Having the ability to discriminate between samples of similar toxicity as well as improving the detection capability of lower toxicity samples with a high level of confidence is especially important for municipal WWTPs that rely on accurate testing of nitrification inhibition to meet the increasingly stringent ammonia discharge limits according to the Wastewater Systems Effluent Regulations (WSER).[17] In addition, our previous work did not yet cater to point-of-use testing which is advantageous in terms of accessibility, convenience and cost-effectiveness that can be utilized throughout the entire WW supply chain beginning at the source, where the biocides are added.

In this proof-of-concept study, we first aimed to improve the resolution of the biocide-induced fluorescence signals of the three bacterial strains (*E. coli*, *B. subtilis*, *B. cereus*) that were the strongest contributors to predicting nitrification inhibition potential.[16] It was important to us to implement simple and easily adaptable techniques that are tunable so that an appropriate version of the technology can be selected according to toxicity level of the sample being tested. For example, higher toxicity samples would not require a version of the technology that is overly sensitive because these samples would likely kill the entire population of the bacteria rendering the response as unmeasurable. On the contrary, lower

toxicity samples would require a high level of sensitivity so that discrimination between samples of similar toxicity is measurable. Because each of the bacterial strains in our previous work were already stored in PBS solution (100% PBS) when exposed to biocide-containing WWs, in this study we explored the variations in the sensitivity of each of the bacterial strains when stored in different concentrations of PBS (0 – 100%). Research has shown that changes in extracellular salinity content plays a critical role in regulating the permeability of cellular membranes,[18] and other cellular structural responses such as changes in cellular, cytoplasmic, periplasmic volume[19] and hence we suspected the sensitivity of the bacterial strains would change.[18] Another simple method of tuning the sensitivity is investigated by manipulating the number of bacteria used in the assay. With this method, the ratio of the number of biocides to bacteria will change and therefore the toxicity per cell will vary. For both methods, two commonly used biocides, CTAB and Grotan® BK, were used as toxic models and tested at a variety of concentrations to represent a spectrum of toxicity levels. The second part of the study demonstrates the transfer of the technology from a bench-top microplate reader to a compact and cost-effective commercially available Quantus™ fluorometer to allow for point-of-use testing.

4.3 Materials and Methods

4.3.1 Preparation of bacterial strains

Three bacterial strains (*Escherichia coli DH5α*, *Bacillus subtilis* and *Bacillus cereus*) were selected in this study. This selection is based on our previous work which determined that strains were the most significant contributors for predicting the nitrification inhibition potential of industrial WW samples.[16] The preparation of the three strains are highlighted:

- *E. coli* were grown for approximately 20 hours in Lysogeny broth (LB) media (Sigma-Aldrich) in 14 mL polystyrene round-bottom Falcon tubes at 37°C via a Thermo MaxQ 8000 Shaker Incubator set to 225 rpm.
- *B. subtilis* were grown for approximately 40 hours in LB media at 26°C. The same tube type and incubator mentioned for *E. coli* were used.
- *B. cereus* were grown under the same conditions as *B. subtilis*.

Sanger sequencing of the bacterial strains confirmed the identity (99%) of all three strains via BLAST search software.

4.3.2 Preparation of varying salinity content solutions and number of bacteria

After culturing each of the bacterial strains, the bacteria-LB solutions from the 14 mL polystyrene round-bottom Falcon tubes were transferred into a single 50 mL polystyrene Falcon tube to create a large stock. The solution was then distributed equally (by volume) into six separate new 14 mL polystyrene round-bottom Falcon tubes and centrifuged at 4000 rpm at 8°C for 8 minutes. The supernants were decanted and the cell pellets were resuspended in six different phosphate buffered saline (PBS) solutions (1:1 LB to PBS) of varying PBS concentrations (0 (Milli-Q water only), 5, 15, 25, 50 and 100%). An exception was made for *B. subtilis* when exposed to biocide Grotan® BK (see section 4.3.3 for biocide information) where the cell pellets were resuspended in PBS at half the volume of LB removed (1:0.5 LB to PBS). This higher concentration for *B. subtilis* was necessary for this particular bacteria-biocide combination so that the control fluorescence signal of the final

dilution in the dilution series was large enough (~1000 RFU) to still discriminate between control and biocide fluorescence signals.

To further improve the limit of detection (LOD) for each bacterial strain, a 1.5 × bacterial strain serial dilution was performed on the bacteria-PBS solution (0, 5, 15, 25, 50, or 100%) that was determined to be the most effective at discriminating between the control (Milli-Q water) and the lowest concentration of biocide Cetyltrimethylammonium bromide (CTAB) and Grotan® BK. For each bacterial strain, the zeroth/no dilution (N0), second (N0 × 1.5^{-2}) and fourth (N0 × 1.5^{-4}) dilutions were tested; N0 corresponds to the number of bacteria tested (exposed to biocides or Milli-Q water) using the bacteria-PBS solution created immediately after resuspending the cell pellet (zeroth dilution) in one of the six PBS solutions. The enumeration via colony forming units (CFUs) was determined from a 10 × serial dilution of the N0 dilution performed in triplicate, followed by plating on an LB-Agar plate, incubating the plate upside down at 37°C (*E. coli*) or 28°C (*B. subtilis*, *B. cereus*) for 20 h, and then counting the colonies visually.

4.3.3 Fluorescence assay and biocide detection

All bacteria-biocide fluorescence experiments were conducted using a LIVE/DEAD BacLight dye solution (L7007 Bacterial Viability Kit), and read using either an Infinite M200 Pro multimode microplate reader (referred to as a Tecan M200 microplate reader) or a compact Quantus™ fluorometer (Promega Corporation). For the Tecan M200 microplate reader, a default gain of 60 and an excitation and emission wavelength of 485 and 530 nm were used. The excitation and emission wavelengths for the Tecan M200 microplate reader

was selected based on the L7007 Bacterial Viability Kit manufacturer's instructions for measuring 'live' bacteria present in a sample.[20] For the Quantus™ fluorometer, the blue 'fluorescent channel' was selected because it is the only setting available that corresponds to a similar excitation (495 nm) and emission wavelength (510-580 nm) to that of the Tecan M200 microplate reader.

For both instruments, 50 µL aliquots of bacteria-PBS solutions (corresponding to the number of bacteria N0, N0 × 1.5^{-2}, N0 × 1.5^{-4}) were mixed by aliquoting 50 µL of either CTAB or Grotan® BK dissolved in Milli-Q water. Details for these two biocides are given below:

- CTAB (Sigma) is a commonly used biocide employed to inhibit corrosion in cooling water systems.[21, 22] In this study, a variety of CTAB concentrations were tested. When PBS concentration was varied, 5, 10, and 20 ppm CTAB was tested. When the number of bacteria was varied, a wider range of CTAB concentrations (0.625, 1.25, 2.5, 5, 10, 20, and 40 ppm) were tested with a focus on CTAB concentrations to see if the LOD improved further.
- Grotan® BK (Commericial Oil) is a well-known biocide used to prohibit demulsification of industrial metal-working fluids.[23] In this study, a variety of Grotan® BK concentrations were tested. When PBS concentration was varied, 125, 500, 2000 ppm Grotan® BK was tested. When the number of bacteria was varied, a wider range of Grotan® BK concentrations (7.8, 15.6, 31.2, 62.5, 125, 250, 500 ppm) were tested with a focus on CTAB concentrations to see if the LOD improved further.

After 5 minutes of biocide exposure, 100 µL of the LIVE/DEAD BacLight dye solution (prepared according to the L7007 manual) was added. After 1 minute, the fluorescence signals were read in a 96-well flat bottom black microplate (Eppendorf) for the microplate reader, and read in 0.5 mL Axygen™ Thin-Wall PCR Tubes for the Quantus™ fluorometer; there is no advantage to waiting longer than 1 minute for the fluorescence signals (see section 4.4.1).

The fluorescence signals between these two fluorometers were compared. After culturing all three strains using same protocol as described in section 4.3.1, the Falcon tubes were centrifuged according to the same protocol as described in section 4.3.2. The supernants were decanted and the cell pellets were resuspended in PBS solution at half the volume of LB removed (1:0.5 LB to PBS) for *B. subtilis* and *B. cereus*, and at quarter the volume of LB removed for *E. coli* (1:0.25 LB to PBS). These dilution factors were selected to ensure that a wide range of fluorescence signals could be obtained. For each bacterial strain, a 5-step (6 concentrations), 2 × serial dilution was performed. The correlation between the two instruments was also generated with fluorecein (Sigma-Aldrich), a commonly used fluorophore for many applications.[24] Fluorescein was prepared in 1M NaOH according to the manufacturer's instructions.[25] A 6-step (7 concentrations), 2 × serial dilution was performed from a 500,000 pM Fluorescein stock solution. This fluorescein concentration was selected since the fluorescence signal produced by this concentration of fluoescein was near the upper bounds of the fluorescence signals achieved for each of three bacteria using the Tecan M200 microplate reader. The fluorescence signals for each dilution were measured in

triplicate (three separate wells in the microplate, three separate PCR tubes) by adding 200 µL of fluorescein solution into the same type of microplate and PCR tube. 200 µL was selected according to the literature,[26] and because this is the same total volume used to measure the fluorescence signal for each of the three bacterial strains.

4.4 Results and Discussion

4.4.1 Effects of varying biocide concentration on the fluorescence signal of *B.subtilis*

To demonstrate the effects of varying the concentration of a biocide on the fluorescence signal of a bacterial strain, *B. subtilis,* a Gram-positive strain, was exposed to five different CTAB concentrations (0.625, 1.25, 2.5, 5, and 10 ppm). The results in **Figure 4-1** show the normalized fluorescence signals one minute after dye addition (time-zero). The normalized fluorescence signals are calculated by dividing the fluorescence signal of the bacterial strain exposed to CTAB (biocide), by the fluorescence signal of the bacterial strain exposed to Milli-Q water (i.e. the control). The results in **Figure C1** (Appendix C) show that there is no advantage to waiting 30 minutes prior to measuring the fluorescence signals (responses and trends are similar); a 30-min wait time is shown since the fluorescence signal appeared to still be changing for most experimental conditions after the recommened 15-min wait time as per the manufacturer instructions (**Figure C2**, Appendix C). Lebaron et al. also concluded that the fluorescence signal (using the same dye) of *S. typhimurium* was still changing after the 15-min mark.[27] Three trials (one per day for three days) of the *B.subtilis*-CTAB experiment (from **Figure 4-3**) were conducted to highlight the reproducibility of the fluorescence signal responses and trend. This particular experiment was selected to be highlighted in **Figure 4-1** because it best represents the variety of fluorescence signal

responses presented in this work. For all three trials, when the concentration of CTAB is increased from 0.625 ppm to 2.5 ppm, the fluorescence signal increases. However, when the CTAB concentration is increased further, the fluorescence signal begins to drop and it eventually falls below the control signal represented by the dashed red line. A two-sample t-test (unequal variances) was conducted comparing the fluorescence signals of the control sample to the fluorescence signals of the 2.5 ppm CTAB sample, corresponding to the peak fluorescence based on the average fluorescence signal. The one-tail P-values for all three trials correspond to 0.024, 0.001, 0.005, and the two-tail P-values correspond to 0.048, 0.01, 0.003, respectively. Since all of these P-values are less than the α value (0.05), we are 95% confident that the increase in the fluorescence signal is statistically significant.

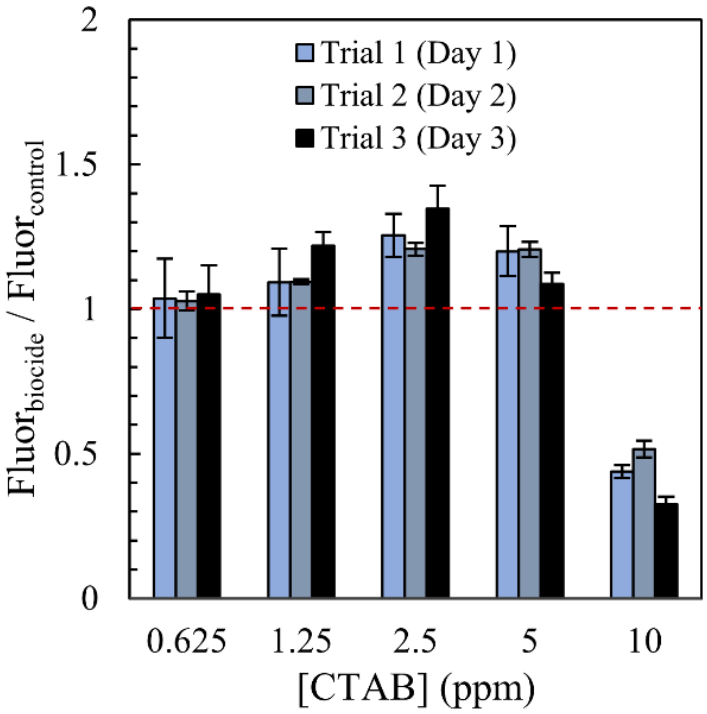

Figure 4-1. Normalized fluorescence signal ($Fluorescence_{biocide}$ / $Fluorescence_{control}$) data for *B. subtilis* prepared in 25% PBS exposed to Milli-Q water (0 ppm CTAB) and five different CTAB concentrations (0.625, 1.25, 2.5, 5, 10 ppm). This result was selected and extracted from Figure 4-3 and was repeated two additional times (three trials total) to highlight the reproducibility of these tests and to highlight an interesting phenomenon (increase in fluorescence signal with an increase in CTAB concentration up to 2.5 ppm). The number of *B. subtilis* was approximately 1.9, 2.0 and 1.9×10^7 for Trial 1, 2, and 3, respectively. Triplicate analysis was recorded for each trial. The error bars correspond to the standard deviation of the triplicate samples.

This result outlines three possible outcomes/effects: an increase, a decrease, and no change in the fluorescence signal with respect to the control fluorescence; the same three outcomes were seen in our previous works.[16, 28] The first effect, where the fluorescence signal is increased, occurs when lower concentrations of CTAB are used. It has been reported that upon exposure to CTAB, small pores in the cellular membrane of bacterial strains are created and have been observed to aid in the diffusion of substrates through the membrane,

thereby increasing the cellular activity of the bacteria.[29] In addition to increased diffusion, an increase in cellular activity may occur due to the expression of stress proteins that are used by the cell to combat the toxic analyte. This phenomenon has been observed in recombinant *E. coli* with the *lux* gene coupled to stress responsive promoters.[30] When *E. coli* was exposed to higher concentrations of dendrimer biocides (e.g., D5ClNC12), stress-responsive promoters led to the expression of the *lux* gene, thereby producing a higher bioluminescence signal than the control (without biocide).[30] Although we did not use bioluminescence, these cellular responses also account for an increase in the fluorescence signal; the SYTO 9 (green-fluorescence nucleic acid stain) component in the dye is known to increase the fluorescence intensity when bound to RNA,[27] which is produced under stressed conditions for the purpose of producing stress proteins.[31] The second effect, where the fluorecence signal is decreased, is the result of an increased disruption of the cellular membrane upon exposure to higher concentrations of CTAB. This phenomenon has been highly reported in the literature,[20, 32, 33] where propidium iodide (red-fluorescence nucleic acid stain) diffuses across a disrupted/damaged cellular membrane to replace SYTO 9 bound to DNA and RNA, effectively decreasing the fluorescence signal. This trend was also observed in the bioluminescence-testing 'equivalent' where a further increase in the dendrimer biocide concentration led to a decrease in the bioluminescence signal due to the higher toxicity resulting in the death of the bacteria.[30] The third effect, where the fluorescence signal is unchanged, occurs when little-to-no CTAB is used. This effect is of particular interest to us, since our aim is to improve the ability to discriminate between biocide-containing samples of similar toxicity as well as improve the LOD with a high level of confidence.

4.4.2 Tuning the sensitivity of bacteria: manipulating salinity content

As a proof-of-concept to increase bacteria susceptibility to biocides, bacteria solutions of varying PBS concentrations (0, 5, 15, 25, 50, 100% PBS) were studied for all three bacterial strains using CTAB and Grotan® BK. We arranged all of these experimental results in a six-panel format shown in **Figure 4-2**. The results show that for all bacterial strains, biocide type, and concentration of biocide tested, lower PBS concentrations appear to increase the sensitivity of bacteria upon exposure to CTAB or Grotan® BK biocides leading to an amplified increase or decrease in fluorescence signal with respect to the control fluorescence signal (exposure to Milli-Q water).

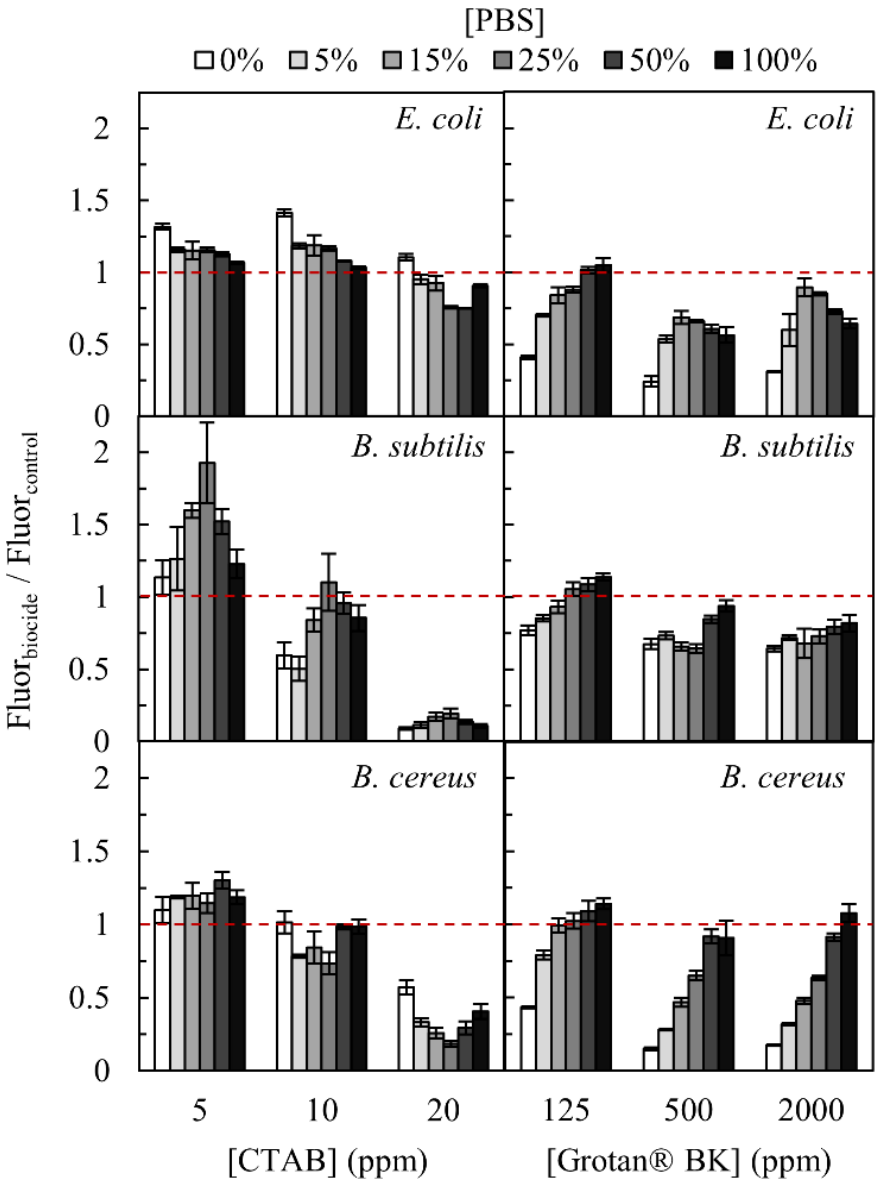

Figure 4-2. *E. coli*, *B. subtilis*, and *B. cereus* bacterial strains exposed to CTAB at 5, 10, 20 ppm and Grotan® BK at 125, 500, 2000 ppm when stored in six different PBS solutions (0, 5, 15, 25, 50, 100%). The responses are reported as the average of duplicate measurements as normalized fluorescence signals ($Fluorescence_{biocide}$ / $Fluorescence_{control}$). The control solution used was Milli-Q water. The number of bacteria exposed to CTAB was approximately $9.1 \pm 0.1 \times 10^7$, $2.5 \pm 0.2 \times 10^7$, and $1.3 \pm 0.1 \times 10^7$ for *E. coli*, *B. subtilis*, and *B. cereus*, respectively. The number of bacteria exposed to Grotan® BK was approximately $7.5 \pm 0.3 \times 10^7$, $5.0 \pm 0.2 \times 10^7$, $1.3 \pm 0.1 \times 10^7$ for *E. coli*, *B. subtilis*, and *B. cereus*, respectively.

This amplified response is clearly seen when *B. cereus* is exposed to Grotan® BK at 125, 500, and 2000 ppm. The result shows that a lower PBS concentration is required to detect lower concentrations of Grotan® BK. For example, when using a 100% PBS solution, the normalized fluorescence signals for all three concentrations of Grotan® BK remain close to 1.0. This implies that *B. cereus* stored in 100% PBS solution cannot be used to detect Grotan® BK at either of these biocide concentrations. However, when a 25% PBS solution is used, the normalized fluorescence signals for 125, 500, and 2000 ppm of Grotan® BK are 1.02 ± 0.05, 0.65 ± 0.03, and 0.63 ± 0.01, respectively. When a 5% PBS solution is used, the normalized fluorescence signals are lower at 0.79 ± 0.02, 0.28 ± 0.01, and 0.32 ± 0.01, respectively. For *B. subtilis*, the trend is similar but the fluorescence signals are less pronounced. This may be due to several reasons that are bacterial strain specific. For example, it has been shown that *B. subtilis* expresses approximately three times as many genes upon exposure to stressful environments (e.g. acidity) compared to *B. cereus*.[34] An increase in the number of bacteria ($\sim 5.0 \times 10^7$ for *B. subtilis* vs. $\sim 1.3 \times 10^7$ for *B. cereus*) that are being exposed to toxic analytes is another explanation for less pronounced fluorescence signals; a greater number of bacteria will reduce the number of biocide molecules per cell.

Table 4-1 highlights the PBS concentration (0, 5, 15, 25, 50, or 100%) which gives the largest decrease or increase in the fluorescence signal for each of the three bacterial strains when exposed to CTAB (5, 10, 20 ppm) and Grotan® BK (125, 500, 2000 ppm). As previously mentioned, lower concentrations of PBS are shown to improve the LOD. High salinity conditions have been shown to reduce the permeability of the membrane of *H. elongatta* via tightening of the cell membrane thereby reducing the amount of toxic analytes

entering the cell.[18] This principle could explain the reduced biocidal tolerance when lower concentrations of PBS are used, which results in an improved detection capability observed by a larger decrease or increase in the fluorescence signal. A larger permeability may allow for a larger influx of the dyes present in the water and thus, in most cases, a decrease in fluorescence signal (propidium iodide has preferential binding) will be observed.

Table 4-1. PBS solution condition which achieved the largest decrease or increase in the fluorescence signal for *E. coli*, *B. subtilis* and *B. cereus* at 5, 10, and 20 ppm CTAB and 125, 500, and 2000 ppm Grotan® BK based on the data in Figure 4-1. The PBS solution condition which achieved the largest decrease of increase in the fluorescence signal for *B. cereus* at 5 ppm CTAB and *B. subtilis* at 2000 ppm Grotan® BK was inconclusive and is therefore represented by a dashed line.

Bacteria	[CTAB] (ppm)			[Grotan] (ppm)		
	5	10	20	125	500	2000
E. coli	0%	0%	25, 50%	0%	0%	0%
B. subtilis	25%	0, 5%	0%	0%	0, 5, 15, 25%	-
B. cereus	-	5, 15, 25%	25%	0%	0%	0%

Interestingly, in some cases (see **Table 4-1**), 0% PBS (pure Milli-Q water) does not result in the lowest LOD. An example of this is seen when *B. subtilis* is prepared in 25% PBS and is exposed to 5 ppm of CTAB (**Figure 4-2**). It is important to note that since slightly more *B. subtilis* bacteria ($\sim 2.5 \times 10^7$) were used in this experiment in comparison to **Figure 4-1** ($\sim 1.9 \times 10^7$), the fluorescence signals are elevated since it becomes more difficult to kill higher amounts/numbers of bacteria (see section 4.3.3). We believe that at this concentration of PBS and CTAB, a fluorescence signal drop is counteracted by an increase in the cellular activity resulting in a net increase of the fluorescence signal. A further decrease in the PBS concentration will lead to an additional increase in the permeability of the membrane resulting in an eventual influx of propidium iodide, thereby reducing the overall net increase

in the fluorescence signal; in most cases, a net decrease in the fluorescence signal is observed. We suspect that these phenomena are not mutually exclusive and lead to the parabolic trend displayed for each of the three CTAB concentrations for *B. subtilis*.

4.4.3 Tuning the sensitivity of bacteria: manipulating number of bacteria

As previously mentioned, decreasing the number of bacteria exposed to biocides is another simple method that can be used in conjunction with manipulating the PBS concentration to improve the LOD of biocides. This effect is highlighted in **Figure 4-3**, where a wider range of CTAB and Grotan® BK concentrations were tested; only the PBS concentration that was deemed to be the most effective at discriminating between the control (Milli-Q water) and the lowest concentration of CTAB and Grotan® BK from **Figure 4-2** was used. For *B. cereus* in combination with CTAB, 25% PBS was selected since it was the most effective and recurrent for both 10 and 20 ppm of CTAB. Lower concentrations of each biocide were selected to show that lower concentrations of biocide could be detected using this simple method. For example, 0.625 ppm of CTAB could only be detected by *E. coli* when diluted 1.5^4-times (~5-times diluted) corresponding to $\sim 1.9 \times 10^7$ cells. For *B. subtilis*, 0.625 ppm of CTAB became detectable (increase in fluorescence signal) when diluted 1.5^2-times (2.25-times diluted) corresponding to $\sim 0.8 \times 10^7$ cells. However, for *B. cereus*, the results show neither of the three concentrations of bacteria could detect 0.625 ppm of CTAB. Nevertheless, decreasing the number of bacteria for *B. cereus* was still effective; the normalized fluorescence signal when using 5 ppm of CTAB dropped from 0.86 ± 0.09 to 0.53 ± 0.05, corresponding to $\sim 0.9 \times 10^7$ cells and $\sim 0.4 \times 10^7$ cells, respectively. Similar trends are

shown when *B. subtilis* and *B. cereus* are exposed to Grotan® BK, however strangely, *E. coli* reports the opposite trend. This *E. coli*-Grotan® BK result was repeated twice and yielded the same result (result not shown). We suspect that the exposure of the selected Grotan® BK concentrations may be the reason for the increase in the fluorescence signal as the number of bacteria decreases; when *E. coli* was exposed to 0.625, 1.25, 2.5, 5, and 10 ppm of CTAB, the fluorescence signal either remained the same, or increased (as with Grotan® BK). However, at 20 and 40 ppm CTAB, the fluorescence signals for *E. coli* decreased as the number of bacteria was decreased (representative of the trends for *B. subtilis* and *B. cereus*). In other words, we believe the trend would have aligned with that of *B. subtilis* and *B. cereus* if higher concentrations of Grotan® BK were tested.

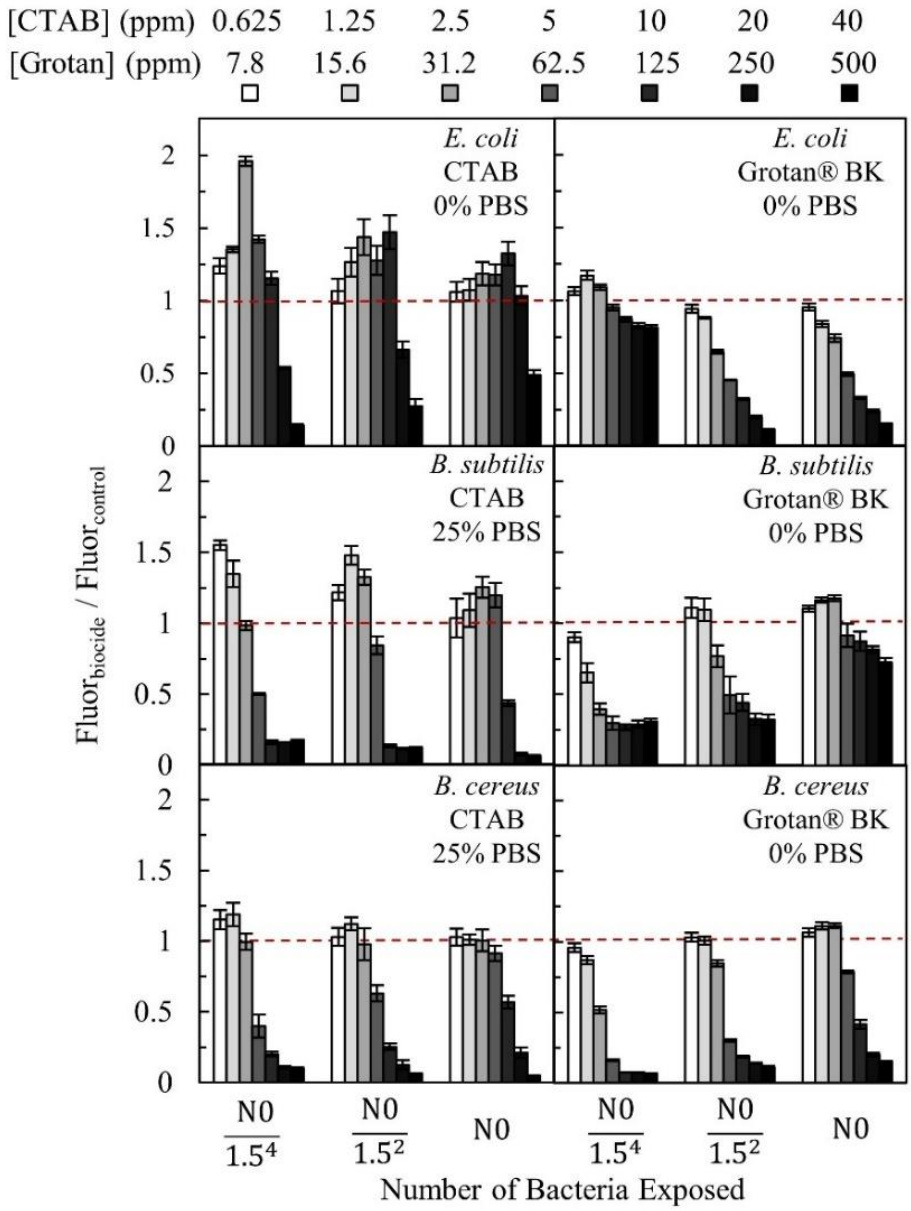

Figure 4-3. Normalized fluorescence signals ($Fluor_{biocide}/Fluor_{control}$) for *E. coli*, *B. subtilis*, and *B. cereus* bacterial strains exposed to CTAB at 0.625, 1.25, 2.5 5, 10, 20 and 40 ppm and Grotan® BK at 7.8, 15.6, 31.2, 62.5, 125, 250, and 500 ppm for three different amounts/numbers of bacteria (N0, N0 diluted 1.5^2-times, N0 diluted 1.5^4-times) for each bacterial strains when stored in the PBS solution which produces the largest increase or decrease in the fluorescence signal when exposed to lowest biocide concentration as shown in **Table 4-1**. The number of bacteria exposed to CTAB for N0 was approximately $9.4 \pm 0.8 \times 10^7$, $1.9 \pm 0.1 \times 10^7$, and $0.9 \pm 0.1 \times 10^7$ for *E. coli*, *B. subtilis*, and *B. cereus*, respectively. The

number of bacteria exposed to Grotan® BK for N0 was approximately and $1.2 \pm 0.1 \times 10^8$, $5.4 \pm 0.8 \times 10^7$, $1.1 \pm 0.2 \times 10^7$ for *E. coli*, *B. subtilis*, and *B. cereus*, respectively.

From a practical point of view, having the ability to manipulate both the number of bacteria and PBS concentration offers advantages when testing the toxicity of biocide-containing samples (e.g. industrial WW samples). For example, depending on the toxicity of the sample, an appropriate number of bacteria for each strain could be selected and tested; 'kits' containing preserved cells of different numbers of bacteria could be readily available (e.g., high range, low range) without having to concentrate or dilute the cells. Our previous work focused on the preservation of *E. coli* as a model bacterial strain to assess the preservation performance of various solutions so that these 'kits' could be stored at room or refrigerated temperatures for extended periods of time (2-3 months).[28] Building on this knowledge and that of the literature,[35, 36] future developments will allow for these three bacterial strains to be stored in sugar-based films/tablets at different numbers of bacteria. The films are anticipated to be readily dissolvable in the PBS solution-of-choice in order to tune the sensitivity within the range of the testing sample's toxicity. For example, lower toxicity samples would require low PBS concentrations and low numbers of bacteria, while higher toxicity samples would require the opposite. The tunability of these three bacterial strains would be particularly useful in the context of testing the nitrification inhibition potential of partially treated industrial WWs (based on our previous work[16]) where there is a wide range in toxicity. Through this proof-of-concept work, it is now expected that samples that exhibit low nitrification inhibition (i.e., containing low concentrations of biocides) could be more easily detected with a greater resolution. For example, when 2.5 ppm and 5 ppm of

CTAB were tested with ~0.9×10^7 *B. cereus* cells, there was no measureable difference (1.00 ± 0.07 vs. 0.91 ± 0.05) between the two samples (poor resolution); both of these results would have predicted the same nitrification inhibition value. However, when ~0.2×10^7 *B. cereus* cells were used, a clear measurable difference (0.99 ± 0.06 vs. 0.40 ± 0.08) is observed.

4.4.4 Point-of-use biocide detection using a compact fluorometer

To improve the testing accessibility and to reduce the overall cost and footprint required to run these fluorescence-based toxicity tests, an inexpensive, compact, and commercially available Quantus™ fluorometer was tested as a proof-of-concept to replace the Tecan M200 microplate reader. The compact fluorometer can be connected a computer to transfer data generated in real-time. **Figure 4-4** shows the relationship between the two instruments for all three bacterial strains. Also, due to its widespread use in labelling and sensing biomolecules,[24] fluorescein dye was tested (without bacteria) to further demonstrate the strong relationship between the two instruments that can be observed based on the linear trend and slope value which is close to 1. We suspect that the slight offset of the slope is due to minor discrepancies of the wavelength parameters between the two instruments (see section 4.3.3).

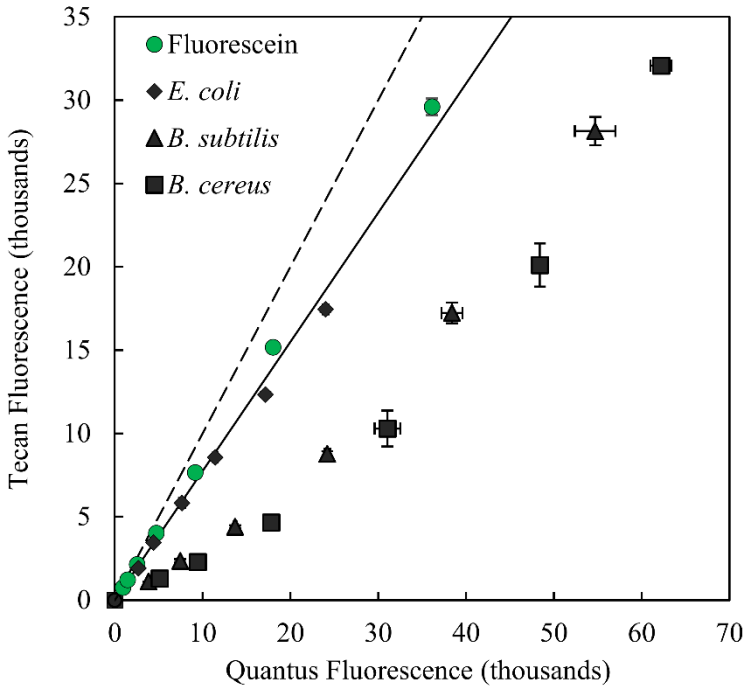

Figure 4-4. Tecan M200 microplate reader to Quantus fluorometer relationship reported as raw fluorescence signals (thousands) for fluorescein dye and for the three bacterial strains *E. coli*, *B. subtilis*, and *B. cereus*. The error bars correspond to the standard deviation of triplicate samples; the data points correspond to the average raw fluorescence signal. The triplicate samples correspond to three separate dilution series originating from the same bacterial stock. The top and bottom diagonal lines have slopes of 1 and 0.775 respectively to illustrate the variation from parity between the measurements from the Tecan and Quantus fluorometers. The solid diagonal line was created to capture a single trend which corresponds to the average slope for fluorescein and *E. coli*.

Interestingly, for both *B. subtilis* and *B. cereus*, the trends are non-linear, while the trend for *E. coli* is linear. It is hypothesized that the emission wavelengths are shifted when in the prescence of *B. subtilis* and *B. cereus*, which may be in part due to the Gram-positive structure of these two bacterial strains. Because the wavelength parameters of each instrument are slightly different, this hypothesized shift in the emission wavelengths would account for an unparalleled response between the two instruments that could contribute to the formation of a non-linear relationship. In a study by Dwarakanath et al.,[37] emission

wavelength shifts of greater than 140 nm were reported for quantum dots, a nano-sized fluorophore, when bound to bacterial strain surfaces. Another possible explanation for the shift in the emission wavelengths could be related to the similarities of the biofilms,[38-40] termed pellicles, for both *B. subtilis* and *B. cereus*, where similar proteins such as *tasA* – responsible for fiber network strengthening of the biofilm – and extracellular DNA (eDNA) have been shown to exist. Interestingly, Vilain et al. used the same fluorescent dye (containing SYTO 9 and propidium iodide) to assess the presence of eDNA present in the biofilm of *B. cereus*.[38] Upon exposure of these two strains to the fluorescent dye, an interaction between the biofilm proteins, eDNA and the dye may exist such that there is a shift in the emission maximum. A study by Koronakis et al.[41] showed that upon the binding of Trinitrophyl-ATP, a fluorescent molecule, to a *GST-bctp* protein (fused protein), the emission maximum decreased from approximately 542 nm to 532 nm.

To further demonstrate the transfer of the technology from the Tecan M200 microplate reader to the compact Quantus™ fluorometer, as a proof-of-concept using only one of the three bacterial strains, *B. cereus* was exposed to 5 ppm and 10 ppm of CTAB and read using both the Tecan M200 microplate reader and the Quantus™ fluorometer (**Figure 4-5**).

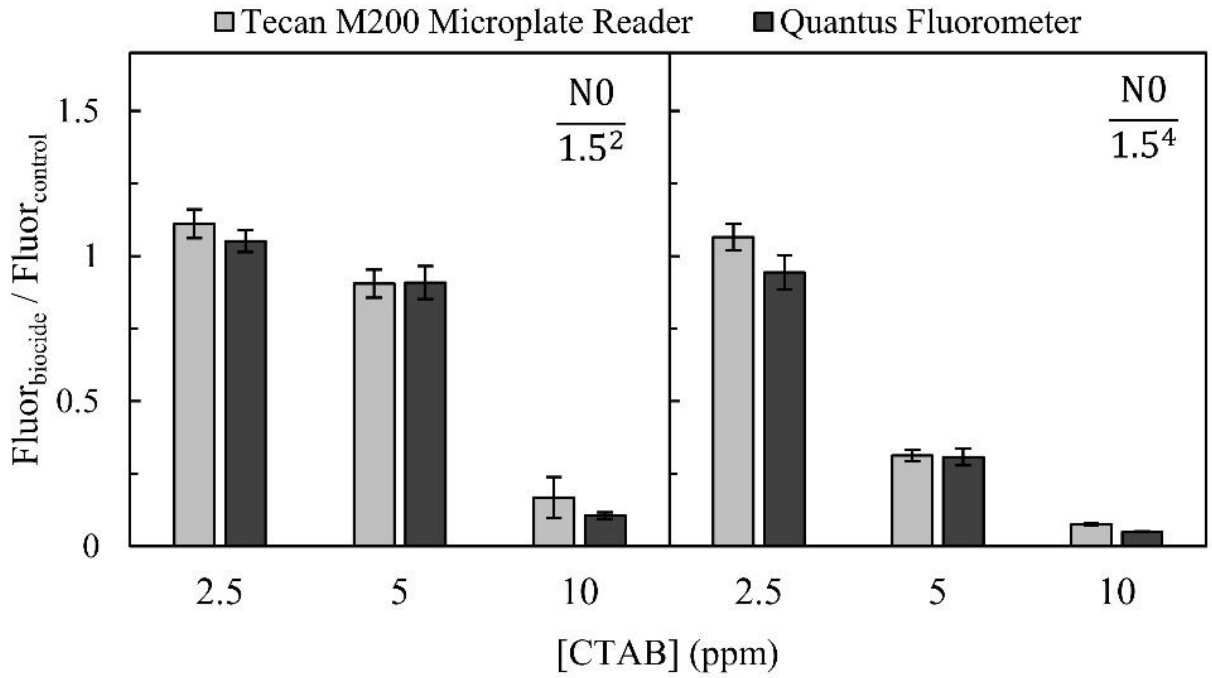

Figure 4-5. Normalized fluorescence signals ($Fluor_{biocide}/Fluor_{control}$) for *B. cereus* in 25% PBS exposed to 2.5 ppm, 5 ppm and 10 ppm CTAB using the Tecan M200 microplate reader and Quantus™ fluorometer. The raw fluorescence signals for the Quantus™ fluorometer were converted to Tecan M200 microplate reader signals according to the relationship in Figure 4-4. The error bars correspond to the standard deviation of triplicate samples. The number of bacteria exposed was approximately $0.6 \pm 0.2 \times 10^7$ for the $N0 \times 1.5^{-2}$ condition.

The raw fluorescence signals generated by the Quantus™ fluorometer were converted into the raw fluorescence signals for the Tecan M200 Microplate Reader via the relationship shown in **Figure 4-4**; this was a necessary step to provide an accurate comparison. This result further confirms that the relationship is reliable and that both instruments respond similarly.

4.5 Conclusion

Simple and easily adaptable methods such as manipulating the salinity content (PBS concentration) and the number of bacteria have been shown to improve the sensitivity of

biocide-induced fluorescence signals of the three bacterial strains (*E. coli*, *B. subtilis*, *B. cereus*) used as cell-based biosensors (CBBs) to predict nitrification performance. These tunable methods have vast implications to municipal and industrial WWTPs that accept WW by allowing for better discrimination of biocide-containing samples of similar toxicity, and improved detection capability of lower toxicity samples. As a result, WWTPs have the potential to make better-informed treatment decisions with a higher level of confidence that the increasingly stringent ammonia discharge requirements will be met. These implications also extend to the industrial companies at which the biocide-containing WWs are produced, however a lack of portable testing allows for inefficiencies that could result in the over-use of biocides. Therefore, this study shows the potential for a transfer of the technology to a compact device (Quantus™ fluorometer) allowing for point-of-use testing and obviating the need for laboratory testing performed using expensive and stationary microplate readers.

4.6 References

1. Vigneshvar, S., et al., *Recent advances in biosensor technology for potential applications–an overview.* Frontiers in bioengineering and biotechnology, 2016. **4**: p. 11.
2. Rodriguez-Mozaz, S., et al., *Biosensors for environmental monitoring A global perspective.* Talanta, 2005. **65**(2): p. 291-7.
3. Gui, Q., et al., *The application of whole cell-based biosensors for use in environmental analysis and in medical diagnostics.* Sensors, 2017. **17**(7): p. 1623.
4. Bousse, L., *Whole cell biosensors.* Sensors and Actuators B: Chemical, 1996. **34**(1-3): p. 270-275.
5. Siripong, S. and B.E. Rittmann, *Diversity study of nitrifying bacteria in full-scale municipal wastewater treatment plants.* Water Res, 2007. **41**(5): p. 1110-20.
6. Farré, M. and D. Barceló, *Toxicity testing of wastewater and sewage sludge by biosensors, bioassays and chemical analysis.* TrAC Trends in Analytical Chemistry, 2003. **22**(5): p. 299-310.
7. Maltby, L., *Small-Scale Freshwater Toxicity Investigations: Volume 1–Toxicity Test Methods*. 2007, Wiley Online Library.

8. Bollmann, U.E., et al., *Biocide Runoff from Building Facades: Degradation Kinetics in Soil.* Environ Sci Technol, 2017. **51**(7): p. 3694-3702.
9. Ortiz de Garcia, S.A., et al., *Ecotoxicity and environmental risk assessment of pharmaceuticals and personal care products in aquatic environments and wastewater treatment plants.* Ecotoxicology, 2014. **23**(8): p. 1517-33.
10. Ellis, J.B., *Pharmaceutical and personal care products (PPCPs) in urban receiving waters.* Environ Pollut, 2006. **144**(1): p. 184-9.
11. Ferrer, I., et al., *Determination of drugs in surface water and wastewater samples by liquid chromatography–mass spectrometry: methods and preliminary results including toxicity studies with Vibrio fischeri.* Journal of Chromatography A, 2001. **938**(1-2): p. 187-197.
12. Kunniger, T., et al., *Release and environmental impact of silver nanoparticles and conventional organic biocides from coated wooden facades.* Environ Pollut, 2014. **184**: p. 464-71.
13. Bye, C.M., R.M. Jones, and P.L. Dold, *Pragmatic Nitrification Inhibition Testing for Robust Plant Design.* Proceedings of the Water Environment Federation, 2012. **2012**(12): p. 4222-4238.
14. Mamais, D., et al., *Comparison of bioluminescence and nitrification inhibition methods for assessing toxicity to municipal activated sludge.* Water Environ Res, 2008. **80**(6): p. 484-9.
15. Jönsson, K., et al., *Occurrence of nitrification inhibition in Swedish municipal wastewaters.* Water Research, 2000. **34**(9): p. 2455-2462.
16. Morkus, P., et al., *A Rapid Assay to Assess Nitrification Inhibition Using a Panel of Bacterial Strains and Partial Least Squares Modeling.* Environ Sci Technol, 2019.
17. Canada, G.o. *Wastewater Systems Effluent Regulations*. 2012 [cited 2022 February 7]; Available from: https://laws-lois.justice.gc.ca/eng/regulations/SOR-2012-139/page-1.html.
18. Vreeland, R.H., R. Anderson, and R. Murray, *Cell wall and phospholipid composition and their contribution to the salt tolerance of Halomonas elongata.* Journal of bacteriology, 1984. **160**(3): p. 879-883.
19. Wood, J.M., *Osmosensing by bacteria: signals and membrane-based sensors.* Microbiology and molecular biology reviews, 1999. **63**(1): p. 230-262.
20. Probes, M., *LIVE/DEAD®BacLight Bacterial Viability Kits*. 2004.
21. Ramesh, S. and S. Rajeswari, *Corrosion inhibition of mild steel in neutral aqueous solution by new triazole derivatives.* Electrochimica Acta, 2004. **49**(5): p. 811-820.
22. Reddy, G.K.K., Y.V. Nancharaiah, and V.P. Venugopalan, *Long alkyl-chain imidazolium ionic liquids: Antibiofilm activity against phototrophic biofilms.* Colloids Surf B Biointerfaces, 2017. **155**: p. 487-496.
23. Mattsby-Baltzer, I., et al., *Microbial growth and accumulation in industrial metal-working fluids.* Applied and Environmental Microbiology, 1989. **55**(10): p. 2681-2689.
24. Zhou, P., et al., *The invalidity of the photo-induced electron transfer mechanism for fluorescein derivatives.* Phys Chem Chem Phys, 2012. **14**(43): p. 15191-8.

25. Sigma-Aldrich, *Fluorescein (F7505) - Product Information Sheet*.
26. BioSystems, T., *A Modulus™ Microplate Fluorometer Method for Fluorescein Measurement*.
27. Lebaron, P., N. Parthuisot, and P. Catala, *Comparison of blue nucleic acid dyes for flow cytometric enumeration of bacteria in aquatic systems.* Applied and environmental microbiology, 1998. **64**(5): p. 1725-1730.
28. Morkus, P., et al., *Optimization of microorganism preservation conditions for the development of an acute toxicity bioassay for biocides.* Chemosphere, 2019. **221**: p. 45-54.
29. D'souza, S., *Microbial biosensors.* Biosensors and Bioelectronics, 2001. **16**(6): p. 337-353.
30. Chen, C.Z. and S.L. Cooper, *Interactions between dendrimer biocides and bacterial membranes.* Biomaterials, 2002. **23**(16): p. 3359-3368.
31. Welch, W.J., *How cells respond to stress.* Scientific American, 1993. **268**(5): p. 56-64.
32. Giao, M.S., et al., *Validation of SYTO 9/propidium iodide uptake for rapid detection of viable but noncultivable Legionella pneumophila.* Microb Ecol, 2009. **58**(1): p. 56-62.
33. Brul, S., J. Nussbaum, and S. Dielbandhoesing, *Fluorescent probes for wall porosity and membrane integrity in filamentous fungi.* Journal of Microbiological Methods, 1997. **28**(3): p. 169-178.
34. Desriac, N., et al., *Bacillus cereus cell response upon exposure to acid environment: toward the identification of potential biomarkers.* Front Microbiol, 2013. **4**: p. 284.
35. Krumnow, A.A., et al., *Preservation of bacteria in natural polymers.* J Microbiol Methods, 2009. **78**(2): p. 189-94.
36. Jahanshahi-Anbuhi, S., et al., *Pullulan encapsulation of labile biomolecules to give stable bioassay tablets.* Angew Chem Int Ed Engl, 2014. **53**(24): p. 6155-8.
37. Dwarakanath, S., et al., *Quantum dot-antibody and aptamer conjugates shift fluorescence upon binding bacteria.* Biochem Biophys Res Commun, 2004. **325**(3): p. 739-43.
38. Vilain, S., et al., *DNA as an adhesin: Bacillus cereus requires extracellular DNA to form biofilms.* Appl Environ Microbiol, 2009. **75**(9): p. 2861-8.
39. Caro-Astorga, J., et al., *A genomic region involved in the formation of adhesin fibers in Bacillus cereus biofilms.* Front Microbiol, 2014. **5**: p. 745.
40. Majed, R., et al., *Bacillus cereus Biofilms-Same, Only Different.* Front Microbiol, 2016. **7**: p. 1054.
41. Koronakis, V., C. Hughes, and E. Koronakis, *ATPase activity and ATP/ADP-induced conformational change in the soluble domain of the bacterial protein translocator HlyB.* Molecular microbiology, 1993. **8**(6): p. 1163-1175.

5 Chapter 5: Miniaturization of an enclosed electrospinning process to enhance the reproducibility in the fabrication of rapidly dissolving cell-based biosensors

In this chapter, experiments were performed by myself, and undergraduate students Stephanie Sibbald, Lauren Choi, and Sarah Rassenberg, under my supervision. This chapter was drafted by myself and edited by a technical editor Kris Pikl along with my academic supervisors, Dr. David R. Latulippe and Dr. Carlos D.M Filipe. This chapter and its appendix were submitted to *Wiley Biotechnology Journal*.

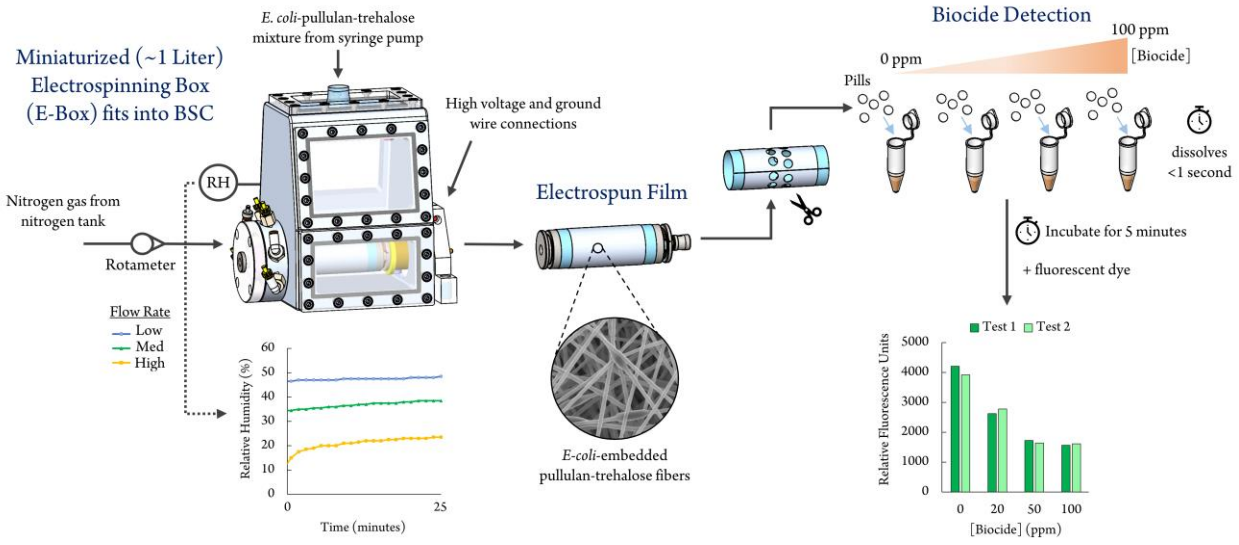

5.1 Abstract

There is widespread interest in using electrospun films produced directly in the presence of biological materials to create a range of products, including fibroblast-embedded tissue patches and bacteria-encapsulated bioanodes. However, the creation of such products can be highly challenging, as electrospinning is difficult, if not impossible, under certain environmental conditions. Furthermore, while a variety of commercial electrospinning systems exist, they are expensive (>$10,000) and few allow users to control environmental conditions (i.e., relative humidity (RH)). In addition, these systems are often too large to fit into biological safety cabinets (BSCs), which necessitates the use of filters/exhaust fans to ensure that the appropriate biosafety levels are met, as well as to mitigate the emission of air pollution. In this work, we build an inexpensive (~$700), miniaturized (one liter), predominantly 3D-printed enclosed electrospinning box (E-Box) that can be integrated with an inexpensive (~$300) computerized numerical control (CNC) machine and easily installed in a typical Class II Type A2 BSC. Using this system, we address the challenges of producing *E. coli*-embedded sugar (pullulan-trehalose) films that are rapidly (<1 second) dissolvable in water. In doing so, we demonstrate our system's ability to enable the rapid control of RH—which significantly impacts the quality of the resultant electrospun films and the properties of the fibers—by conducting electrospinning at 22%, 36%, and 48% RH. Our findings showed that the average fiber diameter decreased from 314 ± 8 to 240 ± 11 nm when the RH was raised from 22% to 48%. Interestingly, the findings also revealed that reproducibility in film production (number of droplets, film width) was greatest at 36% RH. Therefore, "pills" hole-punched from *E-coli*-embedded films at 36% RH were utilized to detect three

concentrations of two model biocides: Grotan® BK and triclosan. A fluorescent dye was used to probe membrane integrity and cellular activity, and a limit of detection of at least 20 ppm was achieved for both biocides. These results confirm that this convenient electrospinning tool can be used to create *E-coli*-embedded sugar films capable of detecting biocides. Moreover, the results of this work demonstrate that the developed device not only makes electrospinning possible for agents that require operation under strict biosafety conditions, but it also enables the production of highly reproducible materials through the accurate and rapid control of RH.

5.2 Introduction

Electrospinning entails the creation of nano-sized polymeric fibers under the influence of a strong electric field.[1] In this process, a sufficient electrical charge is applied to the body of a polymer solution, which creates electrostatic forces capable of overcoming the solution's surface tension. This rupture in the surface tension causes a cylindrical fiber to be drawn from an extruding polymeric droplet, which is then directed towards a grounded conductive roller.[2] Over time, this process results in the production of a dry matured film made up of several fibers. Since first being observed in the late 1960s,[3] this phenomenon has been harnessed in various applications, including nanocatalysis, filtration, and tissue engineering.[4] However, electrospinning is not without its challenges. Solution attributes such as concentration, conductivity, viscosity, surface tension, and homogeneity, and process parameters such as applied voltage, flow rate, distance between the spinneret and collector, and ambient conditions (e.g., temperature, relative humidity (RH), air flow) must all be

considered when attempting to create a desired film, all while ensuring reproducibility.[5] With regards to ambient conditions, it has been well-documented that temperature and RH greatly affects the electrospinning process.[2, 6, 7] Although the exact influence of the ambient conditions may be solution specific, they are known to impact the morphology (e.g., fiber diameter) of the nanofibers in general.[8] In addition, the ambient conditions are also known to impact atmospheric effects in the voltage field, which results in charge dispersion and increases the potential of the fibers being deposited on unwanted surfaces[9] (henceforth referred to as "off-target fiber deposition"). Thus, it is critical to control the ambient conditions during electrospinning.

There are examples of commercially available stand-alone electrospinning systems (e.g., Spinbox Systems®, Inovenso, nanoScience Instruments) that vary in size, complexity, and features offered; however, such systems can cost tens of thousands of dollars.[10] Researchers exploring the use of electrospinning as a tool in proof-of-concept experimental work are often unwilling to spend such large sums, and instead opt to source pre-owned high-voltage supplies and readily available laboratory syringe pumps to develop their own electrospinning systems at a fraction of the cost.[10] One of the major challenges in achieving consistent electrospinning performance is the ability to control the environmental conditions, particularly RH, which, as previously mentioned, greatly affects the electrospinning process. Temperature is less prone to fluctuation in laboratory settings due to pre-existing room-temperature control systems; however if higher- or lower-than-room temperature settings are required, options such as electrically heated coil elements[11] can be used, or the temperature of the solution can be heated or cooled prior to electrospinning.[12]

Researchers have employed a number of approaches to control RH, such as installing humidifiers[13] or dehumidifiers[14, 15] in close proximity to the electrospinning system, or enclosing the electrospinning environment in a self-made enclosed box to allow the inflow of a gas (e.g., air or nitrogen) with a desirable RH, which can be manipulated via a humidifier[16, 17] or desiccator column.[18]

Nonetheless, building an enclosed electrospinning system can be challenging. For those seeking to use biological materials in their electrospinning work and/or protect the user from air pollution caused by solvent evaporation,[11] it is necessary to install auxiliary units such as high-efficiency particulate absorbing (HEPA) or ultra-low particulate air (ULPA) filters and exhaust fans, thus increasing the complexity and overall cost of the setup. Biological safety cabinets (BSCs), which are commonly found in laboratories, are already equipped with the above units and can therefore be used to conduct such "specialty" electrospinning work. However, enclosed electrospinning systems are often large (excluding syringe pumps and high-voltage supply attachments) and do not fit easily (or at all) into BSCs, which presents a significant challenge. As such, there is a clear need to develop a smaller, low-cost enclosed electrospinning system that can easily fit into a BSC, while also allowing the rapid manipulation of RH, which comes with the miniaturization of the electrospinning environment. In this study, we attempt to address this need by designing and constructing an inexpensive (~$700 CAD), miniature (1 L; 100 to 200 times smaller in volume compared to the commercially available enclosed systems shown in **Table D1**), predominantly 3D-printed electrospinning box (E-Box) that can be easily integrated with a readily available and inexpensive (~$300 CAD) computerized numerical control (CNC)

machine to enable collector rotation during electrospinning. The proposed E-Box is operated in a top-down orientation on top of the CNC machine, with the whole unit fitting easily into a common Class II, Type A2 biological safety cabinet, which is compatible with work using biological materials and is equipped to handle pollution caused by solvent evaporation.

The developed miniaturized electrospinning system was applied to create rapidly dissolvable films that contain bacteria, which act as cell-based biosensors capable of quickly (<10 minutes) detecting biocides commonly found in wastewaters. Electrospun films have desirable characteristics (e.g., large surface area, thin profiles) that help to enable rapid dissolution in hydrophilic solutions. Poly(vinyl alcohol) and poly(ethylene oxide) are two common polymers that have been used in electrospinning solutions to encapsulate a variety of biological materials, including bioactive molecules, bacteria, and viruses/phages. However, one common issue with such films is that they require 30-60 minutes to fully dissolve, which is inconvenient for our purpose. For example, a 60 minute dissolution time was used in two different studies involving poly(vinyl alcohol) electrospun films embedded with bacteria (*E. coli*, *S. albus, B. animalis*) and bacterial viruses (T7, T4, λ),[19, 20] while a 30 minute dissolution time of encapsulated T4 phage in a poly(ethylene oxide) film was reported in another study.[21] Since sugars possess properties that facilitate easy dissolution in water, we elected to employ a sugar-based formulation comprised of pullulan and trehalose, as these particular sugars are known for stabilizing biological materials when present in a dried format.[22-24] In this work, we demonstrate the challenges associated with electrospinning this sugar-based solution in our enclosed miniature environment, and we discuss our miniature electrospinning system's applicability for the reproducible production

of *E. coli*-embedded pills—derived from the films—for use in the detection of Grotan® BK, a common industrial biocide,[25] and triclosan, a biocide and contaminant of emerging concern.[26]

5.3 Materials & Methods

5.3.1 Electrospinning casing and system assembly

The miniature E-Box is a custom device made up of six 3D-printed ABS-M30 parts: a frame base, a drive unit tube end, a left/support side roller housing end, a tooling end retainer, a roller housing center support, and an antirotate plate. These components were prepared individually using a FORTUS 450mc 3D printer (Stratasys), which featured a 1 L inner volume and is easy to assemble. The other main parts of the E-Box (not 3D printed) were machined from stainless steel 304, and include the roller center support, the die spring housing, the drive shaft adapter, and the roller (diameter = 2.54 cm; length available for aluminum foil = 7.6 cm). The windows of the E-Box were cut from clear Lexan sheets using the CNC machine, and the seals were manually cut from nitrite rubber sheets (Misumi Corp.). Self-tapping copper inserts (SPIROL Industries Ltd.) were installed in the 3D printed frame base to enable the easy installation and removal of the windows, which were affixed with hex socket head cap screws (McMaster-Carr). Deep groove ball bearings (Misumi Corp) were "snapped in" to the 3D-printed drive unit tube end and the tooling end retainer to allow the roller to rotate inside the E-Box. Assembly and detailed drawings of the electrospinning are shown in Appendix D.

As shown in **Figure 5-1**, the 3D-printed miniaturized E-Box sits just above the base of a CNC 3018 Pro GRBL Control DIY Mini CNC Machine (TopDirect) and between the lathe revolving centre (TopDirect) on the support side and the drive side. The top-facing side of the E-Box contains a cross-section of a standard rubber balloon, with the lip of the balloon facing outwards to allow for the spinneret-fitting assembly to be partially inserted into the E-Box. The spinneret-fitting assembly is held in place by a support plate connected to the spinneret motor. The spinneret motor provides the spinneret-fitting assembly with 3-axis movement, which can be controlled by the user, while the balloon acts as an elastic bellow that allows the spinneret to move freely within the bounds of the top retainer opening, while ensuring an enclosed environment, regardless of the spinneret's positioning. The E-Box is equipped with two ports on the drive side wall. The first port allows an insulated ground wire to be connected between the roller (which sits in a grooved ring) and the ground of the high-voltage power supply (Bertan series 230), while the second port allows an insulated wire to be connected between the high-voltage power supply and the spinneret (18-gauge blunted tip) to supply the charge. These connections allow electrospun fibers to form on the aluminum foil substrate that is wrapped and taped around the roller during the electrospinning process. To replace the substrate, the tooling end retainer is first opened by removing the four hex socket head cap screws affixing it to the E-Box, and the roller is then disconnected from the drive shaft adapter by loosening a set screw; once the substrate has been replaced, the roller is re-installed and the tooling end retainer is re-secured. For rapid (~1 min) substrate replacement, the substrate can be simply peeled off the roller after the front window of the E-Box is removed by unscrewing the hex socket head cap screws. Figures

S1 and S2 of the SI show real images of the designed setup inside of a Baker SterilGARD III Advance° SG403A Class II, Type A2 Biological Safety Cabinet (The Baker Company).

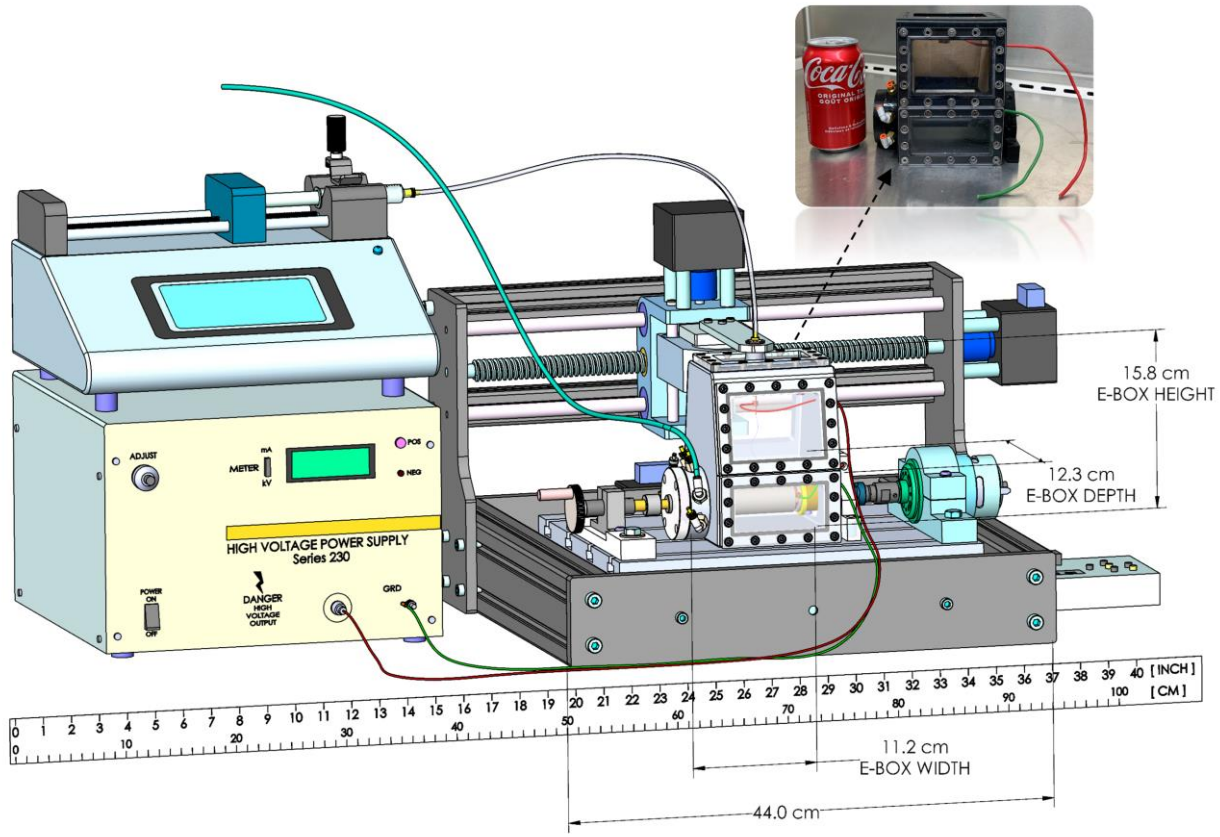

Figure 5-1. CAD design (SolidWorks) of the miniaturized electrospinning system, syringe pump, and Bertan Series 230 High-Voltage Power Supply. The 3D-printed miniaturized E-Box sits between the lathe revolving centre on the support side of the E-Box and the drive side and is placed on the base of the CNC 3018 Pro GRBL Control DIY Mini CNC Machine. A balloon, which acts as an elastic bellow, is fitted on the top portion of the E-Box to allow for spinneret access and the added benefit of 2-axis spinneret movement via the spinneret motor. The long blueish-green tubing exiting the E-Box connects to a nitrogen tank, which allows for the manipulation of the RH inside the E-box. A 1:1 scale bar in inches and centimeters is provided. An image of the E-Box next to a Coke is provided to help visualize the small size of the E-Box. Real images of the setup are provided in Figures A5-1 and A5-2.

5.3.2 Formation of electrospun cell-based biosensors

Escherichia coli DH5α, provided by the Biointerfaces Institute at McMaster University, were grown in Lysogeny broth (LB) media (Sigma-Aldrich) in 14mL polystyrene round-bottom Falcon tubes in a Thermo MaxQ 8000 shaker incubator pre-set to 225 rpm for 18 h at 37˚C. Following incubation, 10 tubes, each containing 5 mL of solution, were combined into a 50 mL polystyrene Falcon tube and centrifuged for 8 min at 10˚C (Thermo Scientific Sorvall ST 40R). The supernatant was removed and replaced with 5 mL of the sugar solution to yield an *E. coli* concentration of approximately 2.3×10^9 cells/mL. The sugar solution consisted of 20% w/v 100 kDa desalinized pullulan (Polysciences, Inc.) and 0.5 M Trehalose dihydrate (Sigma) in Milli-Q water. Electrospinning runs were conducted with the sugar solution only (no *E. coli*) when assessing changes in the high-voltage supply and ground connections during the commissioning phase (**Figure 5-3**).

A sterile 5 mL BD syringe was loaded with 2 mL of the desired electrospinning solution (*E. coli*-sugar solution or sugar solution) and connected to the spinneret via a section of tubing. The syringe was then loaded onto a standard laboratory syringe pump, while the spinneret was attached to the top-facing side of the E-Box. From inside the E-Box, the high-voltage supply connection was affixed to the spinneret via a custom cylindrical fitting (see **Figure D4** in Appendix D), leaving 1 cm of space at the bottom of the spinneret; this connection was not manipulated. Clean cardboard inserts matching the shape of the E-Box's sides were wedged into the inside walls to help isolate the grounded roller from the E-Box. The syringe pump was adjusted until a droplet formed at the tip of the spinneret; the droplet was then collected with a tissue prior to beginning the electrospinning sequence.

The electrospinning sequence consisted of the following steps. First, the spinneret was centered 9 cm from tip to roller, which was a convenient distance for the E-Box due its miniature size, and a piece of aluminum foil (9.5 cm by 6.5 cm) was taped onto the roller. Rapid loading and unloading of the substrate was performed by removing the top front window between runs. Prior to electrospinning, one final cardboard insert was placed on the inside of the front window. Once the final cardboard insert had been installed, the CNC machine was turned on and the controller was used to initiate roller spinning at approximately 200 RPM. Simultaneously, the syringe pump was set to 2.5 μL/min, and the power supply was adjusted at a rate of 1kV per second up to the desired voltage of 14 kV. These conditions were selected based on the preliminary work described in Section 3.1. At the end of the electrospinning run, the syringe pump was stopped, the voltage was reduced to zero at a rate of 1kV/s, and the CNC machine was turned off. Next, the top front plate was unscrewed, the front cardboard insert was removed, the spinneret tip was wiped clean, and the now-coated aluminum foil was carefully removed. The cardboard inserts were only replaced between runs if a large degree of off-target fiber deposition (splattering) was observed; small amounts of splattering were wiped off with tissue.

The flow rate of nitrogen gas from of a nitrogen gas cylinder was controlled manually using a needle valve and monitored with a rotameter. The nitrogen gas downstream of the rotameter entered the support side of the E-Box via one of six quick-connect fittings through the long blueish-green tubing shown in **Figure 5-1**. The RH inside the E-box was monitored using a USB-502 RH/Temperature Data Logger (Measurement Computing).

5.3.3 Film characterization

Once the film had been created, the number of droplets dripping from the spinneret onto the film were counted visually and the width of the film was measured with a standard centimeter ruler. One random circular disc (d = 0.6 cm), known as a pill, was cut from each film using a single hole punch and imaged with a TESCAN VEGA-II LSU scanning electron microscope. Fiber diameter characterization was performed with ImageJ. The resultant SEM images (**Figure D6** Appendix D) were first auto-segmented using the Huang method from the Auto Threshold plugin, followed by manual segmentation to ensure that no partial fiber segments were present, the intersections of fibers did not contain black spots, and the segmented fibers accurately represented the fibers' actual diameters without including the background/imaging artifacts. The segmented images were analyzed using the DiameterJ plugin.

5.3.4 Detection of biocides via fluorescence assay of *E. coli*

The technical details for the two biocides used in this study are given below.

- Triclosan, or 5-chloro-2-(2,4-dichlorophenoxy)phenol, is a broad-spectrum antibacterial agent that has been found to be effective against many Gram-negative and Gram-positive bacteria.[27]

  Triclosan is sparingly soluble in aqueous buffers; thus, a 100 ppm stock was prepared in a 1:3 solution of ethanol:PBS solution on days when experiments were being conducted with triclosan.

- Grotan® BK (Commercial Oil) contains 78.5% of Hexahydro-1,3,5,tris(2-hydroxyethyl)triazine and is commonly used to prevent the demulsification of metalworking fluids by controlling bacterial growth.[25, 28] A 100 ppm stock solution was prepared by diluting the as-received liquid solution with Milli-Q water.

After the creation of a film via electrospinning, 20 pills were punched out from its middle portion (1 cm left and 1 cm right from the center of film) and along its whole length. Note that film irregularities such as droplets were avoided during this process. The 20 pills were split randomly into four groups of 5 pills, with each group being dissolved in 1.7 mL microfuge tubes containing 100 µL of Milli-Q water. During dissolution, the microfuge tubes were vortexed twice for 10 seconds and pulsed twice using a Micro Centrifuge (Fisher Scientific).

After the pills had been dissolved, half of the solution (50 µL) in each tube was pipetted into a well in a 96-well Flat Bottom Black microplate (Eppendorf), followed by the addition of 50 µL of either Milli-Q water (control) or a biocide solution (Grotan® BK 20, 50, 100 ppm in Milli-Q water or triclosan 10, 20, 50 ppm in 1:3 solution of ethanol:PBS). After five minutes, 100 µL of dye solution was also added to each well, as per the instructions of the LIVE/DEAD™ BacLight™ Bacterial Viability Kit L7007 (Invitrogen). The plate was immediately placed inside an Infinite M200 Pro plate reader (TECAN) and the fluorescence signal was recorded over a 15-minute period. While the first fluorescence signal was recorded one minute after adding the dye, little change was observed in the signals over the 15-minute monitoring period (**Figure D7** in Appendix D). The fluorescence signal

monitoring was conducted using a default gain of 60, with excitation and emission wavelengths of 485 nm and 530 nm, respectively.

5.4 Results & Discussion

5.4.1 Mitigating off-target fiber deposition in the production of rapidly dissolvable electrospun films

Electrospinning in an enclosed miniaturized environment has its challenges. Although fiber deposition in electrospinning is focused on the grounded collector, other surfaces in the vicinity are also potential targets. Since fibers are highly charged, they are attracted to any surface (i.e., unwanted surfaces) close to the ground state.[9] This phenomenon is particularly problematic during electrospinning in an enclosed miniature environment, as these unwanted surfaces are much closer to the spinneret and jet trajectory. In this section, we highlight the challenges associated with electrospinning a pullulan-trehalose sugar solution in an enclosed miniature environment (E-Box) that is 100 to 200 times smaller by volume than commercially available enclosed electrospinning systems (see **Table D1** in Appendix D for dimensions). Pullulan has become widely used as a fast-dissolving sugar material in food products such as breath strips,[29] oral films for drug delivery,[30] paper-based colorimetric biosensors,[31] and microfluidic devices,[32] and it is also a well-documented stabilizing agent for many different biological materials, including bacteria,[22] bacteriophages, and enzymes.[23] Furthermore, the combination of trehalose and pullulan has been shown to be a particularly excellent pairing for bacteriophage antimicrobials.[24, 33] Electrospun films composed of pullulan are especially known for their fast-dissolving capability. In one study, Mehdi et al.[34] electrospun pullulan directly in the presence of the

migraine drug, rizatriptan, to form a fast-dissolving (within 1 s) oral drug-embedded fibrous material. **Figure 5-2** illustrates the rapid rate (near instant; < 1 s) at which our electrospun pullulan-trehalose strip (cut from a film) dissolves in water. As can be seen, the strip disappears upon breaching the air-water interface.

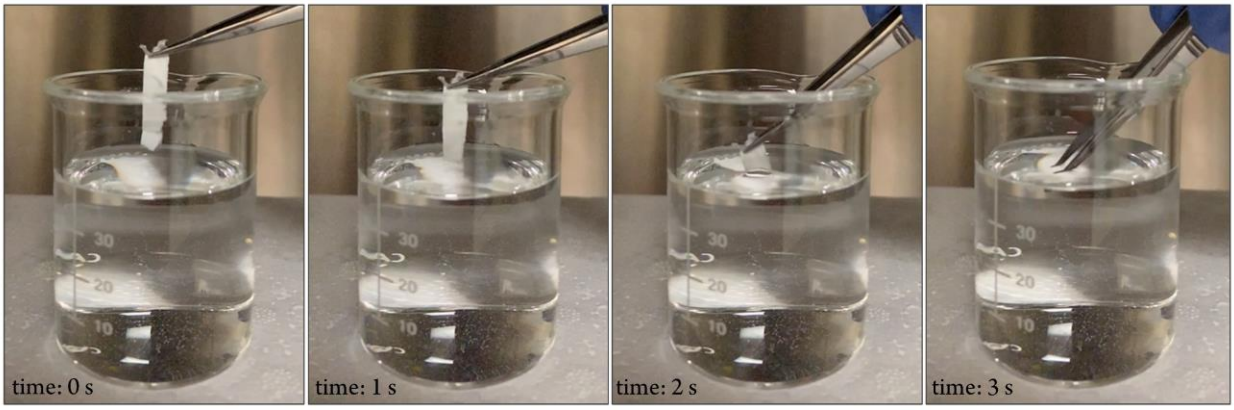

Figure 5-2. Timelapse of a section of a pullulan-trehalose film dissolving in water.

To successfully create a film in our miniaturized electrospinning environment, a series of design changes were investigated. Ultimately, electrospinning conditions of 2.5 µL/min at 14 kV were selected to reduce the amount of voltage-induced stress the *E. coli* would undergo, and to maximize the number of films that could be generated in a single day (by maximizing flow rate). These investigations revealed that it was difficult to form *E-coli*-embedded electrospun films at voltages below 14 kV, with efforts at 12 kV or below being entirely unsuccessful. At a higher flow rate (e.g., 3 µL/min), there was an imbalance between the solution flow rate and the fiber-formation rate, which resulted in the formation of an unstable droplet at the tip of the spinneret. The selected conditions allowed for the creation of 16 films over an 8-hour period (30 minutes per film: 24 minutes of electrospinning and 6 minutes for loading and unloading aluminum foil substrate). We began with a typical

electrospinning setup wherein the high-voltage supply is connected to the spinneret with an alligator clip, and we then varied the ground connection and spinneret location (**Figure 5-3** (*A*, *B*, *C*, *D*)). In *A*, the electrospun film (grey-filled rectangle) was consistently (tested three times) located off-center towards the drive side (right) of the roller where the ground was attached. The proximity of the outer right edge of the film to the edge of the roller led us believe that the fibers were most attracted to the location of the ground connection. Thus, the ground connection was relocated to the support side of the roller (*B*). As can be seen in *B,* this relocation caused the film to shift accordingly (left of *A*). Although the film location was centered, there was off-target fiber deposition (spattering) on some of the walls; the location and severity of this spatter is indicated by the colored circles (see **Figure A5-3** for an example of severe spatter). Neither changing the location of the ground connection (so it was on both the drive and support side (*C*)), nor the spinneret (*D*) was able to eliminate this off-target fiber deposition. We suspected that the irregular shape of the alligator clip—commonly used in electrospinning apparatuses[35-37]—led to an irregular electric field distribution, thus resulting in off-target fiber deposition on the inner walls of the E-Box. As such, we returned the ground connection to its original position on the drive side and changed the orientation of the alligator clip so it was positioned downwards/inline with the spinneret (*E→F)*. A visual inspection revealed that this change led to a reduction in the quantity of fibers deposited on the inner support, front, and drive-side walls of the E-Box. To improve on this outcome, the high-voltage connection was redesigned as a slim cylindrical fitting that was in-line and concentric with the spinneret (see middle image in **Figure D4** in Appendix D), which resulted in little-to-no splatter (no obvious visual indication) on all of

the inner E-Box walls. As shown in *G* and *H*, the developed cylindrical fitting enables the operation of the E-Box with different spinneret locations, while minimizing off-target fiber deposition. In the end, the center (0u, 0u) was selected as the final spinneret location (film result not shown). To further improve on this cylindrical design, a new cylindrical fitting equipped with a set screw was created to prevent spinneret-fitting slippage, thus establishing a stronger connection during electrospinning (see **Figure D4** in Appendix D). This modified cylindrical fitting was able to provide the same results as with the original slim cylindrical fitting.

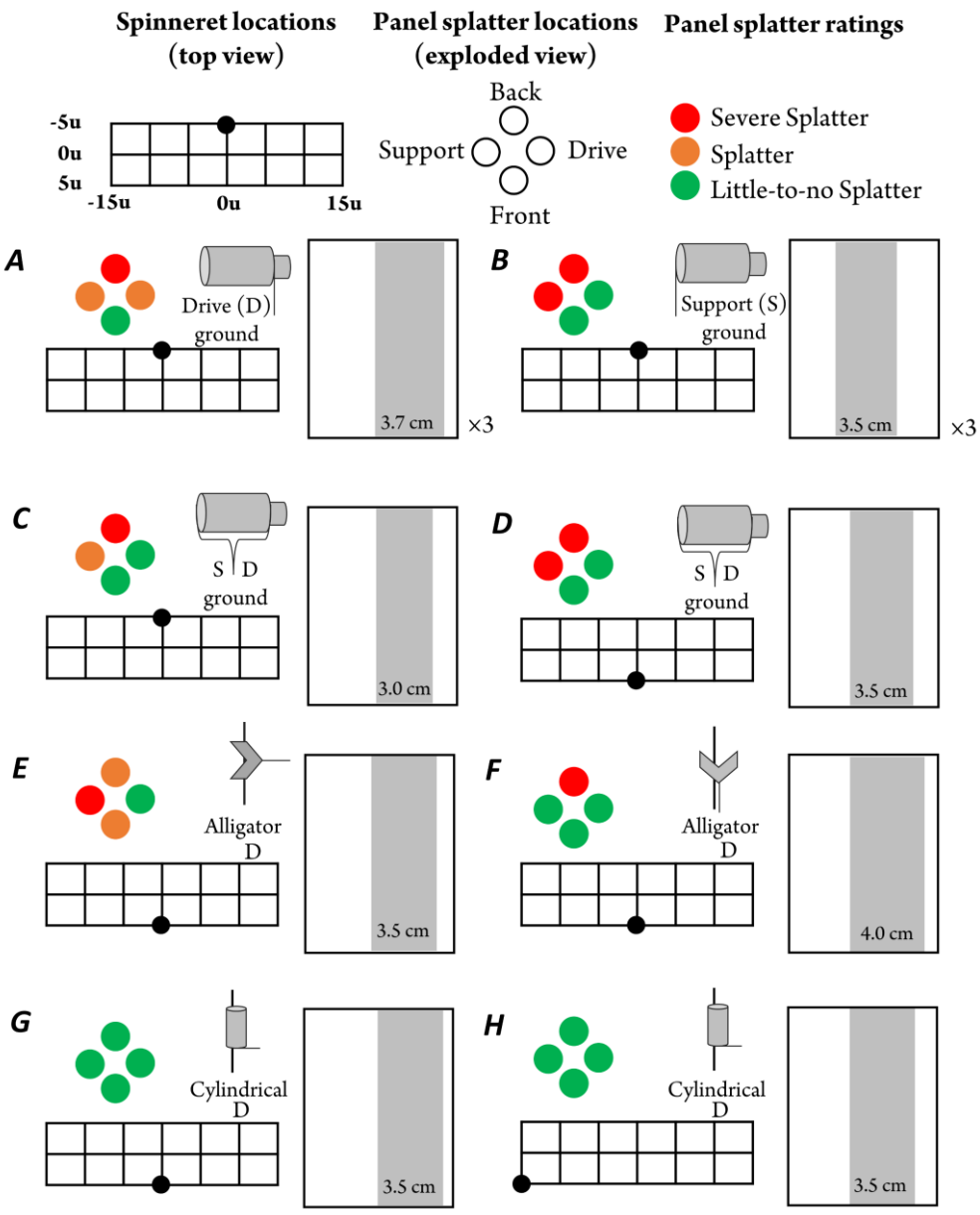

Figure 5-3. Eight different operating conditions (A-H) with varying ground connection orientations (ground attached to the support, drive, or support and drive side), top-view locations of the spinneret (black-filled circle), and high-voltage-to-spinneret connections (alligator, cylindrical). The grey-filled rectangle inside the larger white rectangle corresponds to the electrospun film after electrospinning on the aluminum foil substrate. All eight experiments were conducted using the standard 20% w/v pullulan-0.5 M trehalose solution, with a solution flow rate of 2.5 µL/min and a voltage of 14 kV. Conditions A-F used an alligator clip, while conditions E-H used a drive ground connection. Conditions E and F show different alligator clip orientations on the spinneret. In some cases (A and B),

experiments were conducted in triplicate (×3), as indicated next to the large white rectangle. E-H were operated with the ground connection on the drive side of the roller.

5.4.2 Relative humidity effects on electrospinning performance in a miniature environment

One of the main goals in this work was to create highly reproducible *E. coli*-embedded films that can be used to detect biocides. To this end, we electrospun a pullulan-trehalose sugar solution containing *E. coli* to make a film that could function as a sensor. Eight films were created back-to-back over a four-hour period under two conditions: one in which RH was uncontrolled, and one wherein RH was controlled within the E-Box by passing 5 LPM N_2 into the system for 3 minutes between electrospinning runs. Each run was 24 minutes in length, with an additional 6 minutes dedicated to RH manipulation (specific for an RH controlled experiment), unloading the sugar film-covered aluminum foil substrates, and reloading fresh aluminum foil substrates. As shown in **Figure 5-4**, increases in RH during an electrospinning run corresponded to the evaporation of water in the electrospinning solution; this effect was more pronounced in our miniature environment. In contrast, the decreases in RH corresponded to the opening of the E-Box between runs (uncontrolled condition) and the flow of nitrogen into the E-Box (controlled condition). Compared to the controlled RH condition, the electrospun films produced in the uncontrolled condition showed greater variation with respect to the number of droplets that hit the surface of the film, having a standard deviation of 10. Over the 4-hour production period, the RH increased from 26% to 44%; however, when the RH was controlled within a 4% range (34-38%) via nitrogen purging between runs, the variation in the number of droplets that hit the electrospun film had a standard deviation of 2. **Figure 5-4** also shows examples of an

uncontrolled and controlled film, which contain 17 and 7 droplets, respectively. During the electrospinning process, droplets are formed at the tip of the spinneret where there is an electrical potential difference between the droplet and the roller.[38] Unstable droplets are created due to a variety of reasons, which commonly include an imbalance in solution conditions (e.g., viscosity, surface tension), ambient conditions (e.g., temperature, RH), and electrospinning conditions (e.g., flow rate, voltage, spinning time, spinning orientation).[38] For example, long spin times and/or low surface-tension solutions are known to increase the tendency to disrupt fiber jets, which can lead to dripping.[39] Thus, it is not uncommon for droplets to drip downwards from the spinneret onto the collector when working with a top-down electrospinning setup.[39] In our case, this result was not surprising for the films generated at higher RHs in the uncontrolled condition, as environments with a higher RH are more conducive to the formation of new conductive pathways between the spinneret and collector, which can cause the droplets to be pulled in different directions, thus further destabilizing them.[40] Furthermore, a higher RH slows down solvent evaporation,[39] and thus, the gravitational effect on the droplet, which also increases the tendency for destabilization.

Although not explored in this study, our design allows the alignment of the spinneret and roller to be offset via the spinneret motor to help divert the droplets away from the roller. This feature also lends an element of customization to the electrospinning process, as it allows the user to harness a portion of the performance properties of a horizontal setup (as a result of the offset) while still predominantly operating in a top-down orientation. As documented in the literature, the orientation impacts the electrospinning process in a number of ways.[39] For example, a top-down orientation has been shown to provide greater

homogeneity in the electrospun film compared to horizontal systems.[39] This difference may be due to the fact that horizontal systems have gravity-affected trajectories.[41]

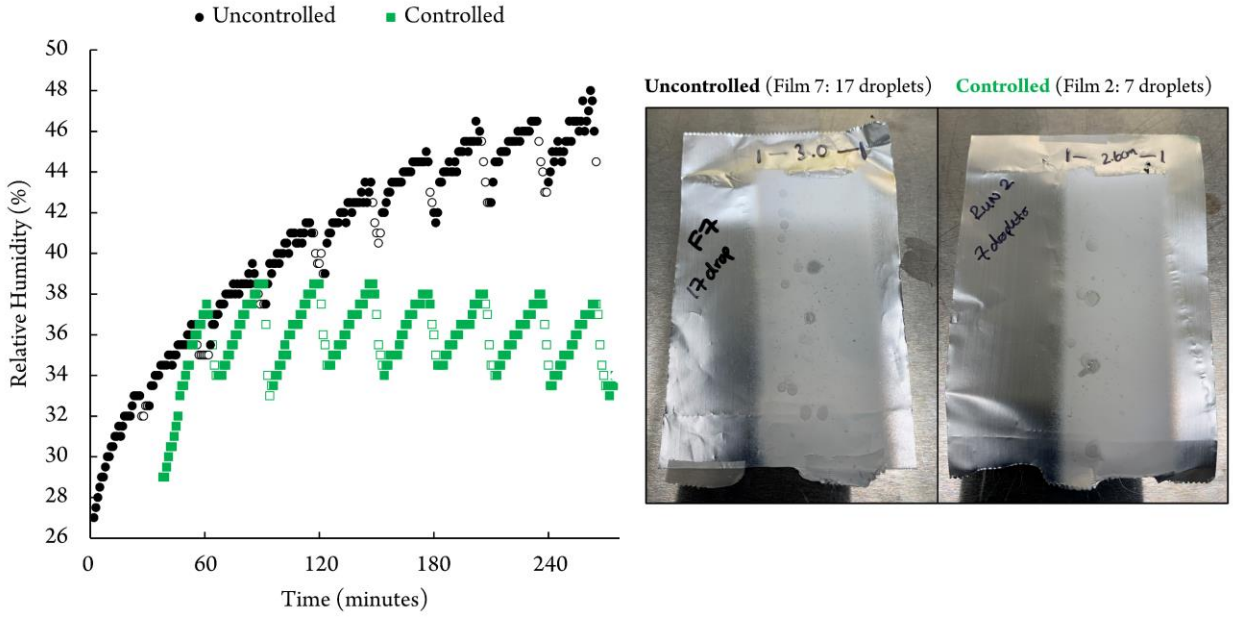

Figure 5-4. Left: RH measurements at 1-minute increments for 8 films created sequentially in uncontrolled (black filled circles) and controlled (green filled squares) settings. In the controlled condition, 5 LPM N_2 was passed into the system for 3 minutes between runs. The empty circles and empty squares correspond to the RH measurements between runs. Right: Image of an uncontrolled (Film 7) and controlled film (Film 2) showing the number of droplets on each film.

The ability to rapidly manipulate RH is one of the many benefits of electrospinning in a miniaturized enclosed environment. The results in **Figure 5-5** (left) demonstrate that the RH of the electrospinning system can be easily controlled at 22%, 36%, and 48% by nitrogen purging the E-Box for only a few minutes between runs. However, to achieve these RH targets from ambient conditions (prior to the first run), the E-Box was either nitrogen purged (for 22%), left at ambient RH (for 36%), or a table-top humidifier (Honeywell) was used to deliver humid air (for 48%) via a large flexible tubing to the front side of the E-Box after

removing the front window. The three films created at each target RH were controlled by passing 2 LPM N_2 (22%), 5 LPM N_2 (36%), and 10 LPM N_2 (48%) into the E-Box for 3, 3, and 6 minutes, respectively.

The fiber diameter distributions and average fiber diameters of the two films produced in the 22% and 48% RH conditions were compared. The middle panel of **Figure 5-5** shows the fiber-diameter distributions, which were generated via ImageJ (see section 2.3) using one SEM image from each of the four films. Bin sizes (e.g., 113-226, 226-339 nm) were also automatically generated in ImageJ. The y-axis of the bar graph denotes the number of fiber segments, with new fiber segments being defined by the intersection of one fiber with another. The right panel in **Figure 5-5** shows a section of an SEM image that was used to generate the fiber-diameter distribution for the 48% RH condition. As expected, the findings showed that controlling the RH had a significant impact in regulating both the fiber-diameter distribution and the average fiber diameter. The fiber-diameter distributions for the two RH conditions were offset from one another, with the 22% and 48% RH conditions having the largest number of fiber segments in the 226-339 nm bin (9534 ± 95 fiber segments, including standard deviation) and 113-226 nm bin (13326 ± 877 fiber segments, including standard deviation), respectively. The average fiber diameters (also determined using ImageJ) and the standard deviations for the 22% and 48% RH conditions were 314 ± 8 nm and 240 ± 11 nm, respectively. These results were expected, as lower RH increases the rate of solvent evaporation,[5, 39] which reduces the stretching/thinning of the fiber jet[42] as it travels towards the collector. However, electrospinning at 48% RH resulted in spattering on the inner walls

of the E-Box, whereas the inner walls of the system remained clean during operation at 22% and 36% RH. The off-target fiber deposition observed at 48% RH was likely due to an increase in the conductivity of the medium (moist air) inside the E-Box.[40] The use of moist air may cause the formation of new conductive pathways between the spinneret and collector, which can result in the formation of secondary jets, thus leading to off-target fiber deposition.[40]

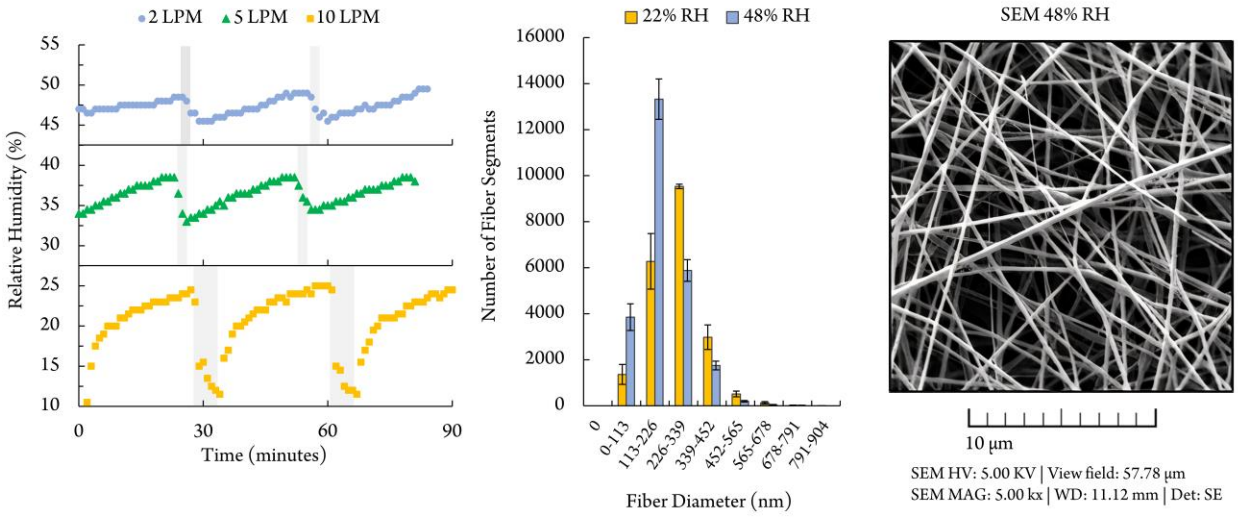

Figure 5-5. Left: RH measurements at 1-minute increments for three films created sequentially in experiments wherein RH was controlled at an average of 48% (blue solid circles), 36% (green solid triangles), and 22% (yellow solid squares). For dips in RH between runs/films (i.e., between Film 1 and Film 2, or Film 2 and Film 3), the background is highlighted in grey and corresponds to the nitrogen purging step required to reset the RH prior the next electrospinning run. Middle: Fiber-diameter distribution for two films produced at 22% RH (blue bars) and two films produced at 48% RH (yellow bars). Fiber-diameter distributions were generated by analyzing SEM images (one from each film) using ImageJ; an SEM image of a film created at the 48% RH condition is shown on the right. This analytical procedure is described in greater detail in Section 2.3. For each bin (e.g., 0-113, 113-226), the error bars correspond to the standard deviation of the number of fiber segments from two different films. Bin sizes were automatically generated in ImageJ.

Since the 48% RH condition resulted in excessive spattering, we explored the developed system's ability to produce 16 films back-to-back over an 8-hour period at 22% and 36% RH (**Figure 5-6**). A standard deviation of 2 was achieved for the number of droplets in both conditions (same result as in **Figure 5-3**). Interestingly, operating the system at 36% RH resulted in more consistent film formation with respect to film width size (2.7 ± 0.1 cm) compared to the 22% RH condition (3.5 ± 0.5 cm). This result suggests that there is an optimal RH for consistently producing films with similar widths. We believe that this outcome is a result of different jet-whipping instabilities,[43] which are dependent on the RH of the electrospinning environment. During the electrospinning process, the electrically charged jet undergoes whipping instability wherein it bends to form many expanding loops as it travels towards the collector.[44] It has been shown that poly(ethylene oxide) fibers electrospun at higher RHs have smaller radii of curvatures compared to those electrospun at lower RHs.[45] This finding suggests that fibers deviate further away (large radii of

curvature)[43] along the path to the collector at lower humidities, which explains the larger average film width (3.5 cm) observed at 22% RH compared to 48% RH (2.7 cm).

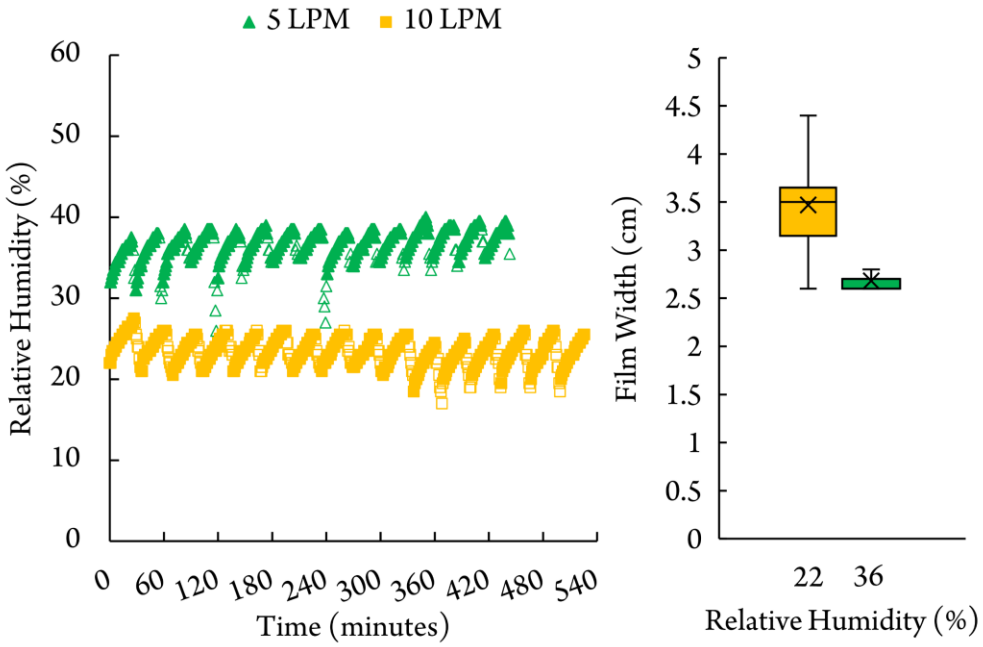

Figure 5-6. Left: RH measurements at 1-minute increments for 15 films created sequentially at 36% RH (green triangles) and 16 films created sequentially at 22% RH (yellow squares). Right: Box and whisker plot demonstrating the spread of the film widths after the electrospinning process at 22% and 36% RH. Dips in RH between runs/films are shown as empty green triangles and yellow squares and correspond to the nitrogen purging step required to reset the RH prior to the next electrospinning run.

5.4.3 Biocide detection as an application using *E. coli*-embedded sugar films

To demonstrate the practical applicability of our reproducible rapidly dissolving sugar films, we conducted a proof-of-concept study wherein we used the films to prepare *E. coli*-embedded pills, which served as biosensors for the detection of two different model biocides: Grotan® BK and triclosan. A commercially available fluorescent dye (see Section 2.4) was used to stain the *E. coli* after biocide exposure, and a fluorescence plate reader was used to read the fluorescence signal. The films prepared at 36% RH (**Figure 5-6)** were used

in this section of the study; the films prepared at 22% RH were not used due to the larger variation in film width from run to run. A total of four films prepared at 36% RH were randomly selected for use in this study: Film 1, Film 6, Film 11, and Film 13. Pills (see Section 2.4) derived from Film 11 and Film 13 were used to detect Grotan® BK, while pills derived from Film 1 and Film 6 were used to detect triclosan. The fluorescence signals, expressed in relative fluorescence units (RFU), are shown in **Figure 5-7**, with each bar corresponding to the fluorescence signal obtained by combining five pills from a corresponding film. The control fluorescence signals (exposure to Milli-Q water) were 4207 and 3922 for Film 11 and Film 13, and 3687 and 4197 for Film 6 and Film 1, respectively. As shown by the red line in **Figure 5-7**, the fluorescence signal of these films was 100 in the absence of the bacteria. Increasing the concentration of Grotan® BK caused the fluorescence signals of the two films to decrease to 2624 (Film 11) and 2779 (Film 13) RFU at 20 ppm, 1725 (Film 11) and 1639 (Film 13) RFU at 50 ppm, and 1564 (Film 11) and 1614 (Film 13) at 100 ppm. Similarly, the results revealed that increasing the triclosan concentration also caused the fluorescence signal to decrease: while the fluorescence signal remained approximately the same at 3790 (Film 6) and 3307 (Film 1) at 10 ppm, it decreased to 2205 (Film 6) and 2463 (Film 1) at 20 ppm and 407 (Film 6) and 422 (Film 1) at 50 ppm. These findings demonstrate that two randomly selected *E. coli*-embedded sugar films made at different times and exposed to different concentrations of different biocides are capable of yielding similar results across a wide range of fluorescence signals. While the attained limits of detection (at least 20 ppm for both Grotan® BK and triclosan) were significantly higher than those of traditional detection techniques, including gas chromatography-mass spectroscopy,[46] our technique is rapid (<10

minutes) and can be applied for the point-of-use detection of biocides if accompanied with a portable fluorometer, such as a Quantus™ Fluorometer (Promega).

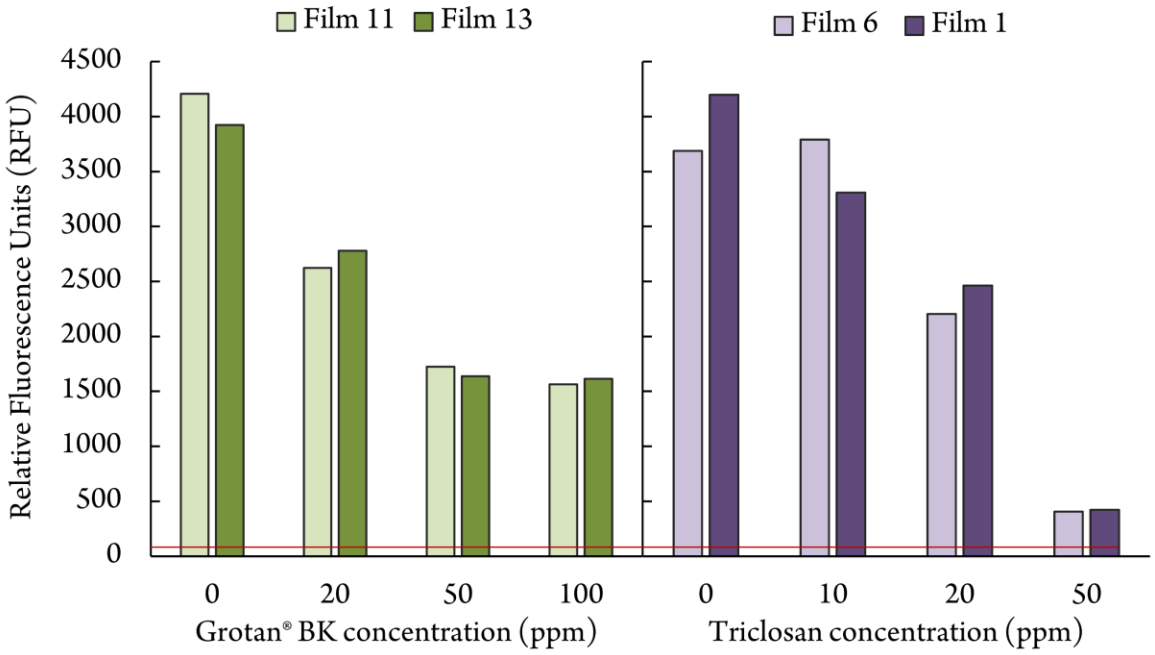

Figure 5-7. Fluorescence signals after exposing *E.coli*-pullulan-trehalose electrospun pills derived from films created at 36% RH (Figure 5) to three different concentrations of Grotan® BK (20, 50, 100 ppm) and triclosan (10, 20, 50 ppm) and a control (Milli-Q water). Each bar corresponds to the fluorescence signal obtained by combining 5 pills from a corresponding film. Film 11 and Film 13 were selected at random for the detection of Grotan® BK, while Film 6 and Film 1 were selected at random for the detection of triclosan. The red line corresponds to the fluorescence signal (100) of a control film with no bacteria

5.5 Conclusion

The electrospinning system presented in this paper obviates the need for HEPA filtration and ventilation system add-ons, as it easily fits into a commonly used Class II, Type A2 biological safety cabinet, which is already equipped to handle biological materials and pollutant solvent evaporation. In testing our in-house-built E-Box—which is miniature in

size, inexpensive, and predominantly 3D printed—we first found that it was necessary to change the high-voltage supply to the spinneret connection from a commonly used alligator clip to a cylindrical in-line and concentric fitting in order to mitigate off-target fiber deposition. Next, we demonstrated that RH is an important parameter that can easily be manipulated (in just a few minutes due to the relatively small 1 L electrospinning environment volume) to improve film quality reproducibility and to regulate the average fiber diameter and fiber-diameter distribution. We characterized film quality by visually inspecting variations in film width and the number of droplets originating from the outlet of the spinneret from run to run. Of the three different RHs tested, it was found film quality reproducibility was maximized at an RH of 36%. Finally, as a proof-of-concept, we prepared rapidly dissolvable *E. coli*-embedded pills derived from the films produced at 36% RH and demonstrated their ability to be used for the rapid detection (< 10 minutes) of two model biocides, namely, Grotan® BK and triclosan.

5.6 References

1. Xue, J., et al., *Electrospinning and electrospun nanofibers: Methods, materials, and applications.* Chemical reviews, 2019. **119**(8): p. 5298-5415.
2. Hardick, O., B. Stevens, and D.G. Bracewell, *Nanofibre fabrication in a temperature and humidity controlled environment for improved fibre consistency.* Journal of materials science, 2011. **46**(11): p. 3890-3898.
3. Taylor, G.I., *Electrically driven jets.* Proceedings of the Royal Society of London. A. Mathematical and Physical Sciences, 1969. **313**(1515): p. 453-475.
4. Bhardwaj, N. and S.C. Kundu, *Electrospinning: a fascinating fiber fabrication technique.* Biotechnology advances, 2010. **28**(3): p. 325-347.
5. Haider, A., S. Haider, and I.-K. Kang, *A comprehensive review summarizing the effect of electrospinning parameters and potential applications of nanofibers in biomedical and biotechnology.* Arabian Journal of Chemistry, 2018. **11**(8): p. 1165-1188.
6. De Vrieze, S., et al., *The effect of temperature and humidity on electrospinning.* Journal of materials science, 2009. **44**(5): p. 1357-1362.

7. Pelipenko, J., et al., *The impact of relative humidity during electrospinning on the morphology and mechanical properties of nanofibers.* International journal of pharmaceutics, 2013. **456**(1): p. 125-134.
8. Fashandi, H. and M. Karimi, *Comparative studies on the solvent quality and atmosphere humidity for electrospinning of nanoporous polyetherimide fibers.* Industrial & Engineering Chemistry Research, 2014. **53**(1): p. 235-245.
9. Feltz, K.P., et al., *A review of electrospinning manipulation techniques to direct fiber deposition and maximize pore size.* Electrospinning, 2017. **1**(1): p. 46-61.
10. Velasco Barraza, R., et al., *Designing a low cost electrospinning device for practical learning in a bioengineering biomaterials course.* Revista mexicana de ingeniería biomédica, 2016. **37**(1): p. 7-16.
11. Holmarc. *Nano Fiber Electrospinning Unit with Support*. 2020; Available from: https://www.holmarc.com/compact_nano_fiber_electrospinning_unit_with_support.php.
12. Ramazani, S. and M. Karimi, *Investigating the influence of temperature on electrospinning of polycaprolactone solutions.* e-Polymers, 2014. **14**(5): p. 323-333.
13. Xu, S., et al., *Electrospinning of native cellulose from nonvolatile solvent system.* Polymer, 2008. **49**(12): p. 2911-2917.
14. Lu, P. and Y. Xia, *Maneuvering the internal porosity and surface morphology of electrospun polystyrene yarns by controlling the solvent and relative humidity.* Langmuir, 2013. **29**(23): p. 7070-7078.
15. Jang, S., et al., *Optimization of electrospinning parameters for electrospun nanofiber-based triboelectric nanogenerators.* International Journal of Precision Engineering and Manufacturing-Green Technology, 2019. **6**(4): p. 731-739.
16. Ding, B., et al., *Formation of novel 2D polymer nanowebs via electrospinning.* Nanotechnology, 2006. **17**(15): p. 3685.
17. Casper, C.L., et al., *Controlling surface morphology of electrospun polystyrene fibers: effect of humidity and molecular weight in the electrospinning process.* Macromolecules, 2004. **37**(2): p. 573-578.
18. Huang, L., et al., *Controlling electrospun nanofiber morphology and mechanical properties using humidity.* Journal of polymer science part B: Polymer physics, 2011. **49**(24): p. 1734-1744.
19. Salalha, W., et al., *Encapsulation of bacteria and viruses in electrospun nanofibres.* Nanotechnology, 2006. **17**(18): p. 4675.
20. López-Rubio, A., et al., *Encapsulation of living bifidobacteria in ultrathin PVOH electrospun fibers.* Biomacromolecules, 2009. **10**(10): p. 2823-2829.
21. Korehei, R. and J.F. Kadla, *Encapsulation of T4 bacteriophage in electrospun poly (ethylene oxide)/cellulose diacetate fibers.* Carbohydrate polymers, 2014. **100**: p. 150-157.
22. Krumnow, A.A., et al., *Preservation of bacteria in natural polymers.* J Microbiol Methods, 2009. **78**(2): p. 189-94.
23. Jahanshahi-Anbuhi, S., et al., *Pullulan encapsulation of labile biomolecules to give stable bioassay tablets.* Angew Chem Int Ed Engl, 2014. **53**(24): p. 6155-8.

24. Leung, V., et al., *Long-term preservation of bacteriophage antimicrobials using sugar glasses.* ACS Biomaterials Science & Engineering, 2017. **4**(11): p. 3802-3808.
25. Urwin, C., J.C. Richardson, and A.K. Palmer, *An evaluation of the mutagenicity of the cutting oil preservative Grotan BK.* Mutation Research/Genetic Toxicology, 1976. **40**(1): p. 43-46.
26. Jagini, S., et al., *Emerging contaminant (triclosan) identification and its treatment: a review.* SN Applied Sciences, 2019. **1**(6): p. 1-15.
27. Nudera, W.J., et al., *Antimicrobial effect of triclosan and triclosan with Gantrez on five common endodontic pathogens.* Journal of endodontics, 2007. **33**(10): p. 1239-1242.
28. Mattsby-Baltzer, I., et al., *Microbial growth and accumulation in industrial metal-working fluids.* Applied and Environmental Microbiology, 1989. **55**(10): p. 2681-2689.
29. Kulkarni, A., et al., *Exploration of different polymers for use in the formulation of oral fast dissolving strips.* J Curr Pharm Res, 2010. **2**(1): p. 33-35.
30. Qin, Z.-y., et al., *Fast dissolving oral films for drug delivery prepared from chitosan/pullulan electrospinning nanofibers.* International journal of biological macromolecules, 2019. **137**: p. 224-231.
31. Kannan, B., et al., *Printed paper sensors for serum lactate dehydrogenase using pullulan-based inks to immobilize reagents.* Analytical chemistry, 2015. **87**(18): p. 9288-9293.
32. Jahanshahi-Anbuhi, S., et al., *based microfluidics with an erodible polymeric bridge giving controlled release and timed flow shutoff.* Lab on a Chip, 2014. **14**(1): p. 229-236.
33. Carrigy, N.B., et al., *Trileucine and pullulan improve anti-campylobacter bacteriophage stability in engineered spray-dried microparticles.* Annals of biomedical engineering, 2020. **48**(4): p. 1169-1180.
34. Mehdi, M., et al., *Fabrication and characterization of rizatriptan loaded pullulan nanofibers as oral fast-dissolving drug system.* Materials Research Express, 2021. **8**(5): p. 055404.
35. Kang, S., et al., *Energy-saving electrospinning with a concentric teflon-core rod spinneret to create medicated nanofibers.* Polymers, 2020. **12**(10): p. 2421.
36. He, J.-H., et al., *Micro sphere with nanoporosity by electrospinning.* Chaos, Solitons & Fractals, 2007. **32**(3): p. 1096-1100.
37. Islam, M.S. and M.R. Karim, *Fabrication and characterization of poly (vinyl alcohol)/alginate blend nanofibers by electrospinning method.* Colloids and Surfaces A: Physicochemical and Engineering Aspects, 2010. **366**(1-3): p. 135-140.
38. Yarin, A.L., S. Koombhongse, and D.H. Reneker, *Taylor cone and jetting from liquid droplets in electrospinning of nanofibers.* Journal of applied physics, 2001. **90**(9): p. 4836-4846.
39. Suresh, S., A. Becker, and B. Glasmacher, *Impact of apparatus orientation and gravity in electrospinning—A review of empirical evidence.* Polymers, 2020. **12**(11): p. 2448.
40. Medeiros, E.S., et al., *Effect of relative humidity on the morphology of electrospun polymer fibers.* Canadian Journal of Chemistry, 2008. **86**(6): p. 590-599.

41. Khenoussi, N., L. Schacher, and D. Adolphe, *Nanofiber production: study and development of electrospinning device.* Experimental Techniques, 2012. **36**(2): p. 32-39.
42. Cai, Y. and M. Gevelber, *The effect of relative humidity and evaporation rate on electrospinning: fiber diameter and measurement for control implications.* Journal of Materials Science, 2013. **48**(22): p. 7812-7826.
43. Šimko, M. and D. Lukáš, *Mathematical modeling of a whipping instability of an electrically charged liquid jet.* Applied Mathematical Modelling, 2016. **40**(21-22): p. 9565-9583.
44. Nezarati, R.M., M.B. Eifert, and E. Cosgriff-Hernandez, *Effects of humidity and solution viscosity on electrospun fiber morphology.* Tissue Engineering Part C: Methods, 2013. **19**(10): p. 810-819.
45. Tripatanasuwan, S., Z. Zhong, and D.H. Reneker, *Effect of evaporation and solidification of the charged jet in electrospinning of poly (ethylene oxide) aqueous solution.* Polymer, 2007. **48**(19): p. 5742-5746.
46. Wu, J.-L., et al., *Triclosan determination in water related to wastewater treatment.* Talanta, 2007. **72**(5): p. 1650-1654.

6 Chapter 6: An atomizer-integrated electrospinning system for capturing aerosolized bacteria within an easy-to-dissolve sugar fibrous network

In this chapter, experiments were performed by myself, and undergraduate students Lauren Choi, Stephanie Sibbald, and Sarah Rassenberg, under my supervision. Graduate students Scott Laengert and Ryan J. LaRue provided support with the building of the diffusion dryer. This chapter was drafted by myself and will be edited by my supervisors Dr. David R. Latulippe and Dr. Carlos D. M. Filipe for future publication.

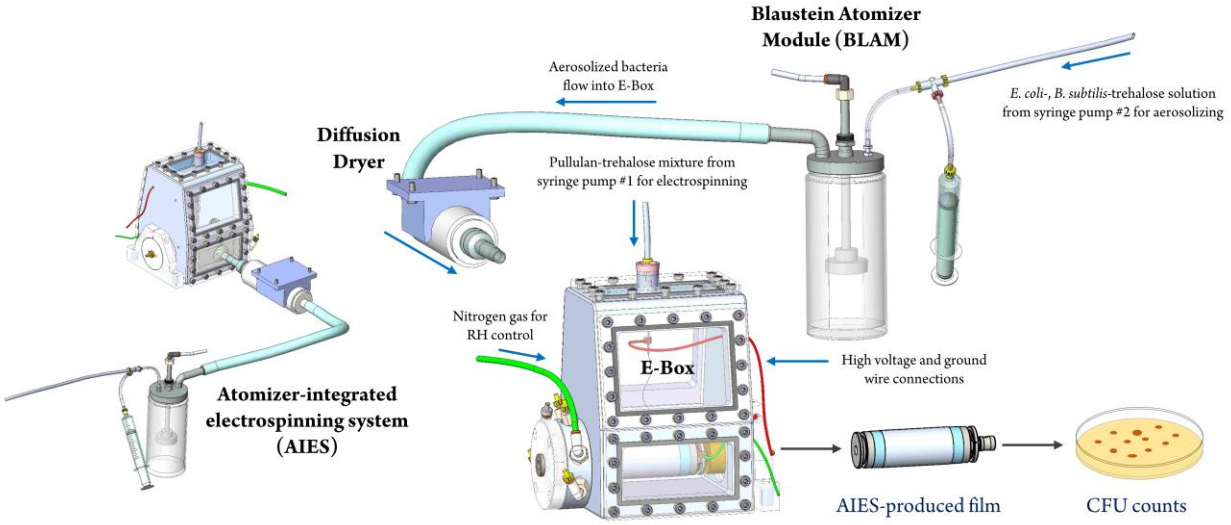

6.1 Abstract

Producing fibrous networks directly in the presence of biological materials through electrospinning has received widespread interest among researchers for creating functional food products involving probiotics, drug delivery products involving controlled release of bioactive compounds, and many others. However, electrospinning is far from a robust method for encapsulating biological materials; there is a wide range of performances measured in terms of cell culturability (e.g., 0.01 – 100% for bacteria) that have been reported that limit its potential for further widespread use. Ensuring there is a high level of cell culturability or viability of these materials once embedded within electrospun matrix is critical to the successful deployment of many of these products. Thus, in this study, we focused on modifying the traditional electrospinning process by integrating atomization (via an atomizer) as a gentle process of incorporating aerosolized bacteria with electrospun fibers to create bacteria-embedded electrospun fibrous networks/films. A sugar mix of pullulan and trehalose in Milli-Q water, known for its ability to stabilize biological materials, was utilized as an electrospinning solution. Once electrospun, this dried sugar mix is rapidly (<1 second) dissolvable and thus has benefits for variety of applications as orally dissolving films for drug delivery purposes, or as per our previous work, can be used to rapidly reanimate cell-based biosensors that detect toxic chemicals commonly found in wastewater. The first work in this study involved the use of fluorescent green microspheres (FGMs) as oversimplified surrogates of bacteria for rapid screening of process and design changes of this atomizer-integrated electrospinning system (AIES). The outcome of this work enabled the successful integration of *E. coli* (Gram-negative) and *B. subtilis* (Gram-positive) aerosols

with electrospun sugar fibers. These bacteria were selected as models of biological materials since they are easily culturable and are known to be susceptible to the stressful forces associated with the traditional electrospinning process. Interestingly, we discovered that incorporating trehalose sugar with the *E. coli* solution (solution to be atomized) was key in obtaining culturable counts. As we increased the concentration of trehalose from 0 to 0.88 M, the percent culturability increased from 0 to 3.1%. For *B. subtilis*, there was no statistical difference in percent culturability as the trehalose concentration increased; the average percent culturability for *B. subtilis* was 1.2%. The significance of this work highlights the AIES as a potentially gentler method of incorporating biological materials into electrospun films that could be beneficial across a wide range of applications where a high level of viability is desirable.

6.2 Introduction

Electrospinning is a common technique used to fabricate networks/films of nano- or micro-fibrous materials with a myriad of applications that span a wide range of disciplines including drug delivery, tissue engineering, filtration, sensing and many others.[1] Electrospun fibrous networks have also been produced directly in the presence of cells to improve long-term cell viability and culturability, adhesion and cell proliferation. In one such study by Xu et al.,[2] tissue patches were created via a reactive electrospinning technique to produce hydrazone-cross-linked poly(oligo ethylene glycol methacrylate)-based hydrogel nano-fibrous networks embedded with fibroblasts and myoblasts. Bacterial cells have also been subject to electrospinning where in one study by Sanchez and Laberty-Robert,[3] electroactive

bacteria, *Shewanella oneidensis*, were encapsulated in poly(ethylene oxide)-poly(ε-caprolactone) fibers to produce a bioanode for a microbial fuel cell application. Although both studies targeted different types of living cells (eukaryotic, prokaryotic) and for vastly different applications, both studies share a common outcome: the electrospun network was found to conserve cell viability and biological activity.

Although electrospinning has shown promise in preparing cell-encapsulated electrospun films for a variety of applications, there are inherent technological constraints owing to the method of forming these films that limit its potential for widespread use. The act of fiber stretching upon applying a sufficient electric charge causes shear stress (on top of the stress caused by the electric field) on the cells present within the fibers.[2] For bacteria, electrospinning has been shown to have a wide range of success (0.01 – 100%)[4-11] in terms of culturability immediately after electrospinning. Also, because the method of forming cell-encapsulated electrospun fibers requires the electrospinning solution and cells to be mixed prior to fiber formation, the rheological behavior of electrospinning solution can be greatly affected and thus the concentration, size and shape of the cells or other biological materials must be carefully considered. One possible strategy to remove these constraints, while still allowing for the simultaneous integration of electrospun fibers and cells in a continuous film creation process, would be to decouple the electrospinning solution from the cells by introducing atomization as a complimentary technique to electrospinning. Atomization, also referred to as aerosol generation, is a well-known technique that is utilized for testing bacterial filtration efficiencies (BFE) of face mask and respirator materials.[12] The BFE test relies on the survival of bacteria in a dry aerosol format after atomization to measure a

material's resistance to bacterial penetration. Thus, because of the gentle process of generating bacteria aerosols via atomization,[13] we investigated the use of integrating this technique with electrospinning as new method of creating bacteria-embedded electrospun films.

In this study, we retrofitted an existing miniature (1L inner volume) and fully enclosed electrospinning box (E-Box) designed and built in-house from a previous study (Chapter 5) to integrate atomization as a complimentary technique to electrospinning. As previously mentioned, the purpose of atomization in this newly developed atomizer-integrated electrospinning system (AIES) is to allow for a gentle incorporation of bacteria, or other biological materials in the form of dry aerosols, into electrospun films. A sugar mix of pullulan and trehalose in Milli-Q water was selected as the electrospinning solution in this work as it is a well-known and promising formulation that can be used to stabilize biologicals present in a dry format.[14-16] This work is divided into two parts: the first part includes proof-of-concept work with fluorescent green microspheres (1-5µm diameter) to act as oversimplified surrogates of bacteria, while the second part includes work with *E. coli* (Gram-negative) and *B. subtilis* (Gram-positive). In our previous work (Chapter 3), *E. coli* and *B. subtilis* were found to be particularly useful as cell-based biosensors in assessing toxicity of industrial wastewaters. These two common bacteria possess different structural characteristics (Gram-negative, Gram-positive) and biological functions (e.g., non-spore forming, spore forming) and thus were conveniently used as models to assess the performance of AIES measured via colony forming unit counts. The AIES is particularly advantageous: the rheological behavior of the electrospinning solution is independent of the

size, structure, concentration/quantity, or type of materials (e.g., particles, bacteria, or other biologicals) to be embedded in the electrospun film. The film that is generated by the AIES also differs from traditional electrospinning in that a portion of bacteria embedded within the film exist outside of electrospun fibers, as opposed to being encapsulated within the fibers. To the best of our knowledge, this is the first attempt at combining these two processes and we believe this approach for forming bacteria-embedded electrospun films may draw interest from a variety of other disciplines and for a range of applications.

6.3 Materials and Methods

6.3.1 Atomizer integrated electrospinning system (AIES) components

The AIES is made up of the following main components:

(1) A readily available and inexpensive (~$300 CAD) 3018 Pro GRBL Control DIY Mini CNC Machine (TopDirect) and lathe revolving centre (TopDirect) to allow for collector rotation and spinneret movement.

(2) A custom miniaturized (1 L inner volume) and predominantly 3D printed E-Box designed and built by us to integrate with the CNC machine. Our previous work (Chapter 5) describes the benefits of the E-Box; relative humidity (RH) can be rapidly manipulated (few minutes) and easily fits into a Class II, Type A2 Biological Safety Cabinet (BSC) equipped to work with biological materials and handle solvent evaporation. The assembly and detailed drawings of E-Box are also available in this previous work. The E-Box is fully enclosed, except for a single quick-connect port to which a 0.45μm filter is attached so that atmospheric pressure inside the box can be

maintained and so that airborne microspheres and bacteria aerosols do not escape the E-Box.

(3) A high voltage power supply (Bertan 230 series) to enable formation of electrospun fibers.

(4) A single-jet low flow Blaustein Atomizing Module (BLAM; CHTech) aerosol generator for the atomization of fluorescent green microspheres (Cospheric) and non-pathogenic bacteria (*DH5α E. coli*, *B. subtilis*).

(5) Two laboratory syringe pumps; one for feeding the pullulan-trehalose sugar solution to the spinneret (18 gauge blunted tip needle) for electrospinning, and one for feeding the fluorescent green microspheres (Cospheric) and bacteria solution to the Blaustein Atomizing Module (BLAM) for atomization.

(6) A home-made diffusion dryer (**Figure E1** Appendix E**;** medium (MD) size dryer was used) made from a standard binder divider, and a stainless-steel mesh filled with silica gel beads 2-4 mm in size (Dry & Dry). Silica gel beads are housed between two concentric cylinders, the outer cylinder and inner cylinder is made of made of rolled-up binder divider and rolled-up stainless-steel mesh, respectively. The diffusion dryer dries the particles that are atomized prior to reaching the E-Box to avoid dissolving the highly hygroscopic sugar film.

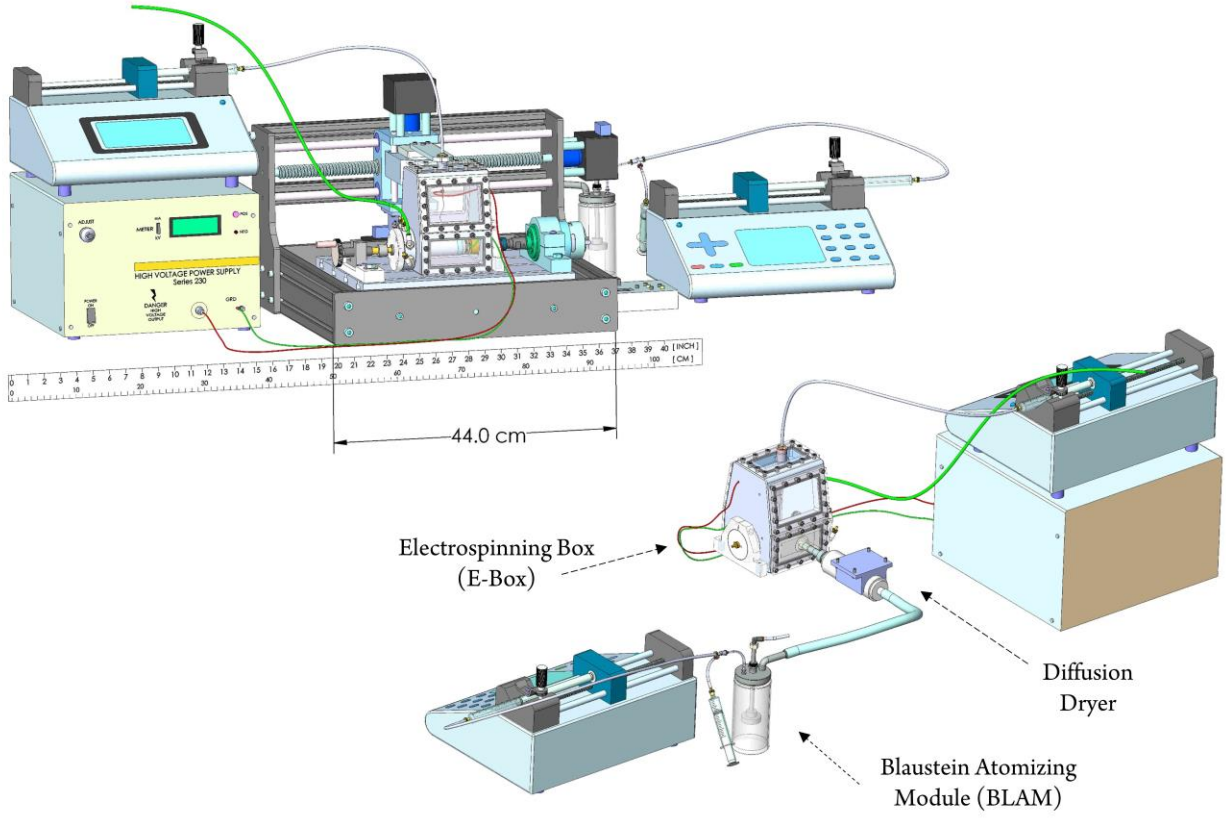

Figure 6-1. Front and back view of AIES; the CNC machine is removed in the back view to highlight the diffusion dryer with the purple mount downstream of the BLAM (transparent jar with grey lid) and upstream of the back-facing side of the E-Box. Two syringe pumps are located on either side of the CNC machine-E-Box assembly. The blueish green tube corresponds to the nitrogen gas feed line entering one of the quick-connect ports on the support side of the E-Box. The red and green wires on high voltage power supply correspond to the power supply and ground wires, respectively. A ruler (1:1 scale) is shown.

6.3.2 Creating an AIES film with embedded fluorescence green microspheres or bacteria

Electrospinning conditions (flow rate, relative humidity (RH), sugar solution, voltage) were selected according to previous work in Chapter 5. Prior to running an experiment, the AIES was set up: first, removable cardboard inserts were cut and wedged to the inner walls of the E-Box to help isolate the grounded roller and thus improve the roller's affinity to the fiber jet. Next, a 2 mL solution of 20% w/v Pullulan, 0.5M Trehalose in Milli-Q water was loaded into a sterile 5 mL BD syringe and secured onto a standard laboratory syringe pump

with the solution flow rate set to 2.5 μL/min. One end of a flexible piece of tubing was connected to the syringe and the other end was connected to the spinneret-fitting assembly located on the top section of E-Box (see **Figure 6-1**). The red wire carrying the power (**Figure 6-1**) from the high voltage power supply was inserted through a small opening on the drive side of the E-Box and affixed to a cylindrical fitting which attaches to the 18-gauge spinneret. The bottom of the fitting was positioned approximately 1 cm from the tip of the spinneret (see **Figure E2** in Appendix E); the tip of the spinneret was positioned 9 cm away from the roller. The green ground wire (**Figure 6-1**) was inserted through another small opening on the drive side of the E-Box and looped loosely around a groove located on the drive-side of the roller. Two sterile 10 mL BD syringes were connected to the inlet of the BLAM via a three-way valve fitting with one of the syringes filled with Milli-Q (for rinsing the BLAM before and after atomization), and the other filled with either a fluorescent green microsphere (FGM) solution or bacteria (*E. coli* or *B. subtilis*) solution. Preparation of the FGM and bacteria solutions were as follows:

- FGMs purchased from Cospheric are 1-5 μm bright green, fluorescent spherical polymer particles and were dissolved in Milli-Q water to create 0.2 mg/mL solution for atomization. The density of these particles is advertised as approximately 1.3 g cm^{-3} and at this concentration can simply be suspended in Milli-Q water with minimal settling over an 8-hour period.
- *E. coli* was provided by Biointerfaces Institute at McMaster University. The *E. coli* were cultured for 18 h at 37°C with 5 mL of Lysogeny broth (LB) in 40 sterile 15 mL

polystyrene round-bottom Falcon tubes inside of a Thermo MaxQ 8000 shaker incubator with a rotation speed of 225 rpm. After culturing, the contents of the tubes were combined into a sterile Erlenmeyer flask to a create a single solution. The single solution was redistributed into four sterile 50 mL Falcon tubes in equal volumes and centrifuged at 10°C for 8 min using a Thermo Scientific Sorvall ST 40R centrifuge. The supernatants were replaced with 15 mL of Milli-Q water containing 0g, 1.25g, 2.5g, or 5g of trehalose dihydrate (Sigma). The four concentrations of trehalose correspond to 0 M, 0.22 M, 0.44 M, and 0.88 M of trehalose, respectively. The concentration of *E. coli* in each tube was approximately 2.3×10^9 cells/mL.

- *B. subtilis* was also provided by the Biointerfaces Institute at McMaster University. The *B. subtilis* were cultured for 40 h in 5 mL of LB in 15 sterile polystyrene round-bottom Falcon tubes using the same equipment and conditions as *E. coli*. After culturing, the same steps as those for *E. coli* were conducted. The concentration of *B. subtilis* in each tube was approximately 7.1×10^7 cells/mL.

For FGMs, the syringe pump was set to a flow rate of 0.5 mL/min and 15 mL was loaded into a 20 mL BD syringe. For *E. coli*, *B. subtilis*, the same flow rate as for FGMs was used but only 10 mL of solution was loaded into a 10 mL BD syringe. The 0.5 mL/min flow rate remained unchanged for all experiments.

To begin creating the AIES-produced film, the RH in the E-Box was adjusted to 30% by feeding nitrogen gas into the E-Box. The RH was recorded by inserting a USB-502 RH/Temperature Data Logger (Measurement Computing) into the E-Box before and after

film creation. Next, the front window of the E-Box was opened (for 2-3 minutes), and an aluminum foil (Fisher) substrate was wrapped around the roller (roller diameter = 2.54 cm, roller length available for aluminum foil = 7.6 cm). The syringe pump for the pullulan-trehalose solution was temporarily turned on until a small droplet appeared at the tip of the spinneret. The front window was reattached with hex socket head cap screws (McMaster-Carr) and the CNC machine was turned on to begin roller rotation (80-100 RPM). Electrospinning was initiated first by turning on the high voltage power supply and the voltage was increased by 1 kV per second to the desired voltage of 9 kV for bacteria and 14 kV for FGM. Electrospinning was operated for 10 minutes prior to atomization to ensure a sugar-film was produced on the aluminum foil substrate. Atomization was initiated by setting the BLAM pressure to 5 PSI and turning on the syringe pump containing the syringe loaded with the desired solution to be aerosolized. The BLAM pressure was adjusted via a needle valve located downstream of the nitrogen tank and monitored via a pressure gauge downstream of needle valve. Atomizing was conducted for a total of 20 min and 30 min for bacteria and FGMs, respectively. After producing the film, both syringe pumps, the high voltage power supply, and CNC machine were turned off. The needle valve controlling the flow of nitrogen gas to the BLAM was closed and the solution collected at the bottom of the BLAM was removed. The front window of the E-Box was temporarily removed and the aluminum foil substrate containing the AIES-produced film was removed. The front window was reattached, and the flow of nitrogen gas was diverted away from the BLAM and towards the E-Box via a three-way valve. The needle valve was reopened to purge the E-Box and reset the RH to 30% for the next run.

6.3.3 Film characterization

Film characterization and quantification for FGMs and bacteria were as follows:

- After FGM film creation, circular discs (d = 0.6 cm), known as pills, were single hole-punched from the middle portion (1 cm left and right from the center) of the 5 cm × 7.9 cm film using a single hole punch. A single pill was imaged with TESCAN VEGA-II LSU scanning electron microscope. Five pills were cut from the pullulan-trehalose film, placed in a single 1.7 mL microfuge tube, and dissolved in 300 µL of Milli-Q water. 200 µL of the 300 µL was aliquoted into a black flat-bottom microplate and read using a Spark 10M microplate reader (Tecan). The average fluorescence signal over a 4-minute period was recorded; the signals were flat over the entire period but fluctuated and thus the average was reported (**Figure E3** Appendix E). Excitation and emission wavelengths were set to 485 nm and 525 nm respectively. The gain was set to the default setting of 60.
- After bacteria (*E. coli* or *B. subtilis*) film creation, a single strip 2 cm × 7.9 cm was cut from 5 cm × 7.9 cm film and peeled off the aluminum foil substrate with tweezers (**Figure E4** Appendix E) and dissolved in 100 µL of phosphate buffered saline (PBS) inside of a 1.7 mL microfuge tube. Duplicates were plated on the same LB-agar culture plates subdivided into two sections; 20µL of solution was aliquoted to each section, spread using a L-shape spreader (VWR), and incubated upside down at 37°C for 20 h. The colonies were then counted visually.

6.4 Results and Discussion

6.4.1 Fluorescent green microspheres for proof-of-concept work

Integrating aerosolized bacteria into an electrospinning process that produces a highly hygroscopic fibrous film within high voltage environment is challenging. There are many sites throughout the process that can kill the bacteria (e.g., shear and rapid drying of the atomization process, high voltage environment) and thus to simplify the problem, fluorescent green microspheres (FGMs) were first used as an oversimplified surrogate of bacteria. The experiments with FGMs were performed using electrospinning conditions that were known to be successful in electrospinning solutions in the presence of *E. coli* (no atomizer) from previous work (Chapter 5). Thus, a voltage of 14 kV and a pullulan-trehalose solution flow rate of 2.5 μL/min was selected. In this previous work, 14 kV was selected to reduce the amount of voltage-induced stress the *E. coli* would undergo; we could not form an electrospun film operating at 12 kV or below. For the atomizing portion of this system, the goal was to select an aerosol generator and set of operating conditions that would minimize the amount of stress the bacteria would undergo. Thus, a Blaustein Atomizing Module (BLAM) was selected in this study as it is considered a gentle aerosol generator primarily because it produces aerosols using a single-pass format (atomized only once). The Collison is another commonly used aerosol generator, however, it operates using a multi-pass format in which the fluid that is not successfully aerosolized is recirculated back into the original feed which can be detrimental to the bacteria. Also, the BLAM can be operated at a lower pressure (7 psi) than the Collison (20 psi) which reduces the magnitude of the forces imparted on the fluid.[17] Although, the lowest BLAM pressure according to CH

Technologies is 7 psi,[17] a pressure of 5 psi was attempted to further minimize the force imparted on the fluid. Although the act of atomizing involves the rapid drying of the atomized material, it was important to ensure that the FGMs were dry enough to avoiding dissolving the hygroscopic electrospun pullulan-trehalose film. Preliminary experiments showed that a diffusion dryer or heating coil downstream of the BLAM was necessary to avoid the aerosols completely dissolving the film. The use of a heating coil was successful in preventing film dissolution; however, it was later replaced with a home-made diffusion dryer to obviate the need for heating. Three different diffusion dryer sizes were made and tested but the only shortest, yet still effective diffusion dryer was selected to avoid unnecessarily over-drying the aerosols (see **Figure E1** Appendix E).

Using this configuration, fluorescence green microspheres (FGMs) and Milli-Q water (control) were atomized into the E-Box, and FGMs were successfully integrated with electrospun fibers. The fluorescence signals for the FGM and control experiment were 7306 ± 394 and 255 ± 50, respectively (**Figure 6-2**).

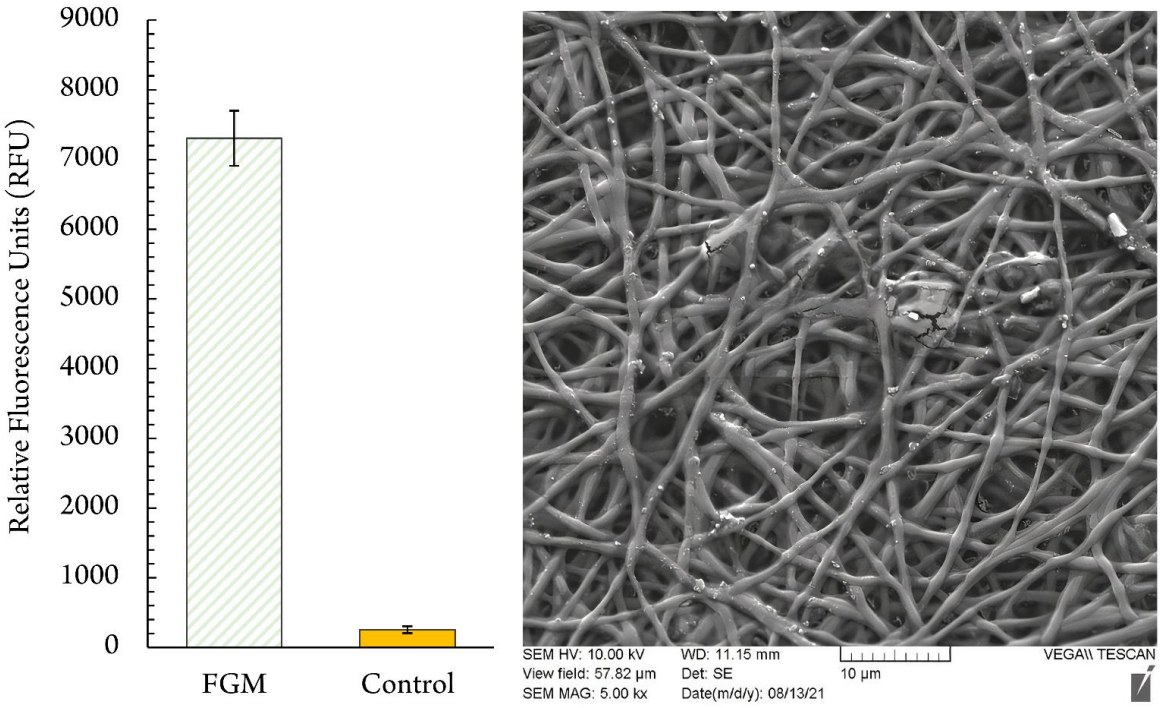

Figure 6-2. Left: Average fluorescence signals measured as relative fluorescence units (RFUs) derived from two fluorescent green microsphere (FGM)-embedded films and two control (atomized Milli-Q water) films. FGM and control experiments were conducted in duplicates (four films in total); for each film, five pills each with a diameter of 0.6 cm were cut via a single hole-punch, combined, dissolved in Milli-Q water, and read using a microplate reader (Tecan). Each bar corresponds to the average fluorescence signal obtained from the two films. The error bars correspond to the standard deviation of the fluorescence signals from those two films. Right: An SEM image of the FGM-embedded film where the white/grey 'artifact-type' materials are the FGMs.

This consistent and large fluorescence difference between the FGM and control test demonstrates that the FGMs are present in the film. An SEM image of one of the films confirms this result where FGMs (light grey/white spots) are present in the fiber matrix. The FGMs were found to be integrated into the fiber matrix in different ways. They were either adhered to, embedded within, or protruding from the fibers. This SEM image indicates that a portion of the atomized FGMs is incorporated into and/or onto the fibers as they travel towards the grounded collector. This result is not surprising since the fibers exiting the

spinneret are not yet fully dried and thus can mix with the atomized FGMs suspended in the E-Box. Interestingly, in early work we discovered that alternating between electrospinning and atomizing three times produced a fluorescence signal at least three times lower (**Figure E5**, Appendix E) when the same amount of FGMs were atomized. The alternating approach relies on the FGMs adsorbing or absorbing to the surface of the film. This observation indicates that the act of electrospinning captures additional atomized FGMs. The miniature size (1 L inner volume) and fully enclosed space of the E-Box is likely partially responsible for the success of this process as it promotes the accumulation of atomized FGMs in a localized space within the electrospinning zone. A larger environment (enclosed or open) would further disperse the atomized materials and by that would decrease the concentration and number of atomized materials available for capture.

6.4.2 AIES performance for *E. coli* and *B. subtilis*

The E-spin and BLAM conditions for the experiments conducted with two bacteria of different types, *E. coli* (gram-negative) and *B. subtilis* (gram-positive), are shown in **Table 6-1**. Voltage is the only condition that was changed when switching from FGM (14 kV) to bacteria (9 kV). It was discovered (after FGM experiments) that with the absence of bacteria in the electrospinning solution, an electrospun film could be formed at a lower voltage of 9 kV; this voltage represents the lowest possible voltage (at 1 kV increments) required to form a film. We attribute the success in electrospinning at 9 kV (36% lower) to the absence of bacteria/material in the pullulan-trehalose electrospinning solution. Because the concentration of *E. coli* in the pullulan-trehalose solution in our previous work was high

(~2.3 × 10^9 cells/mL), the rheological behavior of the solution in the absence of bacteria was likely altered such that it became to easier deform the solution droplet at the tip of spinneret under voltage-induced strain.

Table 6-1. Electrospinning (E-spin) and Blaustein Atomizing Module (BLAM) conditions used for *E. coli* and *B. subtilis* experiments.

E-spin conditions	**Value**
Voltage	9 kV
Pull-Tre solution flow rate	2.5 μL/min
Pullulan, Trehalose	20% w/v Pull, 0.5 M Tre in Milli-Q Water
Roller Speed	80-100 RPM
E-Spin Time	10 min (alone) + 20 min (with BLAM)
Relative Humidity	~30% Start (Before film formation)
BLAM conditions	**Value**
Pressure	5 Psi
Bacteria solution flow rate	0.5 mL/min
Bacteria Concentration	*E. coli*: 2.3×10^9 cells/mL *B. subtilis*: 7.1×10^7 cells/mL
BLAM time	20 mins
Relative Humidity	~40% End (After film formation)

The first experiment was conducted according to the conditions in **Table 6-1** with *E. coli* and showed that zero culturable *E. coli* were present in the electrospun film. In a second experiment, only the BLAM was operated and a petri-dish containing LB-Agar was placed into the E-Box at outlet of the atomizer. The results (**Figure E2** in Appendix E) showed that thousands of *E. coli* colonies were present on the surface of the LB-Agar after atomizing for only five minutes. The results from these two preliminary experiments indicated that the cumulative stress of the atomization and diffusion drying process weakened the *E. coli*, and the act of electrospinning killed them. To reduce the amount stress on the *E. coli* induced by

the atomization and diffusion drying process, *E. coli* was suspended in Milli-Q water containing 0, 0.22, 0.44, and 0.88 M of trehalose, a well-known stabilizing agent when present in a dry format.[14, 15] Pullulan is also known to stabilize biological materials,[14] however, typically used pullulan concentrations (5-15% w/v)[14, 18, 19] for biological stability purposes were too viscous and thus could not be processed through the BLAM. The results in **Figure 6-3** show that use of trehalose in the atomization process was successful in obtaining culturable counts in the film for *E. coli*. As the concentration of trehalose increased from 0 M to 0.88 M, the number of culturable *E. coli* per square centimeter of film increased from 0 up to 3341 (for run 4). The average number of culturable *E. coli* for 0, 0.22, 0.44, and 0.88 M trehalose and their corresponding standard deviations were 0, 9 ± 5, 42 ± 11, and 1967 ± 1156, respectively. For *B. subtilis*, the results show that as the concentration of trehalose increased, the number of culturable *B. subtilis* per square centimeter of film remained the same; the number of culturable bacteria for 0, 0.22, 0.44, and 0.88 M trehalose and their corresponding standard deviations were 51 ± 12, 32 ± 10, 37.5 ± 6, 44 ± 23, respectively. The average number of culturable bacteria and their standard deviations were calculated from duplicate runs, and in one case (*E. coli* at 0.88 M trehalose), in quadruplicate, with each run conducted on different days using newly cultured stocks of bacteria. The lower numbers of culturable *B. subtilis* in comparison to *E. coli* at 0.88 M trehalose is likely and partially due to the lower concentration (32 times lower than *E. coli*) of *B. subtilis* atomized.

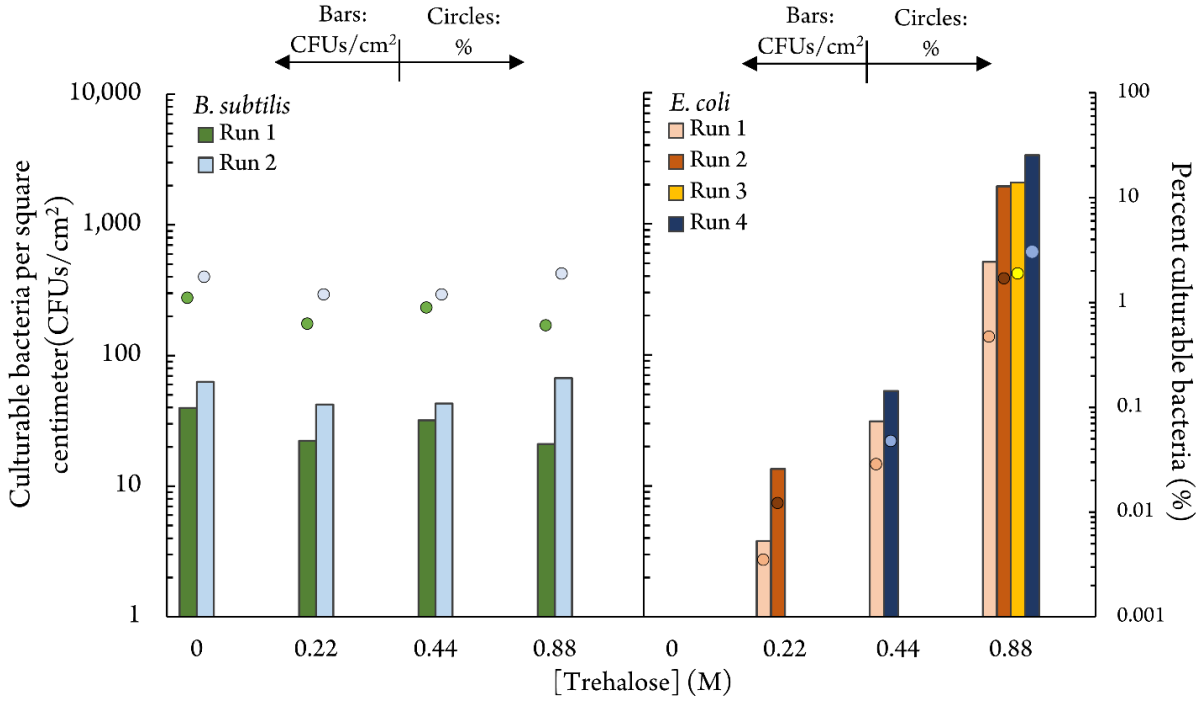

Figure 6-3. Number of culturable bacteria (*B. subtilis* on the left, *E. coli* on the right) per square centimeter (CFUs/cm²) after producing a film (corresponding a single bar) with the AIES operating at different concentrations (0, 0.22, 0.44, 0.88 M) of trehalose present in the atomizing solution. Each run (1-4) was conducted on a different day and thus a different stock of bacteria was used for each run. The circles correspond to the percent of culturable bacteria in the film as calculated using Equation 1 which was derived from FGM experimentation.

The cell wall structure of the bacteria (Gram-positive, Gram-negative) is one reason likely responsible for the trends between these two bacterial strains shown in **Figure 6-3**. Gram-positive bacteria have a cell wall containing peptidoglycan known for providing structural strength that is significantly thicker than that of Gram-negative bacteria. Differing measurement techniques have provided a range of cell wall thicknesses for *E. coli* including 2.5 nm using small-angle neutron scattering,[20] 6.0 nm using atomic force microscopy,[21] and at most, 4 nm using electron cryotomography.[22] In contrast, *B. subtilis* have been measured to have a cell wall thickness of 33 nm using cryo-transmission electron microscopy (TEM),[23]

and 30 – 40nm depending on the site of measurement (e.g., pole, pole-cylinder) using electron microscopy by freeze-substitution.[24] A second reason is that *B. subtilis* is already equipped to handle drastic changes in environmental conditions (i.e., shear and rapid drying caused by atomization, further drying via the diffusion dryer) which cause extreme stress to the bacteria. An endospore, also referred to as a spore or the daughter cell, is formed (begins at the onset of the stationary phase of the bacteria growth curve) inside of a *B. subtilis* cell via asymmetric division.[25] This process of sporulation in *B. subtilis* gives rise to spores that are resistant to extreme environmental stresses. It has been reported that the spores may be resistant to drying stresses since the spore core is slightly dehydrated.[25] A third reason is that *B. subtilis* is surrounded by a self-produced viscous substance known as a biofilm.[26] The major components that serve as key structural elements in biofilms are proteins, extracellular DNA, and coincidently, polysaccharides.[27] As mentioned earlier, polysaccharide pullulan is known to reduce drying stresses on biological materials. This third reason would explain why the addition of a higher concentration of trehalose did not increase the number of culturable bacteria in the AIES-produced film; the extracellular matrix of *B. subtilis* may have already been saturated with these materials, namely the self-produced polysaccharides. Because *E. coli* have a thinner peptidoglycan layer, lack the ability to produce biofilms that contain polysaccharides and other materials, and are non-spore forming, it is not surprising that *E. coli* would require the use of a stabilizing agent such as trehalose to survive the stress induced by the AIES process.

Percent culturability of *E. coli* and *B. subtilis* in **Figure 6-3** was also quantified using the initial work with FGMs. The quantification assumes that these bacteria behave the same as

that of the FGMs when atomized. This is a good assumption since the bacteria (*E. coli*: 1-2 μm long and 0.5 μm wide,[28] *B. subtilis*: 2-6 μm long, 1 μm wide[29]) and FGMs are of a similar size (advertised as 1-5 μm, but smaller sizes are found). With the work from **Figure 6-1**, we compared the total mass of FGMs fed into the BLAM (3 mg) with the total mass of FGMs in the film to determine the percent of bacteria that should have been incorporated into the film; we also assumed that the average size of the FGMs (advertised d50 = 1.5 – 2.0 μm) was the same average size as the two types of bacteria. The total mass of FGMs in the film was determined by taking the same FGM feed stock (0.2 mg/mL) and diluting it with Milli-Q water to a concentration with a volume of 300 μL, of which 200 μL were loaded into a well to achieve the same fluorescence signal of ~7000 RFU (for five pills) as in **Figure 6-1** of section 3.1. This concentration was determined to be 6.7×10^{-5} mg FGM/mL; the same procedure for measuring the fluorescence was used as in **Figure 6-1**. We compared this concentration to the theoretical concentration if all FGMs atomized (3.0 mg) were successfully incorporated into the film and if five pills were cut (3.6% of the film area corresponding to 0.11 mg) and dissolved in 300 μL of Milli-Q water (0.36 mg/mL). With these data, it was determined that 0.019% of FGMs atomized were incorporated into the film. Thus, all culturability percentages shown in **Figure 6-3** were calculated using Equation 1 with the assumption that 0.019% was the maximum percentage of *E. coli* or *B. subtilis* fed into the BLAM that could have been incorporated into the film.

$$\text{Percent culturable (\%)} = \frac{\text{\# of cells in electrospun film}}{(\text{\# of cells fed to BLAM}) \times 0.019\%} \qquad \text{Equation 1}$$

With Equation 1, the percent culturability for *E. coli* and *B. subtilis* ranged between 0-3.1% and 0.6-1.9%, respectively. For *E. coli* to achieve a similar percent culturability to that of *B. subtilis*, 0.88 M of trehalose was required; run 1-4 corresponded to a percent culturability of 0.47, 1.79, 1.92, and 3.1 for *E. coli*, respectively. These results are promising since preliminary work with *E. coli* and *B. subtilis* showed that when bacteria were electrospun directly in the presence (electrospinning only; no atomization) of the same electrospinning solution (20% w/v Pullulan, 0.5M Trehalose in Milli-Q water), and under 'near-optimal' electrospinning conditions (14 kV, 2.5 μL/min), the percent culturability was between 0.05-0.1% for *E. coli* and much lower for *B. subtilis* at approximately 0.001%. Operating at a high voltage is well known in the literature to be harmful to the viability of cells and thus a low voltage can be desirable.[30] For example, preliminary work demonstrated that when traditional electrospinning was conducted in the presence of *E. coli* at 18 kV, the culturability decreased 10-fold when compared to 14 kV (4 kV lower). Thus, we contribute this higher level of culturability partially with the AIES's ability to form bacteria-embedded electrospun films at a lower (5 kV lower) voltage which is made possible by decoupling the electrospinning solution from the bacteria.

6.5 Conclusion

A first of its kind atomizer-integrated electrospinning system (AIES) was investigated as a gentle alternative to traditional electrospinning to produce bacteria-embedded electrospun films. With the use of a Blaustein Atomizing Module (BLAM) and fluorescent green microspheres (FGMs) as oversimplified surrogates of bacteria, we demonstrated that

FGMs, as aerosols, could be successfully embedded into hygroscopic sugar-based electrospun films. However, it was found that a diffusion dryer (built in-house) downstream of the BLAM was necessary to prevent the aerosols from completely dissolving the film. When transitioning to bacteria, it was found that the use of trehalose in the atomizing solution was critical to the survival of *E. coli* in this process; in the absence of trehalose, no culturable *E. coli* were present in the AIES-produced film. As the trehalose concentration increased from 0 to 0.88 M, the number of culturable *E. coli* per square centimeter of film increased from 0 to as high as 3144. However, for *B. subtilis*, trehalose was not a critical factor. It was found that regardless of trehalose concentration, the number of culturable *B. subtilis* per square centimeter remained the same between 32 and 51. Finally, the maximum percent culturability obtained in this study for *E. coli* and *B. subtilis* was calculated (based on FGM work) to be 3.1% and 1.9%, respectively. These values are considerably higher than our previous work with traditional electrospinning; the maximum percent of culturable *E. coli* and *B. subtilis* was 0.1% and 0.001%, respectively. We attribute this improvement to the decoupling of the electrospinning solution from the bacteria which enabled the formation of fibers at a lower voltage (approximately 5 kV lower). The findings of this work are significant and could be beneficial to other fields and applications where high culturability/viability of bacteria or other biological materials is advantageous.

6.6 References

1. Teo, W.E. and S. Ramakrishna, *A review on electrospinning design and nanofibre assemblies.* Nanotechnology, 2006. **17**(14): p. R89.
2. Xu, F., et al., *Single-step reactive electrospinning of cell-loaded nanofibrous scaffolds as ready-to-use tissue patches.* Biomacromolecules, 2018. **19**(11): p. 4182-4192.

3. Sanchez, J.-L. and C. Laberty-Robert, *A novel microbial fuel cell electrode design: prototyping a self-standing one-step bacteria-encapsulating bioanode with electrospinning.* Journal of Materials Chemistry B, 2021. **9**(21): p. 4309-4318.
4. Salalha, W., et al., *Encapsulation of bacteria and viruses in electrospun nanofibres.* Nanotechnology, 2006. **17**(18): p. 4675.
5. Klein, S., et al., *Encapsulation of bacterial cells in electrospun microtubes.* Biomacromolecules, 2009. **10**(7): p. 1751-1756.
6. López-Rubio, A., et al., *Encapsulation of living bifidobacteria in ultrathin PVOH electrospun fibers.* Biomacromolecules, 2009. **10**(10): p. 2823-2829.
7. Nagy, Z.K., et al., *Nanofibrous solid dosage form of living bacteria prepared by electrospinning.* 2014.
8. Heunis, T., M. Botes, and L. Dicks, *Encapsulation of Lactobacillus plantarum 423 and its bacteriocin in nanofibers.* Probiotics and antimicrobial proteins, 2010. **2**(1): p. 46-51.
9. San Keskin, N.O., et al., *Encapsulation of living bacteria in electrospun cyclodextrin ultrathin fibers for bioremediation of heavy metals and reactive dye from wastewater.* Colloids and Surfaces B: Biointerfaces, 2018. **161**: p. 169-176.
10. Fung, W.-Y., K.-H. Yuen, and M.-T. Liong, *Agrowaste-based nanofibers as a probiotic encapsulant: fabrication and characterization.* Journal of agricultural and food chemistry, 2011. **59**(15): p. 8140-8147.
11. Gensheimer, M., et al., *Novel biohybrid materials by electrospinning: Nanofibers of poly (ethylene oxide) and living bacteria.* Advanced Materials, 2007. **19**(18): p. 2480-2482.
12. *BS EN 14683:2019 Medical Face Masks - Requirements and Test Methods.* British Standards Institution, 2019.
13. Otero Fernandez, M., et al., *Transformative approach to investigate the microphysical factors influencing airborne transmission of pathogens.* Applied and environmental microbiology, 2020. **86**(23): p. e01543-20.
14. Krumnow, A.A., et al., *Preservation of bacteria in natural polymers.* J Microbiol Methods, 2009. **78**(2): p. 189-94.
15. Leung, V., et al., *Long-term preservation of bacteriophage antimicrobials using sugar glasses.* ACS Biomaterials Science & Engineering, 2017. **4**(11): p. 3802-3808.
16. Carrigy, N.B., et al., *Trileucine and pullulan improve anti-campylobacter bacteriophage stability in engineered spray-dried microparticles.* Annals of biomedical engineering, 2020. **48**(4): p. 1169-1180.
17. Technologies, C., *BLAM Advantages in Viability Over Collison*.
18. Robert, H. and D. Carlos, *Simple and ultrastable all-inclusive pullulan tablets for challenging bioassays.* Chemical science, 2016. **7**(3): p. 2342-2346.
19. Leathers, T.D., *Biotechnological production and applications of pullulan.* Applied microbiology and biotechnology, 2003. **62**(5): p. 468-473.
20. Labischinski, H., et al., *Direct proof of a" more-than-single-layered" peptidoglycan architecture of Escherichia coli W7: a neutron small-angle scattering study.* Journal of bacteriology, 1991. **173**(2): p. 751-756.

21. Yao, X., et al., *Thickness and elasticity of gram-negative murein sacculi measured by atomic force microscopy.* Journal of bacteriology, 1999. **181**(22): p. 6865-6875.
22. Huang, K.C., et al., *Cell shape and cell-wall organization in Gram-negative bacteria.* Proceedings of the National Academy of Sciences, 2008. **105**(49): p. 19282-19287.
23. Matias, V.R. and T.J. Beveridge, *Cryo-electron microscopy reveals native polymeric cell wall structure in Bacillus subtilis 168 and the existence of a periplasmic space.* Molecular microbiology, 2005. **56**(1): p. 240-251.
24. Hayhurst, E.J., et al., *Cell wall peptidoglycan architecture in Bacillus subtilis.* Proceedings of the National Academy of Sciences, 2008. **105**(38): p. 14603-14608.
25. McKenney, P.T., A. Driks, and P. Eichenberger, *The Bacillus subtilis endospore: assembly and functions of the multilayered coat.* Nature Reviews Microbiology, 2013. **11**(1): p. 33-44.
26. Vlamakis, H., et al., *Sticking together: building a biofilm the Bacillus subtilis way.* Nature Reviews Microbiology, 2013. **11**(3): p. 157-168.
27. Dragoš, A. and Á.T. Kovács, *The peculiar functions of the bacterial extracellular matrix.* Trends in microbiology, 2017. **25**(4): p. 257-266.
28. Board, S.S. and N.R. Council, *Size limits of very small microorganisms: proceedings of a workshop*. 1999: National Academies Press.
29. Errington, J. and L.T. van der Aart, *Microbe Profile: Bacillus subtilis: model organism for cellular development, and industrial workhorse.* Microbiology, 2020. **166**(5): p. 425.
30. Duman, D. and A. Karadag, *Inulin added electrospun composite nanofibres by electrospinning for the encapsulation of probiotics: characterisation and assessment of viability during storage and simulated gastrointestinal digestion.* International Journal of Food Science & Technology, 2021. **56**(2): p. 927-935.

7 Chapter 7: Conclusions and recommended future work

7.1 Conclusions

The overall work in this thesis explores the use of bacteria as a cell-based biosensor platform for detecting toxic compounds, such as biocides, used by industries and later present in contaminated waters/industrial wastewater (WW). The general focus of this work was guided by the current inability to rapidly assess if these waters (containing biocides) derived from industrial facilities, are safe enough to enter a municipal WWTP without disrupting a crucial biologically mediated process, known as nitrification. The presence of these biocides can negatively affect the nitrification process, which is responsible for oxidizing ammonia, a deleterious substance under the Wastewater Systems Effluent Regulations (WSER), into nitrate. The current gold standard specific nitrification rate (SNR) batch test used to assess the impact of these waters on nitrification performance is effective but is painfully tedious, complex, and time-consuming (4 hours). The work conducted to develop a new rapid test/assay would enable industrial and municipal WWTPs to make quicker decisions on what to do with contaminated waters. The test would also enable industrial facilities that produce contaminated waters to rapidly reassess their need to use certain types of biocides or use biocides in their current quantities. This could lead to an overall reduction in their use, both saving money and the environment (e.g., lakes, rivers, oceans), which ultimately receive a portion of these biocides.

My PhD work began with the use of a non-pathogenic *E. coli* (*DH5-α*) used as a model bacterial strain and cell-based biosensor (CBB) platform to detect three different common

biocides (Chapter 2). Recognizing that bacteria inherently possess a complex network of mechanisms that are activated when exposed to stressful environments, the use of a common and commercially available off-the-shelf fluorescent dye was leveraged to the probe the cellular activity and membrane integrity of the *E. coli* after exposure to Grotan® BK, ProClin 300™ and cetyltrimethylammonium bromide (CTAB) biocides. In this same study, a sugar polymer, pullulan, was investigated as a stabilizing agent to preserve the *E. coli*. A design of experiments (DOE) was conducted to understand the influences different factors (e.g., storage temperature, salinity content) would have on the survival (measured via colony forming unit counts) of *E. coli* over a period of approximately three months. Over this same period, the fluorescence response of the *E. coli* when exposed to the three different biocides was also reported. The results demonstrate that storing the *E. coli* in a pullulan-Milli-Q water solution at 4°C yielded the highest number of culturable cells over the three-month period. Also, for a few sets of preservation conditions, of which only temperature (at 4°C) was the common factor, the *E. coli* fluorescence response to each of the three biocides remained similar during the three-month storage period.

Subsequent work (Chapter 3) expanded on the concept of using bacteria as a CBB in combination with the same fluorescent dye by introducing six new bacteria (seven total) of different types (Gram-positive, Gram-negative) and functions (non-nitrifying, nitrifying). Two nitrifying bacteria, *Nitrospira* and *Nitrosomonas europaea*, responsible for nitrification in municipal WWTPs were used. The individual fluorescence response from each of the seven bacteria exposed to a single real industrial WW sample (containing a variety of compounds, including biocides) were combined to form a single unique sequence of seven

numbers ("fingerprint"). The approach was repeated for 28 different industrial WW samples and the sequences were correlated via partial least squares (PLS) modeling to the current gold-standard SNR batch test. A microplate reader (Tecan M200) was used to obtain the fluorescence signals over a 15-minute reading period (as per the instructions provided by the manufacturer of the dye), however it was found that only the initial fluorescence signal, which was retrieved after five minutes of exposure to the WW sample and one minute after the addition of dye, was necessary to achieve a strong correlation to the SNR batch test. When three principal components were used in the PLS model, the R^2 and Q^2 values were 0.84 and 0.75, respectively. Since the Q^2 value is close to the R^2 value and since the R^2 value is large, the model is accurate and not overfit. The results also show that of the seven bacterial strains, four (*Nitrospira*, *Escherichia coli*, *Bacillus subtilis*, *Bacillus cereus*) were identified via PLS modeling to be the most significant contributors for predicting the nitrification performance. Furthermore, by correlating the gas chromatography-mass spectrometry (GC-MS) analysis of the 28 WW samples with the SNR batch test results via PLS modeling, it was possible to identify which chemical compounds contributed to nitrification inhibition. For example, of the 51 compounds identified, it was found that Benzyl alcohol, Octanoic acid and p-Chlorocresol were positively correlated with nitrification inhibition and 2-Ethylhexanol, Dicyclohexylamine and Carbodiimide were negatively correlated with nitrification inhibition (nitrification stimulating). Finally, it is demonstrated that by developing a PLS model between the GC-MS data and the fluorescence data, it became possible to approximate the chemical composition of a WW sample by simply analyzing the fluorescence response of each bacterial strain.

Chapter 4 investigated the use of manipulating number of bacteria used in the assay and salinity content to improve biocide detection sensitivity of the three bacterial strains (*E. coli*, *B. subtilis*, *B. cereus*) identified via PLS modeling in Chapter 3 to be significant contributors in predicting nitrification performance. The results show that these two methods can be used to adjust the sensitivity of each bacterial strain which would lead to a better discrimination of biocide-containing samples of similar toxicity. It was discovered that bacteria suspended in lower salinity conditions (0-25% v/v phosphate buffered saline in Milli-Q water), and in most cases, a lower number of bacteria improved the limit of detection for two previously tested biocides, CTAB and Grotan® BK. Finally, a compact Quantus™ fluorometer was tested and compared to the Tecan M200 microplate reader as a means of enabling point-of-use toxicity testing. A correlation between the two instruments was developed for each of the three bacterial strains and as a proof-of-concept, two different amounts (number of bacteria) of *B. cereus* were exposed to three concentrations of biocide CTAB (used in Chapter 2). The results confirmed that for this experiment with *B. cereus*, the Quantus™ fluorometer could be used as a substitute to the Tecan M200 microplate reader.

Chapter 5 focused on leveraging electrospinning as a tool for preparing thin sugar-based films embedded with *E. coli* that could be used to rapidly detect two model biocides, Grotan® BK and Triclosan. The motivation for creating thin *E. coli*-embedded films as opposed to storing bacteria in solution (Chapter 2), was to harness, to a fuller extent, the documented benefits of sugars (pullulan and trehalose in particular) used as stabilizing agents when present in a dried format. Also, electrospun sugar films possess desirable properties that allow them to be easily dissolved in water and thus were convenient as a

platform for detecting biocides present in water. To allow for the creation of *E. coli*-embedded electrospun films, there was a critical need to control relative humidity (RH). Because commercially available enclosed electrospinning systems are too expensive ($10,000s) and do not easily fit into common biological safety cabinets (BSCs) equipped to handle the safe operation of biological materials, a miniaturized (1 L inner volume; 100-200 times smaller than commercially available systems) inexpensive (~$700 CAD) electrospinning box (E-Box) that surrounds a grounded roller for fiber collection was designed, built, and tested. The E-Box sits on top of an inexpensive (~$300 CAD) commercially available 3D printing machine that controls roller rotation speed and spinneret/needle movement; the combined unit easily fits in a Class II, Type A2 BSC. The results demonstrate that the RH of the E-Box environment can be rapidly (few minutes) manipulated at 22%, 36% and 48% which was found to be critical in controlling electrospun film quality and the diameter of the electrospun fibers. A high level of film-to-film reproducibility was achieved when operating at 36% RH, suggesting that there is an optimal RH for producing these films. Furthermore, small circular cut-outs of these films created at 36% RH, referred to as pills, were shown to be rapidly dissolvable (near instant; <1 s) and capable of detecting Grotan® BK and Triclosan with a limit of detection of at least 20 ppm for both.

In Chapter 6, the same E-Box from Chapter 5 was retrofitted to allow for the integration of two techniques; atomization, and electrospinning which was coined an atomizer-integrated electrospinning system (AIES). These two techniques were combined for the first time to enable a gentler process of creating bacteria-embedded electrospun

films. In this study, the AIES performance differences between two different types of bacteria were investigated: *E. coli* as a Gram-negative strain, and *B. subtilis* as a Gram-positive strain. The AIES process entails aerosolizing the bacteria (*E. coli* or *B. subtilis*) via a single-jet low flow Blaustein Atomizing Module (BLAM) into the miniature E-Box while electrospinning a bacteria-absent pullulan-trehalose solution. Interestingly, it was found that the addition of trehalose sugar to the atomizing solution was necessary in obtaining any culturable counts for *E. coli*; however, for *B. subtilis*, trehalose had no impact to the number of culturable counts in the film. Using the best conditions from this study for both the AIES and electrospinning alone, the percent of culturable bacteria in a film increased to 3.1% and 1.9% from 0.1% and 0.001% for *E. coli* and *B. subtilis*, respectively. The findings in this Chapter are significant as the AIES could be a valuable tool and alternative to traditional electrospinning for embedding stress-sensitive biological materials into electrospun films.

7.2 Recommended Future Work:

7.2.1 Improved prediction of nitrification inhibition potential of industrial wastewaters using separate models

In Chapter 3, 28 industrial wastewater (WW) samples derived from various facilities (e.g., automotive, food) across Ontario (Canada) were tested using the specific nitrification rate (SNR) batch test and using the cell-based biosensor (CBB) panel of bacterial strains test developed. Each sample tested was a hodgepodge of industrial WWs batched together from a variety of clients across many industries that were pretreated in batch mode using various physicochemical processes at an industrial WW treatment facility in Brantford (our industrial partner), tested, and sewered to the same municipal WWTP. The results from both

tests (SNR, CBB) were used to create a partial least squares (PLS) model, and with it, the CBB test results could be used to predict the nitrification inhibition potential of industrial WWs. Although the model was successful in its prediction (R^2 = 0.84, Q^2 = 0.75), it is suggested that individual/separate models be generated for each industrial WW facility and for companies/clients (those that produce contaminated waters) who intend to treat and sewer industrial WWs. This suggestion is due to the following reasons:

(1) Industrial WW facilities and companies (potential clients) that plan to treat industrial WW operate in different regions and their local WWTP may be more or less susceptible (in comparison to other WWTPs) to nitrification inhibition. Early work from Margrethe Winther-Nielsen and Jes la Cour Jansen found that percent nitrification inhibition of six different types of influent WWs was heavily influenced by the type of activated sludge used from three different WWTPs.[1] The type/amount of industries in the catchment area for each WWTP differed tremendously with the first, second, and third WWTPs receiving WW mainly from the food industry, from various industries (strong industrial activity), and from very few industries (very low industrial activity), respectively. This early study is cited by the international standard (ISO) 9509 (water quality – toxicity test for assessing the inhibition of nitrification of activated sludge) that was reviewed and confirmed in 2015,[2] and thus it is important to evaluate the nitrification inhibition potential using activated sludge from the receiving WWTP.

(2) As new models are generated for different clients and their corresponding local WWTPs, the CBB test could be used to predict which WWTP would be best equipped

to handle a particular batch of industrial WW. This knowledge could provide insight to the local WWTP (intended to receive the industrial WW) and tweak their treatment processes and conditions by consulting the WWTPs that were deemed better equipped to handle that batch; it could also be shipped and treated at those better equipped WWTPs. This collaborative approach may lead to an overall improvement in the treatment of a variety of wastewaters leading to a reduction in the total amount of harmful chemicals such as biocides into receiving water bodies.

(3) There is a plethora of biocides that exist, and the use of obscure/atypical biocides may skew a universal model and thus negatively influence the prediction performance for other potential clients. The use of so-called green biocides is becoming increasingly desirable in various applications to reduce the overall negative environmental impact of biocidal products.[3] Thus, future work with CBB and SNR testing should include industrial WW samples (e.g., marine-based applications) that are partially composed of these biocides.

Interestingly, in Chapter 3 it was also discovered that certain chemical compounds such as 2-Ethylhexanol and 1-Octanol were negatively correlated with nitrification inhibition and therefore were indicative of improving nitrification. Thus, SNR batch tests should be conducted with a list of the compounds identified in Chapter 3, and others with similar properties to those in the list, to verify the findings.

7.2.2 Outlook on the future of biocides: focus on green/eco-friendly low environmental toxicity biocides

There are a vast number of different biocides that exist that can be segmented into 23 product types of which there are hundreds of biocidal products.[4] However, the future of biocide selection used for various processes operated in institutions, businesses, commercial and industrial facilities will continue to be influenced by Sewer Use By-Laws which are becoming increasingly stringent over time. As a result, new broad-spectrum antimicrobials referred to as green, or eco-friendly biocides are becoming popular alternatives to meet these regulations which yield low levels of environmental toxicity. Coumarins, such as osthole and imperatorin, isolated from plant (*Cnidium monnieri*) extracts, and coumarin derivatives, namely 2'-deoxymetranzin hydrate, demonstrated excellent inhibitory activities against *Balanus albicosatus* larval settlements in marine applications including shipping facilities, seawater pipelines, and vessels.[5] These particular biocides are attractive alternatives to metal-based biocides such tributyltin and cuprous oxide as they are derived from the environment and are biodegradable.[5] There are also examples of so-called green biocide enhancers including ethylenediamine disuccinate (EDDS) that have been used to reduce the need for high concentrations of common biocides such as glutaraldehyde used for treating sulfate-reducing bacteria (SRB) biofilms.[3] D-tyrosine and other D-amino acids have also been used as green biocide enhancers for tetrakis hydroxymethyl phophonium sulfate (THPS) against SRB biofilms for microbiological influenced corrosion (MIC) control.[6]

7.2.3 Streamlined preparation and biocide testing using freshly cultured bacteria as cell-based biosensors using automated high-throughput systems

As discussed in Section 7.2.1, there are many compelling reasons to switch to creating separate models for clients, however, building them will take more time than a single large

universal model. The preparation phase and testing phase of the SNR test requires approximately 2 and 4 hours, respectively, while the CBB test can take up to four weeks and 1/6 of an hour (10 minutes), respectively. The lengthy CBB preparation time is owed solely to the culturing process of the bacterial strains; for example, nitrifying bacteria, *Nitrospira* (used in the CBB test), were grown for four weeks prior to their use. However, the successful implementation of preserved bacterial strains to form operationally stable CBBs for several months will eliminate preparation as the 'rate-limiting step'. The challenges of preparing a subset of the bacterial strains from the CBB test in various ways (solution and dry thin-film formats) for preservation purposes were addressed in Chapters 2, 5 and 6, however, there is more work to be done; see section 7.2.4. Until then, freshly cultured bacteria should be used to build-out these models.

Fortunately, easily culturable (<48 hours) bacterial strains *E. coli*, *B. subtilis*, and *B. cereus* were found to be strong contributors to predicting nitrification inhibition potential (Chapter 3) and thus waiting several days for the growth of *Nitrospira* may not be required; these three bacterial strains alone could be used for predictions. Apart from culturing bacteria as part of the preparation phase, the CBB test still necessitates the replacing of growth media of the bacterial strains to the testing media (phosphate buffered saline), followed by the transferring of the bacteria-testing media into microplates where industrial WWs (beginning of testing phase) and fluorescent dye are subsequently added. These steps can become a labor-intensive task if seeking to test hundreds of industrial WW samples either sequentially or in parallel. High-throughput systems such as the Liquid Handling Robot TECAN Freedom Evo® 200 exist to manage workflow automation from sample

preparation through to detection. These systems are conveniently equipped to handle the step-by-step process of aliquoting the necessary solutions (cultured bacterial strains, fluorescent dye, industrial wastewater) into a 96-well plate (or other plate configurations) and reading the fluorescence signals via a built-in fluorescence plate reader in a fully automated manner. The use of such systems would accelerate model development by minimizing workloads and enabling multiple samples to be tested in parallel. Such systems would also ensure accurate dispensing of liquids, and precise timing of liquid additions and fluorescence signal read-outs.

7.2.4 Survival and preservation performance of AIES-produced cell-embedded films

Preservation of CBBs at room or refrigerated temperatures is a key component in advancing testing capabilities. It allows CBB products to be shipped and stored without specialized cold chain requirements (e.g., ultra-low temperature freezers), and in wastewater applications it enables seamless on-site testing which is desirable for facilities that produce or receive WW on a regular basis. As demonstrated in Chapter 2, creating operationally stable CBBs such that their activity remains unchanged over the long-term is challenging. Harnessing, to a fuller extent, the well documented benefits of sugars such as pullulan and trehalose as stabilizing agents for biological materials in dried format, and using them to create rapidly dissolvable CBBs was the basis of Chapters 5 and 6. The atomizer-integrated electrospinning system (AIES) in Chapter 6 was shown to be a new valuable tool for creating bacterial-embedded films with a high degree of culturability for *E. coli* and *B. subtilis* (two common bacterial strains), but the preservation performance of the bacteria

over a storage period of months was not explored. It is recommended that future work with the AIES should consist of a well-thought-out Design of Experiments (DOE) evaluating a variety of factors, mainly including the atomizer operating pressure, diffusion dryer size, electrospinning voltage, sugar formulation (varying pullulan and trehalose concentrations), and bacteria type and concentration to maximize bacteria culturability and detection stability of biocides over a period of months. Other work should include obtaining confocal images of electrospun films to analyze the distribution of fluorescent green microspheres throughout the matrix.

The AIES system may also cater to other biological materials. In particular, it may be useful in tissue engineering applications where cells, such as fibroblasts, have been shown to exhibit a large degree of cell proliferation when present outside of electrospun fibers;[7] to this end, the AIES is ideally suited since the fibroblasts and other biological materials interacting with the electrospun fibers are aerosolized and thus are not forced into encapsulation within the fibers as with a traditional electrospinning process. With traditional electrospinning used to encapsulate mesenchymal stems cells, The AIES should also be investigated as a gentler alternative to embed other biological materials including mesenchymal stem cells and mononuclear cells which has shown viabilities of 19.6% and 8.38% after electrospinning, respectively.

7.3 References

1. Winther-Nielsen, M. and J. la Cour Jansen, *The role of the sludge in nitrification inhibition tests.* Water Science and Technology, 1996. **33**(6): p. 93-100.
2. Standard, I., *Water quality — Toxicity test for assessing the inhibition of nitrification of activated sludge microorganisms*, in *ISO 9509*. 2006: Switzerland.

3. Ashraf, M.A., et al., *Green biocides, a promising technology: current and future applications to industry and industrial processes.* Journal of the Science of Food and Agriculture, 2014. **94**(3): p. 388-403.
4. Singer, H., et al., *Determination of biocides and pesticides by on-line solid phase extraction coupled with mass spectrometry and their behaviour in wastewater and surface water.* Environmental pollution, 2010. **158**(10): p. 3054-3064.
5. Wang, Z.-C., D.-Q. Feng, and C.-H. Ke, *Coumarins from the herb Cnidium monnieri and chemically modified derivatives as antifoulants against Balanus albicostatus and Bugula neritina larvae.* International Journal of Molecular Sciences, 2013. **14**(1): p. 1197-1206.
6. Xu, D., Y. Li, and T. Gu, *A synergistic D-tyrosine and tetrakis hydroxymethyl phosphonium sulfate biocide combination for the mitigation of an SRB biofilm.* World Journal of Microbiology and Biotechnology, 2012. **28**(10): p. 3067-3074.
7. Xu, F., et al., *Single-step reactive electrospinning of cell-loaded nanofibrous scaffolds as ready-to-use tissue patches.* Biomacromolecules, 2018. **19**(11): p. 4182-4192.

Appendix A

The effects of 'partial' desiccation (evaporative stress) where a portion of the cell solution was desiccated were investigated. The relative humidity (RH) during desiccation was set to 25 ± 3% in an xL Bel-Art Vacuum Desiccator. 100g of Drierite Desiccant-Anhydrous was used for both microplates and microtubes. If microplates were prepared, one plate was placed between two Sigma-Aldrich Nalgene Microfuge Tube Racks which were stacked on top of each other, and the other plate was placed on the top rack. Only the inside wells of the 96-well Flat Bottom Low Evaporation Lid Tissue Culture Plate were used (**Figure A1**).

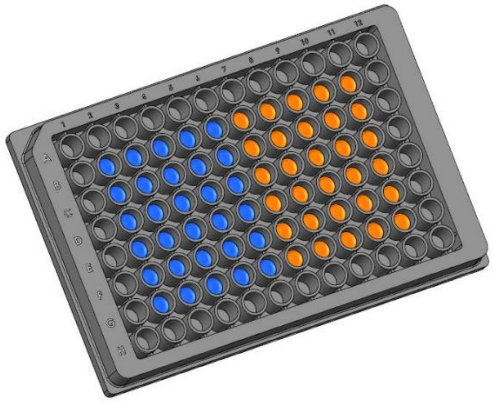

Figure A1. Microplate configuration: 60 wells were used per plate (30 wells per preservation condition). A total of 240 wells were used (8 preservation conditions) of which only 192 wells were tested (6 extra wells per condition). Model designed in SolidWorks.

If tubes were prepared, two racks each containing 49 tubes were stacked on top of one another with tube caps open (**Figure A2**). All 98 tubes contained 150µL of cell-solution

(preservation conditions determined based on the DOE). The stacked tube racks were then placed in the desiccator

Figure A2. Left: two tube-holding racks (stackable). Right: Two tube-holding racks stacked and placed into an xL Bel-Art Vacuum Desiccator.

Prior to desiccation, a Measurement Computing USB-502 RH/Temperature Data Logger was placed inside the desiccator to monitor RH as a function of time. **Figure A3** shows RH as a function of desiccation time for microplates and microtubes.

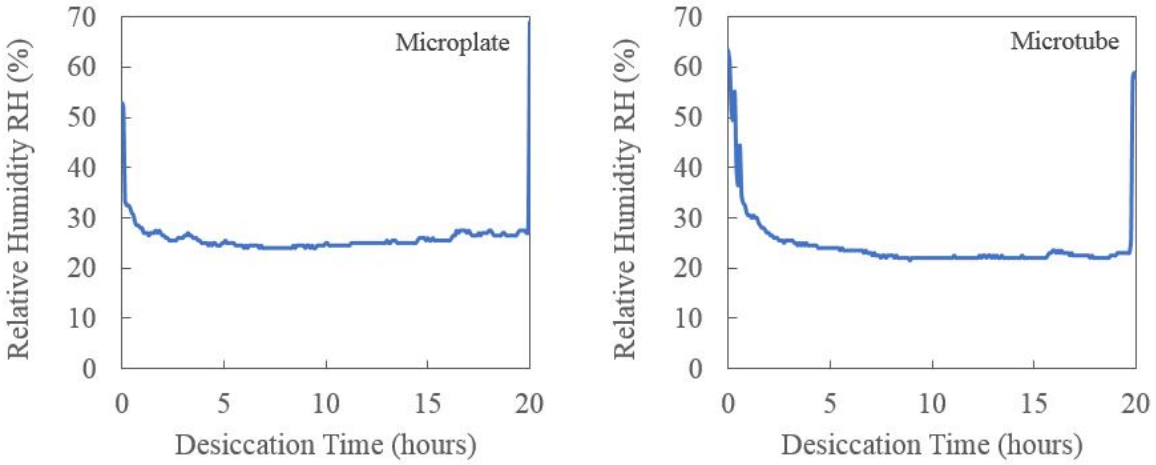

Figure A3. Partial desiccation time period in a 96-well microplate for Condition 2, 8, 12, and 14 (left). Partial desiccation time period in microtubes for Condition 4, 6, 10, and 16 (right). RH goal was 25% over a 20-hour desiccation period.

Post-Desiccation Analysis:

Figure A4 show depression development on an AbsorbMax™ film two weeks after cell preservation preparation in an Eppendorf 96-well Flat Bottom Black Plate. A sterile mechanical punch was used to allow re-homogenization and removal of the cell solution using a 200 µL micropipette. After the cell solution was re-homogenized, a portion of a new AbsorbMax™ film was cut, the hole was covered, and the microplate was placed back in its respective preservation condition (4 °C fridge, or 20 °C drawer). Some conditions showed differences in depression depth (visible in **Figure A4)** where Condition 12 (left side) produced deeper depressions compared to Condition 14 (right side)). For Condition 14, there were visible differences between depressions (bottom right vs top right). Although other conditions are not shown, it was hypothesized that these variations may have

explained for the dips and peaks in the fluorescence signals from week to week for certain conditions stored in microplates. It can also be seen that some depressions did not form at all. It was also noted that plates that were stored at 20 °C, had developed deeper depressions than plates stored at 4 °C.

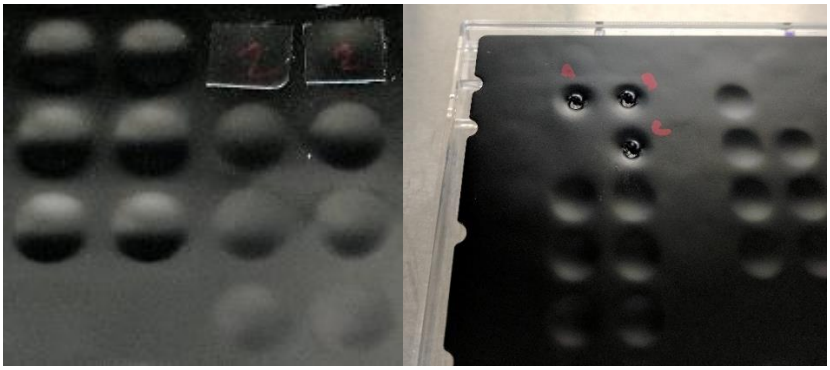

Figure A4. Left: Condition 12 (left half), Condition 14 (right half). Lighter depressions appear in Condition 14 for certain wells. Right: Holes in AbsorbMax™ film prior to re-homogenization of cell solution for Condition 12.

Maximum Live Fluorescence to Culturability Relationship at Room Temperature:

The Maximum Live Fluorescence (MLF) was plotted against culturability (CFU/mL) for all 8 conditions stored at 20 °C (i.e. Conditions #9 through #16) for all eight timepoints. The results in **Figure A5** show a similar trend for all conditions where the MLF is positively correlated with CFU/mL (concentration of culturable cells inside the microtube or microplate well).

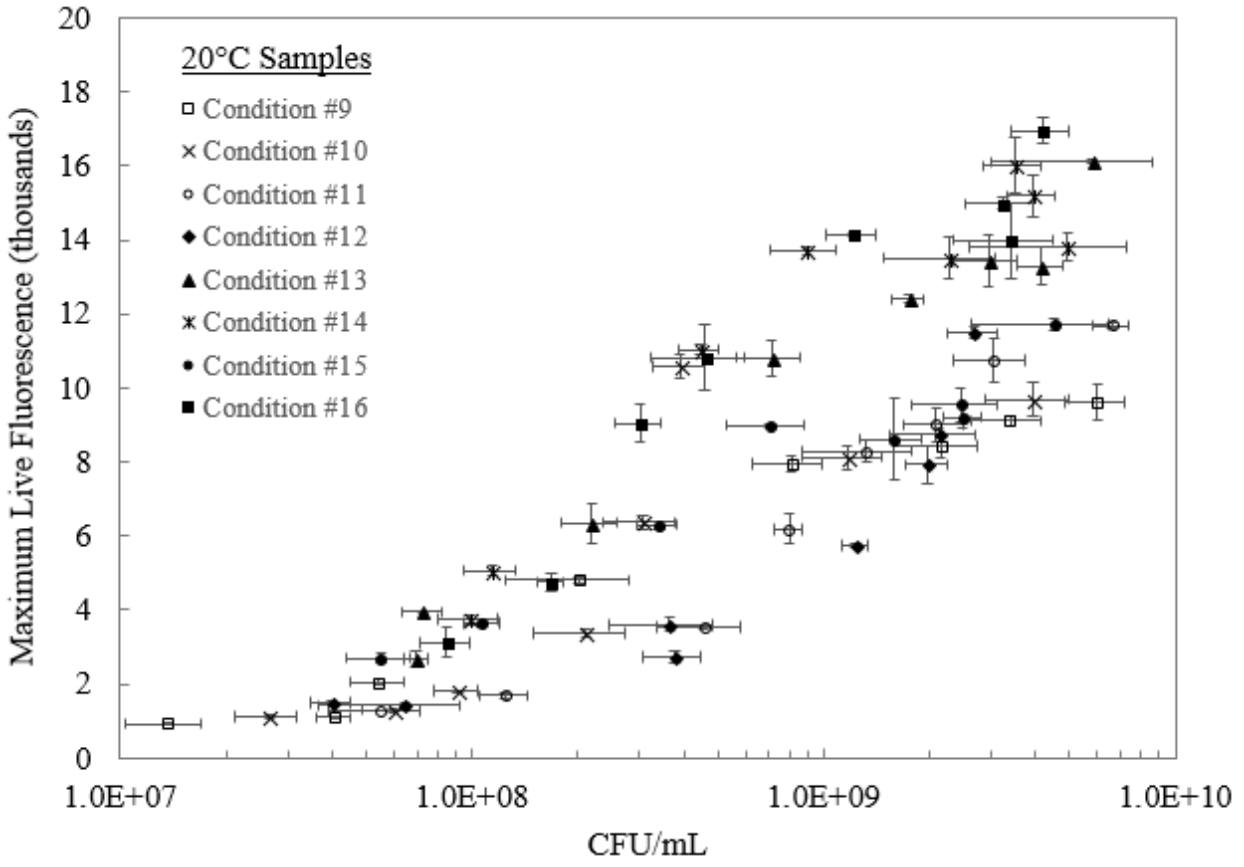

Figure A5. Comparison of eight preservation conditions stored at 20 °C from the 2^{5-1} DOE study in terms of the relationship between CFU/mL (x-axis) and Maximum Live Fluorescence (y-axis) across the eight timepoints of the 14-week storage period. The error bars for the CFU/mL data series and Maximum Live Fluorescence data series correspond to the standard deviation from the analysis of triplicate (three microtubes or microplate wells, each measured three times) and duplicate samples (two microtubes or microplate wells, each measured once) respectively. The factors pertaining to each condition are found in Figure 2-1 of Chapter 2.

RNA Results:

During the 14-week storage period, both Conditions #1 and #10 were found to have relatively low CFU counts but very different MLF values. After 28 weeks of storage, the RNA concentrations were measured using a Thermo Scientific™ Nanodrop™ One^{C} UV-Vis spectrophotometer with the results displayed in **Table A1**.

Table A1. OD_{600} (absolute), CFU/mL, maximum live fluorescence, and intracellular RNA concentration (measured using Nanodrop One^c instrument) for Conditions 1 and 10 in duplicate after 28 weeks of storage.

Results	Condition 1		Condition 10	
	A	B	A	B
Cell Storage Temperature	4°C	4°C	20°C	20°C
OD_{600} (absolute)	0.1051	0.1042	0.0413	0.0418
CFUs per mL of Storage (10^4)	2	8	280	317
Maximum Live Fluorescence (thousands)	8.7	8.3	1.1	1.1
Nanodrop One^c RNA (ng/µL)	1.18	1.25	0.14	0.09
RNA/OD_{600}	11	12	3	2
Fluorescence / RNA	7	7	8	12

Growth Curve and Biocide Exposure Tests:

Growth curve profiles (OD_{600}) for weeks 0, 2, 7, 10, and 14 were evaluated for all 16 conditions with the results shown in **Figures A6**, **A7**, **A8**, and **A9**. Biocide exposure using Proclin™ 300 (300 ppm, 9 ppm active ingredient), CTAB (20 ppm), and Grotan BK (1500 ppm) were conducted on all 16 preservation conditions over a 14-week period with the results shown in **Figures A10**, **A11**, **A12**, and **A13**.

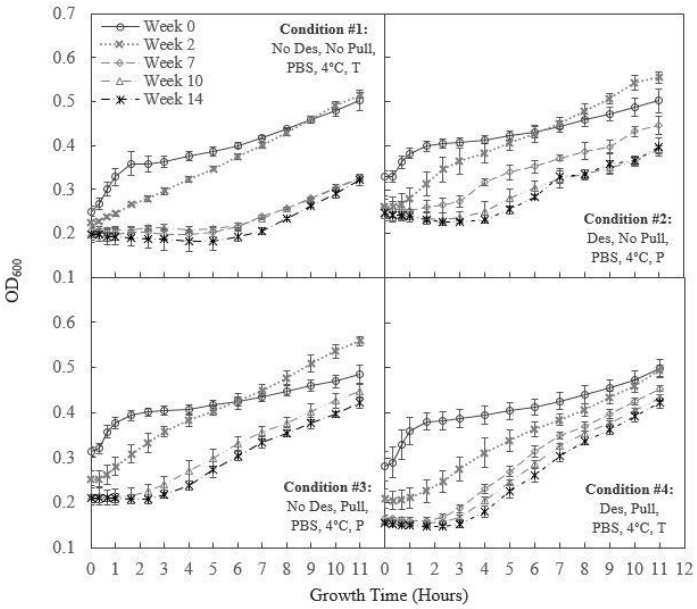

Figure A6. OD_{600} growth curves over an 11-hour period at 37 °C for the four preservation conditions corresponding to panels 1, 2, 3, and 4 in Figure 2-1. Refer to the caption for Figure 2-3 for a detailed explanation of the captions on each panel.

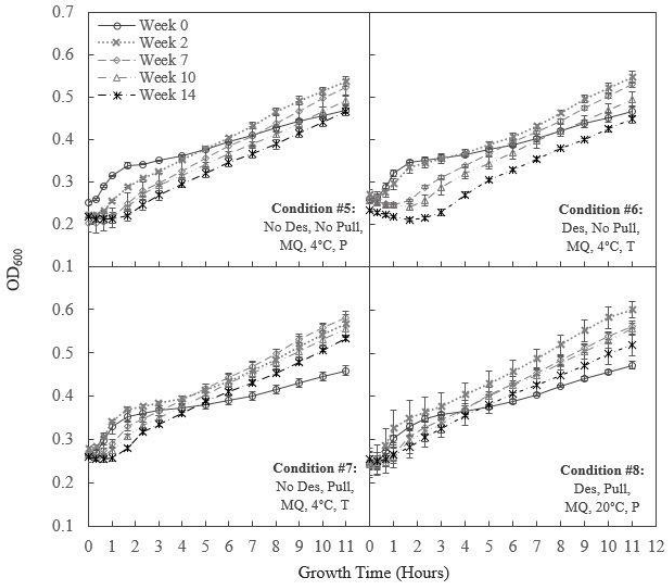

Figure A7. OD_{600} growth curves over an 11-hour period at 37 °C for the four preservation conditions corresponding to panels 5, 6, 7, and 8 in Figure 2-1. Refer to the caption for Figure 2-3 for a detailed explanation of the captions on each panel.

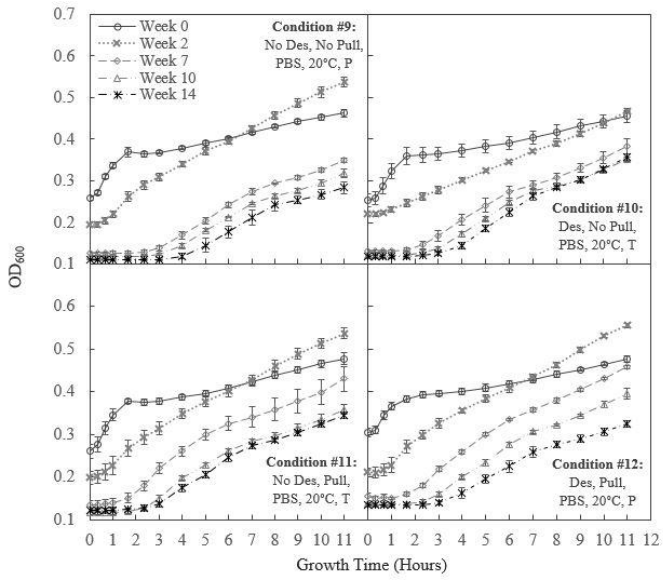

Figure A8. OD_{600} growth curves over an 11-hour period at 37 °C for the four preservation conditions corresponding to panels 9, 10, 11, and 12 in Figure 2-1. Refer to the caption for Figure 2-3 for a detailed explanation of the captions on each panel.

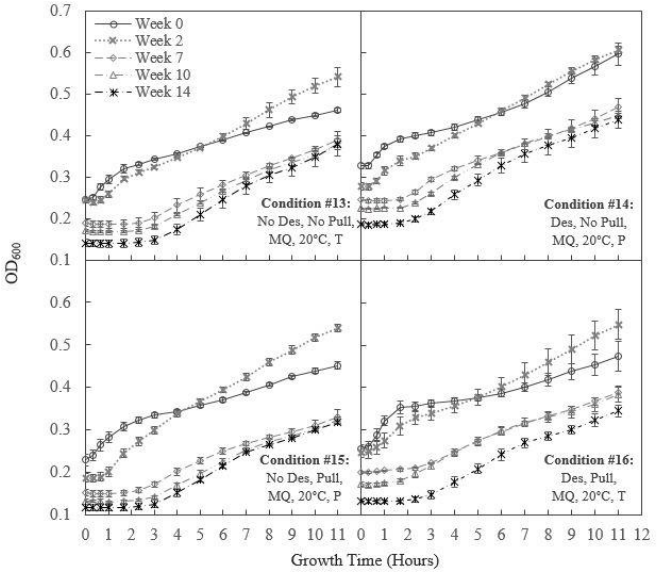

Figure A9. OD_{600} growth curves over an 11-hour period at 37 °C for the four preservation conditions corresponding to panels 13, 14, 15, and 16 in Figure 2-1. Refer to the caption for Figure 2-3 for a detailed explanation of the captions on each panel.

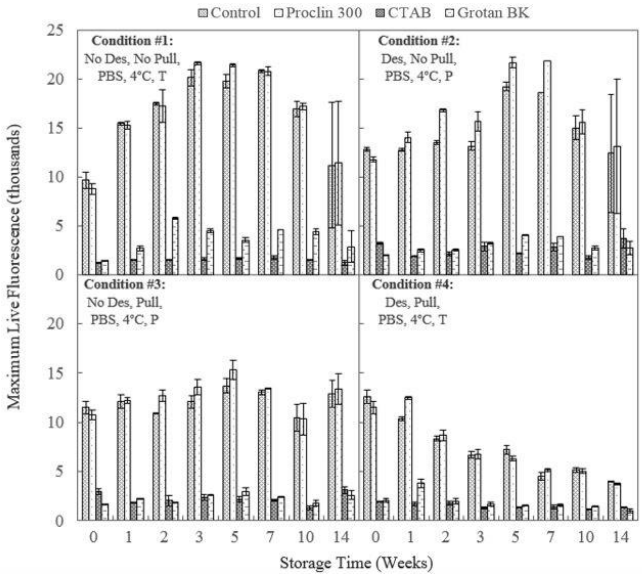

Figure A10. Comparison of the effect of biocide exposure on the Maximum Live Fluorescence values for the four preservation conditions corresponding to panels 1, 2, 3, and 4 in Figure 2-1. The different bars at each timepoint correspond to the samples that were exposed to the control (i.e., Milli-Q water) and ProClin™ 300, CTAB, and Grotan® BK samples with concentrations of 300 ppm (9 ppm active ingredient), 20 ppm, and 1500 ppm respectively. Refer to the caption for Figure 2-3 for a detailed explanation of the captions on each panel.

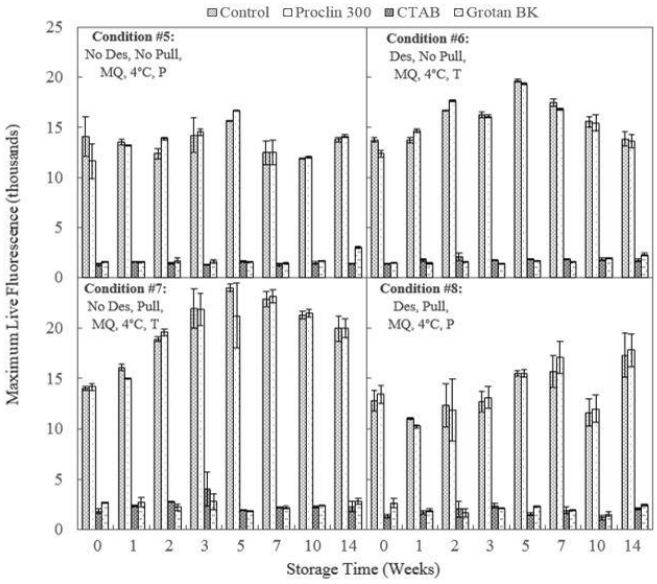

Figure A11. Comparison of the effect of biocide exposure on the Maximum Live Fluorescence values for the four preservation conditions corresponding to panels 5, 6, 7, and 8 in Figure 2-1. The different bars at each timepoint correspond to the samples that were exposed to the control (i.e., Milli-Q water) and ProClin™ 300, CTAB, and Grotan® BK samples with concentrations of 300 ppm (9 ppm active ingredient), 20 ppm, and 1500 ppm respectively. Refer to the caption for Figure 2-3 for a detailed explanation of the captions on each panel.

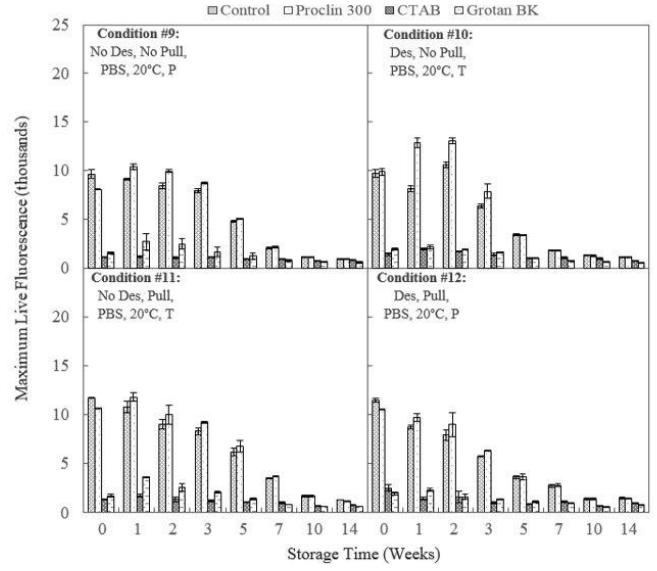

Figure A12. Comparison of the effect of biocide exposure on the Maximum Live Fluorescence values for the four preservation conditions corresponding to panels 9, 10, 11,

and 12 in Figure 2-1. The different bars at each timepoint correspond to the samples that were exposed to the control (i.e., Milli-Q water) and ProClin™ 300, CTAB, and Grotan® BK samples with concentrations of 300 ppm (9 ppm active ingredient), 20 ppm, and 1500 ppm respectively. Refer to the caption for Figure 2-3 for a detailed explanation of the captions on each panel.

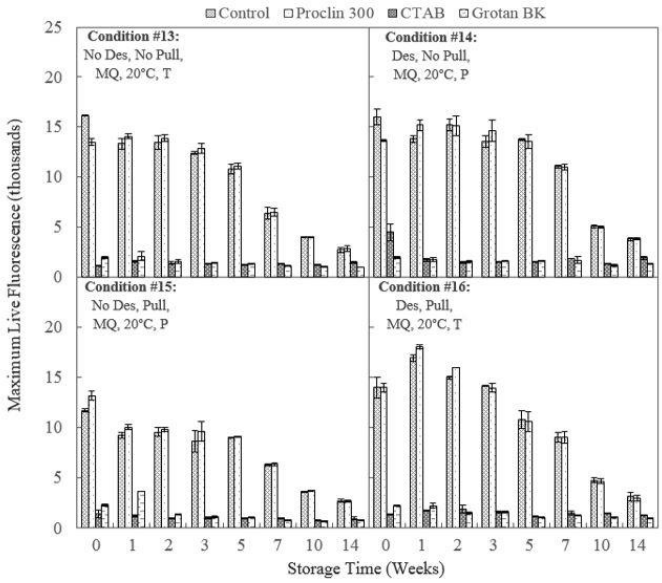

Figure A13. Comparison of the effect of biocide exposure on the Maximum Live Fluorescence values for the four preservation conditions corresponding to panels 13, 14, 15, and 16 in Figure 2-1. The different bars at each timepoint correspond to the samples that were exposed to the control (i.e., Milli-Q water) and ProClin™ 300, CTAB, and Grotan® BK samples with concentrations of 300 ppm (9 ppm active ingredient), 20 ppm, and 1500 ppm respectively. Refer to the caption for Figure 2-3 for a detailed explanation of the captions on each panel.

Multiple Linear Regression R Code:

CFU:

```
x1 <- c(-1, +1, -1, +1, -1, +1, -1, +1, -1, +1, -1, +1, -1, +1, -1, +1)
x2 <- c(-1, -1, +1, +1, -1, -1, +1, +1, -1, -1, +1, +1, -1, -1, +1, +1)
x3 <- c(-1, -1, -1, -1, +1, +1, +1, +1, -1, -1, -1, -1, +1, +1, +1, +1)
x4 <- c(-1, -1, -1, -1, -1, -1, -1, -1, +1, +1, +1, +1, +1, +1, +1, +1)
x5 <- c(+1, -1, -1, +1, -1, +1, +1, -1, -1, +1, +1, -1, +1, -1, -1, +1)
```

```
yx14 <- c(0.00121, 0.01797, 0.044129, 0.01151, 0.04138, 0.045092, 0.333235, 0.28365,
0.00228, 0.00675, 0.00833, 0.0149, 0.012, 0.02819, 0.01216, 0.02485)
mod.full <- lm(yx14 ~ x1*x2*x3*x4*x5)
summary(mod.full)
library(pid)
paretoPlot(mod.full)
yield = yx14
library(car)
qqPlot(yield)
```

Multiple Linear Regression (MLR) Aliasing Notations:

X1 (Desiccation) → A
X2 (Stabilizer) → B
X3 (Solution) → C
X4 (Storage Temp) → D
X5 (Storage Unit) → E

There are many aliasing combinations, however only a few are shown.

$$E = ABCD, I = ABCDE$$

X1:X5 which appeared to have a high coefficient value in the MLR, is confounded with the best condition; Condition 7 and Condition 8 (Pullulan, Milli-Q Water, and 4 °C). By multiplying both sides of the identity by AE, the left side produce AE, and the right side produces BCD (AE is cancelled with itself).

$$I = ABCDE$$

$$AE = BCD$$

$$X1:X5 = X2:X3:X4 = (\text{Stabilizer})(\text{Solution})(\text{Temperature})$$

Since Condition 7 and Condition 8 are both involved in the calculation, and both record relatively large CFU fractions, the coefficient value for X1:X5 has been largely increased.

Appendix B

Table B1. Comparison of results for 28 industrial WW samples for the SNR test (highlighted in gray) and the CBB panel fluorescence data (highlighted in orange). The error (standard deviation) associated with the fluorescence signals was between 1-5% based on duplicate testing. Duplicate analysis of WW sample 2 and 18 showed that the % SNR Difference values and their errors were approximately 4 ± 2 and 26 ± 5, respectively.

WW Sample	SNR Outcome	Bacterial Strain Fluorescence Signal						
	% SNR difference	*Nitrospira*	*N. europaea*	*E. coli*	*B. subtilis*	*B. cereus*	*S. saprophyticus*	*S. laurentii*
1	0.58 (Fail)	3072	4279	5984	18258	9682	4956	22007
2	3.93 (Fail)	3194	4719	8063	17817	10221	4618	22183
3	5.65 (Fail)	3137	5412	5244	19517	10289	4592	21800
4	6.35 (Fail)	3082	4278	7717	16312	9508	3997	19418
5	15.45 (Fail)	3406	4867	5774	19640	12206	5580	22162
6	-12.58 (Pass)	2756	4350	6198	18142	8855	3976	21993
7	1.51 (Fail)	3411	4897	7727	19716	10913	4237	21643
8	-13.53 (Pass)	2561	4425	6694	18781	8964	4725	21569
9	5.45 (Fail)	3380	5358	6745	19027	10007	5551	23272
10	-1.43 (Pass)	2882	4414	6116	17844	8724	4906	21163
11	-9.66 (Pass)	2731	4419	5571	19038	9453	4855	22923
12	-3.89 (Pass)	2869	4362	6013	19312	9250	5041	22038
13	13.64 (Fail)	3100	5048	7010	17058	9195	4851	23851
14	-7.60 (Pass)	2747	4383	5902	18322	8669	4840	24482
15	-1.17 (Pass)	3220	4876	5665	19849	9936	5303	23295
16	-6.84 (Pass)	2734	4517	6011	19352	9103	4868	21432
17	29.66 (Fail)	2937	3986	7044	16750	8003	4294	22108
18	26.01 (Fail)	3029	4035	9438	13754	7863	4064	21836
19	0.23 (Fail)	3349	4531	6034	18156	10027	5118	22834
20	0.90 (Fail)	2880	4134	8630	20688	11062	4475	23363
21	5.66 (Fail)	3471	3955	6802	18051	8832	5102	23121
22	2.00 (Fail)	2938	3217	8747	19146	9729	4538	22602
23	-7.48 (Pass)	2611	4079	5192	17903	9216	4572	22942
24	1.24 (Fail)	2497	3676	6709	18076	9910	4532	22226
25	3.38 (Fail)	2972	3815	6018	19141	10004	4798	22130
26	-15.54 (Pass)	3024	3713	6653	20500	8959	5002	22556
27	-6.04 (Pass)	2619	2492	6203	19902	8856	4798	24028
28	13.95 (Fail)	2778	2583	6942	19085	10687	5834	26079

Table B2. Gas Chromatography-Mass Spectrometry (GC-MS) and % SNR difference. The GC-MS values (highlighted in green) correspond to the integral peak area normalized by integral peak area of the internal standard; zero values are used to indicate that the corresponding chemical compound was not detected. Table continued on next page.

WW Sample	SNR Outcome	Gas Chromatography-Mass Spectrometry (normalized integral peak area)							
	% SNR difference	Butanoic acid	Ethylene glycol	Propylene glycol	β-Eudesmol	Heptanoic acid	p-Anisic acid	Triethylene glycol butyl ether	1-Octanol
1	0.58	1.154	0	0	0	2.063	0	0	0
2	3.93	24.463	0	0	0	6.908	0	9.981	0
3	5.65	0	0	0	0	0	0	0.984	0
4	6.35	0	0	0	0	0	0	0	0
6	-12.58	0	0.195	0	0	0	0	0.227	0.296
7	1.51	0	0	0.540	1.409	0	0	0.514	0.371
8	-13.53	0	0	0	0	0	0	0.608	0.362
9	5.45	0	0.610	0.505	0.758	0	0	0.286	0.389
10	-1.43	0	0	0	0	0	0	1.512	0
11	-9.66	0	0	0	0	0	0	0	0
12	-3.89	0	0	0	0	10.989	0	0	0
13	13.64	0	0	0	0	5.092	0	5.855	0
14	-7.60	0	0	0	0	0	0	0	0
16	-6.84	0	0	1.445	1.793	0	0	0	0
20	0.90	0	0	0	0	1.409	0	0	0
22	2.00	0.494	0	0	0	0	0	0	0
24	1.24	0	0	1.567	0	0	0.250	0	0
27	-6.04	0	0	0	0	0	0	0	0
28	13.95	0	0	0	0	0	0	0	0

WW Sample	Gas Chromatography-Mass Spectrometry (normalized integral peak area)										
	Ethylhexanoic acid	2-Phenylethanol	Nonanoic acid	Isoeugenol	Phenol	(E)-Cinnamic acid	Pentanoic acid	2-Butoxyethanol	Hexanoic acid	Benzyl alcohol	Decanoic acid
1	1.632	0.418	0	0	0.274	0	0.593	8.277	0.460	0.663	0
2	5.882	0	2.739	0	3.868	0	0	14.682	3.335	3.397	0
3	5.055	0	0	0	0	0	0	5.077	0	1.191	0
4	50.659	0	0	0	0	0	0	16.241	0	12.898	6.463
6	0	0	0	0	0	0	0	0	0	0	0
7	0	0	0	0.849	0	0	0.258	6.570	0	5.410	0
8	0	0	0	0	0.255	0	0.332	2.310	0	0.231	0
9	0	0.388	0	0.761	0	0	0.370	0	0	1.732	0
10	0	0	0	0	0	0	0	7.001	0	2.010	0
11	0	0	0	0	0	0	0	3.090	0	0	0
12	19.567	0	4.345	0	0	0	0	28.942	0	0	0
13	0	0	2.058	0	0	0	0	0	0	4.856	0
14	0	0	0	0	1.271	0	0	4.556	0	0	0
16	0	0	0	0	0	0	0	5.686	0	4.419	0
20	1.532	0	0.566	0	1.494	0	0	0	0	1.223	0
22	1.779	0	0.304	0	0.324	0	0	2.550	0.489	1.251	0
24	2.287	0	0	0	0	0.216	0	2.043	0.673	1.619	0
27	0	0	0	0	0.646	0	0	4.442	0	1.462	0
28	32.435	0	12.503	0	0	0	0	60.597	0	15.977	0

…Table B2. Continued on next page.

WW Sample	Gas Chromatography-Mass Spectrometry (normalized integral peak area)										
	Octanoic acid	Benzoic acid	Diethylene glycol butyl ether	Phenoxy ethanol	Cyclohex anamine	Sebacic acid	Undecane dioic acid	Dodecane dioic acid	1-Hexanol	1-Phenyletha nol	Ricinoleic acid
1	2.755	0.711	4.619	0	0	1.095	3.347	2.535	0	0	0
2	13.015	6.125	16.021	0	0	5.553	14.980	12.162	0	0	0
3	5.322	1.995	3.210	0	0	2.873	1.424	1.250	0	0	0
4	9.829	5.941	13.728	0	0	4.351	6.532	5.270	0	0	0
6	0	0	0.400	0	0	0	0	0	0	0	0
7	0	0	3.233	0	0	0	0	0	0	3.017	0
8	0	0	3.302	0	0	0	0	0	0	0	0
9	0	0	2.043	0.855	0.360	0	0	0	0	0.302	0
10	0	0	1.808	0	0	0	0	0	0.627	1.440	0
11	0	0	1.007	0	0	0	0	0	0	0	0
12	31.668	5.025	18.775	0	0	13.513	32.021	35.599	0	0	0
13	8.967	4.682	10.111	0	0	3.037	8.292	6.947	0	0	0
14	0	0	2.090	0	0	0	0	0	0	0	0
16	0	0	2.395	2.470	0	0	0	0	0	0.921	0
20	2.421	0.697	0.809	0	0	0.387	2.009	1.056	0	0	0
22	2.616	0.876	0.997	0	0.379	0.613	1.290	1.207	0.574	0	0.563
24	2.336	3.027	0.870	0	0	0.455	4.164	2.067	0	0	0
27	0	0	1.279	0	0	0	0	0	0	0.632	0
28	72.978	16.239	32.955	0	0	43.884	56.705	48.564	0	0	0

…Table B2. Continued on next page.

WW Sample	Gas Chromatography-Mass Spectrometry (normalized integral peak area)										
	Linalool	L-α-Terpineol	Dicyclohexylamine	Palmitic Acid	Carbodiimide	Dibutyl phthalate	3,6,9,12,15-Pentaoxahexadecan-1-ol	Cresol	2-Butoxyethyl	Cinnamyl Alcohol	3-Hydroxyisovaleric acid
1	0	0	0.899	0	0	0	0	0	0	0	0
2	0	0	3.752	0	0	0	0	0	0	0	0
3	0	0	0	0	0	0	0	0	0	0	0
4	0	0	0	0	0	0	0	0	0	0	0
6	0	0	0	0	0.181	0.146	0	0	0	0	0
7	0.680	1.263	0.687	0	0.171	0	0	0	0	0.306	0
8	0	0	1.284	0	0.182	0	0.255	0	0	0	0
9	0.645	0.958	1.691	0.114	0	0	0	0	5.425	0.212	0
10	1.652	0	0	0	0	0	0	0	0	0	0
11	0	0	0	0	0	0	0	0.248	0	0	0
12	0	0	8.415	0	0	0	0	0	0	0	0
13	0	0	2.220	0	0	0	0	0	0	0	0
14	0	0	0	0	0	0	0	4.496	0	0	0
16	2.346	0	2.480	0	0	0	0	0	0	0	7.129
20	0	0	0.387	0	0	0	0	0	3.800	0	0
22	0	0	0	0	0	0	0	0	0	0	0
24	0	0	0	0	0	0	0	0	0	0	0
27	0	0	0	0	0	0	0	2.002	0	0	0
28	0	0	0	0	0	0	0	0	0	0	0

…Table B2. Continued on next page.

WW Sample	Gas Chromatography-Mass Spectrometry (normalized integral peak area)									
	Carbitol	2,3-Butanediol	2-Ethylhexanol	5-Phenylnonane	2,6-Dimethylphenol	Cyclohexanol	2-Butanol	Trifluoroacetamide	Dehydroabietic acid	p-Chlorocresol
1	0	0	0	0	0	0	0	0	0.758	0
2	0	0	0	0	0	0	0	0	0	2.345
3	0	0	0	0	0	0	0	14.769	0	0
4	0	0	0	0	0	0	0	0	0	0
6	0	0	0	0	0	0	0	0	0	0
7	0.311	0.945	0	0	0	0	0	0	0	0
8	0	0	0	0	0	0	0	0	0	0
9	0	0	0	0	0	0	0	0	0	0
10	0	1.285	0	0	0	0.555	1.796	0	0	0
11	0	0	0.672	0.304	0	0	0	0	0	0
12	0	0	0.185	0	0	0	0	0	0	0
13	0	0	0	0	0	0	0	0	0	1.555
14	0	0	0	0	1.846	0	0	0	0	0
16	0	0	0	0	0	0	0	0	0	0
20	1.081	0	0	0	0	0	0	0	0	0
22	1.347	0	0	0	0	0	0	0	0	0
24	1.188	0	0	0	0	0	0	0	0	0
27	0	2.731	0	0	0	0	0	0	0	0
28	0	0	0	0	0	0	0	0	0	0

…Table B2.

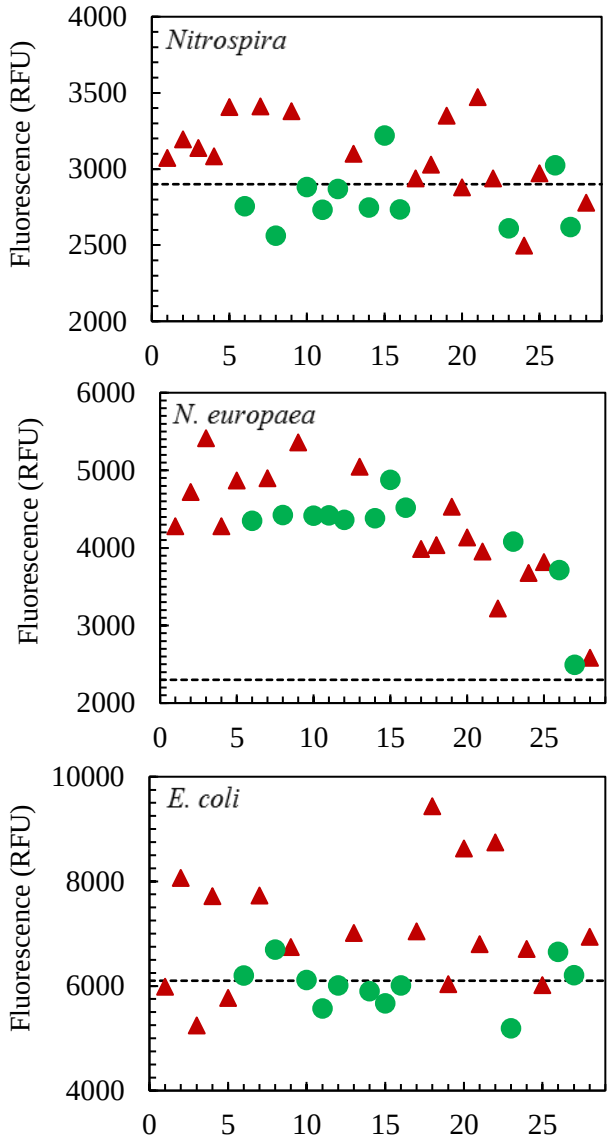

Figure B1. Fluorescence comparison for each bacterial strain (fluorescence signals are plotted using the data shown in **Table B1**). The dotted line represents the control signal (i.e., addition of Milli-Q water instead of WW) for each bacterial strain. The red triangles identify those WW samples that failed the SNR batch test (i.e., had % SNR difference greater than zero). The green circles identify those WW samples that passed the SNR batch test (i.e., had % SNR difference less than zero). Figure continued on next page.

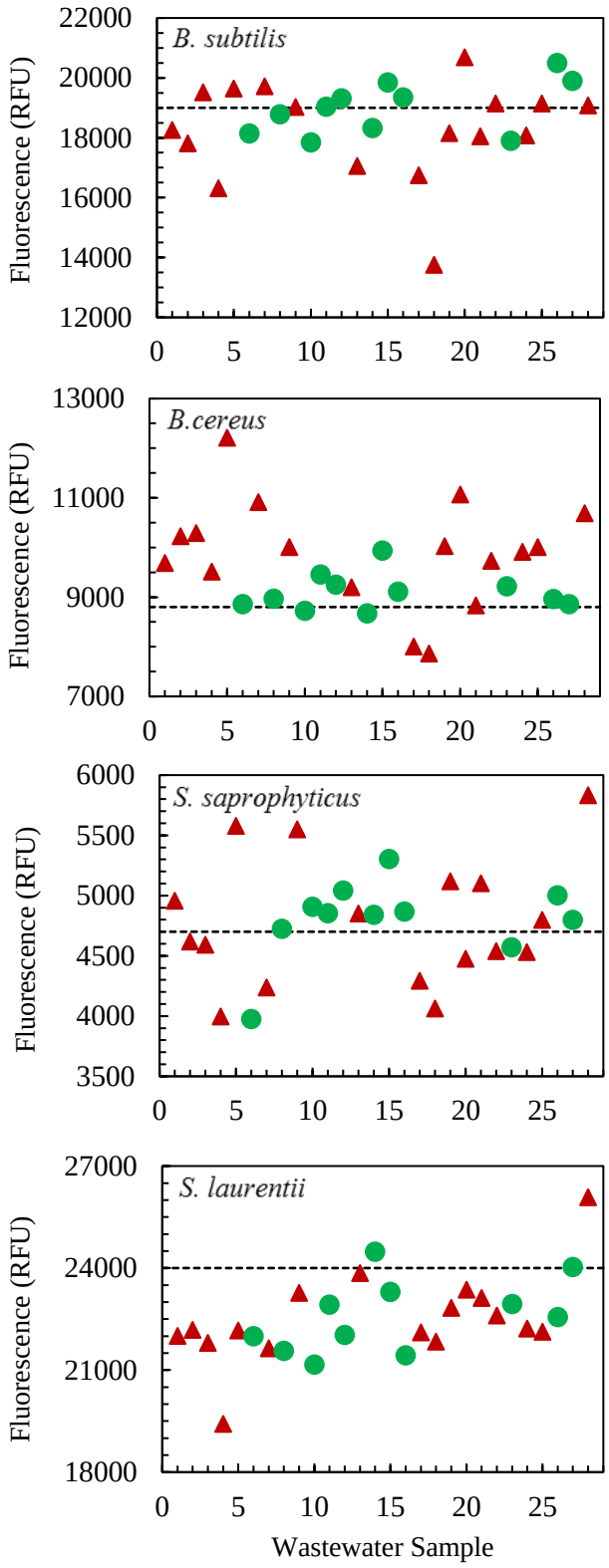
B. subtilis
B.cereus
S. saprophyticus
S. laurentii
Fluorescence (RFU)
Wastewater Sample

…Figure B1.

Figure B2. SNR experimental setup: pH meter, dissolved oxygen meter, seven 100 mL Erlenmeyer flasks containing return activated sludge, mineral medium, COD medium, and the corresponding WW sample. This figure shows a user sampling an SNR batch reactor for measurement of nitrite-N and nitrate-N concentrations. The clear Erlenmeyer flask was not used in this study; typically, this flask would represent the SNR control and would look identical in color to the other flasks (Milli-Q water exposure instead of a WW sample).

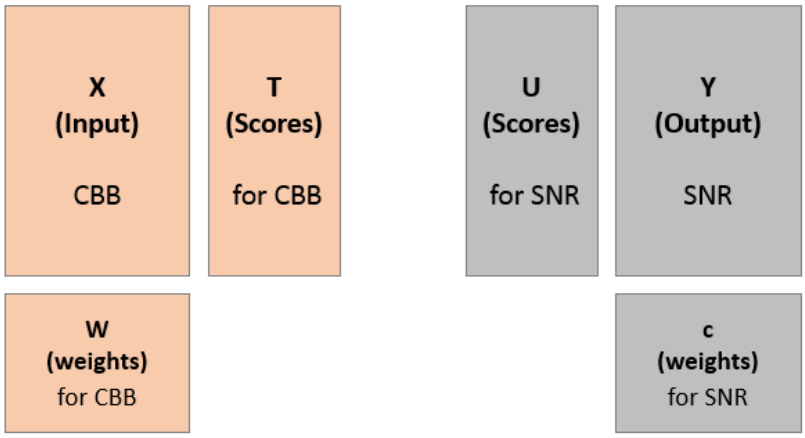

Figure B3. CBB to SNR PLS Model Setup. The X space (input) corresponds to the CBB fluorescence data. The weights (W) and scores (T) for the CBB fluorescence data are shown to the bottom and right of the X space (typical layout), respectively. The Y space corresponds to the % SNR difference data. The weights (c) and scores (U) for the % SNR difference data are shown to the bottom and left of Y space (typical layout), respectively. PLS modeling is used to calculate the values present in the W, T, c, and U spaces.

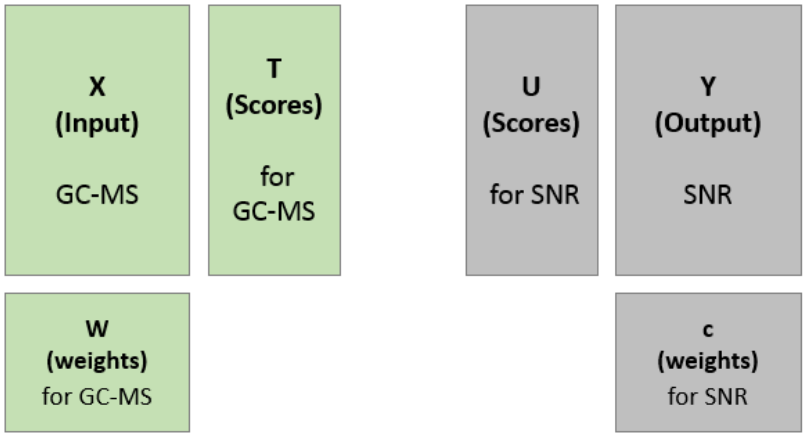

Figure B4. GC-MS to SNR PLS Model Setup. The X space (input) corresponds to the GC-MS data. The weights (W) and scores (T) for the GC-MS data are shown to the bottom and right of the X space (typical layout), respectively. The Y space corresponds to the % SNR difference data. The weights (c) and scores (U) for the % SNR difference data are shown to the bottom and left of Y space (typical layout), respectively. PLS modeling is used to calculate the values present in the W, T, c, and U spaces.

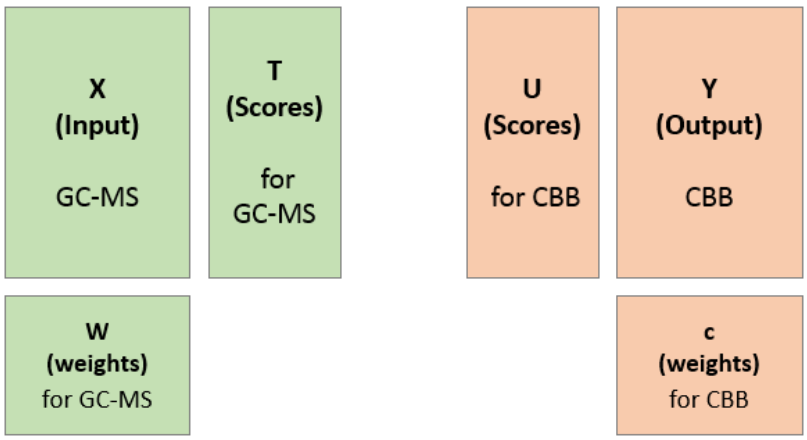

Figure B5. GC-MS to CBB PLS Model Setup. The X space (input) corresponds to the GC-MS data. The weights (W) and scores (T) for the GC-MS data are shown to the bottom and right of the X space (typical layout), respectively. The Y space corresponds to the CBB panel fluorescence data. The weights (c) and scores (U) for the CBB panel fluorescence data are shown to the bottom and left of Y space (typical layout), respectively. PLS modeling is used to calculate the values present in the W, T, c, and U spaces.

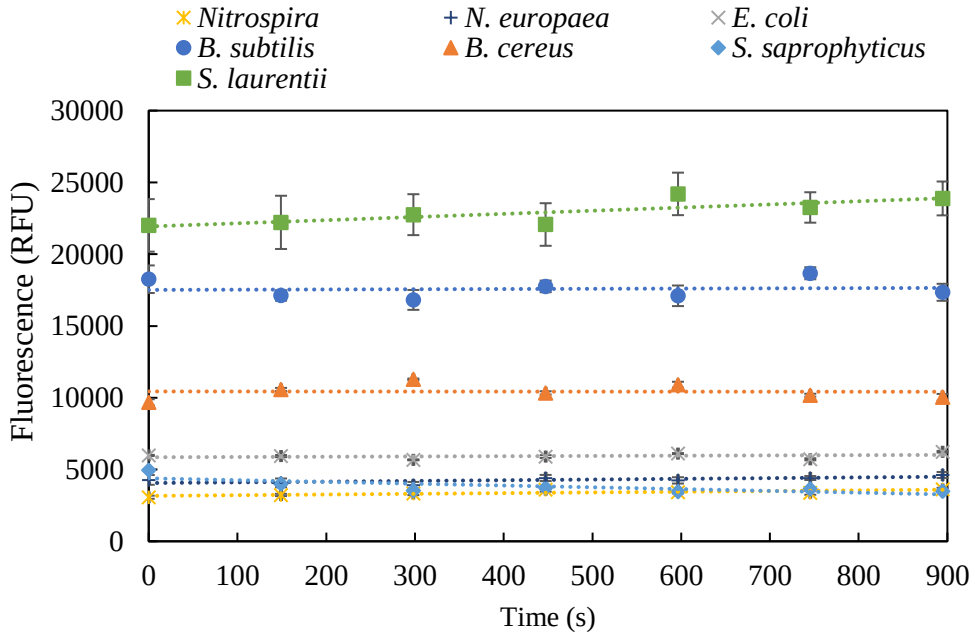

Figure B6. An example of the stability of the fluorescence signals over 15 minutes for all seven strains used in the CBB panel exposed to WW #1.

Table B3. R^2 and Q^2 values for different principal components for seven separate GC-MS to bacterial strain fluorescence PLS models; the same GC-MS data as shown in Figure B2 was correlated with the fluorescence signals of each bacterial strain separately using PLS modeling.

Number of principal components used	*Nitrospira*		*N. europaea*		*E. coli*		*B. subtilis*		*B. cereus*		*S. saprophyticus*		*S. laurentii*	
	R^2	Q^2	R^2	Q^2	R^2	Q^2	R^2	Q^2	R^2	Q^2	R^2	Q^2	R^2	Q^2
1	0.74	0.16	0.52	**-0.02**	0.70	0.09	0.44	**-0.17**	0.57	**-0.15**	0.64	**-0.52**	0.51	**-0.73**
2	0.88	0.24	0.77	**-0.05**	0.86	0.20	0.82	**-0.49**	0.78	**-0.17**	0.88	**-0.43**	0.88	**-0.46**
3	0.97	0.23	0.95	0.03	0.94	0.23	0.91	**-0.45**	0.91	**-0.31**	0.97	**-0.35**	0.95	**-0.27**
4	0.99	0.29	0.99	0.04	0.98	0.24	0.99	**-0.55**	0.98	**-0.29**	0.99	**-0.17**	0.98	0.01
5	1.00	0.36	1.00	0.04	1.00	0.27	0.99	**-0.62**	0.99	**-0.32**	1.00	**-0.10**	1.00	0.11

Table B4. R^2 and Q^2 values for different principal components for the GC-MS to CBB PLS model, where the CBB panel fluorescence data included only the fluorescence signals from *Nitrospira* and *E. coli*. The same GC-MS data as shown in Figure B2 was used.

Number of principal components used	*Nitrospira* & *E. coli*	
	R^2	Q^2
1	0.49	0.05
2	0.73	0.14
3	0.81	0.22
4	0.91	0.20
5	0.94	0.24

Appendix C

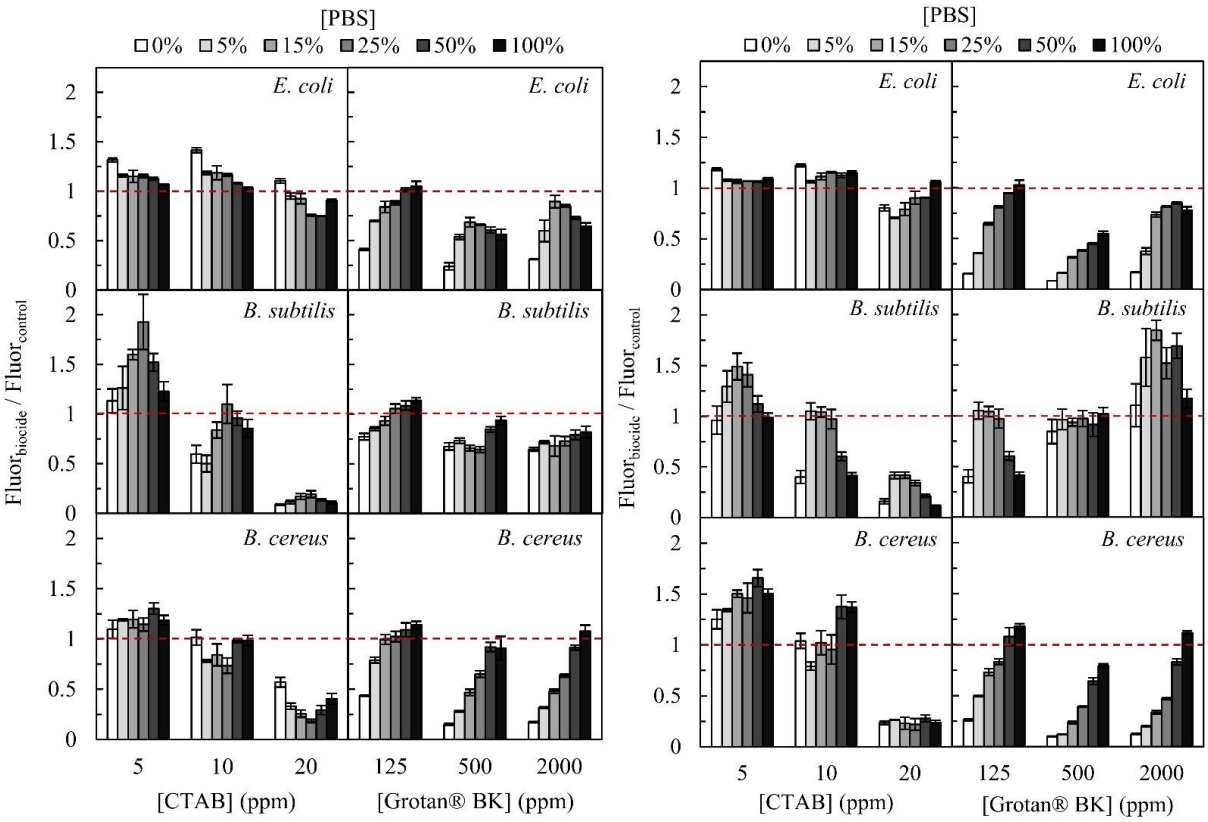

Figure C1. The set of panels on the left and right represent the normalized fluorescence 1 minute and 30 minutes after the dye was added, respectively. Both sets of panels (left and right): *E. coli*, *B. subtilis*, and *B. cereus* bacterial strains exposed to CTAB at 5, 10, 20 ppm and Grotan® BK at 125, 500, 2000 ppm when stored in six different PBS solutions (0, 5, 15, 25, 50, 100%). The responses are reported as the average of duplicate measurements as normalized fluorescence signals ($Fluorescence_{biocide}$ / $Fluorescence_{control}$). The control solution used was Milli-Q water. The number of bacteria exposed to CTAB was approximately $9.1 \pm 0.1 \times 10^7$, $2.5 \pm 0.2 \times 10^7$, and $1.3 \pm 0.1 \times 10^7$ for *E. coli*, *B. subtilis*, and *B. cereus*, respectively. The number of bacteria exposed to Grotan® BK was approximately $7.5 \pm 0.3 \times 10^7$, $5.0 \pm 0.2 \times 10^7$, $1.3 \pm 0.1 \times 10^7$ for *E. coli*, *B. subtilis*, and *B. cereus*, respectively.

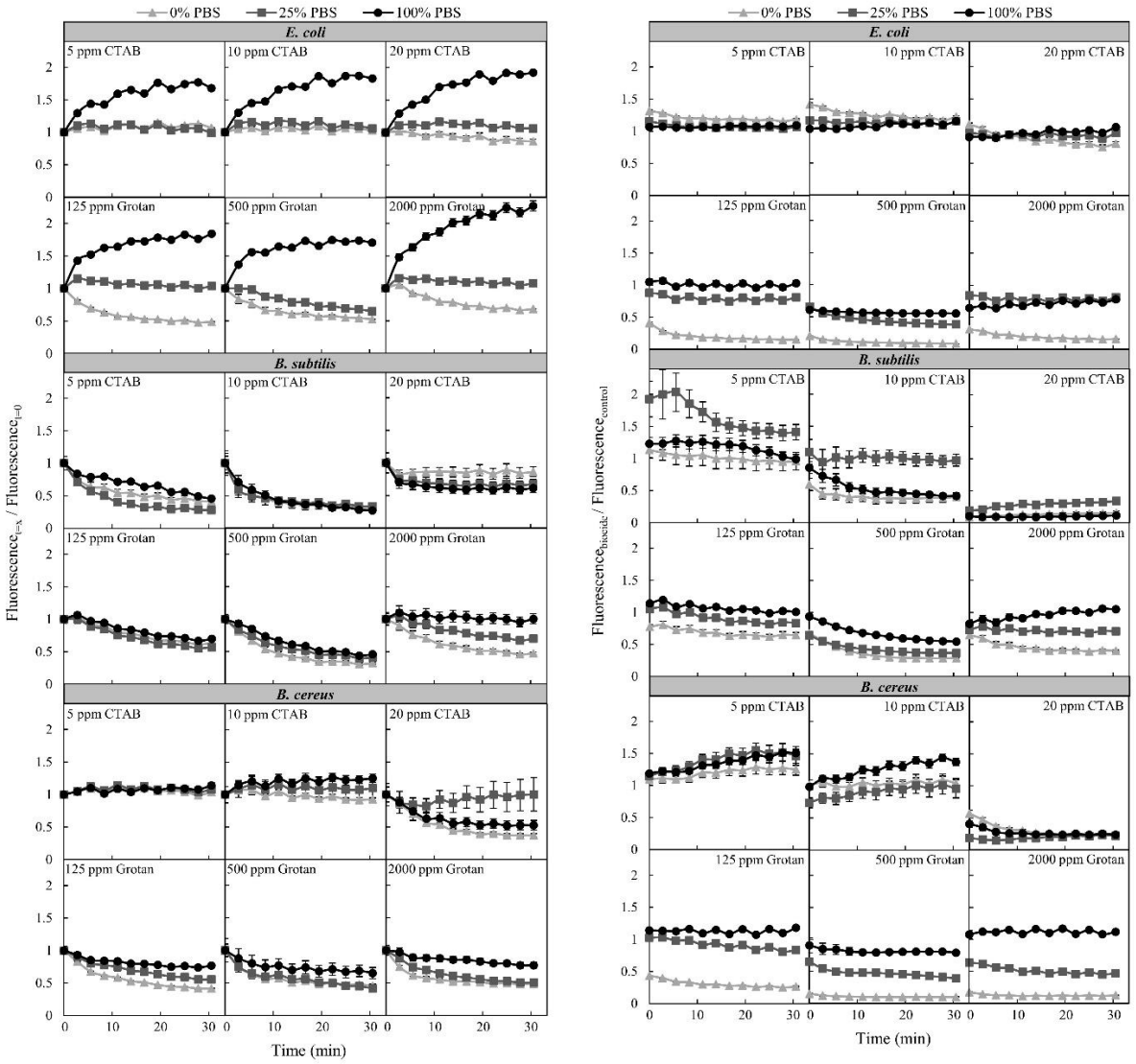

Figure C2. Left set of panels: time-normalized fluorescence signal stability reported as $Fluorescence_{t=x}/Fluorescence_{t=0}$ over a 30-minute reading period where $Fluorescence_{t=x}$ represents the fluorescence signal at time 'x' (as shown x-axis as 'Time (min)'), and $Fluorescence_{t=0}$ represents the fluorescence signal 1 minute after the dye is added. Right set of panels: the normalized fluorescence signal stability reported as $Fluorescence_{biocide}$ / $Fluorescence_{control}$ (as shown in manuscript) over a 30-minute reading period.E. coli, B. subtilis, and B. cereus bacterial strains exposed to CTAB at 5, 10, 20 ppm and Grotan® BK at 125, 500, 2000 ppm when stored in three different PBS solutions (0, 25, 100%). Only these three PBS solutions were selected to be shown to lessen figure complexity and because of their importance as highlighted in Table 4-1. For both sets of panels, the signals are reported as the average of duplicate measurements. The number of bacteria exposed to CTAB and Grotan® BK are the same as in Figure C1.

Appendix D

Table D1. Outer dimensions (cm) of commercially available enclosed electrospinning systems and our electrospinning box (E-Box) with and without a printer bed accessory. Inner dimensions (cm) of Class II, Type A2 Biological Safety Cabinets that are typically used for microbiological and cell culture studies. Inner width of Class II, Type A2 Biological Safety cabinets not included in the table since this dimension is not a limiting factor. The Baker SterilGARD III Advance° SG403A was used in this study.

Electrospinning Systems					
Outer Dimensions (cm)	Spinbox® System	Inovenso	NanoScience Fluidnatek-LE-50	Our E-Box + Printer Bed Accessory	Our E-Box
Width	75	74	85	44	11.2
Depth	55	64.5	57	32	12.3
Height	65	77	85	28	15.8

Class II, Type A2 Biological Safety Cabinets			
Inner Dimensions (cm)	Thermo Scientific Herasafe KS	Thermo Scientific Series A2	Baker SterilGARD®III Advance° SG403A
Depth	63	63	51
Height	78	78	70
Maximum Sash Opening Height	77	53	50

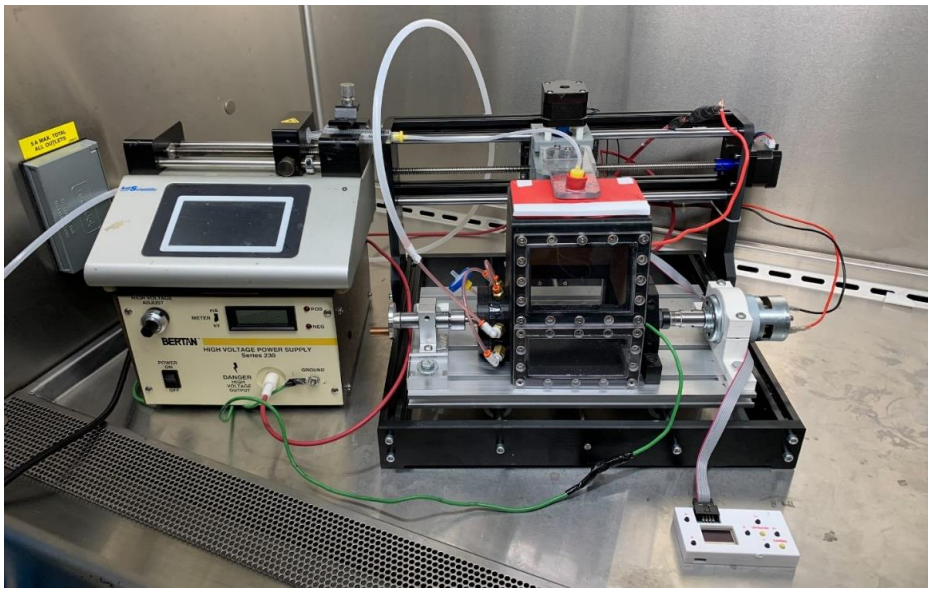

Figure D1. Real image of the electrospinning system shown in Figure 5-1 of the manuscript inside of a Baker SterilGARD III Advance° SG403A Class II, Type A2 Biological Safety Cabinet (The Baker Company).

Figure D2. Electrospinning system in a Baker SterilGARD III Advance° SG403A Class II, Type A2 Biological Safety Cabinet (The Baker Company) with the nitrogen gas cylinder setup including a pressure gauge and a rotameter for controlling nitrogen gas flow rate into the E-Box.

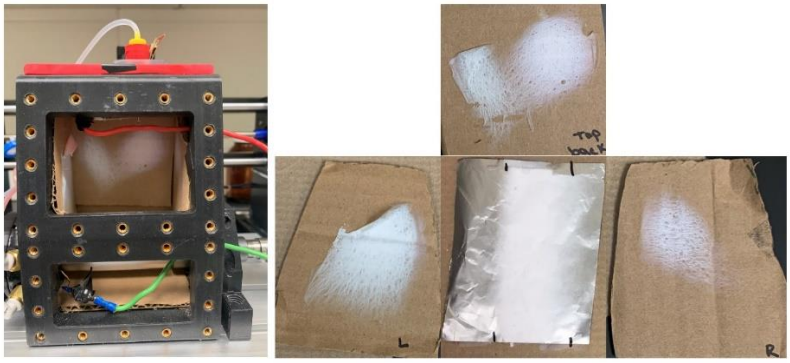

Figure D3. Example of off-target fiber deposition (severe splatter).

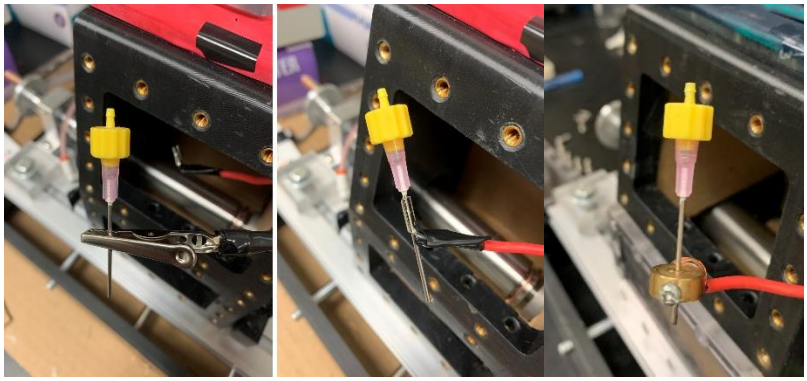

Figure D4. High voltage to spinneret connection types. Images of Alligator clip (left), cylindrical in-line fitting connection (middle), new cylindrical fitting with a set screw for improved connection (right).

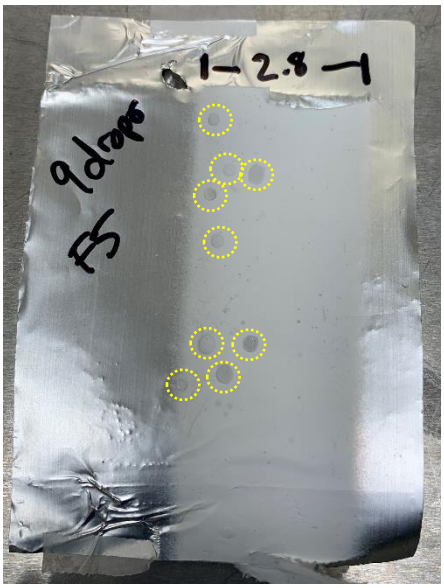

Figure D5. Example of an electrospun film on aluminum foil including droplet count and fiber width (cm) information.

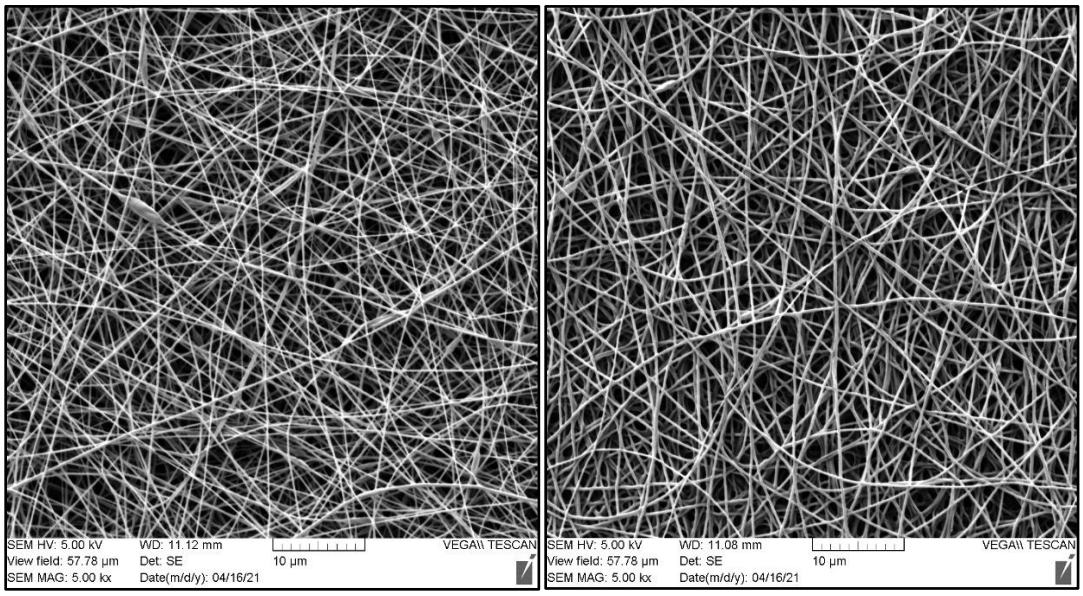

Figure D6. SEM images for a film generated at a relative humidity (RH) of 48% (left) and 22% (right). Three sections (outlined in red) were randomly selected for manual segmentation in ImageJ. The segmented images were analyzed, and fiber diameter data was obtained using the DiameterJ plugin. This process was performed on two different films for both 48% RH and 22% RH conditions.

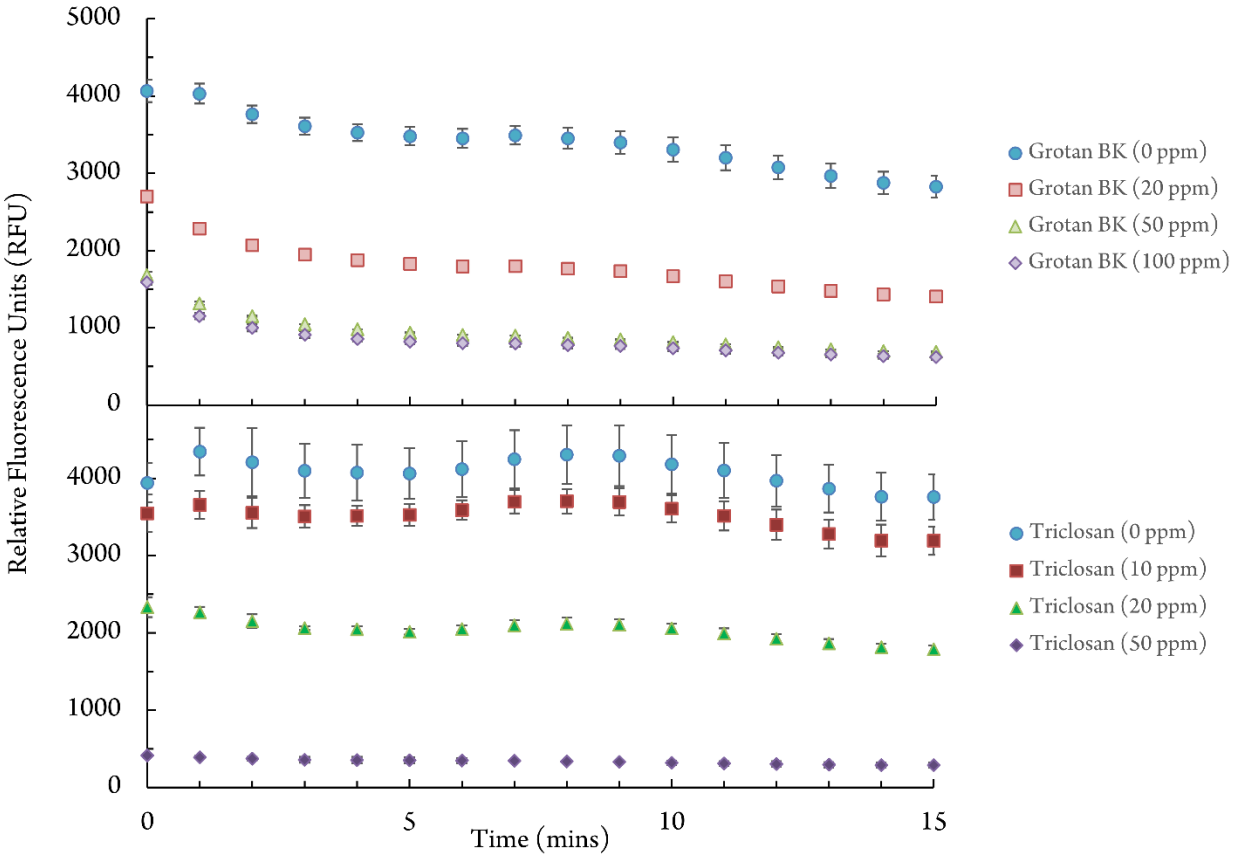

Figure D7. Fluorescence signals measured as relative fluorescence units (RFU) over a 15-minute period after dye addition. Time zero (0 mins) corresponds to the fluorescence signal obtained one minute after dye addition. The same E. coli-pullulan-trehalose electrospun pills used in Figure 4-5 of the manuscript were used to generate this data. Three different Grotan® BK (20, 50, 100 ppm) and Triclosan (10, 20, 50 ppm) concentrations and a control (Milli-Q water; 0 ppm Grotan BK and 0 ppm Triclosan) were tested. Each point corresponds to average fluorescence signal from two different films. Error bars correspond to the standard deviation of the fluorescence signals from the two films.

Electrospinning Box – assembly and detail drawings:

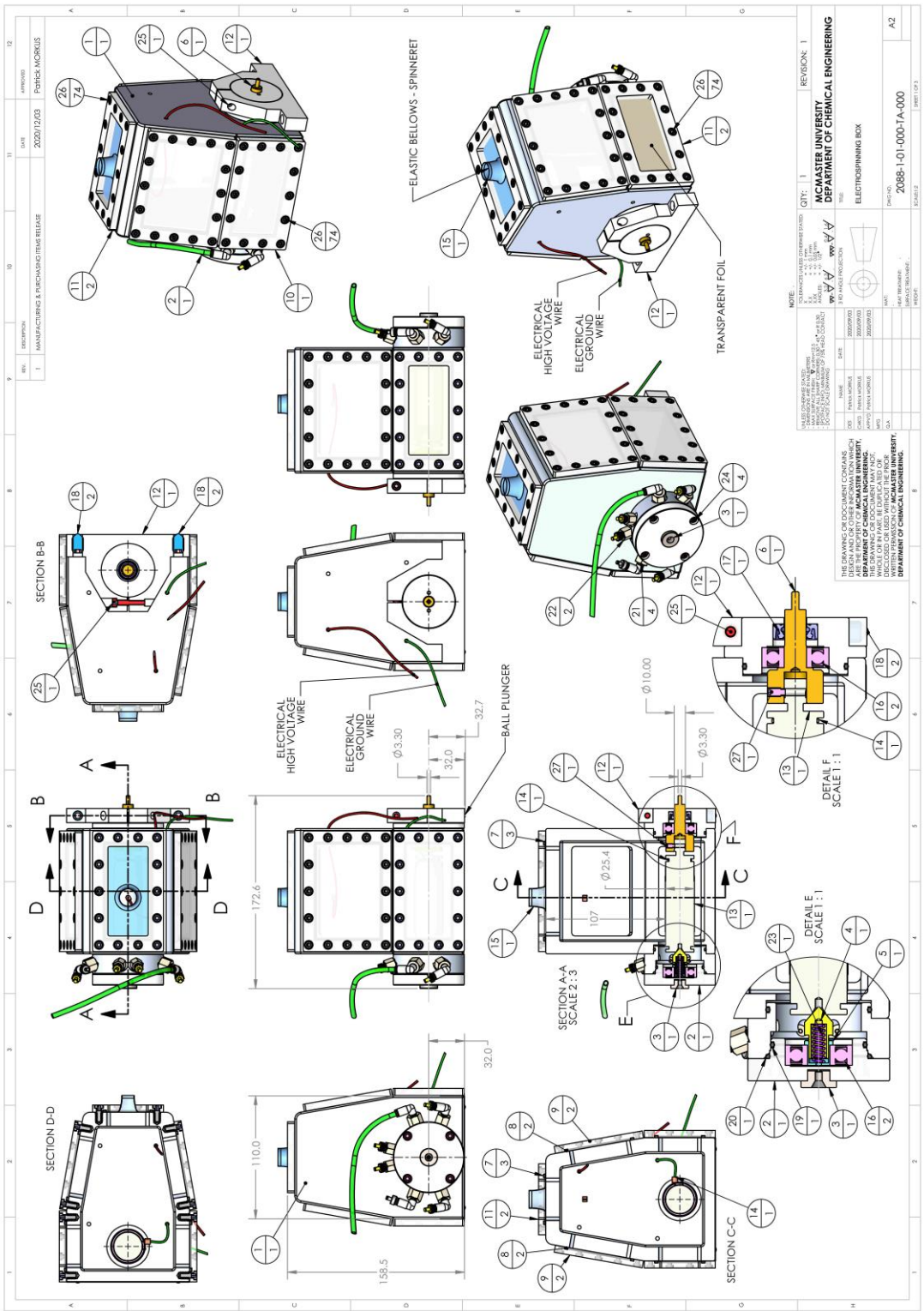

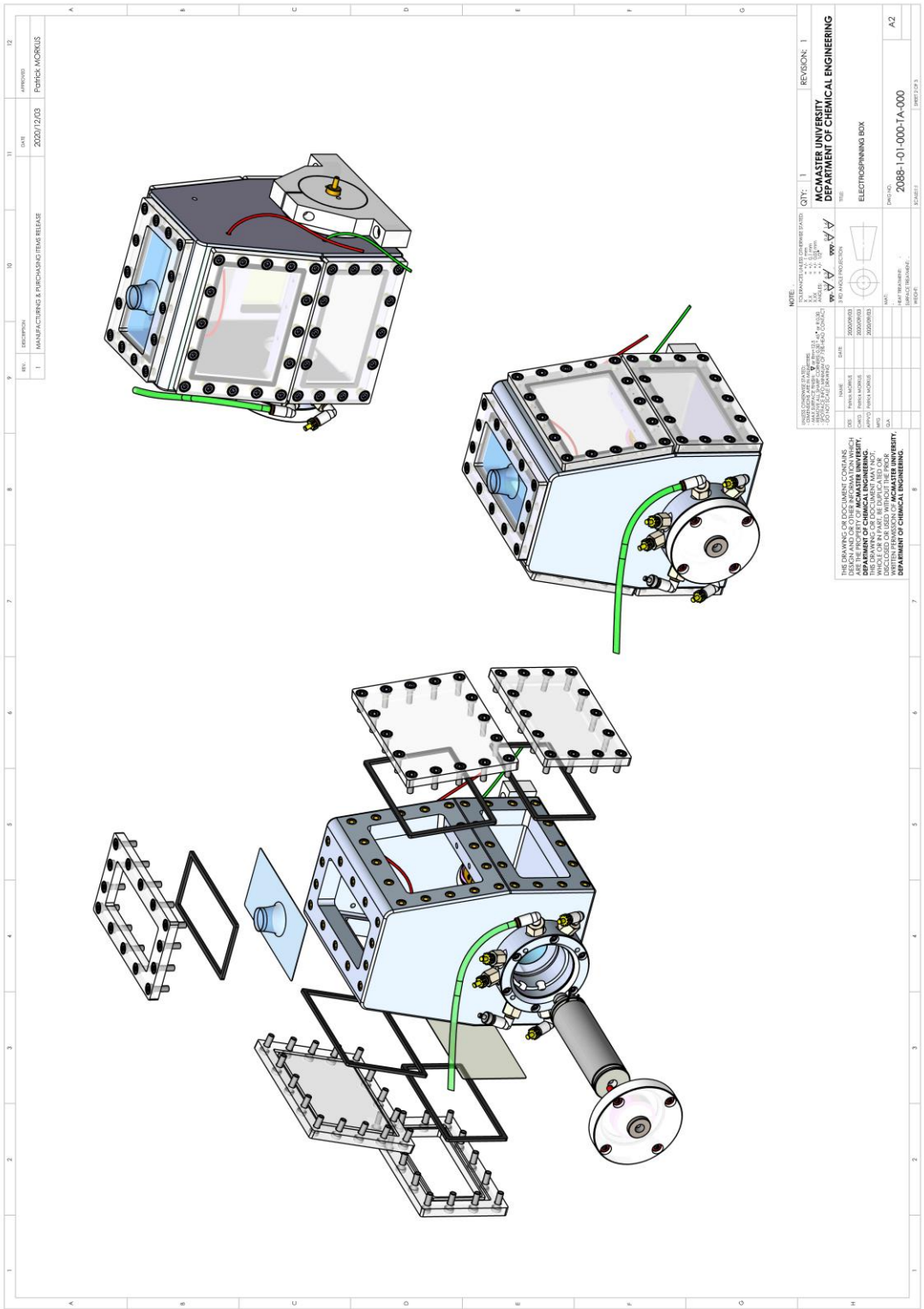
MCMASTER UNIVERSITY
DEPARTMENT OF CHEMICAL ENGINEERING
ELECTROSPINNING BOX
2088-1-01-000-TA-000
A2
REVISION: 1
QTY: 1
Patrick MORKUS
2020/12/03
MANUFACTURING & PURCHASING ITEMS RELEASE

REV.	DESCRIPTION	DATE	APPROVED
1	MANUFACTURING & PURCHASING ITEMS RELEASE	2020/12/03	Patrick MORKUS

BILL OF MATERIALS - BOM

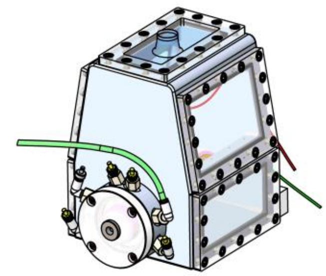

ITEM NO	QTY.	PART NO.	DESCRIPTION	CATALOG NUMBER	SUPPLIER	MATERIAL	HEAT TREATMENT	SURFACE TREATMENT	NOTE
1	1	2088-1-01-000-TA-001	ROLLER HOUSING BASE			GLUED-FASTENED ASSEMBLY			
	1	2088-1-01-000-TA-001A	FRAME BASE			McMASTER UNIVERSITY 3D PRINTED PLASTIC: ABS-M30			
	1	2088-1-01-000-TA-001B	DRIVE UNIT TUBE END			McMASTER UNIVERSITY 3D PRINTED PLASTIC: ABS-M30			
	1	2088-1-01-000-TA-001C	LEFT SIDE ROLLER HOUSING END			McMASTER UNIVERSITY 3D PRINTED PLASTIC: ABS-M30			
	2	2088-1-01-000-TA-001P1	O-RING	NSA44 or NSB44	MISUMI CORP.				do - 43.5 mm, W - 2.0 mm, NITRILE BLACK, (70 +/- 5 HARDNESS or 90 +/- 5 HARDNESS)
	6	2088-1-01-000-TA-001P2	HSCHS M3 * 8	07000 -- 030.008	FABORY METRICAN or McMASTER-CARR				GRADE - 12.9
	6	2088-1-01-000-TA-001P3	HSCHS M3 * 20	07000 -- 030.020	FABORY METRICAN or McMASTER-CARR				GRADE - 12.9
	12	2088-1-01-000-TA-001P4	SELF-TAPPING INSERT M3 x 0.5	INS 10 / M3 x 0.5 / 6.35 EK	SPIROL CANADA				WINDSOR, ON, 1-519-974-3334
	74	2088-1-01-000-TA-001P5	SELF-TAPPING INSERT M4 x 0.7	INS 10 / M4 x 0.7 / 7.92 EK	SPIROL CANADA				WINDSOR, ON, 1-519-974-3334
2	1	2088-1-01-000-TA-002	TOOLING END RETAINER			McMASTER UNIVERSITY 3D PRINTED PLASTIC: ABS-M30			
3	1	2088-1-01-000-TA-003	ROLLER HOUSING CENTER SUPPORT			SS 304: DIA 0.625" - 30 mm			
4	1	2088-1-01-000-TA-004	ROLLER CENTER SUPPORT			SS 304: DIA 0.500" - 35 mm			
5	1	2088-1-01-000-TA-005	DIE SPRING HOUSING			SS 304: DIA 0.500" - 30 mm			
6	1	2088-1-01-000-TA-006	DRIVE SHAFT ADAPTER			SS 304: DIA 1.00" - 70 mm			
7	3	2088-1-01-000-TA-007	RECTANGULAR SEAL	RBTMF2-89-45	MISUMI CORP.	NITRILE RUBBER: RBTMF2-89-45			SHORE 50
8	2	2088-1-01-000-TA-008	RECTANGULAR SEAL - UPPER WINDOW	RBTMF2-89-63	MISUMI CORP.	NITRILE RUBBER: RBTMF2-89-63			SHORE 50
9	2	2088-1-01-000-TA-009	UPPER WINDOW			CLEAR LEXAN or STATIC DISSIPATIVE PVC - CLEAR: 0.250" * 3.150" - 4.250"			CLEAR LEXAN or STATIC DISSIPATIVE PVC - CLEAR: 0.250" * 3.150" - 4.250"
10	1	2088-1-01-000-TA-010	FRONT LOWER COVER WINDOW			CLEAR LEXAN or STATIC DISSIPATIVE PVC - CLEAR: 0.250" * 2.500" - 4.250"			CLEAR LEXAN or STATIC DISSIPATIVE PVC - CLEAR: 0.250" * 2.500" - 4.250"
11	2	2088-1-01-000-TA-011	SEAL RETAINER			CLEAR LEXAN or STATIC DISSIPATIVE PVC - CLEAR: 0.250" * 2.500" - 4.250"			CLEAR LEXAN or STATIC DISSIPATIVE PVC - CLEAR: 0.250" * 2.500" - 4.250"
12	1	2088-1-01-000-TA-013	ANTIROTATE PLATE			AL 6061 T651: 0.500" * 3.00" - 114 mm			
13	1	2088-1-01-000-TA-061	ROLLER			SS 304: DIA 1.000" - 120 mm			
14	1	2088-1-01-000-TA-062	COPPER GROUNDING CLIP			CHROMIUM COPPER C18200: 0.032" x 0.062" - 120 mm			NO DRAWING
15	1	2088-1-01-000-TA-063	ELASTIC BELLOWS - SPINNERET			LATEX (INFLATABLE BALLOON MATERIAL)			NO DRAWING
16	2	2088-1-01-000-TA-201	DEEP GROOVE BALL BEARING	6200ZZ	MISUMI CORP. or NSK				ID10/OD30/B9
17	1	2088-1-01-000-TA-202	OIL FREE SEAL	MUEN10	MISUMI CORP.				
18	2	2088-1-01-000-TA-203	BALL PLUNGER	BSZ10 or BSX10	MISUMI CORP.				
19	1	2088-1-01-000-TA-204	O-RING	NSA40 or NSB40	MISUMI CORP.				do - 39.5 mm, W - 2.0 mm, NITRILE BLACK, (70 +/- 5 HARDNESS or 90 +/- 5 HARDNESS)
20	1	2088-1-01-000-TA-205	O-RING	NSA44 or NSB44	MISUMI CORP.				do - 43.5 mm, W - 2.0 mm, NITRILE BLACK, (70 +/- 5 HARDNESS or 90 +/- 5 HARDNESS)
21	4	2088-1-01-000-TA-221	ONE-TOUCH FITTING -L UNION ELBOW - INCH SIZE - NPT	KQ2L01-33AS	MISUMI CORP. or SMC				
22	2	2088-1-01-000-TA-222	ONE-TOUCH FITTING - STRAIGHT - INCH SIZE - NPT	KQ2H01-33AS	MISUMI CORP. or SMC				
23	1	2088-1-01-000-TA-231	COIL SPRING	SWF6-20 or SWM6-20	MISUMI CORP.				
24	4	2088-1-01-000-TA-264 A	HEX SOCKET HEAD CAP SCREW M4 x 12	07000 --- 040.012	FABORY METRICAN or McMASTER-CARR				GRADE - 12.9
25	1	2088-1-01-000-TA-264 B	HEX SOCKET HEAD CAP SCREW M4 x 25	07000 --- 040.025	FABORY METRICAN or McMASTER-CARR				GRADE - 12.9
26	74	2088-1-01-000-TA-264 C	HEX SOCKET HEAD CAP SCREW WITH LOW HEAD M4 x 12	07090 --- 040.012	FABORY METRICAN or McMASTER-CARR				GRADE - 12.9
27	1	2088-1-01-000-TA-264 S	HEX SOCKET SET SCREW WITH DOG POINT M4 x 8	07820 --- 040.008	FABORY METRICAN or McMASTER-CARR				

NOTE:

UNLESS OTHERWISE STATED:
- DIMENSIONS ARE IN MILLIMETERS
- MAX SURFACE FINISH: ∇ or Rm=12.5
- REMOVE ALL SHARP CORNERS: 0.30 * 45° or R 0.30
- SPOTFACE INFO: MINIMUM OF 75% HEAD CONTACT
- DO NOT SCALE DRAWING

TOLERANCES UNLESS OTHERWISE STATED:
X = +/- 1 mm
X.X = +/- 0.1 mm
X.XX = +/- 0.05 mm
ANGLES: = +/- 1/2°

	NAME	DATE	
DES	Patrick MORKUS		2020/09/03
CHK'D	Patrick MORKUS		2020/09/03
APPV'D	Patrick MORKUS		2020/09/03
MFG			
Q.A			

3 RD ANGLE PROJECTION

MAT:
HEAT TREATMENT:
SURFACE TREATMENT:
WEIGHT:

QTY: 1 REVISION: 1

MCMASTER UNIVERSITY
DEPARTMENT OF CHEMICAL ENGINEERING

TITLE: ELECTROSPINNING BOX

DWG NO. 2088-1-01-000-TA-000 A2

SCALE:1:2 SHEET 3 OF 3

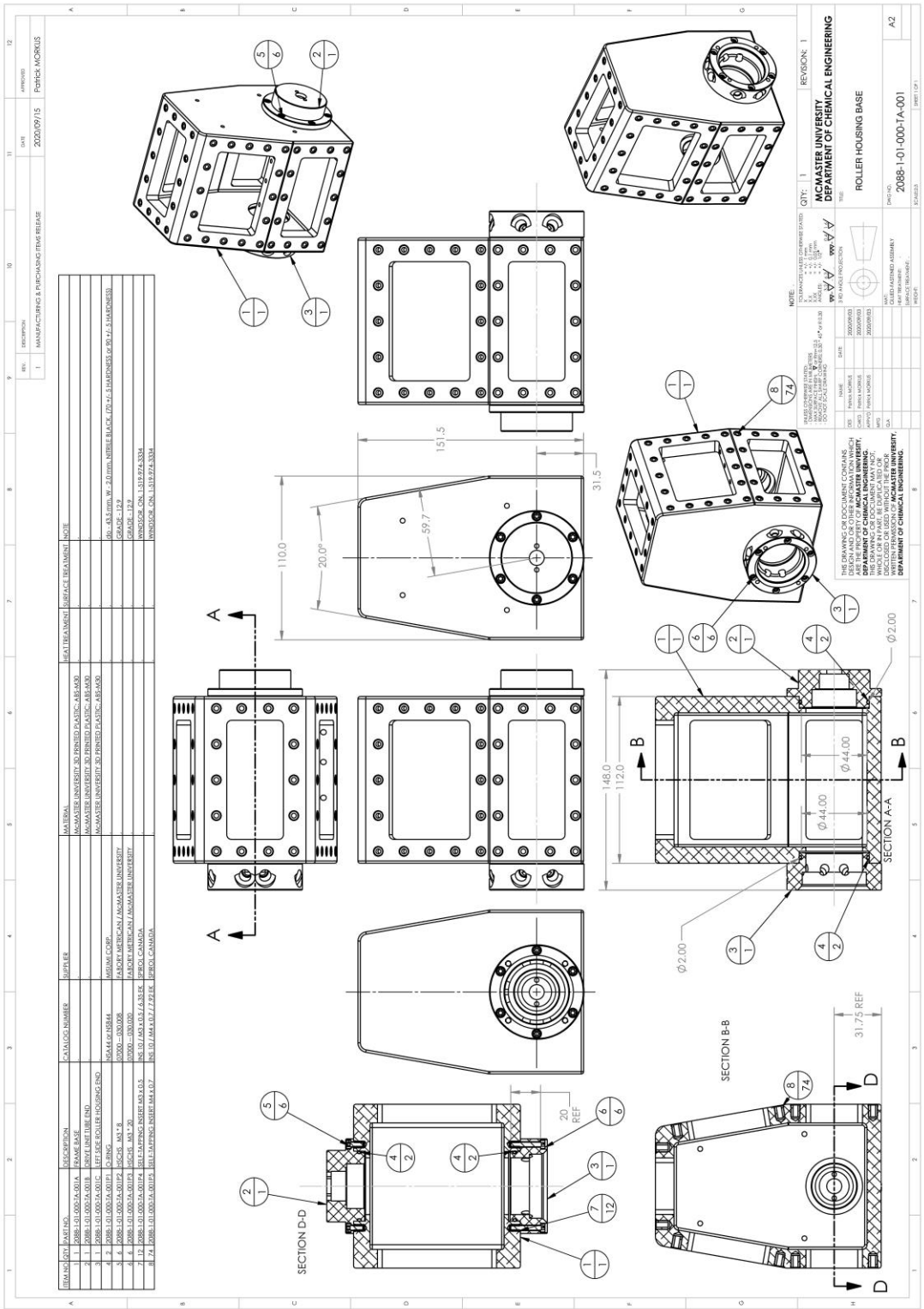
MCMASTER UNIVERSITY
DEPARTMENT OF CHEMICAL ENGINEERING
ROLLER HOUSING BASE
2088-1-01-000-TA-001
A2
REVISION: 1
SECTION A-A
SECTION B-B
SECTION D-D
110.0
20.0°
59.7
151.5
31.5
148.0
112.0
Ø44.00
Ø2.00
20 REF
31.75 REF

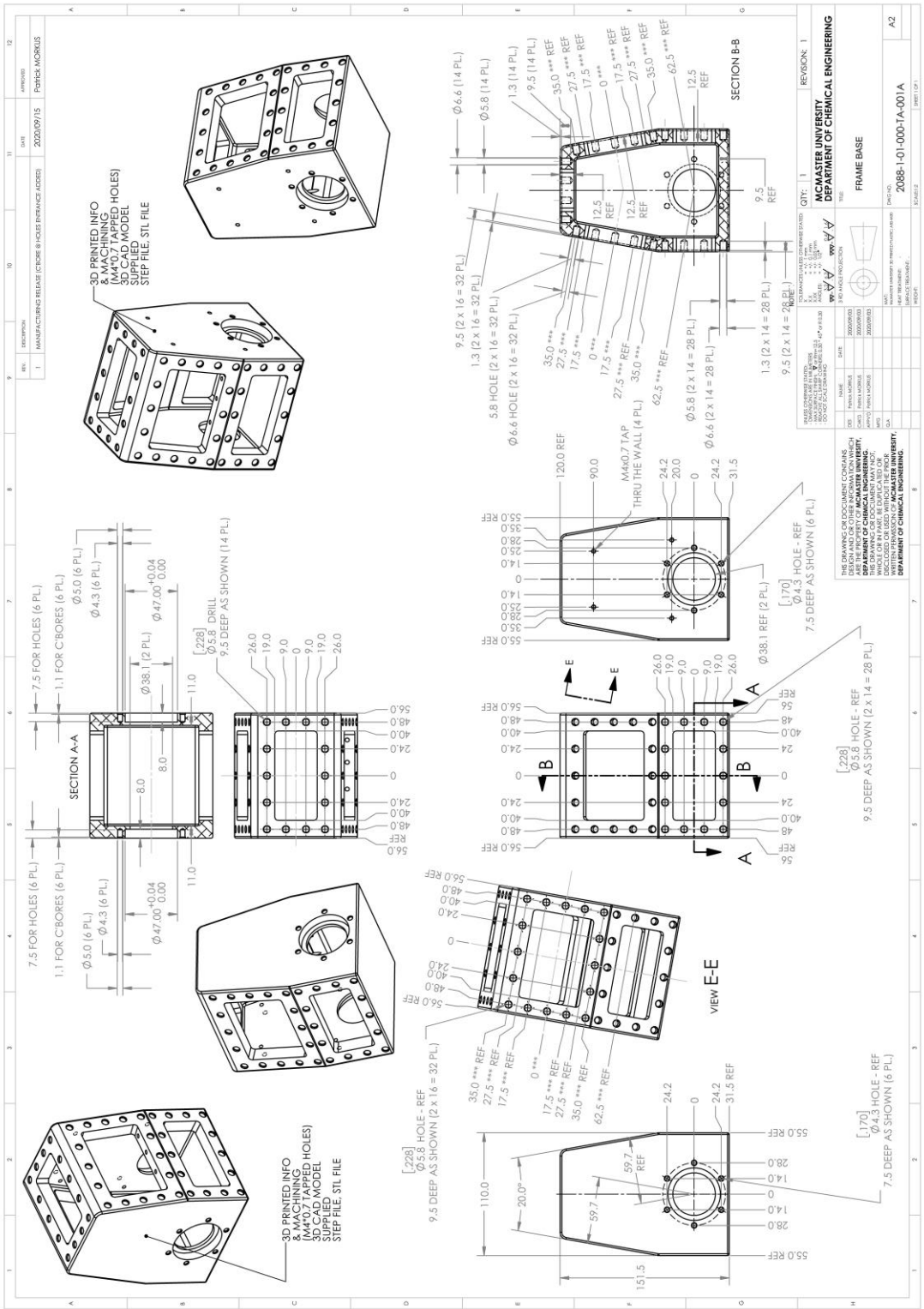
3D PRINTED INFO
& MACHINING
(M4*0.7 TAPPED HOLES)
3D CAD MODEL
SUPPLIED
STEP FILE, STL FILE
SECTION A-A
SECTION B-B
VIEW E-E
7.5 FOR HOLES (6 PL.)
1.1 FOR C'BORES (6 PL.)
Ø5.0 (6 PL.)
Ø4.3 (6 PL.)
Ø47.00 +0.04 0.00
Ø38.1 (2 PL.)
11.0
8.0
[.228] Ø5.8 DRILL 9.5 DEEP AS SHOWN (14 PL.)
26.0
19.0
9.0
0
9.0
19.0
26.0
56.0 REF
48.0
40.0
24.0
0
24.0
40.0
48.0
56.0 REF
Ø6.6 (14 PL.)
Ø5.8 (14 PL.)
1.3 (14 PL.)
9.5 (14 PL.)
35.0 *** REF
27.5 *** REF
17.5 *** REF
0 ***
12.5 REF
62.5 *** REF
9.5 (2 x 16 = 32 PL.)
1.3 (2 x 16 = 32 PL.)
5.8 HOLE (2 x 16 = 32 PL.)
Ø6.6 HOLE (2 x 16 = 32 PL.)
35.0 ***
27.5 ***
17.5 ***
17.5 *** REF
27.5 *** REF
35.0 ***
62.5 *** REF
Ø5.8 (2 x 14 = 28 PL.)
Ø6.6 (2 x 14 = 28 PL.)
1.3 (2 x 14 = 28 PL.)
9.5 (2 x 14 = 28 PL.)
NOTE
120.0 REF
90.0
M4x0.7 TAP
THRU THE WALL (4 PL.)
24.2
20.0
0
24.2
31.5
55.0 REF
52.0
28.0
14.0
0
14.0
28.0
55.0 REF
[.170] Ø4.3 HOLE - REF 7.5 DEEP AS SHOWN (6 PL.)
Ø38.1 REF (2 PL.)
[.228] Ø5.8 HOLE - REF 9.5 DEEP AS SHOWN (2 x 14 = 28 PL.)
[.228] Ø5.8 HOLE - REF 9.5 DEEP AS SHOWN (2 x 16 = 32 PL.)
35.0 *** REF
27.5 *** REF
17.5 *** REF
0 ***
62.5 *** REF
110.0
20.0°
59.7
59.7 REF
151.5
REVISION: 1
QTY: 1
MCMASTER UNIVERSITY
DEPARTMENT OF CHEMICAL ENGINEERING
FRAME BASE
2088-1-01-000-TA-001A
A2
3RD ANGLE PROJECTION
THIS DRAWING OR DOCUMENT CONTAINS DESIGN AND OR OTHER INFORMATION WHICH ARE THE PROPERTY OF MCMASTER UNIVERSITY, DEPARTMENT OF CHEMICAL ENGINEERING. THE INFORMATION CONTAINED HEREIN MAY NOT, WHOLE OR IN PART, BE DUPLICATED OR DISCLOSED OR USED WITHOUT THE PRIOR WRITTEN CONSENT OF MCMASTER UNIVERSITY, DEPARTMENT OF CHEMICAL ENGINEERING.

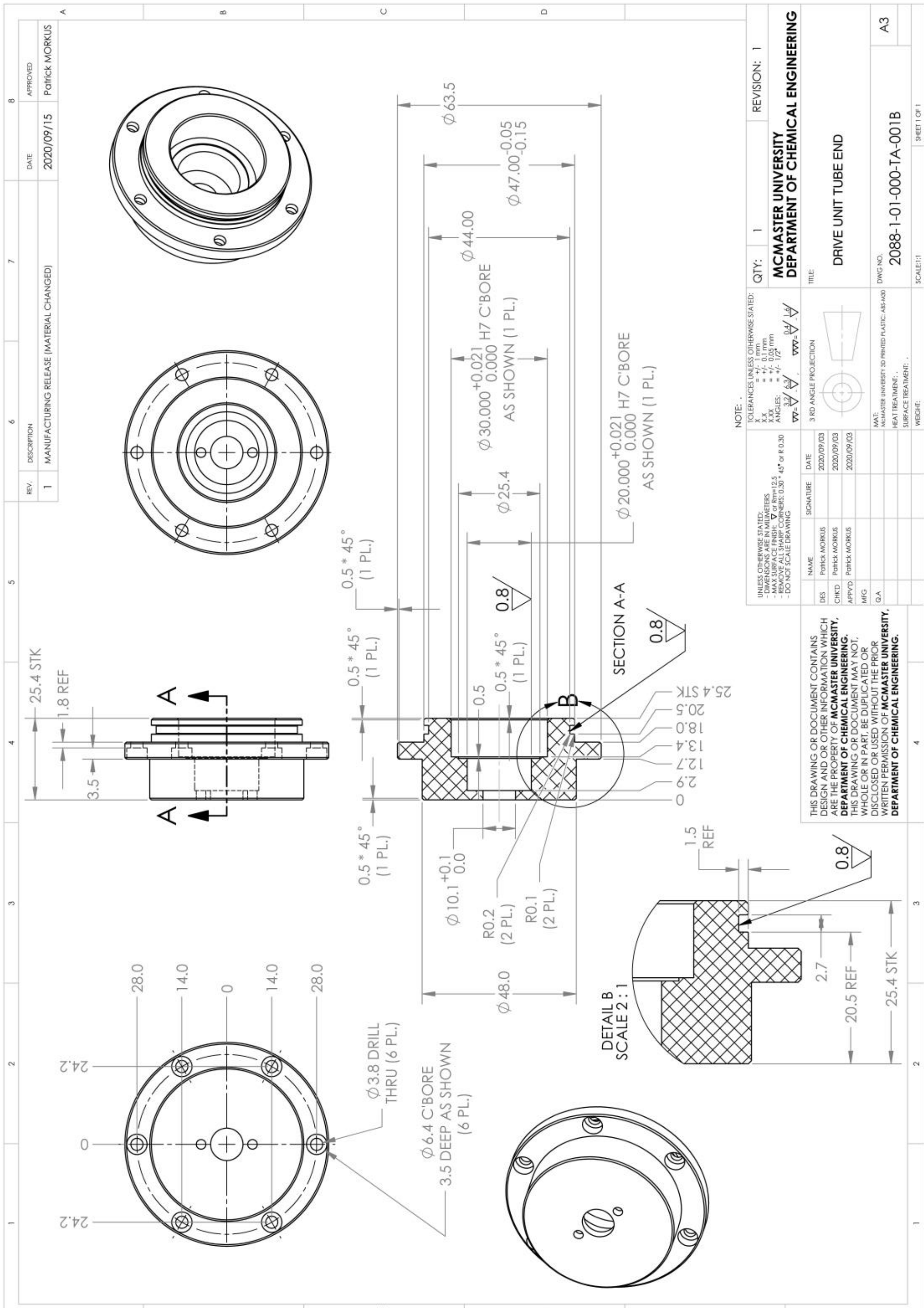
REV. DESCRIPTION DATE APPROVED
1 MANUFACTURING RELEASE (MATERIAL CHANGED) 2020/09/15 Patrick MORKUS
⌀63.5
⌀47.00 -0.05 -0.15
⌀44.00
⌀30.000 +0.021 0.000 H7 C'BORE AS SHOWN (1 PL.)
⌀25.4
⌀20.000 +0.021 0.000 H7 C'BORE AS SHOWN (1 PL.)
0.5 * 45° (1 PL.)
SECTION A-A
25.4 STK
1.8 REF
3.5
A
B
0.5
25.4 STK
20.5
18.0
13.4
12.7
2.9
0
0.8
1.5 REF
⌀10.1 +0.1 0.0
R0.2 (2 PL.)
R0.1 (2 PL.)
⌀48.0
28.0
14.0
0
14.0
28.0
24.2
0
24.2
⌀3.8 DRILL THRU (6 PL.)
⌀6.4 C'BORE 3.5 DEEP AS SHOWN (6 PL.)
DETAIL B SCALE 2 : 1
2.7
20.5 REF
25.4 STK
THIS DRAWING OR DOCUMENT CONTAINS DESIGN AND OR OTHER INFORMATION WHICH ARE THE PROPERTY OF MCMASTER UNIVERSITY, DEPARTMENT OF CHEMICAL ENGINEERING. THIS DRAWING OR DOCUMENT MAY NOT, WHOLE OR IN PART, BE DUPLICATED OR DISCLOSED OR USED WITHOUT THE PRIOR WRITTEN PERMISSION OF MCMASTER UNIVERSITY, DEPARTMENT OF CHEMICAL ENGINEERING.
UNLESS OTHERWISE STATED: - DIMENSIONS ARE IN MILLIMETERS - DO NOT SCALE DRAWING
NAME SIGNATURE DATE
DES Patrick MORKUS 2020/09/03
CHK'D Patrick MORKUS 2020/09/03
APPV'D Patrick MORKUS 2020/09/03
MFG
Q.A
3 RD ANGLE PROJECTION
QTY: 1
REVISION: 1
MCMASTER UNIVERSITY
DEPARTMENT OF CHEMICAL ENGINEERING
TITLE:
DRIVE UNIT TUBE END
DWG NO.
2088-1-01-000-TA-001B
A3
SCALE:1:1
SHEET 1 OF 1

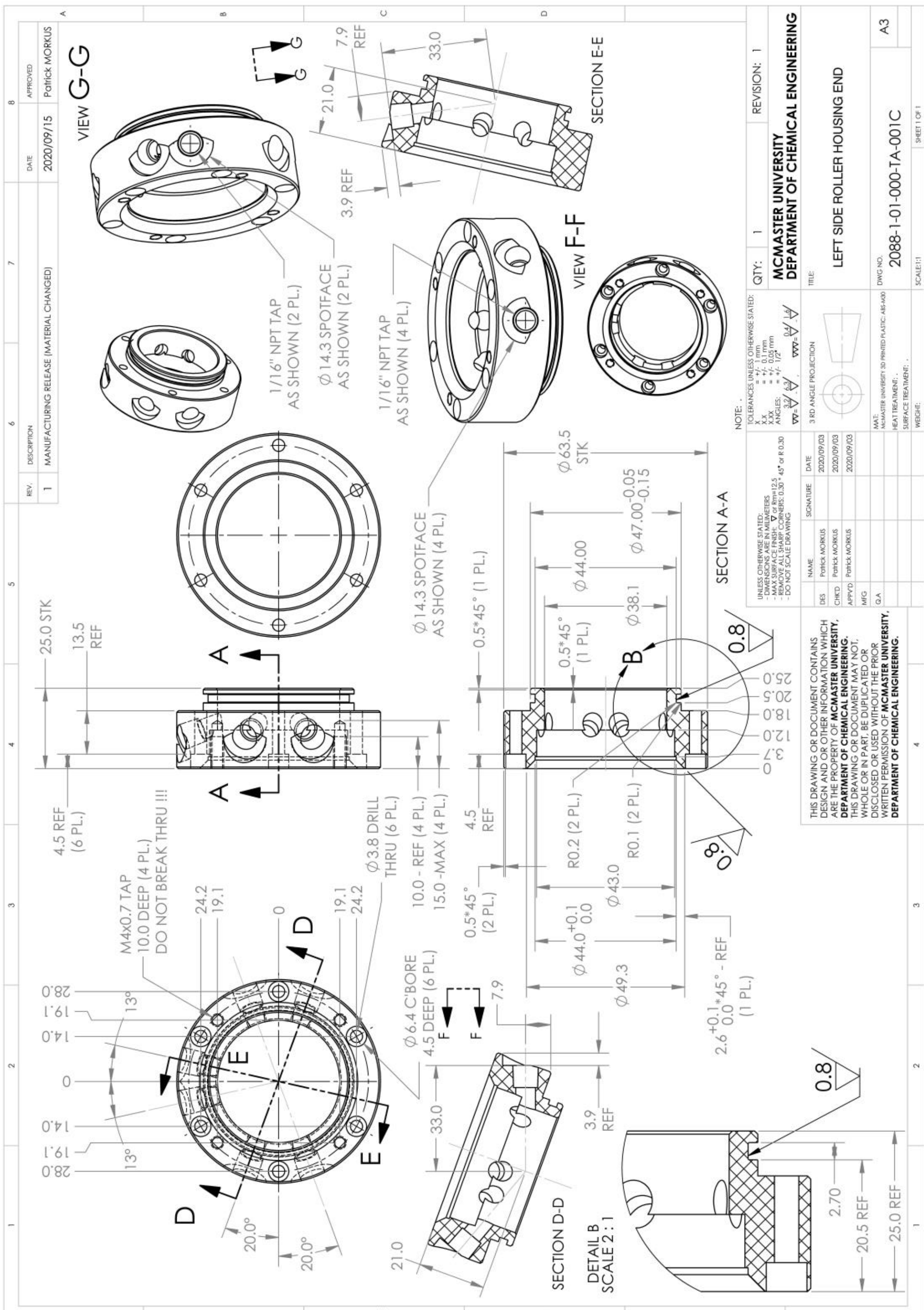
MCMASTER UNIVERSITY
DEPARTMENT OF CHEMICAL ENGINEERING
LEFT SIDE ROLLER HOUSING END
2088-1-01-000-TA-001C
A3
REVISION: 1
QTY: 1
MANUFACTURING RELEASE (MATERIAL CHANGED)
2020/09/15
Patrick MORKUS
SECTION A-A
SECTION D-D
SECTION E-E
VIEW F-F
VIEW G-G
DETAIL B
SCALE 2 : 1

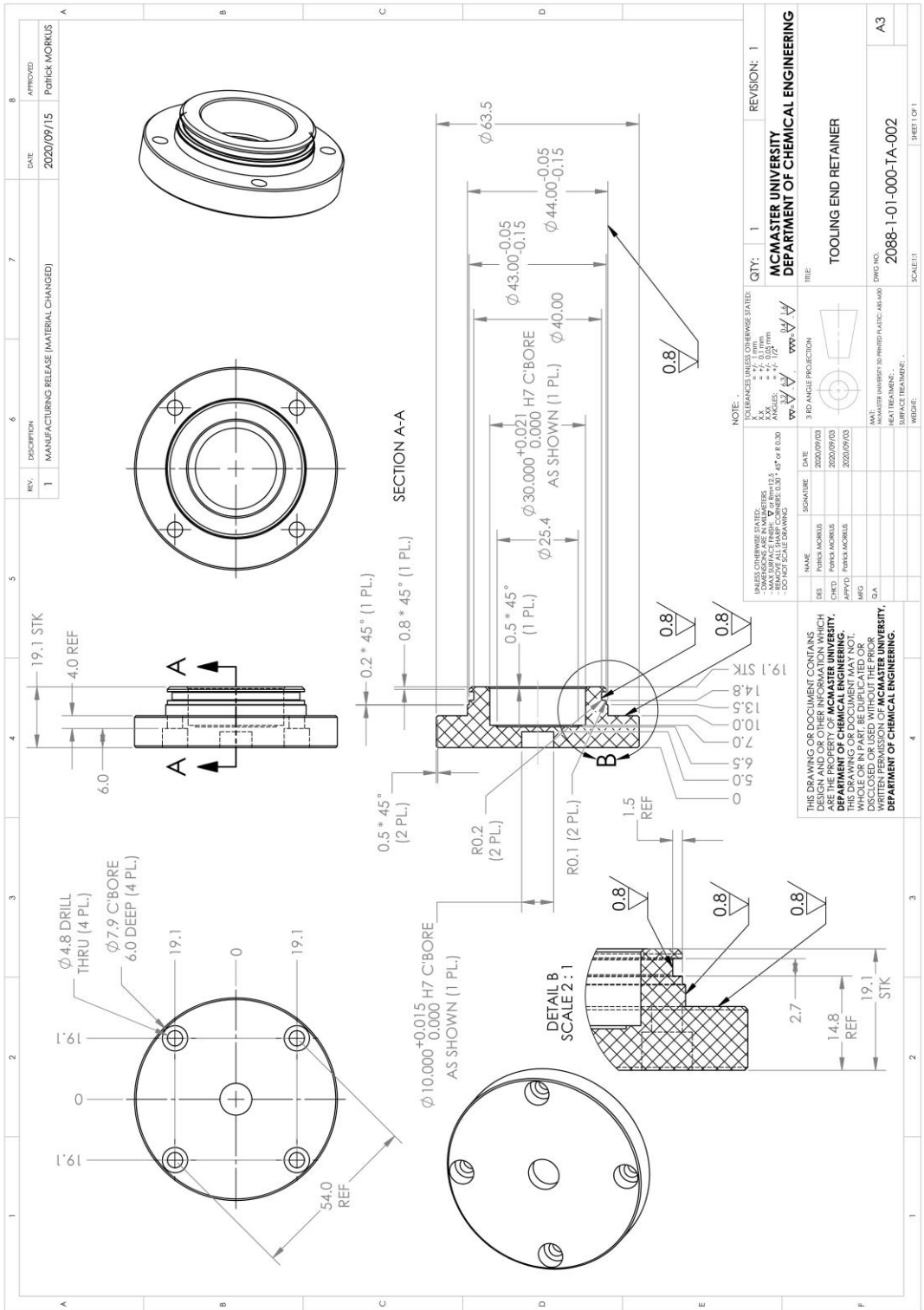
REV. DESCRIPTION DATE APPROVED
1 MANUFACTURING RELEASE (MATERIAL CHANGED) 2020/09/15 Patrick MORKUS
SECTION A-A
DETAIL B SCALE 2 : 1
Ø63.5
Ø44.00 -0.05 -0.15
Ø43.00 -0.05 -0.15
Ø40.00
Ø30.000 +0.021 0.000 H7 C'BORE AS SHOWN (1 PL.)
Ø25.4
Ø10.000 +0.015 0.000 H7 C'BORE AS SHOWN (1 PL.)
Ø4.8 DRILL THRU (4 PL.)
Ø7.9 C'BORE 6.0 DEEP (4 PL.)
19.1 STK
4.0 REF
6.0
0.2 * 45° (1 PL.)
0.8 * 45° (1 PL.)
0.5 * 45° (1 PL.)
0.5 * 45° (2 PL.)
R0.2 (2 PL.)
R0.1 (2 PL.)
1.5 REF
19.1 STK
14.8
13.5
10.0
7.0
6.5
5.0
0
19.1
0
19.1
54.0 REF
2.7
14.8 REF
19.1 STK
0.8
NOTE: -
UNLESS OTHERWISE STATED:
- DIMENSIONS ARE IN MILLIMETERS
- MAX SURFACE FINISH: 3.2 µm Ra cut off 12.5
- REMOVE ALL BURRS AND SHARP EDGES 0.30 x 45° or R 0.30
- DO NOT SCALE DRAWING
TOLERANCES (UNLESS OTHERWISE STATED):
X.X = +/- 0.1 mm
X.XX = +/- 0.05 mm
ANGLES = +/- 1/2°
3RD ANGLE PROJECTION
NAME SIGNATURE DATE
DES Patrick MORKUS 2020/09/03
CHK'D Patrick MORKUS 2020/09/03
APP'D Patrick MORKUS 2020/09/03
MFG
QA
MAT: MCMASTER UNIVERSITY 3D PRINTED PLASTIC: ABS-M30
HEAT TREATMENT: -
SURFACE TREATMENT: -
WEIGHT:
QTY: 1
REVISION: 1
MCMASTER UNIVERSITY
DEPARTMENT OF CHEMICAL ENGINEERING
TITLE:
TOOLING END RETAINER
DWG NO. 2088-1-01-000-TA-002
A3
SCALE:1:1
SHEET 1 OF 1
THIS DRAWING OR DOCUMENT CONTAINS DESIGN AND OR OTHER INFORMATION WHICH ARE THE PROPERTY OF MCMASTER UNIVERSITY, DEPARTMENT OF CHEMICAL ENGINEERING. THIS DRAWING OR DOCUMENT MAY NOT, WHOLE OR IN PART, BE DUPLICATED OR DISCLOSED OR USED WITHOUT THE PRIOR WRITTEN PERMISSION OF MCMASTER UNIVERSITY, DEPARTMENT OF CHEMICAL ENGINEERING.

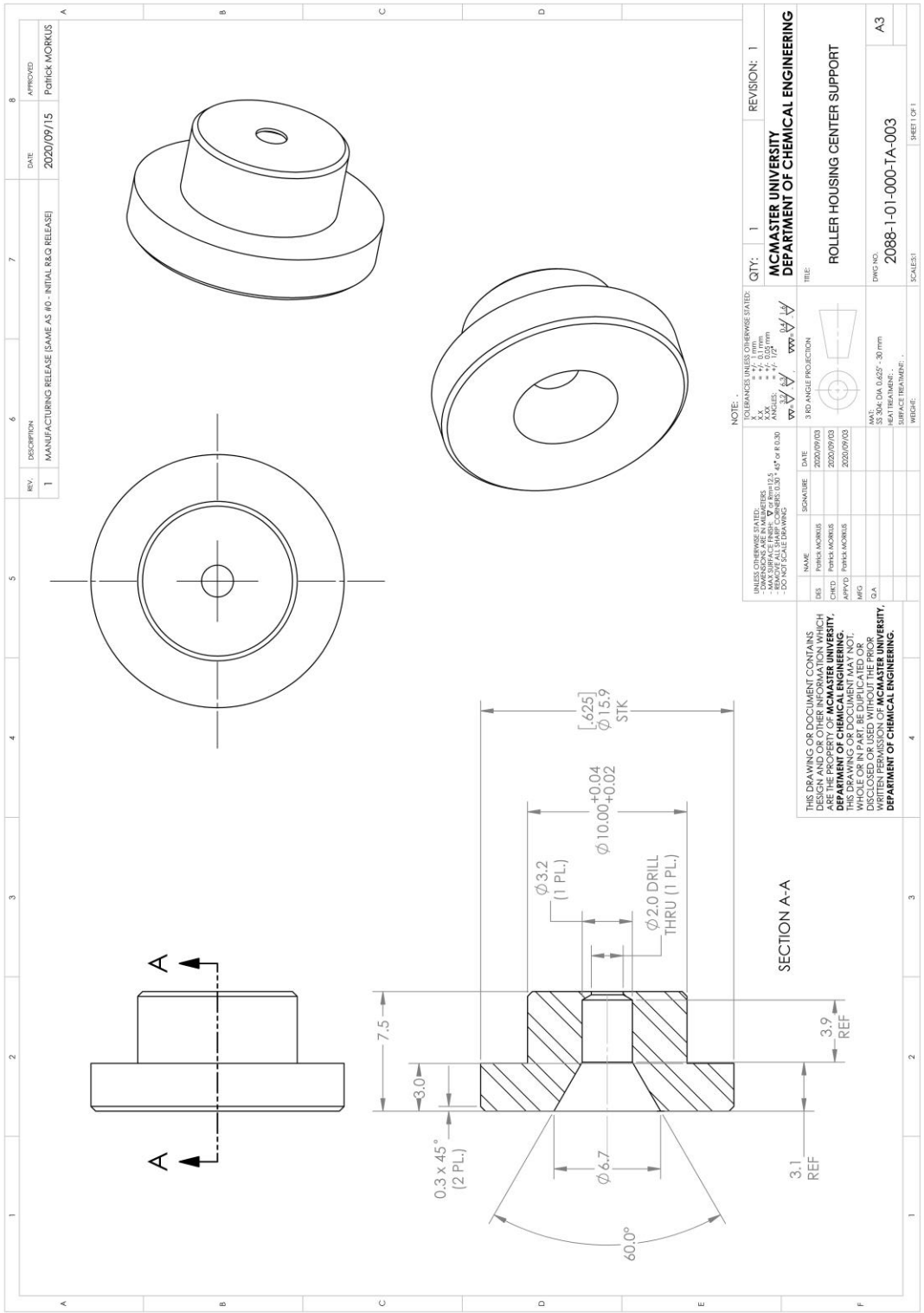
REV.
DESCRIPTION
DATE
APPROVED
1
MANUFACTURING RELEASE [SAME AS #0 - INITIAL R&Q RELEASE]
2020/09/15
Patrick MORKUS
NOTE: -
UNLESS OTHERWISE STATED:
- DIMENSIONS ARE IN MILLIMETERS
- MAX SURFACE FINISH: 3.2 µm Ra or 125 µin
- REMOVE ALL BURRS AND BREAK SHARP EDGES 0.30 x 45° or R 0.30
- DO NOT SCALE DRAWING
TOLERANCES (UNLESS OTHERWISE STATED):
X.X = +/- 0.1 mm
X.XX = +/- 0.05 mm
ANGLES = +/- 1/2°
QTY: 1
REVISION: 1
MCMASTER UNIVERSITY
DEPARTMENT OF CHEMICAL ENGINEERING
3 RD ANGLE PROJECTION
TITLE:
ROLLER HOUSING CENTER SUPPORT
NAME
SIGNATURE
DATE
DES
Patrick MORKUS
2020/09/03
CHKD
Patrick MORKUS
2020/09/03
APPVD
Patrick MORKUS
2020/09/03
MFG
Q.A
MAT:
SS 304: DIA 0.625" - 30 mm
HEAT TREATMENT: -
SURFACE TREATMENT: -
WEIGHT:
DWG NO.
2088-1-01-000-TA-003
A3
SCALE:1:1
SHEET 1 OF 1
THIS DRAWING OR DOCUMENT CONTAINS DESIGN AND OR OTHER INFORMATION WHICH ARE THE PROPERTY OF MCMASTER UNIVERSITY, DEPARTMENT OF CHEMICAL ENGINEERING. THIS DRAWING OR DOCUMENT MAY NOT, WHOLE OR IN PART, BE DUPLICATED, OR DISCLOSED OR USED WITHOUT THE PRIOR WRITTEN PERMISSION OF MCMASTER UNIVERSITY, DEPARTMENT OF CHEMICAL ENGINEERING.
A
A
SECTION A-A
[.625]
Ø15.9
STK
Ø10.00 +0.04 +0.02
Ø3.2
(1 PL.)
Ø2.0 DRILL
THRU (1 PL.)
7.5
3.0
0.3 x 45°
(2 PL.)
Ø6.7
60.0°
3.1
REF
3.9
REF

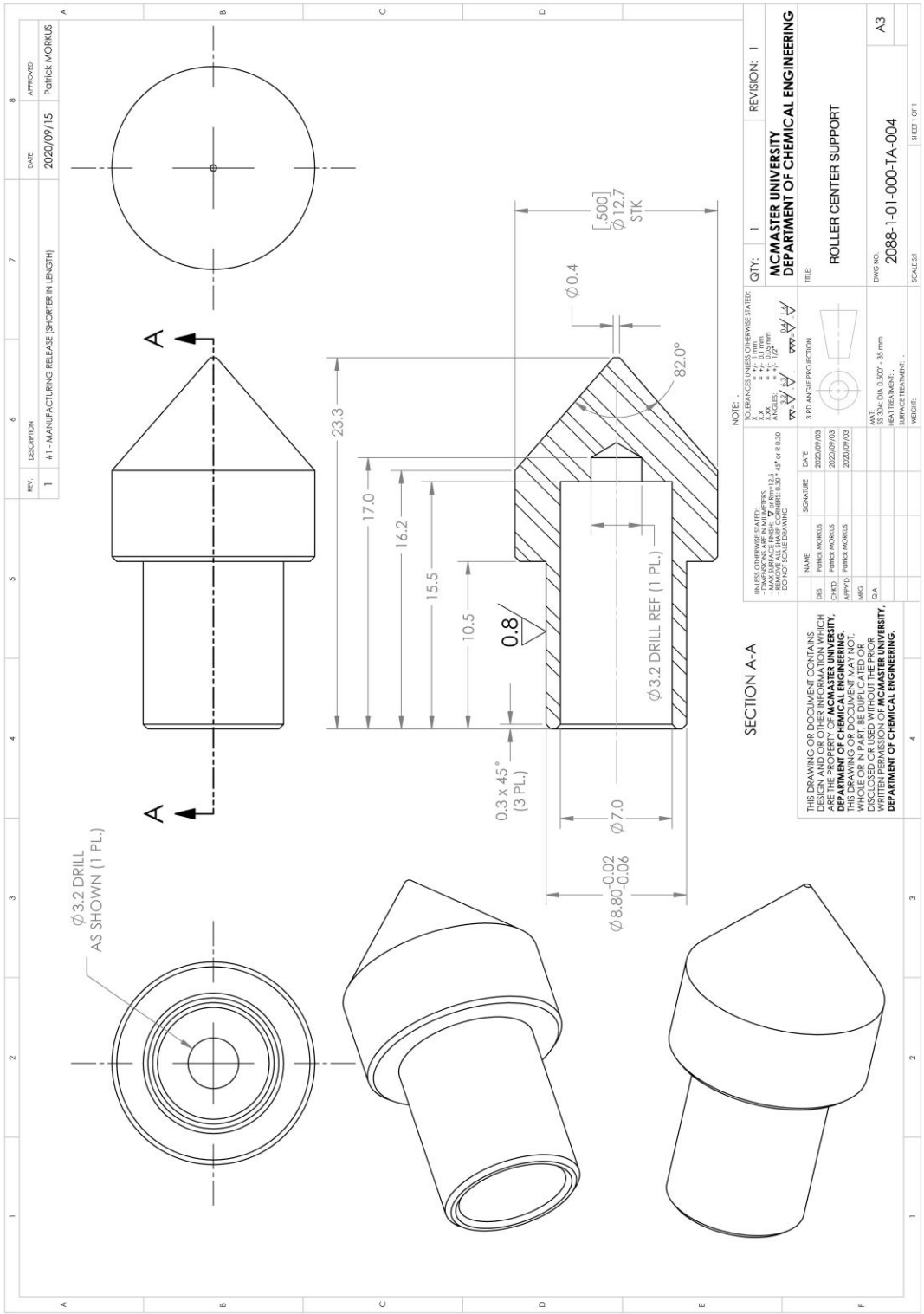
REV.
DESCRIPTION
DATE
APPROVED
1
#1 - MANUFACTURING RELEASE (SHORTER IN LENGTH)
2020/09/15
Patrick MORKUS
A
A
A
SECTION A-A
Ø3.2 DRILL
AS SHOWN (1 PL.)
0.3 x 45°
(3 PL.)
23.3
17.0
16.2
15.5
10.5
0.8
Ø3.2 DRILL REF (1 PL.)
Ø0.4
82.0°
[.500]
Ø12.7
STK
Ø7.0
Ø8.80 -0.02 -0.06
NOTE: -
UNLESS OTHERWISE STATED:
- DIMENSIONS ARE IN MILLIMETERS
- MAX SURFACE FINISH: 3.2 µm Ra or 125 µin
- REMOVE ALL BURRS AND SHARP EDGES
- DO NOT SCALE DRAWING
TOLERANCES (UNLESS OTHERWISE STATED):
X.X = +/- 0.1 mm
X.XX = +/- 0.05 mm
ANGLES = +/- 1/2°
3 RD ANGLE PROJECTION
QTY: 1
REVISION: 1
MCMASTER UNIVERSITY
DEPARTMENT OF CHEMICAL ENGINEERING
TITLE:
ROLLER CENTER SUPPORT
DWG NO.
2088-1-01-000-TA-004
A3
SCALE:1:1
SHEET 1 OF 1
MAT: SS 304: DIA 0.500" - 35 mm
HEAT TREATMENT: -
SURFACE TREATMENT: -
WEIGHT:
DES
CHK'D
APP'D
MFG
Q.A
NAME
SIGNATURE
DATE
Patrick MORKUS
2020/09/03
THIS DRAWING OR DOCUMENT CONTAINS DESIGN AND OR OTHER INFORMATION WHICH ARE THE PROPERTY OF MCMASTER UNIVERSITY, DEPARTMENT OF CHEMICAL ENGINEERING. THIS DRAWING OR DOCUMENT MAY NOT; WHOLE OR IN PART, BE DUPLICATED, OR DISCLOSED OR USED WITHOUT THE PRIOR WRITTEN PERMISSION OF MCMASTER UNIVERSITY, DEPARTMENT OF CHEMICAL ENGINEERING.

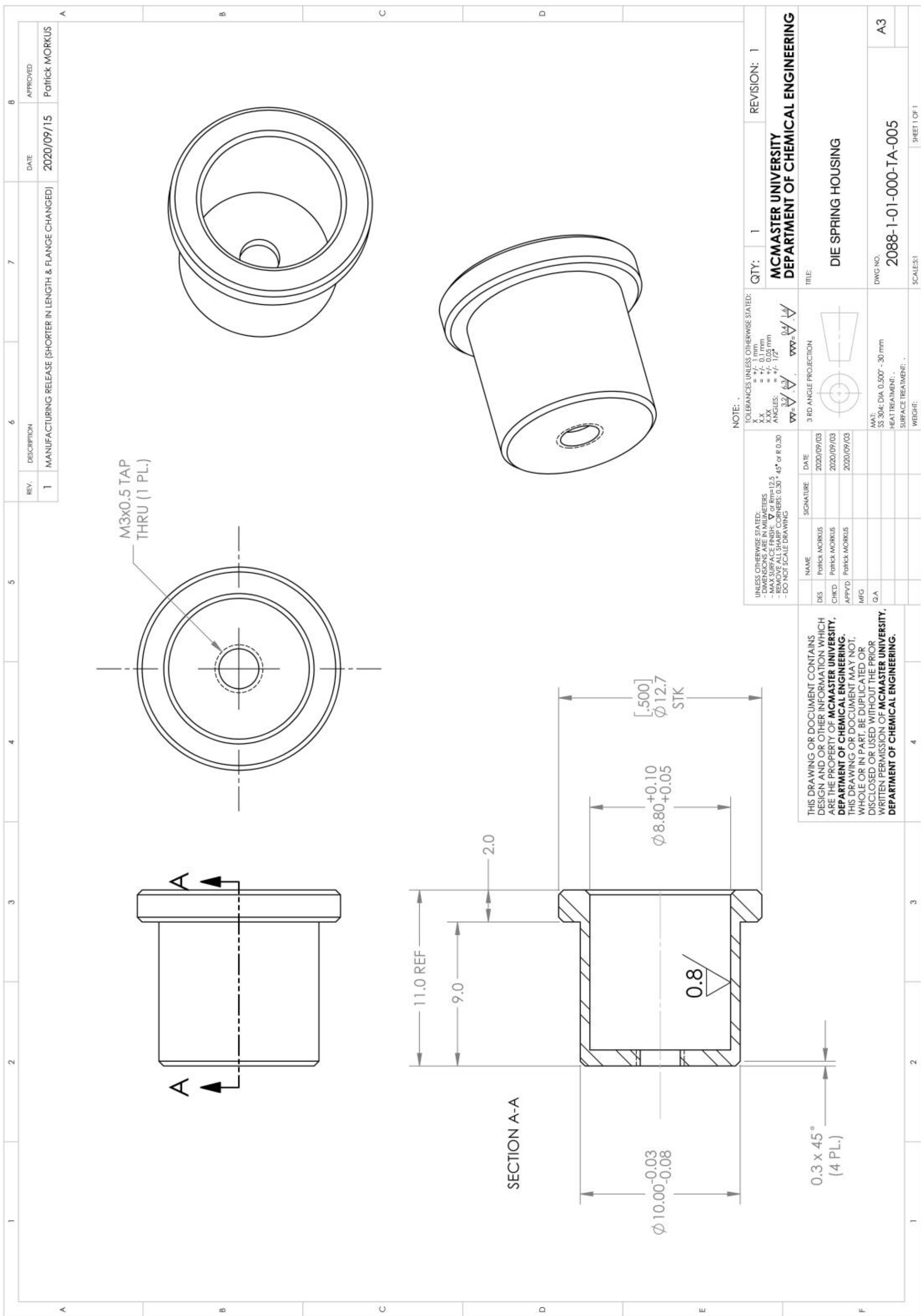

REV. 1 MANUFACTURING RELEASE (SHORTER IN LENGTH & FLANGE CHANGED) 2020/09/15 Patrick MORKUS
M3x0.5 TAP THRU (1 PL.)
[.500] Ø12.7 STK
Ø8.80 +0.10 +0.05
2.0
11.0 REF
9.0
0.8
SECTION A-A
Ø10.00 -0.03 -0.08
0.3 x 45° (4 PL.)
A
A
QTY: 1
REVISION: 1
MCMASTER UNIVERSITY
DEPARTMENT OF CHEMICAL ENGINEERING
DIE SPRING HOUSING
2088-1-01-000-TA-005
A3
MAT: SS 304: DIA 0.500" - 30 mm
3 RD ANGLE PROJECTION
THIS DRAWING OR DOCUMENT CONTAINS DESIGN AND OR OTHER INFORMATION WHICH ARE THE PROPERTY OF MCMASTER UNIVERSITY, DEPARTMENT OF CHEMICAL ENGINEERING.

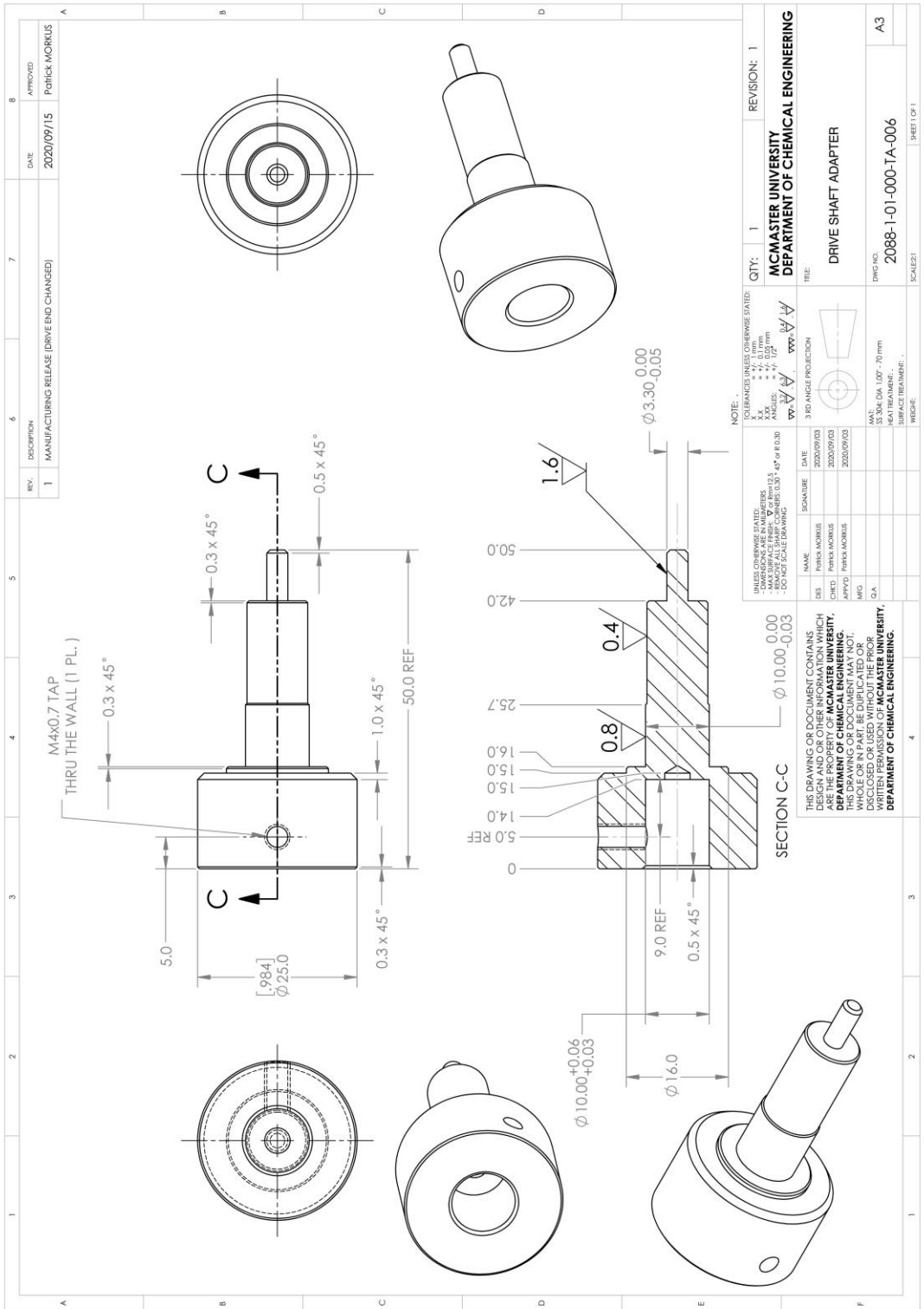
REV. DESCRIPTION DATE APPROVED
1 MANUFACTURING RELEASE (DRIVE END CHANGED) 2020/09/15 Patrick MORKUS
M4X0.7 TAP
THRU THE WALL (1 PL.)
0.3 x 45°
0.3 x 45°
0.5 x 45°
1.0 x 45°
50.0 REF
5.0
[.984]
Ø25.0
0.3 x 45°
C
C
SECTION C-C
Ø3.30 0.00 -0.05
1.6
0.4
0.8
50.0
42.0
25.7
16.0
15.0
15.0
14.0
5.0 REF
0
Ø10.00 0.00 -0.03
9.0 REF
0.5 x 45°
Ø16.0
Ø10.00 +0.06 +0.03
NOTE: -
UNLESS OTHERWISE STATED:
- DIMENSIONS ARE IN MILLIMETERS
- MAX SURFACE FINISH: 125 µin Ra
- REMOVE ALL BURRS AND SHARP EDGES
- DO NOT SCALE DRAWING
TOLERANCES: UNLESS OTHERWISE STATED:
X.X = +/- 0.1 mm
X.XX = +/- 0.05 mm
ANGLES = +/- 1°
3 RD ANGLE PROJECTION
NAME SIGNATURE DATE
DES Patrick MORKUS 2020/09/03
CHK'D Patrick MORKUS 2020/09/03
APP'D Patrick MORKUS 2020/09/03
MFG
Q.A
MAT: SS 304L DIA 1.00" - 70 mm
HEAT TREATMENT: -
SURFACE TREATMENT: -
WEIGHT:
QTY: 1
REVISION: 1
MCMASTER UNIVERSITY
DEPARTMENT OF CHEMICAL ENGINEERING
TITLE:
DRIVE SHAFT ADAPTER
DWG NO. 2088-1-01-000-TA-006
A3
SCALE:2:1
SHEET 1 OF 1
THIS DRAWING OR DOCUMENT CONTAINS DESIGN AND OR OTHER INFORMATION WHICH ARE THE PROPERTY OF MCMASTER UNIVERSITY, DEPARTMENT OF CHEMICAL ENGINEERING. THIS DRAWING OR DOCUMENT MAY NOT; WHOLE OR IN PART, BE DUPLICATED, OR DISCLOSED OR USED WITHOUT THE PRIOR WRITTEN PERMISSION OF MCMASTER UNIVERSITY, DEPARTMENT OF CHEMICAL ENGINEERING.

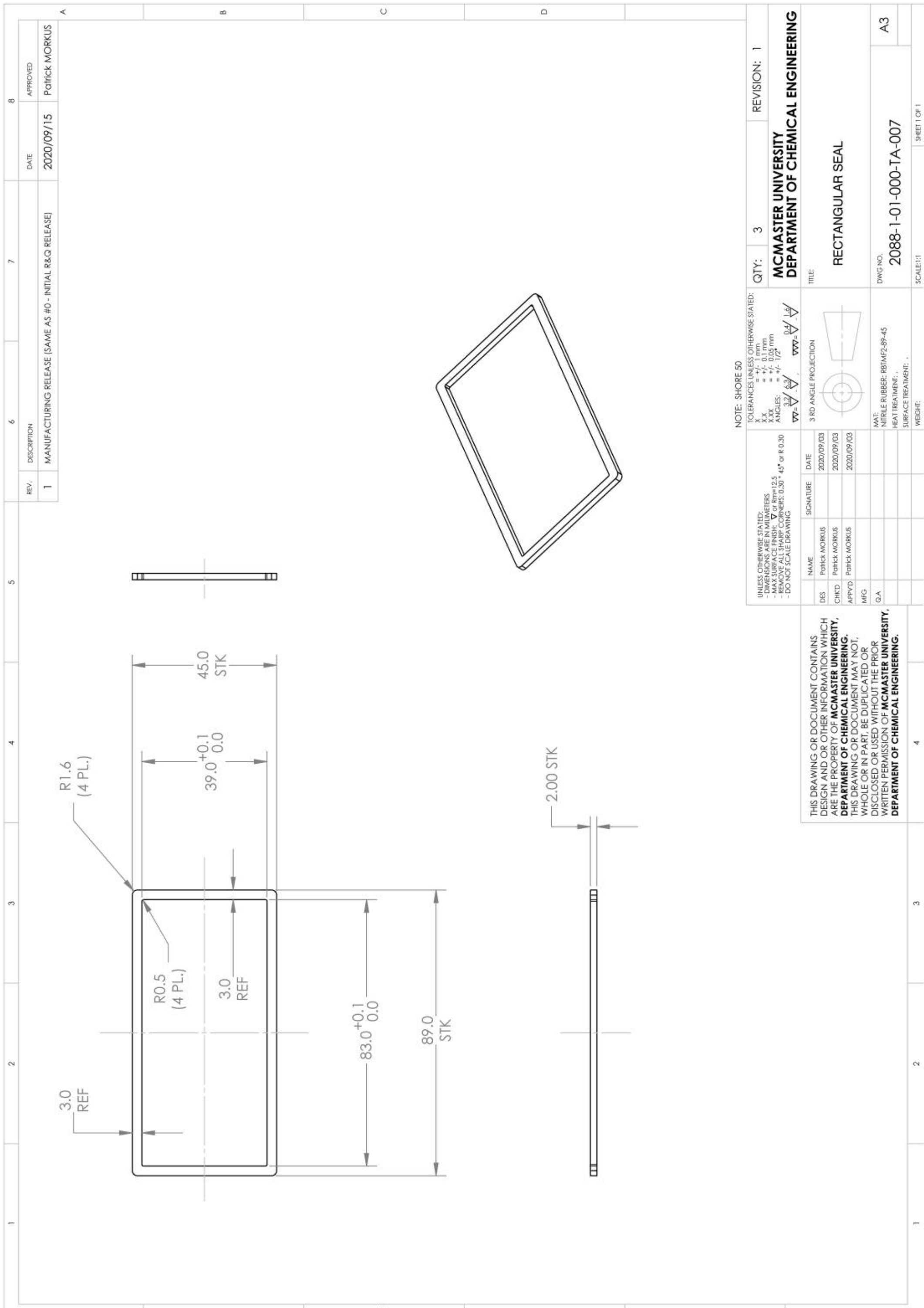
REV.
DESCRIPTION
DATE
APPROVED
1
MANUFACTURING RELEASE (SAME AS #0 - INITIAL R&Q RELEASE)
2020/09/15
Patrick MORKUS
R1.6
(4 PL.)
R0.5
(4 PL.)
3.0
REF
45.0
STK
39.0 +0.1 0.0
83.0 +0.1 0.0
89.0
STK
2.00 STK
NOTE: SHORE 50
QTY: 3
REVISION: 1
MCMASTER UNIVERSITY
DEPARTMENT OF CHEMICAL ENGINEERING
RECTANGULAR SEAL
2088-1-01-000-TA-007
A3
MAT:
NITRILE RUBBER: RB1MF2-89-45
DES Patrick MORKUS 2020/09/03
CHK'D Patrick MORKUS 2020/09/03
APPV'D Patrick MORKUS 2020/09/03
3 RD ANGLE PROJECTION
THIS DRAWING OR DOCUMENT CONTAINS DESIGN AND/OR OTHER INFORMATION WHICH ARE THE PROPERTY OF MCMASTER UNIVERSITY, DEPARTMENT OF CHEMICAL ENGINEERING. THIS DRAWING OR DOCUMENT MAY NOT, WHOLE OR IN PART, BE DUPLICATED OR DISCLOSED OR USED WITHOUT THE PRIOR WRITTEN PERMISSION OF MCMASTER UNIVERSITY, DEPARTMENT OF CHEMICAL ENGINEERING.

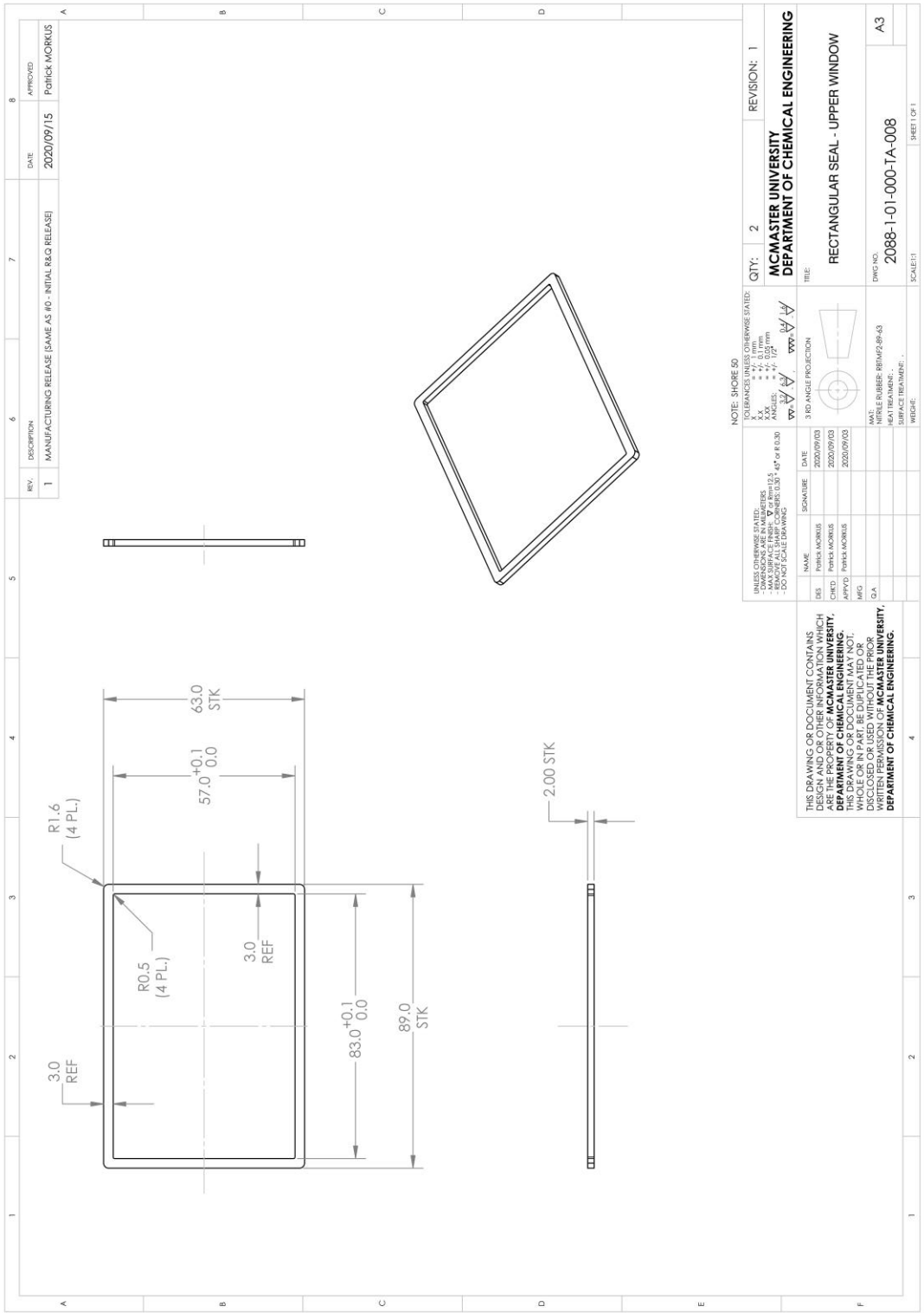
REV.
DESCRIPTION
DATE
APPROVED
1
MANUFACTURING RELEASE (SAME AS #0 - INITIAL R&Q RELEASE)
2020/09/15
Patrick MORKUS
63.0 STK
57.0 +0.1 0.0
R1.6 (4 PL.)
R0.5 (4 PL.)
3.0 REF
3.0 REF
83.0 +0.1 0.0
89.0 STK
2.00 STK
NOTE: SHORE 50
QTY: 2
REVISION: 1
MCMASTER UNIVERSITY
DEPARTMENT OF CHEMICAL ENGINEERING
TITLE:
RECTANGULAR SEAL - UPPER WINDOW
DWG NO.
2088-1-01-000-TA-008
A3
SCALE:1:1
SHEET 1 OF 1
3 RD ANGLE PROJECTION
THIS DRAWING OR DOCUMENT CONTAINS DESIGN AND OR OTHER INFORMATION WHICH ARE THE PROPERTY OF MCMASTER UNIVERSITY, DEPARTMENT OF CHEMICAL ENGINEERING. THIS DRAWING OR DOCUMENT MAY NOT, WHOLE OR IN PART, BE DUPLICATED, OR DISCLOSED OR USED WITHOUT THE PRIOR WRITTEN PERMISSION OF MCMASTER UNIVERSITY, DEPARTMENT OF CHEMICAL ENGINEERING.

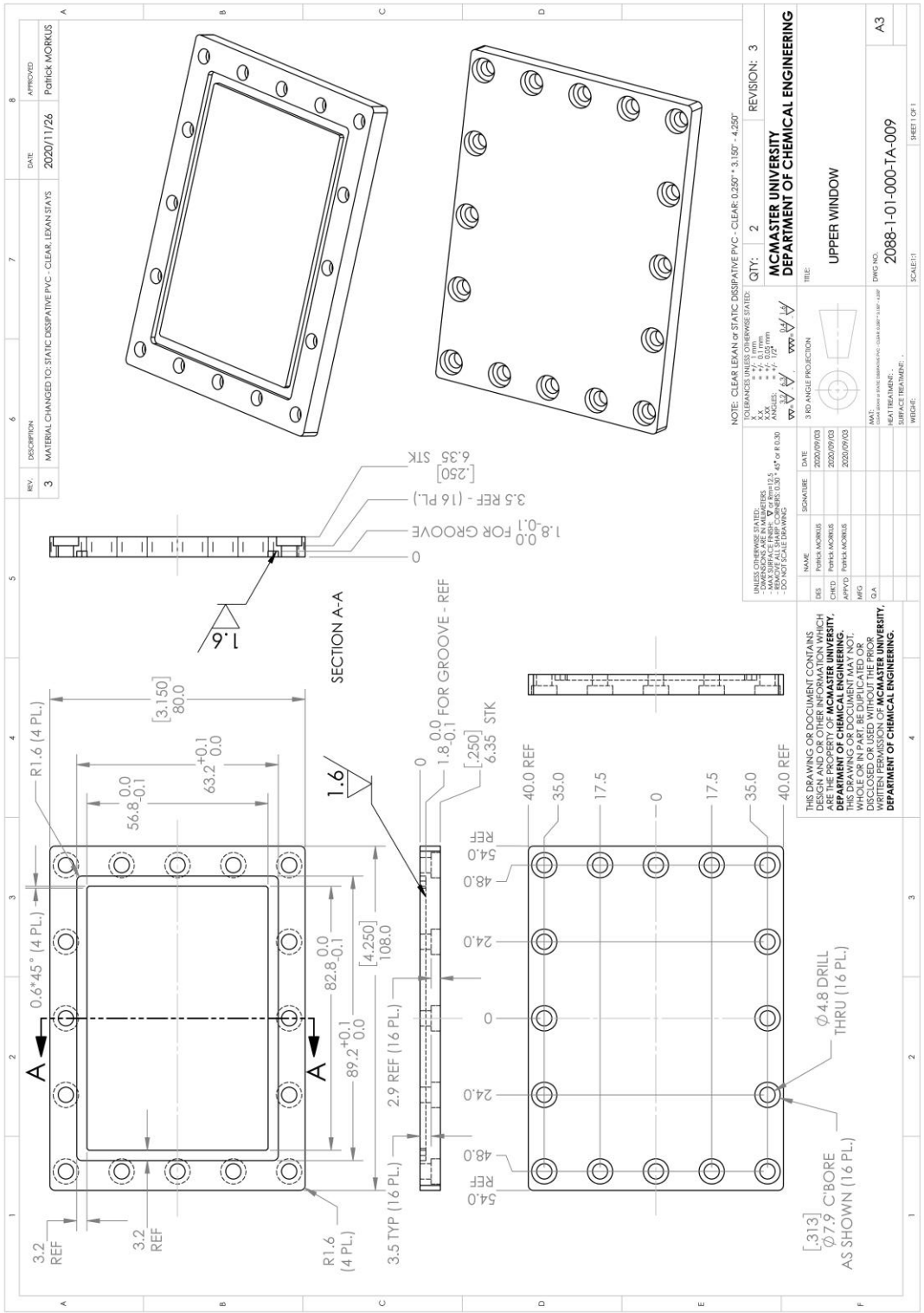
REV. DESCRIPTION DATE APPROVED
3 MATERIAL CHANGED TO: STATIC DISSIPATIVE PVC - CLEAR, LEXAN STAYS 2020/11/26 Patrick MORKUS
NOTE: CLEAR LEXAN or STATIC DISSIPATIVE PVC - CLEAR: 0.250" + 3.150" - 4.250"
QTY: 2
REVISION: 3
MCMASTER UNIVERSITY
DEPARTMENT OF CHEMICAL ENGINEERING
UPPER WINDOW
DWG NO. 2088-1-01-000-TA-009
A3
SCALE:1:1
SHEET 1 OF 1
SECTION A-A
1.6
6.35 STK
[.250]
3.5 REF - (16 PL.)
1.8 -0.1 0.0 FOR GROOVE
0
R1.6 (4 PL.)
[3.150]
80.0
63.2 +0.1 0.0
56.8 0.0 -0.1
0.6*45° (4 PL.)
82.8 0.0 -0.1
89.2 +0.1 0.0
[4.250]
108.0
2.9 REF (16 PL.)
3.5 TYP (16 PL.)
3.2 REF
R1.6 (4 PL.)
1.8 0.0 -0.1 FOR GROOVE - REF
40.0 REF
35.0
17.5
0
24.0
48.0
54.0 REF
Ø4.8 DRILL THRU (16 PL.)
[.313] Ø7.9 C'BORE AS SHOWN (16 PL.)
THIS DRAWING OR DOCUMENT CONTAINS DESIGN AND OR OTHER INFORMATION WHICH ARE THE PROPERTY OF MCMASTER UNIVERSITY, DEPARTMENT OF CHEMICAL ENGINEERING. THIS DRAWING OR DOCUMENT MAY NOT, WHOLE OR IN PART, BE DUPLICATED, OR DISCLOSED OR USED WITHOUT THE PRIOR WRITTEN PERMISSION OF MCMASTER UNIVERSITY, DEPARTMENT OF CHEMICAL ENGINEERING.

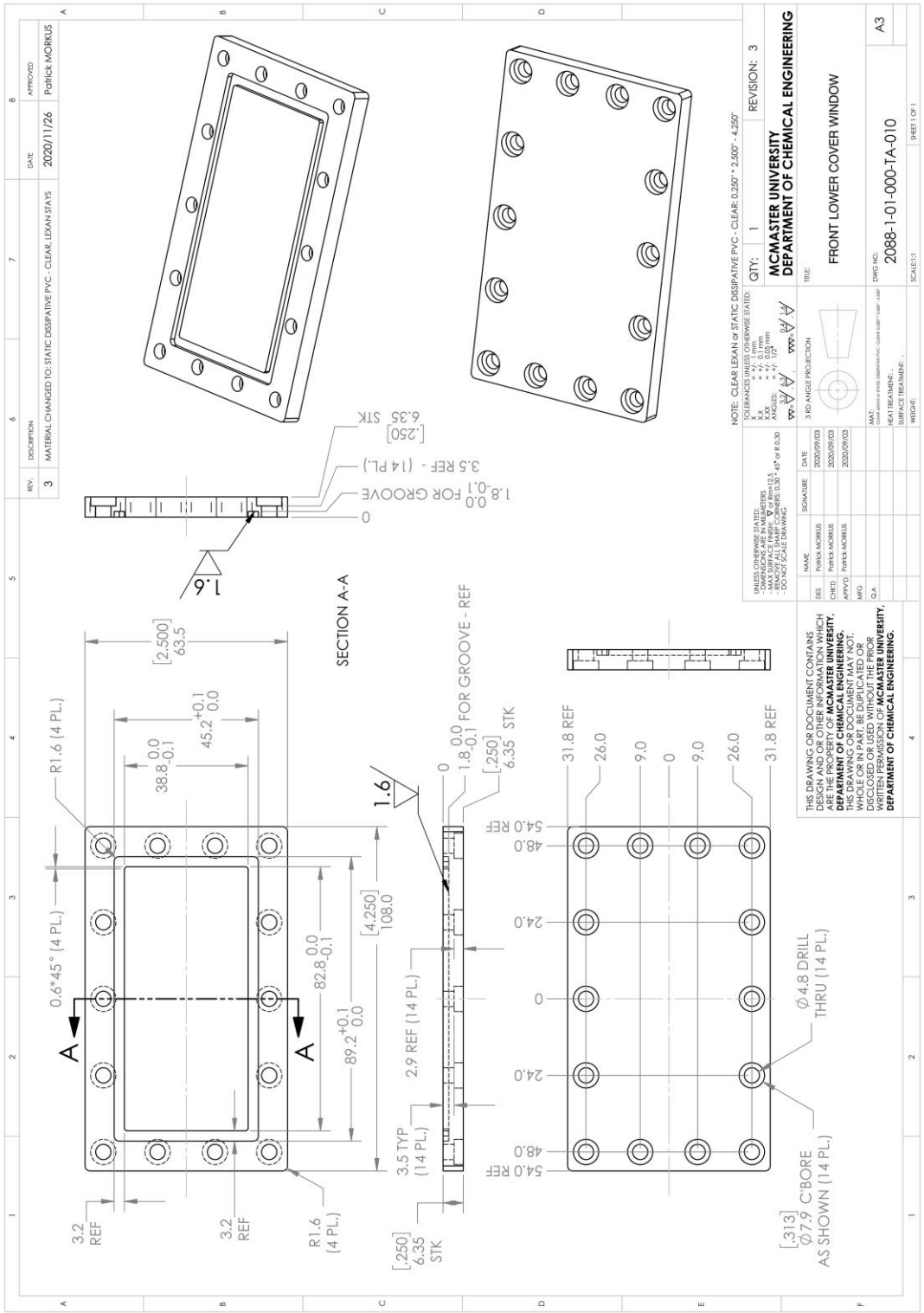
REV. DESCRIPTION DATE APPROVED
3 MATERIAL CHANGED TO: STATIC DISSIPATIVE PVC - CLEAR. LEXAN STAYS 2020/11/26 Patrick MORKUS
NOTE: CLEAR LEXAN or STATIC DISSIPATIVE PVC - CLEAR: 0.250" ± 2.500" - 4.250"
QTY: 1
REVISION: 3
MCMASTER UNIVERSITY
DEPARTMENT OF CHEMICAL ENGINEERING
TITLE:
FRONT LOWER COVER WINDOW
DWG NO. 2088-1-01-000-TA-010
A3
SCALE:1:1
SHEET 1 OF 1
SECTION A-A
[2.500] 63.5
45.2 +0.1 0.0
38.8 0.0 -0.1
R1.6 (4 PL.)
0.6*45° (4 PL.)
82.8 0.0 -0.1
89.2 +0.1 0.0
[4.250] 108.0
3.2 REF
R1.6 (4 PL.)
[.250] 6.35 STK
3.5 TYP (14 PL.)
2.9 REF (14 PL.)
1.6
1.8 0.0 -0.1 FOR GROOVE - REF
[.250] 6.35 STK
31.8 REF
26.0
9.0
0
9.0
26.0
31.8 REF
54.0 REF
48.0
24.0
0
24.0
48.0
54.0 REF
Ø4.8 DRILL THRU (14 PL.)
[.313] Ø7.9 C'BORE AS SHOWN (14 PL.)
1.6
1.8 0.0 -0.1 FOR GROOVE
3.5 REF - (14 PL.)
[.250] 6.35 STK
0
THIS DRAWING OR DOCUMENT CONTAINS DESIGN AND OR OTHER INFORMATION WHICH ARE THE PROPERTY OF MCMASTER UNIVERSITY, DEPARTMENT OF CHEMICAL ENGINEERING. THIS DRAWING OR DOCUMENT MAY NOT; WHOLE OR IN PART, BE DUPLICATED, OR DISCLOSED OR USED WITHOUT THE PRIOR WRITTEN PERMISSION OF MCMASTER UNIVERSITY, DEPARTMENT OF CHEMICAL ENGINEERING.

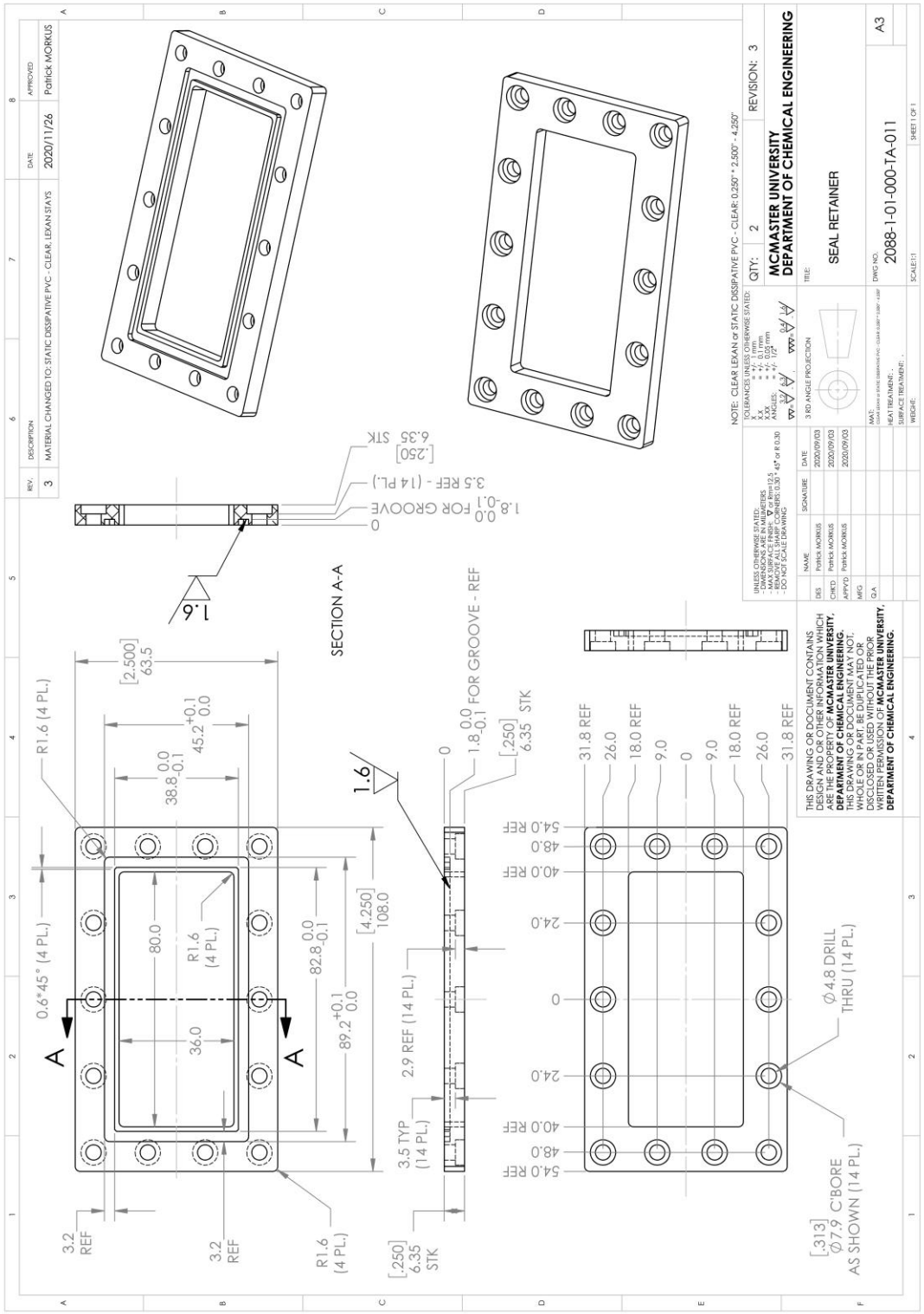
REV. DESCRIPTION DATE APPROVED
3 MATERIAL CHANGED TO: STATIC DISSIPATIVE PVC - CLEAR, LEXAN STAYS 2020/11/26 Patrick MORKUS
NOTE: CLEAR LEXAN or STATIC DISSIPATIVE PVC - CLEAR: 0.250" * 2.500" - 4.250"
QTY: 2
REVISION: 3
MCMASTER UNIVERSITY
DEPARTMENT OF CHEMICAL ENGINEERING
TITLE:
SEAL RETAINER
DWG NO. 2088-1-01-000-TA-011
A3
SCALE:1:1
SHEET 1 OF 1
SECTION A-A
R1.6 (4 PL.)
0.6*45° (4 PL.)
80.0
36.0
R1.6 (4 PL.)
3.2 REF
3.2 REF
R1.6 (4 PL.)
2.9 REF (14 PL.)
3.5 TYP (14 PL.)
[.250] 6.35 STK
1.8 0.0 -0.1 FOR GROOVE - REF
[.250] 6.35 STK
31.8 REF
26.0
18.0 REF
9.0
0
9.0
18.0 REF
26.0
31.8 REF
54.0 REF
48.0
40.0 REF
24.0
0
24.0
40.0 REF
48.0
54.0 REF
Ø4.8 DRILL THRU (14 PL.)
[.313] Ø7.9 C'BORE AS SHOWN (14 PL.)
THIS DRAWING OR DOCUMENT CONTAINS DESIGN AND OR OTHER INFORMATION WHICH ARE THE PROPERTY OF MCMASTER UNIVERSITY, DEPARTMENT OF CHEMICAL ENGINEERING. THIS DRAWING OR DOCUMENT MAY NOT; WHOLE OR IN PART, BE DUPLICATED, OR DISCLOSED OR USED WITHOUT THE PRIOR WRITTEN PERMISSION OF MCMASTER UNIVERSITY, DEPARTMENT OF CHEMICAL ENGINEERING.

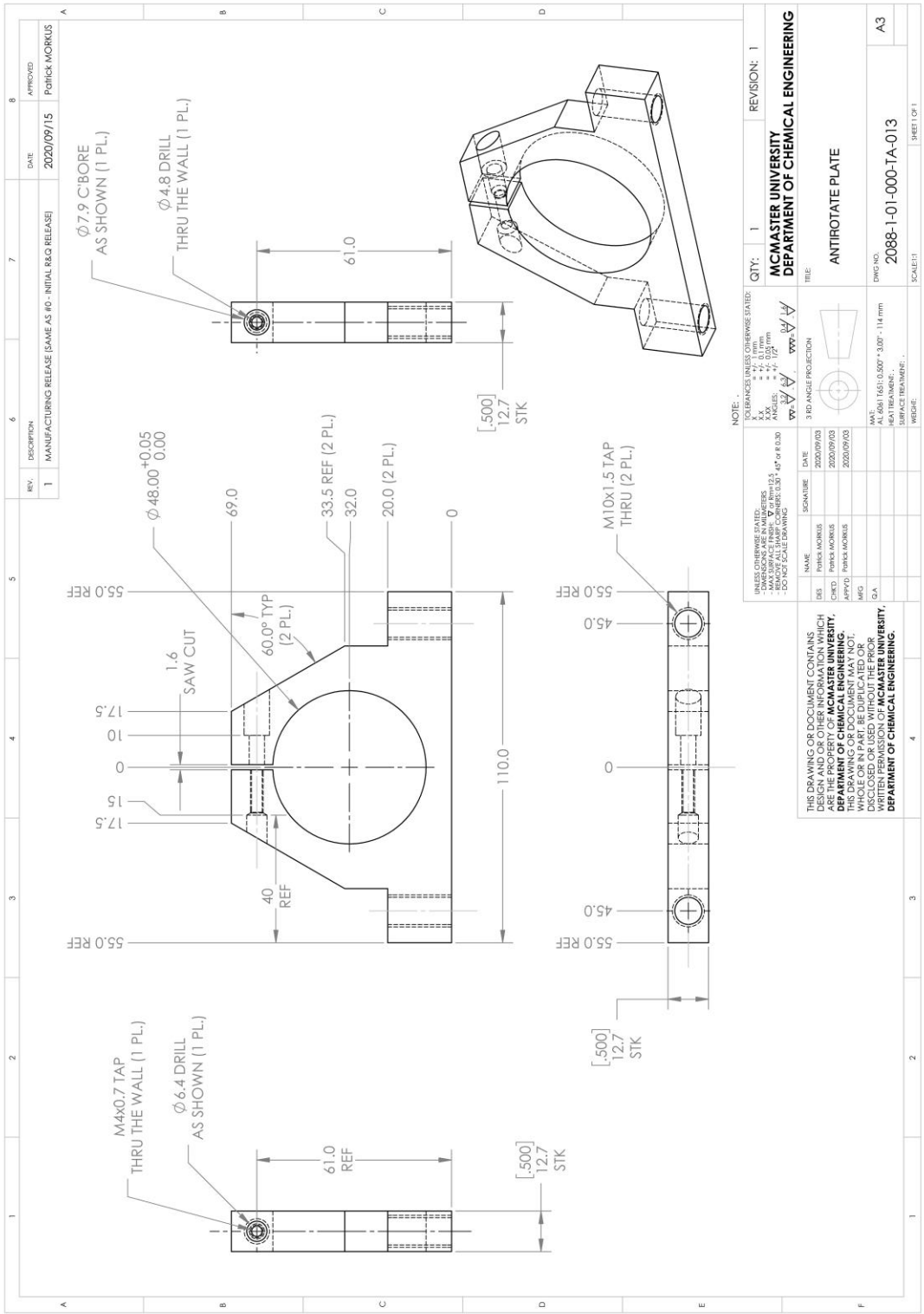
REV. DESCRIPTION DATE APPROVED
1 MANUFACTURING RELEASE (SAME AS #0 - INITIAL R&Q RELEASE) 2020/09/15 Patrick MORKUS
Ø7.9 C'BORE AS SHOWN (1 PL.)
Ø4.8 DRILL THRU THE WALL (1 PL.)
61.0
[.500] 12.7 STK
Ø48.00 +0.05 0.00
69.0
33.5 REF (2 PL.)
32.0
20.0 (2 PL.)
0
M10x1.5 TAP THRU (2 PL.)
55.0 REF
60.0° TYP (2 PL.)
1.6 SAW CUT
17.5
10
0
15
17.5
40 REF
110.0
45.0
M4x0.7 TAP THRU THE WALL (1 PL.)
Ø6.4 DRILL AS SHOWN (1 PL.)
61.0 REF
NOTE: -
UNLESS OTHERWISE STATED:
- DIMENSIONS ARE IN MILLIMETERS
- MAX SURFACE FINISH: 3.2 µm Ra or 125 µinch
- REMOVE ALL BURRS AND SHARP EDGES
- DO NOT SCALE DRAWING
TOLERANCES UNLESS OTHERWISE STATED:
X.X = +/- 0.1 mm
X.XX = +/- 0.05 mm
ANGLES = +/- 1/2°
3 RD ANGLE PROJECTION
QTY: 1
REVISION: 1
MCMASTER UNIVERSITY
DEPARTMENT OF CHEMICAL ENGINEERING
TITLE:
ANTIROTATE PLATE
DWG NO. 2088-1-01-000-TA-013
A3
SCALE:1:1
SHEET 1 OF 1
NAME SIGNATURE DATE
DES Patrick MORKUS 2020/09/03
CHK'D Patrick MORKUS 2020/09/03
APP'D Patrick MORKUS 2020/09/03
MFG
Q.A
MAT: AL 6061 T651 0.500" + 3.00" - 114 mm
HEAT TREATMENT: -
SURFACE TREATMENT: -
WEIGHT:
THIS DRAWING OR DOCUMENT CONTAINS DESIGN AND OR OTHER INFORMATION WHICH ARE THE PROPERTY OF MCMASTER UNIVERSITY, DEPARTMENT OF CHEMICAL ENGINEERING. THIS DRAWING OR DOCUMENT MAY NOT, WHOLE OR IN PART, BE DUPLICATED OR DISCLOSED OR USED WITHOUT THE PRIOR WRITTEN PERMISSION OF MCMASTER UNIVERSITY, DEPARTMENT OF CHEMICAL ENGINEERING.

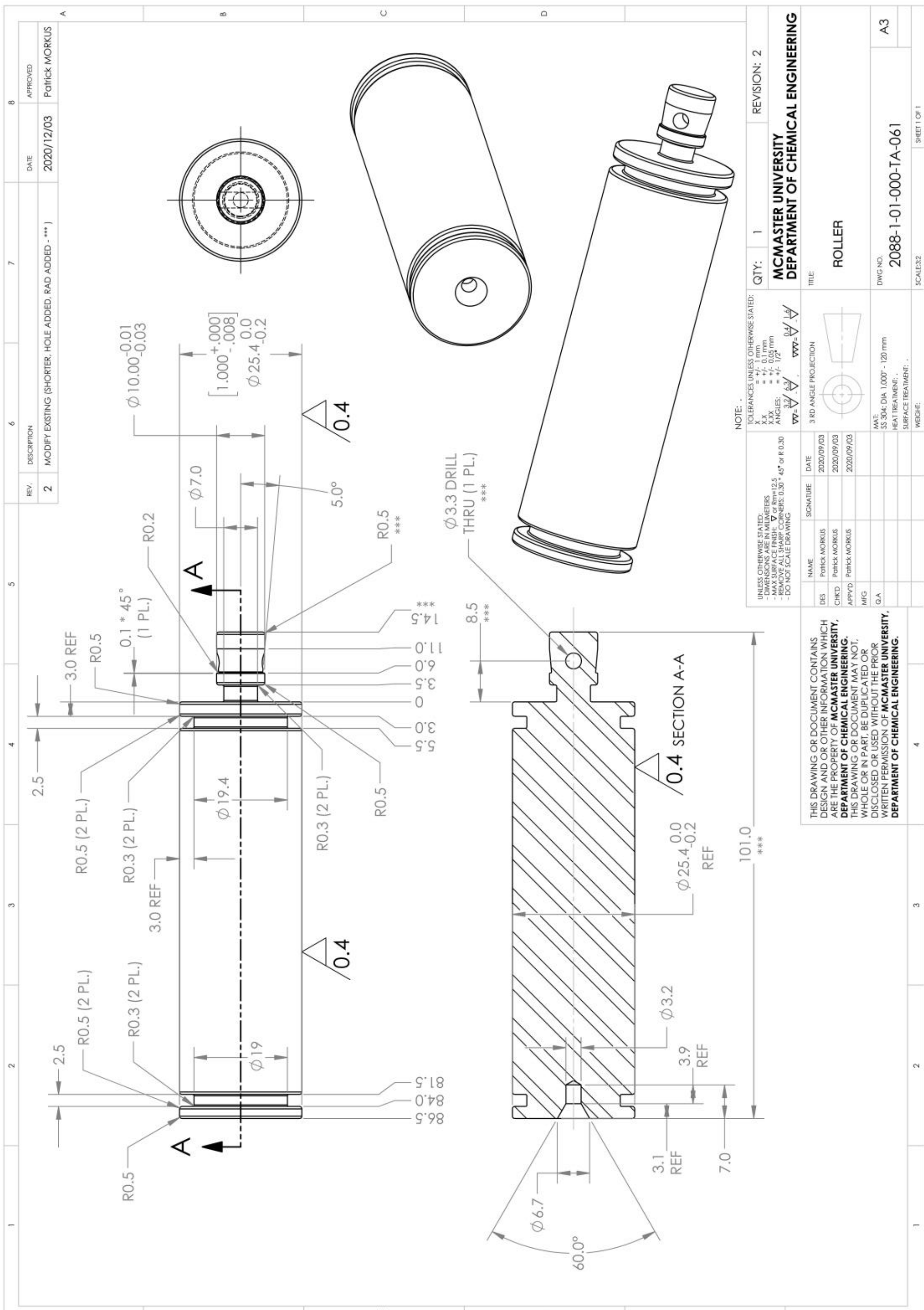
MODIFY EXISTING (SHORTER, HOLE ADDED, RAD ADDED - ***)
2020/12/03
Patrick MORKUS
SECTION A-A
QTY: 1
REVISION: 2
MCMASTER UNIVERSITY
DEPARTMENT OF CHEMICAL ENGINEERING
ROLLER
2088-1-01-000-TA-061
A3

Appendix E

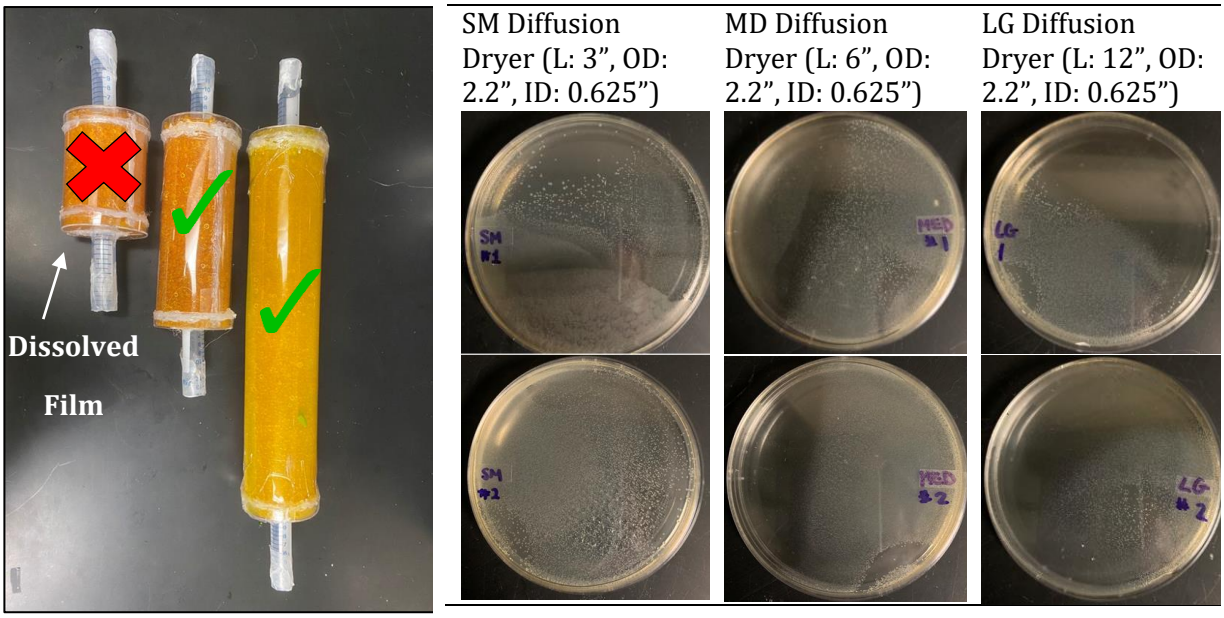

Figure E1. Different sized diffusion dryers used to dry an E. coli aerosol stream prior to entering the E-Box. Petri dishes were placed inside the E-Box at the outlet of the diffusion dryer to ensure bacteria aerosols were reaching the E-Box. Medium (MD) and large (LG) diffusion dryers produce dry aerosols in which thousands of culturable bacteria can adhere to the surface of a LB agar in a petri dish.

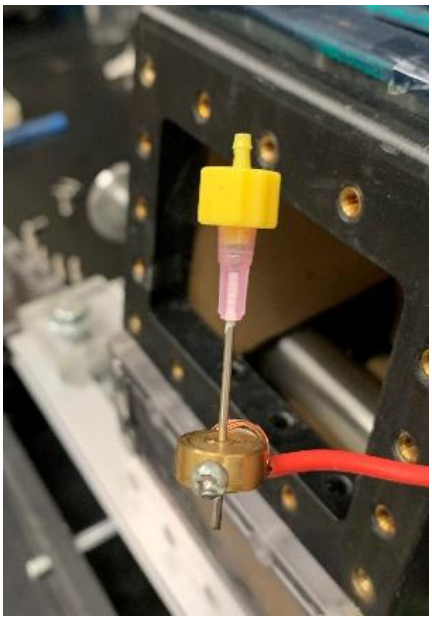

Figure E2. High voltage to spinneret connection. An 18-gauge blunted needle (spinneret) fits snugly into the cylindrical adapter. A set screw is used to gently improve the snugness of the connection.

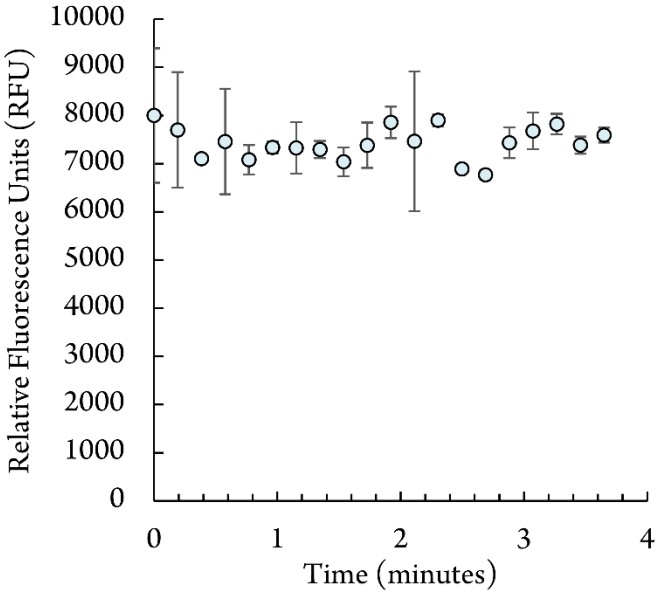

Figure E3. Average fluorescence signal of two different films produced using the AIES with FGMs measured as relatively fluorescence units (RFU) over a 4-minute period. The error bars correspond to the standard deviation. The data is derived from Figure 6-2 in the manuscript.

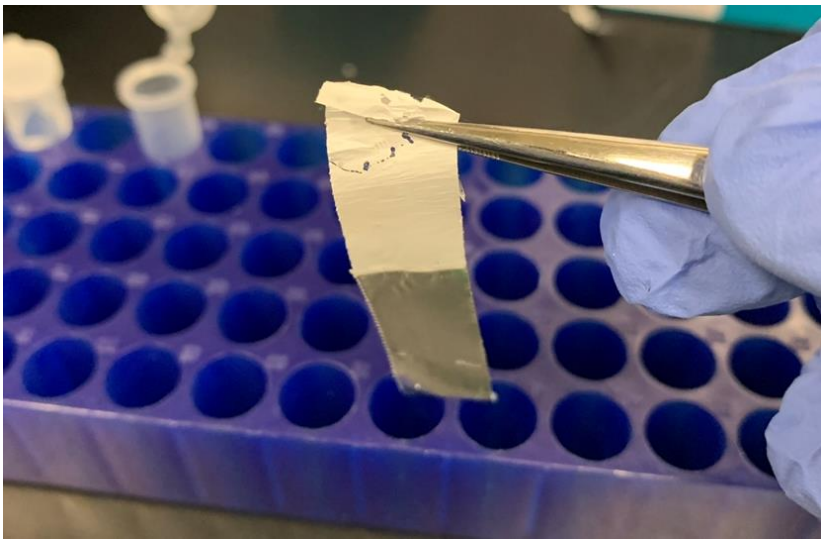

Figure E4. AIES produced *E. coli*-embedded strip (2.5 cm × 7.9 cm) that can easily peel off the aluminum foil substrate.

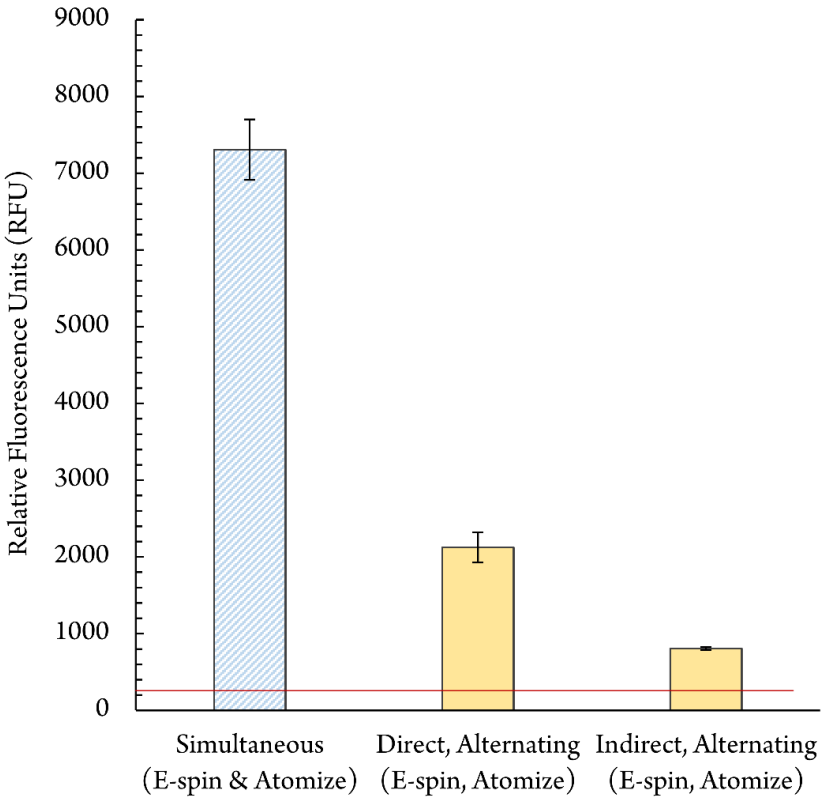

Figure E5. Average fluorescence signals measured as relative fluorescence units (RFUs) for production of FGM-embedded films via simultaneously electrospinning and atomizing and via alternating between electrospinning and atomizing. The simultaneous approach is considered the standard approach and the details of this experiments are outlined in the manuscript. For the alternating approach, electrospinning was conducted first, followed by atomizing; this sequence was repeated a total of three times. The total mass of FGMs atomized (3 mg) was same amongst for both the simultaneous and alternating approach. For the alternating experiment, the roller was stationary throughout the atomizing portion of the experiment to prevent lift of the air surrounding the cylinder and thus the fluorescence signals from pills extracted from two locations on the film ('Direct' and 'Indirect') were reported. 'Direct' corresponds to pills cut from surface of the roller directly exposed to the stream of aerosols exiting the outlet of the atomizer nozzle. 'Indirect' corresponds to the pills cut from the 'back' surface of the roller. Both experiments were conducted in duplicates on separate days and the average fluorescence signal is reported. The error bars correspond to the standard deviation from those two experiments. The red line corresponds to the control fluorescence signal in which only Milli-Q (no FGMs) was aerosolized during an AIES experiment run using the simultaneously/default approach.

Appendix F

Chemical structures of biocides used:

- Cetyltrimethylammonium bromide (CTAB):

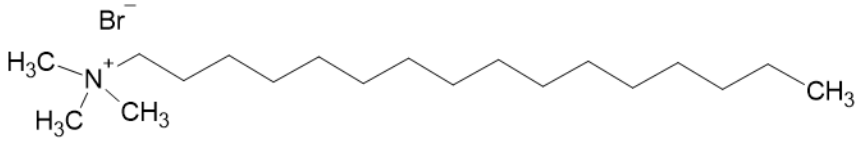

- Grotan® BK (active ingredient: Hexahydro-1,3,5,tris(2-hydroxyethyl)triazine):

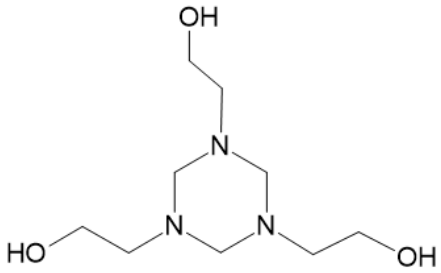

- ProClin 300™ (active ingredients: 5-chloro-2-methyl-4-isothiazolin-3-one (CMIT) and 2-methyl-4-isothiazloin-3-one (MIT)):

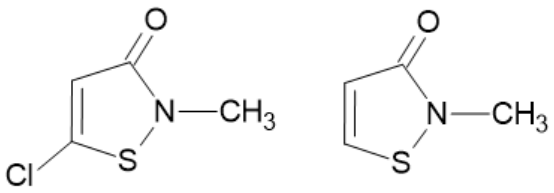

CMIT (left) MIT (right)

- Triclosan: